SPINOPHILIN CELL TYPE-SPECIFICALLY MEDIATES METABOTROPIC GLUTAMATE RECEPTOR 5-DEPENDENT EXCESSIVE GROOMING

Cameron W. Morris

Submitted to the faculty of the University Graduate School
in partial fulfillment of the requirements
for the degree
Doctor of Philosophy
in the Program of Medical Neuroscience,
Indiana University

September 2022

Accepted by the Graduate Faculty of Indiana University, in partial fulfillment of the requirements for the degree of Doctor of Philosophy.

Doctoral Committee

_____
William Truitt, Ph.D., Chair

_____
Brady Atwood, Ph.D.

August 3, 2022

_____
Anthony J. Baucum II, Ph.D.

_____
Yao-Ying Ma, M.D., Ph.D.

_____
David McKinzie, Ph.D.

Dedication

I dedicate this dissertation to the grace that only God can give, which has equipped and sustained me throughout my predoctoral training, and to my wife and family, who have continually encouraged and pushed me toward completion of this dissertation. I am fully convinced that these connections have been the lifeblood of my success; without them I would be a fraction of the man and scientist I am becoming.

Acknowledgements

First and foremost, I would like to thank my mentor, Dr. Anthony J. Baucum II, who has continually invested in my scientific and professional development over the last seven years. I am truly grateful for your commitment to mentoring me, as well as your copious amounts of patience you have shown me over the years! In addition to Dr. Baucum, I would like to specially thank Dr. Mike Edler, Dr. Asma Salek, and Dr. Darryl Watkins for their willingness to answer my never-ending conceptual and technical questions over the years of my training. Additionally, I would like to also thank Dr. Hong Wang and John Ryder for the mentorship they provided during my postbaccalaureate internship at Eli Lilly and Company—your rigorous experimental design and organization skills have been transformative in my scientific development. Lastly, but not least, I would like to acknowledge my lab-mates, Kaitlyn Stickle, Wesley Corey, Basant Hens, Nikhil Shah, and Emily Claeboe, thank you for your friendship and willingness to put up with my over-the-top personality!

In addition to Baucum lab members, I also want to sincerely thank my thesis committee members: Dr. William Truitt, Dr. Anthony J. Baucum II, Dr. Brady Atwood, Dr. Yao-Ying Ma, and Dr. Dave McKinzie. You all have contributed to the development of my thesis project in unique ways, ultimately equipping me with diverse approaches to conceptualize project, design experiments, troubleshoot methods, and interpret results. Additionally, I want to thank Taylor Pennington and the SNRI Electrophysiology Core for performing the field electrophysiology recordings for our recent manuscript

submission. I would also like to give a special thanks to Emma Doud for performing and analyzing our proteomics experiments—you were always eager to help no matter how many times Dr. Baucum and I requested you to renormalize our datasets!

In I addition to my scientific community, I especially thank my wife, Madison Morris, for her continual love, patience, support, and sincere interest in my research despite not having a background in neurobiology! I thank our previous foster children for their friendship and teaching me levels of maturity and sacrifice that graduate school cannot—I will be a better parent and mentor because of you. Mom, thank you for your love and countless prayers over the years—without them I am certain I would not be alive today! Dad, thank you for your concrete example of integrity—it is a quality that lives on in me and will make me a great scientist. Kayla, I am thankful for your friendship, and that at least one person in our family has a background in biology to understand the details of my work! I also thank my mother-, father-, brother-, and sisters-in-law for their friendship and support. I am convinced that the support I have received from all my family members over the last four years has been indispensable in my progress as a graduate student.

Lastly, we want to thank the numerous funding sources that enabled the completion of this project. The proteomics work was supported, in part, by the Indiana Clinical and Translational Sciences Institute funded, in part by Award Number UL1TR002529 from the National Institutes of Health, National Center for Advancing Translational Sciences, Clinical and Translational Sciences Award and the Cancer Center Support Grant for the IU Simon Comprehensive Cancer Center (Award Number P30CA082709) from the National Cancer Institute. We acknowledge and thank Wanda

Filipiak & Galina Gavrilina for embryo injections for the initial generation of Spino$^{Fl/Fl}$ mice as well as the entire excellent Transgenic Animal Model Core (in particular, Anna LaForest, Elizabeth Hughes, Corey Ziebell, and Dr. Thomas Saunders) and the University of Michigan's Biomedical Research Core Facilities for their generation of these mice. Funding for the generation of these mice and completion of studies comes from an R21/R33 award from the National Institutes of Drug Abuse (R21/R33 DA041876 to AJB), Department of Biology/School of Science at IUPUI, Department of Pharmacology and Toxicology Startup Funds, Strategic Research Initiative Funds (Indiana University School of Medicine and Stark Neurosciences Research Institute).

Cameron W. Morris

SPINOPHILIN CELL TYPE-SPECIFICALLY MEDIATES METABOTROPIC GLUTAMATE RECEPTOR 5-DEPENDENT EXCESSIVE GROOMING

Compulsive and repetitive behaviors in obsessive-compulsive spectrum disorders (OCSDs) are associated with perturbations in the sensorimotor striatum. Repetitive behaviors are associated with cell type-specific adaptations in striatal direct- and indirect-pathway medium spiny neurons (dMSNs and iMSNs, respectively). Furthermore, preclinical models for understanding OCSDs, such as constitutive knockout of disks large associated protein 3 (SAPAP3), suggest repetitive motor dysfunction, such as excessive grooming, is associated with increased metabotropic glutamate receptor 5 (mGluR5) activity that increases dMSN function relative to iMSNs in the sensorimotor striatum. However, MSN subtype-specific signaling mechanisms that mediate mGluR5-dependent adaptations underlying excessive grooming are not fully understood.

Reversible phosphorylation of mGluR5's C-terminal domain is one mechanism to regulate mGluR5 signaling, however, unlike kinases, promiscuous phosphatases require targeting proteins to shuttle them into contact with their targets. Therefore, phosphatase targeting proteins may be intimately involved in mediating mGluR5-dependent striatal adaptions underlying repetitive behaviors, such as excessive grooming in SAPAP3 deficient mice. Spinophilin, a major striatal postsynaptic phosphatase targeting protein, regulates striatal function, mGluR5 signaling, and forms a protein-protein interaction

with SAPAP3 that is increased by mGluR5 co-expression. Therefore, we hypothesized that *spinophilin expression in striatal medium spiny neurons mediates mGluR5-dependent excessive grooming*.

To test this, we used a novel conditional spinophilin mouse line combined with functional, behavioral, and molecular approaches to elucidate spinophilin's MSN subtype-specific contributions to rodent excessive grooming behavior associated with increased mGluR5 function. We found that loss of spinophilin in either MSN subtype abrogated plasticity in the sensorimotor striatum associated with increased mGluR5 function and decreased two models of excessive grooming associated with increased mGluR5 function—SAPAP3 deficient mice and global administration of a mGluR5-specific positive allosteric modulator (VU0360172). Additionally, we found that spinophilin's protein interaction with mGluR5 correlates with grooming behavior and loss of spinophilin shifts mGluR5 interactions from lipid-raft associated proteins toward postsynaptic density proteins implicated in psychiatric disorders. Collectively, these results identify spinophilin as a novel striatal signaling hub molecule in MSNs that MSN subtype-specifically mediates striatal adaptations associated with repetitive motor dysfunction in psychiatric disorders.

William Truitt, Ph.D., Chair

Brady Atwood, Ph.D.

Anthony J. Baucum II, Ph.D.

Yao-Ying Ma, M.D., Ph.D.

David McKinzie, Ph.D.

Table of Contents

List of Tables

List of Figures

Chapter One: Introduction

1.1 Neurobiology of Obsessive-Compulsive Spectrum Disorders

Everyone encounters situations that cause them the twirl their hair, pace back and forth, bite their nails, or even double-check to ensure their alarm clock was set for tomorrow's important meeting. As uncomfortable as these situations may be, for most people these intrusive thoughts and corresponding actions subside. However, for a subset of people, these intrusive thoughts and highly repetitive, stereotyped rituals are so severe that they impede on the individual's daily life. These intrusive thoughts and repetitive behaviors, often referred to as obsessions and compulsions, are everyday realities in approximately 3,994,980 adult and 1,260,000 adolescent US citizens living with obsessive-compulsive disorder (OCD) in 2021 (Nazeer et al 2020, NIMH 2017, Walitza et al 2011). Currently, the prototypical treatment for OCD are selective serotonin reuptake inhibitors (SSRIs), such as fluoxetine, however, these drugs are only efficacious in approximately half of OCD patients. To increase the efficacy, SSRIs can also be prescribed in combination with atypical antipsychotics, including risperidone, aripiprazole, and sometimes haloperidol, that target the D2-type dopamine receptor system (described in more detail below) (Thamby & Jaisoorya 2019). However, despite this, efficacious treatments for OCD are still lacking, largely due to our limited understanding of molecular mechanisms that mediate repetitive and compulsive behavior.

The Diagnostic and Statistical Manual of Mental Disorders 4 (DSM IV) classified OCD as an anxiety disorder due to the anxiogenic nature of the obsessions, operating under the assumption that a patient's compulsive behavior was performed in attempt to mitigate or reduce anxious thoughts. However, a direct relationship between anxiety and

compulsive behavior has not only been difficult to prove but is also inconsistent with OCD patient subgroups that assert their compulsive behavior is not due to anxiety. When asked, adults and adolescents with OCD claim they are unsure why they perform the peculiar rituals, and 40% of adolescents deny their compulsive rituals are performed to decrease anxiety (Gillan et al 2014b, Karno et al 1988, Swedo et al 1989). Due to the hit-or-miss role of anxiety in OCD, the psychiatric disorder was recently reclassified in the DSM V under Obsessive-Compulsive and Related Disorders (Robbins et al 2019). In addition to OCD, this new disorder class also includes body dysmorphic disorder, hoarding disorder, trichotillomania (hair-pulling disorder), and excoriation (skin-picking disorder), which are now collectively referred to as obsessive-compulsive spectrum disorders (OCSDs).

1.1.1 The Habit Hypothesis of OCSDs

Given the consistent presentation of compulsive behavior in OCSDs, the habit hypothesis emerged as a neuropsychological theory of OCD. Rather than focusing intently on anxiety as the underlying cause of compulsive behavior, the habit hypothesis postulates that two distinct neural circuits underly goal-directed behavior and habit formation, and that these two circuits oppose one another in their control of action outcome. Furthermore, it is hypothesized that in OCSDs neural circuits promoting goal-directed behavior are out-competed by those promoting habitual behavior (Balleine & O'Doherty 2010), thus leading to an increased propensity to form habits (Graybiel & Rauch 2000), which may be further exacerbated by stress and anxiety (Everitt & Robbins 2016).

In support of the habit hypothesis, healthy control and OCD patients were trained to respond to different picture stimuli using unique discrimination methods (two requiring goal-directed action strategies and one strategy that promotes stimulus-response (habitual) responding) to receive a reward. Although both groups were able to learn the contingencies in the training phase, once the reward was devalued, the OCD participants had impaired knowledge of outcomes (Claire M. Gillan et al 2011), suggesting OCD patients may have impaired goal-directed action strategies. One limitation of this study was that it did not include a core feature of OCD, namely that compulsive behaviors are performed to avoid an outcome (i.e. excessive handwashing to avoid germs). To address this, a groundbreaking experiment was designed that trained healthy control and OCD patients to foot-press a pedal to avoid a shock on their arm. Although, both patient groups successfully learned the contingency, after overtraining (an experimental variable that promotes habitual action strategies) OCD patients persisted in their response to avoid the shock even after the aversive shock was removed from one arm (Gillan et al 2014b). Collectively, these key studies, among others (Gillan et al 2014a, Vaghi et al 2019), suggest OCD patients not only have impaired goal-directed action strategies, but also have an increased propensity to habitually respond to stimuli to avoid aversive outcomes. One of the major limitations of the habit hypothesis is the lack of experimental data supporting the idea that decreased goal-directed action strategies concomitantly increase habitual action strategies, such that the neural substrates underlying these unique action strategies are dependent on one another. Despite ongoing human behavior studies to

refine the habit hypothesis, neuroimaging studies in OCSD patients over the last three decades strongly implicate neural circuits associated with goal-directed and habitual behavior.

1.1.2 Neural Correlates of OCSDs

Subregions of the mammalian prefrontal cortex (PFC) are intimately involved in higher-order brain function and work in concert with the basal ganglia—a collection of midbrain nuclei involved in refining motor function—to transform goal-directed action strategies into intentional, voluntary actions. Specifically, subregions of the medial PFC (mPFC) communicate with the caudate, a major basal ganglia input nucleus, to promote goal-directed actions (Valentin et al 2007). Alternatively, neuronal communication between motor cortical regions, such as the pre-supplementary and primary motor cortices, and the putamen, another major basal ganglia input nucleus, promote stimulus-response action strategies associated with habit formation (Balleine & O'Doherty 2010, Yin et al 2004). Converging evidence from diverse neuroimaging studies suggest disrupted structure, neural communication, and activity between prefrontal cortical regions and the basal ganglia in OCSDs. Indeed, structural and function magnetic resonance imaging (MRI) and positron emission tomography studies from both OCD and trichotillomania patients found volumetric changes of the mPFC, the caudate and putamen (collectively referred to as the striatum), and the thalamus, but the directionality of these changes have been inconsistent across studies (Atmaca et al 2007, Chamberlain et al 2008, Isobe et al 2018, O'Sullivan et al 1997, Pujol et al 2004b). However, despite these inconsistencies, the most reproducible finding in OCSDs is increased activity of the cortico-striatal-thalamo-cortico (CSTC) motor loop (Anticevic et al 2014, Baxter et al

1987, Beucke et al 2013, Harrison et al 2013, Hou et al 2014, Rauch et al 1994, Stein et al 2002). Consistent with the habit hypothesis, a recent functional MRI study aimed to evoke compulsive behaviors from OCD patients during imaging to identify neural correlates of compulsive behavior. Interestingly, during compulsions OCD patients had reduced neural activity in brain regions associated with goal-directed behavior (mPFC and caudate nucleus) and increased activation of regions involved in habit learning (pre-supplementary motor area and putamen). Moreover, post hoc analyses determined the putamen and mPFC most robustly correlated with urges and compulsions, suggesting both cognitive and motor dysfunction underly compulsions (Banca et al 2015).

In summary, the collection of studies detailed above suggest compulsive behavior in OCSDs is associated with decreased goal-directed action strategies and increased stimulus-response action strategies that promote habit formation. Furthermore, neuroimaging studies strongly implicate increased activity of the CSTC motor loop, and that compulsive behaviors in real-time correlate with neural activity in the putamen—the striatal nucleus associated with stimulus-response relationships and habit formation. Collectively, these data suggest there may be at least two unique strategies to decrease compulsive behavior: 1) increase goal-directed behavior in OCD patients, or 2) decrease habitual behavior. Given that there is no guarantee increasing goal-directed behavior will naturally decrease habit-related behavior, the reminder of this dissertation will focus on modulating habit-related nuclei in the basal ganglia as a means to decrease habitual and repetitive motor outputs associated with OCSDs.

1.2 Roles of the Basal Ganglia in Adaptive Behavior

1.2.1 Functional Networks of the Basal Ganglia

The basal ganglia are a group of midbrain nuclei that refine action selection to promote intentional, cohesive, and nearly-automatic movements. The striatum, composed of the caudate and putamen in humans, is the canonical basal ganglia input nucleus. The striatum receives excitatory and modulatory afferents from diverse cortical, thalamic, and subcortical structures, including brain regions that regulate cognitive and affective functions, thus positioning the striatum as a key nuclei for integrating a plethora of neuronal information to optimize action selection (Alexander et al 1986). This vast, multifaceted function of the striatum is achieved by a unique topographical organization of how the cortex innervates the striatum, such that functionally diverse cortical and subcortical regions project in parallel to discrete striatal subregions (Hunnicutt et al 2016, McGeorge & Faull 1989, Nakano 2000). As a result, activity within these diverse cortico-striatal networks increase the activity of unique striatal subregions, which in turn promote unique functional consequences. The striatum is composed of three main functional subdivisions, known as the associative striatum, sensorimotor striatum, and limbic striatum (Jahanshahi et al 2015a, Mailly et al 2013). While all these cortico-striatal circuits modulate aspects of motor function, the context by which they do so vastly differs.

The associative striatum, composed primarily of PFC projections to the caudate, is critical for associating movements with outcomes (Valentin et al 2007). Given this, the associative striatum couples cognition with movement to promote goal-directed behavior, a striatal circuit that is decreased in OCD patients (Gillan et al 2011). The sensorimotor

striatum consists of motor cortical projections to the putamen, which are indispensable for grouping complex movements together (riding a bike or driving a car) to decrease cognitive demand, thus enabling the performance of complex behaviors almost automatically with very little thought required (Graybiel 1998, Tricomi et al 2009). Collectively, the associative and sensorimotor striatum comprise the dorsal striatum, whereas the limbic striatum, often referred to as the ventral striatum, refines motor function in the context of incoming emotional and motivational information from the PFC, amygdala, and hippocampus (Jahanshahi et al 2015a, Kang et al 2021). These three versatile subdivisions of the striatum receive glutamatergic inputs from cortical, thalamic, and subcortical structures to shape motor output in the face of diverse external (environmental) and internal (affective) stimuli.

1.2.2 Glutamatergic Inputs into the Basal Ganglia

The most dense population of excitatory inputs into the striatum arise from the cortex, however, these diverse cortical regions project to distinct subdivisions of the striatum (Hunnicutt et al 2016). Specifically, the dorsomedial striatum (DMS) receives excitatory inputs from the dorsal and ventral anterior cingulate cortex, dorsal, ventral, and medial orbital cortex, visual cortex, prelimbic cortex, infralimbic cortex, and amygdala. Interestingly, many of these cortical regions innervating the DMS synapse in the anterior segment of the striatum (Hunnicutt et al 2016). Alternatively, the dorsolateral striatum (DLS) receives an exuberance of glutamatergic input from the frontal association cortex, primary and supplementary motor cortex, primary and supplementary somatosensory cortex, and insular cortices. Opposed from the DMS, most of these DLS afferents are uniform across anterior and posterior regions of the striatum. Lastly, the ventral striatum

receives overlapping glutamatergic afferents from frontal association cortex, motor cortices, somatosensory cortices, insular cortices, prelimbic and medial orbital cortex, and amygdala. However, the ventral striatum also receives unique afferents (relative to DMS and DLS) from the ecto-/peri-/ento-rhinal cortex, temporal association cortices, and the hippocampal subiculum. In addition to cortical afferents innervating the striatum, the thalamus also sends excitatory efferents into the striatum that can converge with cortical afferents (Hunnicutt et al 2016). However, opposed to cortical-striatal synapses, which predominantly form at the head of dendritic spines, the majority of thalamic synapses form on dendritic shaft regions of postsynaptic neurons (Smith et al 2004).

1.2.3 Basal Ganglia Circuitry

Despite vast anatomical and functional differences throughout the striatum, the cellular make-up of the striatum is by-and-large similar across striatal subregions. Approximately 90-95% of neurons in the striatum are γ-aminobutyric acid (GABA)ergic projection neurons, often referred to as medium-sized spiny neurons (MSNs), that inhibit downstream basal ganglia nuclei (Kreitzer 2009). However, striatal MSNs are subdivided into direct- and indirect- pathway MSNs (dMSNs and iMSNs, respectively) based on differential projections that form unique polysynaptic connections on downstream basal ganglia nuclei (Gerfen & Surmeier 2011). Classically, the majority of dMSN efferents release GABA to inhibit GABAergic neurons in the substantia nigra pars reticulata (SNr), the major basal ganglia output nucleus. However, dMSN efferents also project to inhibit GABAergic neurons in the internal segment of the globus pallidus (GPi), another basal ganglia output nucleus. Due to this organization, excitation of striatal dMSNs decreases the inhibitory efferents arising from SNr/GPi, thus disinhibiting downstream targets of

the basal ganglia (discussed in detail below). Alternatively, GABAergic iMSN efferents inhibit GABAergic neurons in the external segment of the globus pallidus (GPe), which disinhibits activity of the subthalamic nucleus (STN), another basal ganglia nucleus composed of excitatory neurons. In turn, increased STN activity excites GABAergic neurons in the SNr and GPi, thus increasing the level of inhibitor control basal ganglia output nuclei exert on downstream targets. Lastly, a unique basal ganglia pathway, termed the hyperdirect pathway, which consists of motor cortical regions directly exciting the STN (Monakow et al 1978). Similar to the indirect pathway, increased STN activity via glutamatergic innervation in turn increases GABA release from SNr and GPi, thus decreasing basal ganglia output, suggesting the hyperdirect pathway provides a unique top-down mechanism to cancel or stop motor programs (Nambu et al 2000, Nambu et al 2002). Overall, the complex anatomy and circuitry of the basal ganglia create a unique neural system, such that excitation of dMSNs increase basal ganglia output, whereas activation of iMSNs and/or the hyperdirect pathway provide two unique circuits to decrease basal ganglia output.

1.2.4 Basal Ganglia Output Pathways

The basal ganglia refine action selection primarily via two groups of output pathways. First, the most abundant basal ganglia output pathway from the SNr and GPi consist of GABAergic efferents to the deep superior colliculus (SC) and downstream midbrain and brainstem premotor areas, such as the tectum, red nucleus, and pontine reticular areas (Dudman & Krakauer 2016, Yttri & Dudman 2018), which then integrate with descending corticofugal output—a neural pathway intimately involved in filtering sensory stimuli to increase attention to environmentally relevant stimuli (Nuñez &

Malmierca 2007). Therefore, these basal ganglia output pathways provide feedforward control over the SC and brainstem premotor areas. For example, disinhibition of the SNr/GPi output (via increased direct pathway) can facilitate, whereas inhibition of the SNr/GPi output (via increased indirect or hyperdirect pathways) suppress the SC and descending motor pathways. Given this circuitry, it was originally hypothesized that SNr/GPi output gated motor functions of the SC and brainstem motor nuclei (Chevalier et al 1985, Hikosaka et al 2000); however, more recent studies suggest these outputs rather provide a system of continuous fine-tuning of actions, such that acute changes in these basal ganglia output pathways modulate the velocity and kinematics of actions (for detailed reviews see (Dudman & Krakauer 2016, Park et al 2020)).

In addition to SNr/GPi providing feedforward control over SC and brainstem motor nuclei, a significant proportion of basal ganglia efferents also project into higher-order motor nuclei of the thalamus, such as the ventroanterior, ventromedial, and interlaminar nuclei, which integrate cortical, basal ganglia, and cerebellar afferents (Alexander et al 1986, Bosch-Bouju et al 2013). In turn, the ventroanterior thalamic nucleus sends dense efferents exclusively to cortical regions associated with the sensorimotor striatum, including frontal association cortex, motor cortices, and somatosensory cortices (Hunnicutt et al 2014). Alternatively, efferents from the ventromedial thalamic nucleus diffusely synapse in the insular cortex, lateral orbital cortex, frontal association cortex, primary motor cortex, and somatosensory cortices (Hunnicutt et al 2014). Functionally, basal ganglia output to the motor thalamus also refines descending corticothalamic activity in a manner like how the SNr/GPi refine SC and brainstem motor nuclei. Specifically, rather than basal ganglia-thalamic output gating

descending corticothalamic pathways (Deniau & Chevalier 1985), current models suggest basal ganglia afferents serve as a gain modulator of motor signals, such that the direct pathway increases the gain, whereas the indirect and hyperdirect pathways decrease the gain of descending motor pathways (Dudman & Krakauer 2016, Gandhi & Katnani 2011).

Despite the basal ganglia having diverse output pathways, neuroimaging studies from OCSD patients suggest that repetitive and compulsive behaviors are associated with basal ganglia feedback into the thalamus, particularly the CSTC motor loop (Robbins et al 2019). Therefore, the remainder of the introduction will focus on the CSTC motor loop, with an emphasis on the striatal direct and indirect pathways given their dichotomous roles in modulating basal ganglia output to the thalamus (Gerfen & Surmeier 2011). In addition, basal ganglia functions and circuitry detailed above are by-and-large conserved across mammals, particularly between humans and rodents (Balleine & O'Doherty 2010, Calipari et al 2012). While the human striatum is composed of both the caudate and putamen, these striatal nuclei are merged into one structure in rodents. Despite this anatomical difference, basal ganglia functions in promoting goal-directed and stimulus-response behavior via topographically organized cortical inputs into discrete striatal subregions, the direct, indirect, and hyperdirect pathways, and basal ganglia output pathways, are all conserved between human and rodent (Balleine & O'Doherty 2010). Therefore, rodents, such as mice and rats, are an ideal low-order species to understand basal ganglia function and its contribution to repetitive and compulsive behavior associated with OCSDs. Due to this, the remainder of this dissertation will primarily focus on striatal manipulations in rodents that can be leveraged to understand

adaptive basal ganglia functions, as well as maladaptive functions associated with psychiatric disorders, such as repetitive and compulsive behavior for understanding OCSDs.

1.2.5 Striatal Contributions to Motor Function

Given the basal ganglia's role in modulating motor output, and the fact that the striatum is the major basal ganglia input nucleus, it is reasonable to hypothesize that manipulating striatal function will impact motor behavior. Indeed, this hypothesis has been tested in a variety of species using lesion experiments, electrical stimulation, and electrophysiology recordings over the last two centuries (see (Kravitz & Kreitzer 2012) for detailed historical review). Overall, these studies suggest the striatum is indispensable for both the generation and inhibition of movement, particularly contralateral movements (head turning or body circling), contraversive limb movements, and even arrest or freezing behavior.

In addition to regulating locomotion (Barbera et al 2016), the striatum has emerged as a critical basal ganglia structure required for action selection (Corbit & Janak 2010, Kimchi & Laubach 2009, Seo et al 2012, Yin et al 2005), learning and grouping motor sequences together in motor units, called chunks (Barnes et al 2005, Jin & Costa 2010, Jin et al 2014, Kupferschmidt et al 2017, Martiros et al 2018, Sheng et al 2019, Thorn et al 2010, Yin et al 2009), and the transition from goal-directed toward habitual actions (Graybiel 1998, Graybiel 2008, Jog et al 1999). One of the most consistent findings in these studies is the emergence of distinct firing patterns in the DMS (associative striatum) and DLS (sensorimotor striatum) as a recently learned motor sequence transitions into a skill or habit. Specifically, while increased DMS function is

associated with learning a novel task, striatal activity shifts from the DMS to favor DLS function as the task is mastered or transformed into a habit (which can be achieved in rodents by decreasing the association between the task and outcome and/or increasing the number of training sessions). Eventually, after the task is mastered or the habit is formed, striatal activity in the DLS spikes at the action bounds (beginning and end of the action but not during the action), suggesting the multi-step motor program required to perform the task was dynamically encoded into a single action (Jin & Costa 2010, Thorn et al 2010). While these studies highlight the critical function the DLS plays in grouping motor programs together to promote skill mastery and habit formation, recent lesion studies suggest decreased DMS function may gate these DLS functions (Turner et al 2022), suggesting habitual behavior may not be as simple as DMS and DLS competing to control habitual behavior. Despite this, these studies do not detail if these dorsal striatal functions are due to changes exclusively in dMSN or iMSN activity.

1.2.6 Striatal MSN Subtype-Specific Contributions to Motor Function

The two striatal MSN subtypes, dMSNs and iMSNs, differ in the anatomical projections to downstream basal ganglia nuclei, such that increased dMSN activity disinhibits, whereas iMSN activity inhibits, basal ganglia output to the thalamus (see 1.2.2). Given that these MSN subtypes bidirectionally regulate basal ganglia output, it was long hypothesized that dMSNs increased motor function and iMSNs decreased motor function, like a gas and brake pedal of car. While numerous studies support this hypothesis (Albin et al 1989, Alexander & Crutcher 1990, DeLong 1990), one of the most convincing studies to date detailed that optogenetic activation of dMSNs increases movement, whereas optogenetic activation of iMSNs promotes freezing and bradykinesia

(Kravitz et al 2010). However, in recent years, this hypothesis has been challenged due to studies reporting both dMSNs and iMSNs are simultaneously active during action initiation (Cui et al 2013) and that a balance in dMSN/iMSN activity is required for contraversive movements (Tecuapetla et al 2014). Given these dichotomous findings, models of dMSN and iMSN contributions to motor output have been refined. While optogenetic activation of iMSNs can decrease overall motor output, under physiological conditions it is more probable that specific ensembles of iMSNs are activated to inhibit competing motor programs. Specifically, current models postulate that increased dMSN activity promotes action selection, whereas increased iMSN activity refines motor programs by inhibiting competing motor programs. Together, both MSN subtypes function in concert by integrating a plethora of chemical neurotransmitter signals to group complex motor programs into simplified actions.

1.2.7 Striatal MSN Neurotransmitter Systems

Striatal MSNs receive excitatory glutamatergic inputs from the cortex and thalamus, and modulatory dopaminergic inputs from the ventral tegmental area (VTA) and substantia nigra par compacta (SNc) (Calipari et al 2012). In addition to striatal MSNs integrating diverse afferents, the striatum contains at least three major classes of interneurons and a dense population of astrocytes that also modulate MSN function (Khakh 2019, Tepper & Bolam 2004). Lastly, to further refine and optimize striatal output, MSNs communicate with each other through local axon collaterals (Tepper et al 2008, Tunstall et al 2002), enabling ensembles of MSNs to inhibit nearby MSNs while simultaneously communicating with downstream basal ganglia nuclei (see 1.2.2). This

complex organization within the striatum, termed striatal microcircuitry, is critical to filter and fine-tune the activity of striatal projection neurons, which can influence basal ganglia control over thalamic motor nuclei.

Both MSN subtypes express postsynaptic ionotropic α-amino-3-hydroxy-5-methyl-4-isoxazolepropionic acid receptors (AMPARs) and N-methyl-D-aspartate receptors (NMDARs), as well as metabotropic glutamate receptors (mGluRs) to receive excitatory neurotransmission coming from the cortex, thalamus, and local release from cholinergic interneurons (CINs) (Chen et al 1996, Shigemoto et al 1993, Tallaksen-Greene et al 1998, Testa et al 1995). Although both MSN subtypes receive dopaminergic inputs from the VTA and SNc, dMSNs express D1-type dopamine receptors (D1Rs) whereas iMSNs express D2-type dopamine receptors (D2Rs) (Gerfen et al 1990, Surmeier et al 1996). Additionally, dMSNs express M1- and M4-type muscarinic acetylcholine receptors (mAChRs) and iMSNs express M1-type mAChR to receive neurotransmission from CINs (Bernard et al 1992, Lim et al 2014, Yan et al 2001). While glutamate, dopamine, and acetylcholine are released from presynaptic vesicles to modulate MSN function, adenosine within the striatum is produced in the synaptic cleft by converting adenosine-triphosphate (ATP) released from presynaptic and astrocytic vesicles to adenosine by membrane-bound ectonucleases (Cunha & Ribeiro 2000, Zhang et al 2003, Zimmermann 2000). Extracellular adenosine differentially impacts dMSNs and iMSNs due to dMSNs expressing A_1 adenosine receptors and iMSNs expressing A_{2A} receptors (Cunha 2001, Ferré et al 1997, Schiffmann et al 2007). Lastly, both MSN subtypes express inhibitory ionotropic and metabotropic GABA receptors to receive neurotransmission from fast-spiking striatal interneurons, low-threshold spiking striatal

interneurons, and crosstalk between MSNs (Lacey et al 2005). Collectively, these diverse striatal cell types and neurotransmitter receptors expressed in MSNs, which are not an exhaustive list, provide an expansive "molecular language" by which MSNs can adapt to changes in cortical, subcortical, and thalamic afferents.

1.2.8 Modes of Striatal Adaptations

The integration of robust and frequent neurotransmitter signals can cause short- and long-term changes in corticostriatal synaptic function, a process frequently referred to as synaptic plasticity. In turn, synaptic plasticity promotes use-dependent changes in striatal output for adaptive behavior, including motor learning and habit formation (Perrin & Venance 2019). While the phrase synaptic plasticity is used in many different contexts, ranging from changes in synaptic transmission, structure, or even intracellular signaling molecules, here, synaptic plasticity will be discussed in the context of altered synaptic transmission within striatal MSNs that can modulate striatal output. Long-term potentiation (LTP) and long-term depression (LTD) are classical forms of synaptic plasticity; however, a long-standing paradigm in the field of striatal plasticity suggested LTP could only be induced by removing extracellular magnesium to promote NMDAR function (Calabresi et al 1996, Lovinger & Tyler 1996, Reynolds & Wickens 2002). Given this, extensive work has detailed how diverse neurotransmitter systems impact striatal LTD, which can be induced in ex-vivo brain slices by applying a high frequency stimulation at the corpus callosum to stimulate cortical fibers innervating the striatum (corticostriatal synapses). In more recent years, the use of other ex-vivo plasticity induction protocols and in-vivo electrophysiology approaches have led to a curated view of striatal plasticity that now recognizes both the physiological importance of LTD and

LTP (Mahon et al 2004). Therefore, both striatal LTD and LTP will be introduced to detail how unique striatal neurotransmitter systems promote adaptations in striatal circuits for modulating motor function.

A longstanding method to induce LTD in DLS MSNs is to depolarize the postsynaptic cell while simultaneously applying a high frequency stimulation on the lateral segment of the corpus callosum (Calabresi et al 1992, Choi & Lovinger 1997). The stimulation promotes neurotransmitter release whereas the depolarization opens L-type voltage gated calcium channels (VGCCs). This plasticity induction protocol, termed HFS-LTD, causes a robust release of glutamate and dopamine within the synaptic cleft, which then act on postsynaptic ionotropic and metabotropic receptors. The concurrent activation of L-type VGCCs and group 1 mGluRs (mGluR1 and mGluR5) results in the production of endocannabinoids (eCB) in the postsynapse that diffuse retrogradely to activate the presynaptically expressed cannabinoid 1 receptor (CB1R). In turn, CB1R decreases presynaptic neurotransmitter release, resulting in a depression of synaptic transmission (Choi & Lovinger 1997, Kreitzer & Malenka 2005, Kreitzer & Malenka 2007, Wu et al 2015). While some groups consistently detect HFS-LTD in both MSN subtypes, other groups have only been able to induce HFS-LTD in striatal iMSNs. These inconsistencies have largely been attributed to different stimulator electrode sizes, such that macrostimulation may cause robust eCB production in iMSNs that can spill over to decrease synaptic efficacy of neighboring dMSNs.

In addition to L-type VGCCs and group 1 mGluRs, numerous studies indicate D_2-dopamine receptor (D_2R) signaling is intimately involved in promoting HFS-LTD (Calabresi et al 1992, Calabresi et al 1997, Kreitzer & Malenka 2005, Kreitzer &

Malenka 2007, Wang et al 2006); however, the location in which D_2R functions to mediate LTD has been a topic of much debate (Mathur & Lovinger 2012). Although D_2R is not expressed in striatal dMSNs, pharmacological blockade of D_2R signaling prevents HFS-LTD in both MSN subtypes. This peculiar finding led to the hypothesis that D_2R signaling in CINs can indirectly modulate plasticity in MSNs. Indeed, Wang et al. determined that D_2R signaling in CINs promotes a pause in CIN spiking that decreases acetylcholine release. In turn, this decrease signaling through M1-mAChR in MSNs that inhibits eCB production, thus increasing HFS-LTD in both MSN subtypes (Wang et al 2006). Recent studies using conditional D_2R mice determined that D_2R expression in iMSNs only regulates HFS-LTD cell-autonomously, but depletion of D_2R from CINs decreased HFS-LTD in both dMSNs and iMSNs (Augustin et al 2018).

Although it has been documented that striatal LTD predominates in both MSN subtypes using macrostimulation to induce plasticity, some colleagues suggest macrostimulation does not represent physiological neurotransmission and rather suggest that microstimulation protocols may hold more physiological relevance. Not only have investigators found different HFS-LTD results using micro- versus macro-stimulation (see above), it has also been determined that both MSN subtypes undergo LTP using a different microstimulation protocol, termed spike-timing dependent plasticity (STDP) (Caporale & Dan 2008). Although dMSNs don’t undergo HFS-LTD using microstimulation protocols, it has been found that both MSN subtypes undergo LTP and LTD using a unique STDP induction protocol (Caporale & Dan 2008). STDP uses focal stimulation near synaptic sites to pair presynaptic neuron activity and postsynaptic depolarization in a close temporal window (within 10 milliseconds (ms)). By stimulating

a presynaptic neuron prior to depolarizing a postsynaptic neuron (positive timing), LTP can be induced in striatal MSNs. Alternatively, reversing this order, such that postsynaptic depolarization precedes presynaptic stimulation (negative timing), induces LTD in striatal MSNs. Comprehensive work by Shen et al. detailed how glutamatergic, dopaminergic, and adenosinergic neurotransmission impacts STPD in each MSN subtype (Shen et al 2008).

In dMSNs, LTP induced by a positive timing STDP protocol required postsynaptic NMDA receptors and D1R. Interestingly, the negative timing protocol alone was not sufficient to induce LTD in dMSNs, however, antagonism of D1R permitted LTD in dMSNs that required presynaptic CB1R function. LTD induced in dMSNs by inhibiting the D_1-dopamine receptor (D_1R) was blocked by pharmacological inhibition of mGluR5, suggesting mGluR5 signaling can cause LTD, but D_1R can attenuate mGluR5 actions (Shen et al 2008). Opposed to dMSNs, both positive and negative timing STDP protocols induced LTP or endocannabinoid-mediated LTD in iMSNs, respectively. LTP in iMSNs required NMDA and A_{2A} receptors, whereas LTD required D2R and mGluR5 signaling. However, A_{2A} and D2R signaling can oppose each other in promoting LTP and LTD, respectively. A_{2A} signaling (combined with D2R antagonism) can induce LTP despite a negative timing STDP induction protocol, and D2R signaling can induce LTD even when a positive timing STDP protocol is used (Shen et al 2008).

The use of STDP protocols expands our understanding of striatal plasticity outside of HFS-LTD, and further implies functional roles for both LTD and LTP in striatal MSNs. Consistent with these ex-vivo studies, diverse studies have determined these forms of striatal plasticity are associated with motor learning (Koralek et al 2012,

Rothwell et al 2015, Yin et al 2009), occluded in some rodent models of basal ganglia dysfunction (Nazzaro et al 2012, Shen et al 2008), and improves motor function associated with neurological disorders in-vivo, including preclinical models for understanding Parkinson's disease, addiction, and habit formation (Kreitzer & Malenka 2007, Ma et al 2018, Trusel et al 2015).

While the above introduction to striatal plasticity is not an exhaustive synopsis (i.e. there are many other forms of striatal synaptic plasticity not discussed), these studies provide a foundation detailing how postsynaptic neurotransmitter receptors promote functional changes in striatal circuits for modulating basal ganglia function. Not only do these foundational experiments consistently implicate signaling through group 1 mGluRs and dopamine receptors as mediators of long-term changes to MSN function, they also demonstrate that the integration of diverse neurotransmitter systems can promote MSN subtype-specific adaptions in the DLS. Therefore, synaptic plasticity in striatal MSNs provides a molecular framework underlying MSN subtype-specific adaptations, which, as discussed below, are consistently implicated in repetitive motor behaviors.

1.3 MSN Subtype-Specific Functions in Repetitive Behavior

The ability to learn and group motor sequences together is advantageous to simplify complex behaviors. However, perturbations in striatal circuits can increase the propensity to form habits and repetitively execute previously learned motor sequences, such as excessive washing and grooming symptoms in OCSDs. Rodent models have been utilized to understand the function of dMSNs or iMSNs in promoting repetitive and/or habitual behaviors, such as habitual lever pressing for reward, performing a novel sequential motor sequence on an accelerating rotarod, and excessive grooming behavior

(**Table 1**). Using ex-vivo two-photon calcium imaging, O'Hare et al. determined that the transition from goal-directed to habitual level pressing in an outcome devaluation task is associated with a shift in the timing of MSN firing, such that dMSN activity precedes iMSNs in the DLS (O'Hare et al 2016). Interestingly, this study also determined that breaking this lever-pressing habit is associated with both restoring the timing in dMSN/iMSN activity and an overall decrease in dMSN amplitude (O'Hare et al 2016). These experiments are consistent with other groups demonstrating that synaptic depression in iMSNs correlates with habitual lever pressing in a similar outcome devaluation task (Shan et al 2015). Moreover, Rothwell et al. also identified dMSN-specific roles in the initiation and completion of a complex sequential lever pressing task

Behavior	dMSN Function	iMSN Function	Reference
Increasing Repetitive Motor Tasks			
Rotarod Learning	↑	↓	Rothwell et al. 2014
Rotarod Maximal Performance	↑	↓	Rothwell et al. 2014
Motor Sequence Initiation	↑	↓	Rothwell et al. 2015
Motor Sequence Completion	↑	↓	Rothwell et al. 2015
Habitual Lever-pressing	↑	↓	O'Hare et al. 2016
Repetitive Grooming	↑	↓	Ade et al. 2016 Wang et al. 2017
Decreasing Repetitive Motor Task			
Breaking Habitual Lever-pressing	↓	—	O'Hare et al. 2016
Disrupting Motor Sequence Completion	—	↑	Rothwell et al. 2015
Rescuing Repetitive Grooming	—	↑	Wang et al. 2017

Table 1: MSN Subtype-Specific Adaptations Underlie Repetitive Motor Tasks. Increased repetitive motor tasks in rodents is associated with increased (↑) dMSN function and/or decreased (↓) iMSN function. Alternatively, decreasing previously acquired repetitive motor tasks in rodents is associated with decreasing dMSN function or increasing iMSN function—two unique mechanisms to decrease the dMSN/iMSN balance in activity.

(Rothwell et al 2015). Specifically, using an elegant adeno-associated viral (AAV) approach to inhibit dMSNs or iMSNs in the DLS they determined that dMSN activity is required for the completion of complex sequential motor programs, including a serial-order lever pressing task and accelerating rotarod performance, but optogenetic activation of iMSNs impaired the sequence completion in the lever pressing task (Rothwell et al 2014, Rothwell et al 2015). Furthermore, learning this sequential motor sequence was associated with a potentiation of cortical projections from premotor cortex (M2) to dMSNs in the DLS (Rothwell et al 2015).

In addition to above experiments using wild-type C57BL/6 mice, numerous animal models have been created to understand the neurological basis of repetitive behavior associated with psychiatric disorders, including OCSDs and autism spectrum disorders (ASDs). Indeed, genetic mutation, deletion, or pharmacological manipulation of numerous striatal-enriched postsynaptic scaffolding proteins or receptors are associated with psychiatric disorders (Ting et al 2012). In rodents, most of these manipulations result in pathological rodent self-grooming behavior—an evolutionarily conserved basal motor program that can become pathologically initiated and sustained (Kalueff et al 2016). Interestingly, MSN subtype-specific adaptations are associated with excessive grooming following constitutive knockout of SH3 and multiple ankyrin repeat domains 3 (SHANK3) or synapse associated protein-90 (SAP-90)/postsynaptic density-95 (PSD-95)-associated protein 3 (SAPAP3), two different postsynaptic density (PSD) scaffolding proteins that anchor mGluR5 in the extrasynaptic membrane (Peça et al 2011, Welch et al 2007). Excessive grooming in SHANK3b knockout (KO) mice is associated with decreased iMSN function relative to dMSNs in the DLS, whereas SAPAP3 KO mice

have increased dMSN activity in the DLS relative to neighboring iMSN (Ade et al 2016, Wang et al 2017). Although there are differences between these two models, both are characterized by MSN subtype-specific adaptations that cause increased dMSN function compared to iMSN function. Moreover, these MSN subtype-specific adaptations associated with excessive grooming are consistent in directionality with other behaviors in wild-type mice that require repetitive execution of sequential motor programs, suggesting increased dMSN activity, relative to iMSNs in the DLS, may be a generalized adaptation associated with repetitive behaviors.

Repetitive motor behaviors are a core symptom cluster of both OCSDs and ASDs; however, repetitive grooming has limited face validity with ASDs. Despite this, grooming dysfunction is a core phenotype associated with the OCSD, trichotillomania. Furthermore, mutations in SAPAP3 have been detected in trichotillomania patients (Zuchner et al 2009). Due to this, we elected to focus on excessive grooming in the SAPAP3 KO model to further understand MSN subtype-specific adaptions underlying repetitive behaviors.

1.4 Neurological Contributions to Rodent Self-Grooming

Excessive grooming is a common phenotype in preclinical models for understanding OCSDs and ASDs; however, the translational value of this phenotype has been a topic of debate. Excessive grooming has face validity with human grooming and skin-picking disorders, such as trichotillomania and excoriation. However, the construct validity, particularly regarding the extent to which corticostriatal circuits regulate grooming dysfunction, is critical for determining if this phenotype can provide insight into the mechanisms underlying repetitive behavior.

Grooming behavior is an evolutionarily conserved motor program across numerous species, including primates, that is composed of a highly stereotyped action sequence (Berridge & Whishaw 1992, Kolb & Milner 1981). In rodents, grooming strokes targeting the face begin to emerge in the early postnatal days, but after only several weeks of age rodents develop a complex grooming motor program that sequentially targets four main regions of the body along the cephalocaudal axis (Golani & Fentress 1985). Specifically, the grooming action sequence, frequently referred to as grooming syntax, is composed of at least 20 unique, predictable movements that are linked together on a millisecond time scale. Collectively, these movements target four unique regions of the body beginning at the nose, then progressing to the eyes, ears, then body (cephalocaudal rule) (Berridge et al 1987, Kalueff et al 2007). Grooming syntax accounts for approximately 10-15% of all grooming behavior, whereas the reminder of the time spent grooming corresponds to flexible grooming, which still adheres to the cephalocaudal rule. Given that grooming is composed of an innate complex motor sequence, it is hypothesized that understanding the neural circuits, cell types, and molecules that regulate grooming behavior will increase our understanding of how complex motor programs are initiated and completed, which may provide generalizable insight into mechanisms underlying increased habit formation and execution in OCSDs (Kalueff et al 2016).

Rodent grooming behavior is composed of a complex motor sequence, suggesting corticostriatal circuits may be intimately involved in its initiation and execution. However, it is critical to note that grooming behavior can be modulated via numerous biological processes, including changes in affective states, hormone signaling, motor

coordination, and pattern generation (Kalueff et al 2016). Given this, diverse brain regions can influence grooming behavior, including the amygdala, hypothalamus, cerebellum, and brainstem; however, evidence suggest these regions influence grooming behavior in unique ways. For example, the amygdala can regulate context-specific grooming associated with stress and social behavior (Hong et al 2014), and the hypothalamus can increase grooming by facilitating hormone signaling, such as corticotropin-releasing hormone (CRH) and adrenocorticotropic hormone (ACTH) (Dunn 1988, Dunn et al 1987, Dunn et al 1979, Kruk et al 1998, Roeling et al 1993). Lesion of the cerebellum resulted in subtly increased grooming behavior and impaired coordination of grooming strokes without significantly impacting overall grooming syntax (Berridge & Whishaw 1992). However, decerebration experiments determined that brainstem structures are sufficient to generate grooming patterns, however, the completion of grooming sequences in decerebrated rats was significantly decreased, suggesting higher-order brain structures are essential for the completion of grooming syntax (Berntson et al 1988, Berridge 1989). Interestingly, lesion of the neocortex resulted in decreased grooming behavior, however, after numerous experimental observations the deficit in grooming duration recovered and was not different than control (Berridge & Whishaw 1992).

Despite these diverse regions regulating grooming behavior, lesion of basal ganglia output nuclei significantly decrease overall grooming behavior, and site-specific excitotoxic lesion of the DLS or nigrostriatal-dopamine projections abrogated grooming sequence completion (Cromwell & Berridge 1996). Collectively, these results suggest basal ganglia output is required for increased grooming duration, and that the

dopaminergic signaling in the DLS is indispensable for the completion of grooming sequences. Recent genetic and pharmacology studies further support this hypothesis (Berridge & Aldridge 2000a, Berridge & Aldridge 2000b, Berridge et al 2005). Pharmacological activation of D_1R via intraperitoneal (I.P.) injection or intraventricular administration significantly increased grooming duration and sequence completion (Berridge & Aldridge 2000a, Berridge & Aldridge 2000b, Taylor et al 2010). However, co-administration of the D_2R antagonist, haloperidol (which also has a promiscuous off-target profile), occluded the D_1R-dependent increase in grooming duration and sequence completion, and systemic activation of D_2R with quinpirole significantly decreased grooming duration and grooming sequence completion (Berridge & Aldridge 2000a, Taylor et al 2010). While these studies suggest a complex interplay between D_1R and D_2R signaling in the regulation of rodent grooming behavior, it was unclear if these effects were due to these receptors functioning in concert or independently of each other. Recently, Fredrick et al. determined that D_1R knockout prevents, whereas D_2R knockout does not affect, the D_1R agonist-dependent effect in promoting increased grooming duration and sequence completion, suggesting D_1R and D_2R signaling regulate grooming by functioning independently of each other (Frederick et al 2015).

One limitation of the above D_1R and D_2R pharmacology experiments is the inability to confirm the behavioral effects are solely due to striatal dMSN or iMSN function, respectively. However, despite this limitation, it is worth noting that the directionality of these pharmacology experiments is consistent with known dMSN and iMSN roles in mediating complex sequential motor programs (see 1.3). Specifically, given that D_1R is expressed in striatal dMSNs (but not iMSNs), studies by Berridge et al.

further suggest that increased rodent grooming duration and sequence completion may be associated with a balance in dMSN and iMSN function, such that increased grooming behavior is associated with shifting the balance to favor dMSN function. Interestingly, these results are consistent with reported striatal abnormalities in the SAPAP3 KO model for understanding OCSDs (Ade et al 2016). However, grooming dysfunction in SAPAP3 KO mice is associated with increased mGuR5 signaling that promotes MSN subtype-specific adaptations.

1.5 The SAPAP3 Knockout Model for Understanding OCSDs

SAP-90/PSD-95 associated proteins (SAPAPs) are a family of four (SAPAP1-4) postsynaptic scaffolding proteins enriched in glutamatergic synapses, particularly within the postsynaptic density (PSD). Generally speaking, SAPAPs interact with other PSD scaffolding proteins, including PSD-95, synaptic Ras GTPase-activating protein (SynGAP), and SH3 and multiple ankyrin repeat domains proteins (SHANKs) to facilitate crosstalk between ionotropic and metabotropic glutamatergic neurotransmission (Rasmussen et al 2017). Despite overlapping molecular functions, the expression profile of each member of the SAPAP family is unique, such that SAPAP3 is the most abundant SAPAP expressed in the striatum (SAPAP2 is also expressed in the striatum but to a lesser extent) (Welch et al 2004).

Single nucleotide polymorphisms (SNPs) in the genes encoding SAPAPs, disks large associated proteins 1-4 (DLGAP1-4) have been consistently reported in OCSD patients. Genome-wide association studies have identified SNPs within the SAPAP1 gene in OCD patients, and one SAPAP3 SNP is associated with contamination and excessive washing symptoms in OCSD patients (Mattheisen et al 2015, Naaz et al 2020, Stewart et

al 2013, Wu et al 2013). Furthermore, SNPs and mutations in SAPAP3 are associated with human grooming disorders, including trichotillomania patients (Bienvenu et al 2009, Zuchner et al 2009). Consistent with human genetics studies, constitutive knockout of SAPAP3 in mice results in excessive grooming behavior, a phenotype that has face validity with grooming disorders like trichotillomania (Welch et al 2007). Therefore, the SAPAP3 KO mouse has become one of the most popular preclinical models for understanding mechanisms underlying OCSDs, particularly grooming disorders.

The initial characterization of SAPAP3 KO mice by Welch et al. determined that loss of SAPAP3 recapitulated core phenotypes associated with OCSDs, such as increased anxiety, compulsive behavior, and perturbations in corticostriatal synaptic transmission in the DLS, suggesting the preclinical model has both face and construct validity for understanding OCSDs (Welch et al 2007). Additionally, Welch et al. found that treatment with the prototypical OCD therapeutic, fluoxetine, significantly decreased grooming and reduced measures of anxiety, suggesting the SAPAP3 KO model also has predictive validity. Lastly, viral repletion of SAPAP3 protein expression throughout the striatum (dorsal and ventral) in SAPAP3 deficient mice improved grooming dysfunction, anxiety-like behavior, and corticostriatal synaptic transmission, demonstrating striatal dysfunction underlies OCD-like phenotypes in SAPAP3 KO mice (Welch et al 2007). Further highlighting the construct validity of the SAPAP3 KO model, other groups have determined that optogenetic stimulation of corticostriatal circuits associated with goal-directed behavior decreased grooming dysfunction (Burguiere et al 2013), suggesting an imbalance between goal-directed and habitual behavior may underlie compulsive behavior is SAPAP3 KO mice. Consistent with this, Linda Simmler and colleagues found

that SAPAP3 KO mice are insensitive to reward devaluation, suggesting the model has an increased propensity to form habitual motor routines (Hadjas et al 2019). Collectively, these studies demonstrate that the SAPAP3 knockout model has face, construct, and predictive validity for understanding striatal mechanisms underlying OCSDs, such as trichotillomania.

SAPAP3 is highly expressed in the striatal PSD and facilitates crosstalk between ionotropic and metabotropic glutamatergic receptors. Therefore, Nicole Calakos and colleagues conducted foundational electrophysiological experiments to measure AMPAR and NMDAR function in striatal MSNs. Increased NMDAR function in SAPAP3 KO MSNs has been reported in several studies; however, there have been inconsistent results when assessing projection-specific deficits in NMDAR function in the DLS (Corbit et al 2019, Hadjas et al 2020, Wan et al 2011). However, decreased corticostriatal AMPAR currents have been reproduced in both MSN subtypes by multiple labs with few inconsistencies (Hadjas et al 2020, Wan et al 2014, Wan et al 2011). Consistent with the role of SAPAP3 in facilitating ionotropic and metabotropic glutamate receptor cross talk, mechanistic experiments suggest that decreased AMPAR function in SAPAP3 KO MSNs is caused by increased mGluR5 signaling (Wan et al 2011). Specifically, pharmacological antagonism of mGluR5 increased the frequency of quantal AMPAR-mediated currents in SAPAP3 KO MSNs, and augmenting mGluR5 signaling with a positive allosteric modulator (PAM) decreased the frequency of quantal AMPAR current in wild-type mice (Wan et al 2011). Classically, decreases in quantal AMPAR current frequency are attributed to decreased neurotransmitter release from the presynapse, however, this report found no change in other measures of presynaptic release probability that could explain

this effect. Alternatively, they demonstrated that blocking postsynaptic AMPAR endocytosis restored the frequency of AMPAR currents in SAPAP3 KO MSNs. Taken together, it is hypothesized that increased mGluR5 signaling in SAPAP3 KO MSNs promotes AMPAR endocytosis, thus decreasing corticostriatal synaptic transmission (Wan et al 2011, Welch et al 2007).

Although the mGluR5-dependent decrease in AMPAR function is suggested to be a postsynaptic effect, it is important to note that increased mGluR5 signaling in SAPAP3 KO MSNs increased eCB-mediated short-term depression (STD)—a presynaptic form of plasticity (Chen et al 2011). Specifically, STD (lasting 15 minutes) was induced in the DLS by decreasing the inter-stimulation interval of a pair of stimuli (50 ms apart) from 90s to 10s (Chen et al 2011). Importantly, this STD was associated with decreased presynaptic release probability, which was blocked by a CB1R antagonist, confirming this is an eCB-mediated form of plasticity. The resulting STD was enhanced in field DLS recordings and whole-cell recordings from MSNs in SAPAP3 KO mice. Interestingly, this form of STD was pharmacological blocked by antagonism mGluR5 and was increased in wild-type brain slices treated with an mGluR5 positive allosteric modulator (PAM) (CDPPB), such that wild-type and SAPAP3 KO mice were no longer different. Despite increased STD in SAPAP3 KO mice, no genotype effects were found on HFS-LTD, suggesting mGluR5-dependent eCB signaling may be more sensitive in SAPAP3 KO mice, but does not increase the ceiling of eCB-mediated plasticity. Mechanistically, increased mGluR5-dependent eCB-mediated STD in SAPAP3 KO mice was attributed to increased mGluR5 surface expression in primary striatal cultures, thus providing a possible mechanism that could explain increased mGluR5 activity (Chen et al 2011).

Collectively, the above studies suggest constitutive loss of SAPAP3 results in decreased corticostriatal synaptic transmission that is associated with increased mGluR5 surface expression and signaling in MSNs. However, until recently, it was unclear if increased mGluR5 signaling in SAPAP3 KO mice caused excessive grooming behavior. Recently, Ade et al. determined that global administration of an mGluR5 negative allosteric modulator (NAM) decreased excessive grooming in SAPAP3 KO mice (Ade et al 2016). Importantly, this mGluR5 NAM also increased action potentials in the DLS (measured by in-vivo electrophysiology), further suggesting changes in grooming behavior could be due to increased DLS synaptic transmission. In addition to decreasing excessive grooming, the mGluR5 NAM also restored striatal circuit abnormalities in the DLS. Specifically, using ex-vivo 2-photon calcium imaging to measure dMSN and iMSN function simultaneously following electrical stimulation of the corpus callosum, it was determined that loss of SAPAP3 promoted dMSN activity relative to iMSNs in the DLS. Incredibly, bath application of the mGluR5 NAM, MTEP, restored the balance in MSN activity, similar to the dMSN/iMSN balance in wild-type mice (Ade et al 2016). Finally, Ade et al. reported that pharmacologically increasing mGluR5 signaling in wild-type mice with the mGluR5 PAM, VU0360172 (VU'172), is sufficient to cause repetitive grooming. This VU'172-grooming effect (as well as increased grooming from vehicle injection) was absent in mGluR5-KO mice, confirming the specificity of the VU'172 grooming response to mGluR5 function (Ade et al 2016).

Overall, the above studies suggest the core electrophysiological and behavior phenotypes in the SAPAP3 KO model for understanding OCSDs are all caused by increased mGluR5 function in striatal MSNs. Therefore, given that the SAPAP3 KO

model has face, construct, and predictive validity, understanding molecular mechanisms that mediate increased mGluR5 function in SAPAP3 KO mice may elucidate future disease-modifying therapeutic targets capable of improving corticostriatal deficits and compulsive behavior in OCSDs.

1.6 mGluR5 Signaling and Its Regulation

Glutamate, the primary excitatory neurotransmitter in the brain, activates postsynaptic ionotropic and metabotropic receptors. Classically, ionotropic glutamate receptors are localized at the head of dendritic spines and depolarize the postsynaptic cell (fast synaptic transmission), whereas mGluRs, particularly group 1 mGluRs (mGluR1 and mGluR5) are localized in the extrasynaptic membrane of dendritic spines and signal through second messengers (slow synaptic communication) to modulate fast synaptic transmission (Greengard 2001, Nusser et al 1994). When presynaptic glutamate release is low, most of the glutamatergic synaptic transmission is through proximal ionotropic receptors; however, a hyper-glutamatergic state results in glutamate spillover from the synaptic toward extrasynaptic region, in turn activating group 1 mGluRs. Both mGluR1 and mGluR5 are expressed in nearly all neuron types within striatum; however, in-situ hybridization studies suggest mGluR5 mRNA levels are greater than mGluR1 mRNA in the striatum (Shigemoto et al 1993, Tallaksen-Greene et al 1998, Testa et al 1995). Despite mGluR1 expression hypothesized to be lower than mGluR5 in the striatum, mGluR1 is known to have important roles in striatal physiology (Conquet et al 1994, Gubellini et al 2001). However, this introduction will focus on mGluR5 given its role in causing striatal dysfunction in SAPAP3 KO mice (see 1.5).

1.6.1 mGluR5 Structure, Synaptic Localization, and Protein Interactions

Like many other G-protein coupled receptors (GPCRs), mGluR5 is composed of an extracellular N-terminal domain (NTD), cystine rich domain, seven intracellular loops, and a C-terminal domain (CTD) (Niswender & Conn 2010). Upon agonist binding to the NTD, extensive confirmational changes take place beginning in the NTD that subsequently impact the conformation of the remaining protein domains. Basally GPCRs, including mGluR5, interact with a heterotrimeric complex of G-proteins, consisting of Gα, β, and γ subunits. Upon agonism, the confirmation change in mGluR5 causes the activation of $G_{\alpha q/11}$ by exchanging GDP for GTP, thus causing it to dissociate from the β and γ subunits. Classically, the β and γ subunits stay near the membrane, whereas the liberated Gα subunit can briefly diffuse from the membrane to regulate second messenger systems. (Specific signaling pathways associated with mGluR5 will be introduced below).

Canonically, mGluR5 is localized in the extrasynaptic (or perisynaptic) membrane region of dendritic spines (Nusser et al 1994). From this region, mGluR5 directly and indirectly interacts with diverse classes of proteins, including scaffolding proteins, lipid raft proteins, cell adhesion molecules, and signaling molecules, such as kinases and phosphatases. mGluR5 interacts with a network of PSD scaffolding proteins through its direct interaction with specific isoforms of homer proteins. Specifically, homer 1b, 1c, 2, and 3 directly interact with mGluR5's CTD and contain a C-terminal coiled-coiled domain that facilitates tetramerization of homer molecules (Hayashi et al 2006). Tetramerization of homer proteins not only link mGluR5 to intracellular calcium stores (Fagni et al 2000), but the mesh-like structure also enables mGluR5 to indirectly interact

with SHANK and SAPAP proteins (Sheng & Kim 2000, Tu et al 1999). Given that SAPAPs directly interact with SynGAP and PSD-95, the mesh-like network of homer proteins indirectly bridge mGluR5 from the extrasynaptic membrane into the PSD (Sheng & Hoogenraad 2007). Unlike the homer 1b/c isoforms that are constitutively expressed and contain a C-terminal coiled-coiled domain, expression of the homer 1a isoform is induced by neuronal activity and lacks a coiled-coiled domain, preventing tetramerization (Bockaert et al 2021). Although homer 1a can still directly interact with mGluR5, this homer isoform does not facilitate mGluR5's indirect interactions with PSD scaffolding proteins, which can dramatically alter mGluR5 signaling pathways associated with psychiatric disorders (discussed in more detail below) (Ade et al 2016, Ronesi et al 2012, Wang et al 2016).

mGluR5 also associates with lipid rafts (Francesconi et al 2009)—protein complexes localized to discrete extrasynaptic microdomains that function as rigid islands in the membrane bringing receptors and signaling molecules into close proximity for temporally controlled regulation of signaling (Allen et al 2007). Some of the most well-known molecular markers of lipid rafts are caveolin and flotillin proteins. Caveolar-containing lipid rafts are usually found in nonneuronal cell or non-mature neurons (i.e. primary neuronal cultures) and form small invaginations in the membrane to organize signaling complexes and promote rapid activity-dependent receptor endocytosis (Allen et al 2007). However, in contrast to caveolar-containing lipid rafts, flotillin 1 and 2 are expressed in mature neurons and form planar lipid rafts which are also hypothesized to organize signaling complexes and promote clathrin-independent receptor endocytosis (Allen et al 2007, Lang et al 1998). Lipid rafts are composed of

glycosylphosphatidylinositol (GPI)-anchored proteins—a class of lipid-associated membrane proteins that regulate diverse processes, including cell adhesion, synaptic plasticity, and dendritic spine shape (Um & Ko 2017). Interestingly, mGluR5 was recently found to interact with the GPI-anchored protein, prion protein (PrP^C), and this interaction is suggested to be critical for mGluR5 to promote dendritic spine loss and learning/memory deficits in a preclinical model of familial Alzheimer's Disease (Um et al 2013).

Classically, cell adhesion molecules are expressed in both synaptic and extrasynaptic regions of dendritic spines and function in nervous system development to link pre- and post-synapses in close proximity (Elste & Benson 2006, Yamagata et al 2003). Interestingly, numerous classes of adhesion molecules are also GPI-anchored proteins, suggesting they may also co-localize to lipid raft domains. While there currently is not much known about mGluR5 interactions with cell adhesion molecules, it has been reported that mGluR5 interacts with the neurexin family cell adhesion molecule, contactin-associated protein 1 (CASPR1), which is suggested to be required for increased mGluR5 signaling to promote memory formation (Morató et al 2018).

mGluR5 forms transient interactions with a range of signaling molecules, including kinases, phosphatases, and regulators of G-protein signaling (RGS) proteins. mGluR5 interactions with these proteins directly regulate mGluR5 signaling, which will be discussed in detail below. In addition to interacting with G-protein receptor kinases (GRKs), mGluR5 also interacts with serine/threonine kinases, such as protein kinase C (PKC), calcium/calmodulin-dependent kinase II (CaMKII), and protein kinase A (PKA), which directly phosphorylate mGluR5's C-terminal tail (Francesconi & Duvoisin 2000,

Gereau & Heinemann 1998, Kim et al 2005, Ko et al 2012, Raka et al 2015, Uematsu et al 2015). mGluR5 also interacts with calmodulin (CaM) in its calcium-free state (Lee et al 2008). In addition, tyrosine kinases, such as Src family kinases, also interact with mGluR5 to phosphorylate tyrosine residues (Mao & Wang 2016, Orlando et al 2002). A structural biology study determined that mGluR5 directly interacts with the serine-threonine phosphatase, protein phosphatase 1 (PP1) (Croci et al 2003), and one functional study suggests mGluR5 also interacts with protein phosphatase 2A (PP2A) (Mao et al 2005a). Little is known about mGluR5 interactions with tyrosine phosphatases; however, striatal-enriched protein tyrosine phosphatase (STEP) is known to interact with ionotropic glutamate receptors to regulate receptor endocytosis, raising the possibility STEP may also interact with metabotropic glutamate receptors (Pelkey et al 2002, Zhang et al 2008). Lastly, although literature suggests mGluR5 interacts with both RGS4 and RGS9, most evidence suggest RGS4 facilitates a critical negative feedback mechanism required for locomotor sensitization to psychostimulants (Saugstad et al 1998, Schwendt & McGinty 2007, Schwendt et al 2012).

The totality of mGluR5 interacting proteins, which are not fully described here, position mGluR5 in specific microdomains to modulate neuronal function through diverse signaling pathways. Furthermore, mGluR5 interactions with numerous signaling molecules provide a mechanism to bidirectionally regulate mGluR5 signaling for appropriate initiation, maintenance, and termination of signaling.

1.6.2 mGluR5 Signaling Pathways

Agonism of mGluR5 results in the activation $G_{\alpha q/11}$ promoting its dissociation from heterotrimeric G-protein complex. Classically, liberation of $G_{\alpha q/11}$ from the β and γ G-protein subunits enables the activation of the second messenger, phospholipase C (PLC). In turn, PLC cleaves inositol phospholipids to increase the production of diacylglycerol (DAG) and inositol 1,4,5-triphosphate (IP3). In turn, IP3 increases intracellular calcium (Ca^{2+}) levels by activating IP3-gated calcium channels in the endoplasmic reticulum (ER) membrane. In turn, DAG and/or intracellular Ca^{2+} released from the ER can activate diverse isoforms of PKC (Berridge & Irvine 1984, Callender & Newton 2017, Fagni et al 2000, Sugiyama et al 1987). Activation of these second messengers not only increase protein phosphorylation of diverse synaptic molecules, but also increase the activation of calcium-gated potassium and calcium channels, further exciting the neuron (Fagni et al 2000). Although these are the canonical signaling pathways associated with mGluR5 activation, mGluR5 can also influence the signaling through mitogen-activated protein kinase (MAPK) and mammalian target of rapamycin (mTOR) pathways to modulate protein translation (Page et al 2006). Interestingly, the pathway through which mGluR5 signals is determined by its protein interactions.

Tetramerization of the long homer isoforms (1b/c, 2, and 3) both link mGluR5 in close proximity to IP3-gated calcium channels in ER membrane and also bridge mGluR5 into the PSD. Given this, mGluR5 interaction with the long homer isoforms is required for increased intracellular Ca^{2+} mobilization. Furthermore, mGluR5 interactions with long homer isoforms are also required for mGluR5-dependent increases in MAPK signaling (Mao et al 2005b). In contrast, the short homer isoform, homer 1a, is an

immediate early gene due to its expression being increased by neuronal activity. Interestingly, homer 1a cannot multimerize, therefore, it competes with the long homer isoforms to interact with mGluR5 (Xiao et al 2000). As a result, the canonical mGluR5 signaling pathways (PKC, calcium signaling, and MAPK) are reduced when mGluR5 interacts with homer 1a. Under conditions of activity, the mGluR5-homer 1a complex increases the activation of unique signaling pathways, such as mTOR signaling, and can also increase depolarizing conductance through N-type calcium and M-type potassium channels (Holz et al 2019, Kammermeier et al 2000, Page et al 2006). Moreover, mGluR5 interaction with homer 1a is associated with agonist-independent signaling, resulting in constitutive mGluR5 activity (Ango et al 2001). Numerous models for understanding ASDs and OCSDs are associated with constitutive mGluR5 signaling presumably through homer 1a, including the SAPAP3 KO model (Ade et al 2016, Ronesi et al 2012, Wang et al 2016), suggesting mGluR5 dysfunction may be a point of convergence across these psychiatric disorders (Matosin & Siegel 2016). Collectively, these studies suggest that mGluR5 interactions with long homer isoforms, such as homer 1b/c, link mGluR5 to the ER and PSD to increase canonical signaling pathways (PKC, calcium signaling, and MAPK). However, homer 1a can outcompete homer 1b/c for the homer-binding site on mGluR5, resulting in constitutive mGluR5 activity associated with excessive grooming in SAPAP3 KO mice (Ade et al 2016).

mGluR5 signaling is also modulated by the activity of other striatal GPCRs, including D_1R, A_{2A} receptor, and D_2R. Co-activation of mGluR5 and D_1R activity results in an augmented PKC-dependent increase in MAPK signaling in primary striatal cultures (Voulalas et al 2005), and mGluR5 and the A_{2A} receptor are suggested to work

synergistically in promoting MAPK signaling (Ferré et al 2002). Additionally, basal D_2R activity is suggested to decrease mGluR5 phosphorylation, preventing mGluR5 trafficking to the PSD (Mao & Wang 2016). It is unclear how D_2R impacts mGluR5 signaling; however, as described above, modulating mGluR5 phosphorylation and trafficking to the PSD can have robust consequences on which pathways are activated by mGluR5. Therefore, it is possible that mGluR5 signaling could have unique impacts on dMSN and iMSN function by integrating with other MSN subtype-specific GPCRs (see 1.2.6); however, to date, MSN subtype-specific mGluR5 signaling pathways have not been reported.

1.6.3 Termination of mGluR5 Signaling

mGluR5 signaling can be terminated via indirect and direct modulation, both of which are achieved through signaling molecules. Upon GPCR agonism, the G_α subunit exchanges GDP for GTP, causing it to dissociate from the heterotrimeric G-protein complex. To counter-balance this process, RGS proteins increase the rate of GTP hydrolysis on the G_α subunit, causing it to reassemble into the heterotrimeric complex, thus decreasing GPCR signaling (Xie & Martemyanov 2011). Additionally, as mGluR5 signaling increases, kinases, including GRKs, PKC, and CaMKII, which phosphorylate mGluR5's intracellular regions to promote mGluR5 desensitization and/or endocytosis, provide critical negative feedback mechanism(s). Protein phosphatases, such as protein phosphatase 1 (PP1), are hypothesized to counterbalance these phosphorylation-dependent negative feedback mechanisms, thus stabilizing mGluR5 expression in the membrane for reactivation (Kliewer et al 2017). Given that increased mGluR5 signaling

underlies excessive grooming (Ade et al 2016), promoting the termination or preventing the resensitization of mGluR5 signaling may be one strategy to decrease mGluR5-dependent excessive grooming.

Classically, GRKs phosphorylate the intracellular regions of mGluR5 that promote receptor clustering in clathrin-coated pits for endocytosis (Kliewer et al 2017). While these phosphorylation events are reversible, arrestin proteins, such as β-arrestin, preserve these phosphorylated residues by binding to mGluR5 in its phosphorylated state. In addition to GRKs promoting activity-dependent endocytosis, kinases downstream of mGluR5 activation can also feedback to modulate mGluR5 signaling and desensitization.

PKC phosphorylation of serine (Ser) 839 on mGluR5 is required for increased calcium oscillations (Kim et al 2005). However, this PKC-dependent increase in mGluR5 signaling is also associated with mGluR5 desensitization (Gereau & Heinemann 1998). While some reports suggest PKC can desensitize mGluR5 without causing endocytosis, PKC phosphorylation at Ser 901 (Ser 908 in rodents) is known to cause mGluR5 desensitization through endocytosis. Specifically, CaM directly interacts with mGluR5 to stabilize mGluR5 in the neuronal membrane; however, phosphorylation of mGluR5 at Ser 908 destabilizes the interaction of mGluR5 with CaM and favors the interaction of mGluR5 with the E3 ligase seven in absentia homolog (Siah)-1A, thus promoting mGluR5 endocytosis (Ko et al 2012). In addition, CaMKIIα decreases mGluR5-depdendent MAPK signaling and promotes mGluR5 endocytosis; however, the phosphorylation events underlying these effects are not fully understood

(Raka et al 2015). Lastly, mGluR5 phosphorylation by PKA at Ser 870 promotes agonist-induced calcium oscillations, suggesting GPCRs that signal through $G_{\alpha i/o}$ and $G_{\alpha s/olf}$ can also modulate mGluR5 function (Uematsu et al 2015).

The above studies demonstrate that kinases activated by mGluR5 signaling can provide phosphorylation-dependent feed-forward increases in signaling, but at the same time, this increased signaling can also increase negative feedback by promoting receptor endocytosis. Kinase activity can be counter-balanced by phosphatase activity, such that protein phosphatases are critical for suppressing phosphorylation-dependent increases in signaling, as well as restoring GPCR expression in the neuronal membrane. Interestingly, the gamma-1 isoform of PP1 (PP1γ1) can directly interact with mGluR5, suggesting PP1 function may be important for stabilizing mGluR5 signaling and membrane expression. However, unlike kinases that partly target their catalytic function through consensus sequences, promiscuous phosphatases like PP1 require targeting proteins to shuttle them into contact with their targets (Cohen 2002). Therefore, phosphatase targeting proteins may reverse the phosphorylation events that promote the feedforward and feedback mechanisms described above that regulate mGluR5 signaling.

1.7 Spinophilin: The Most Abundant PP1 Targeting Protein in the Striatal PSD

The human genome encodes more than 350 serine/threonine protein kinases to facilitate site-specific phosphorylation of diverse proteins (Cohen 2002). While scaffolding proteins, such as A-kinase anchoring proteins, can group signaling molecules in close proximity to their targets, the amino acid residue(s) a kinase can phosphorylate are built into their structure (Brautigan & Shenolikar 2018). Alternatively, the human genome only encodes ~40 serine/threonine phosphatases that are highly promiscuous in

nature; these protein phosphatases can dephosphorylate nearly any serine or threonine site (Virshup & Shenolikar 2009). Given this, phosphatases almost never exist on their own; they rather complex with regulatory subunits, termed phosphatase targeting proteins, that shuttle phosphatases to specific substrates within discrete subcellular compartments (Brautigan & Shenolikar 2018, Cohen 2002). For example, one of the most abundantly expressed serine/threonine phosphatases in mammalian tissues, PP1, gains its substrate specificity by complexing with over 200 targeting proteins (Brautigan & Shenolikar 2018). In turn, these phosphatase targeting proteins enrich PP1 in specific regions of a cell, including nuclear, cytoplasmic, and postsynaptic regions of a neuron (Cohen 2002).

Spinophilin is the most abundant PP1 targeting protein in the striatal PSD and therefore is hypothesized to be a critical regulator of reversible protein phosphorylation in striatal dendritic spines (Allen et al 1997, Colbran et al 1997, Hsieh-Wilson et al 1999, Ouimet et al 2004). In addition to complexing with PP1, spinophilin also has other protein domains that facilitate its interaction with cytoskeletal proteins, PSD scaffolding proteins, and GPCRs (Baucum et al 2010, Di Sebastiano et al 2016, Grossman et al 2004, Salek et al 2019, Schuler & Peti 2008, Smith et al 1999). In addition, spinophilin contains a C-terminal coiled-coiled protein domain that enables homer- and hetero-dimerization with itself and its protein homolog, neurabin. Therefore, spinophilin can target PP1 to, or even sequester PP1 from (Ragusa et al 2010), myriad protein classes in the PSD to regulate dendritic spine morphology (Evans et al 2015, Feng et al 2000, Terry-Lorenzo et al 2005), PSD protein networks (Baucum et al 2010, Watkins et al 2018), fast synaptic transmission through ion channels (Allen et al 2006, Yan et al 1999), and slow synaptic

transmission from modulatory GPCRs (Wang et al 2004, Wang et al 2007, Wang et al 2005), including D_2R (Allen et al 2006) and mGluR5 (Di Sebastiano et al 2016). Although spinophilin interacts with diverse protein classes that can have wide-spread consequences, which are reviewed in (Sarrouilhe et al 2006), the remainder of the introduction will focus on spinophilin's interactions with GPCRs and its regulation on GPCR signaling given its potential relevance to mGluR5 dysfunction in repetitive grooming.

The majority of what is known regarding the mechanisms and consequences of spinophilin regulating GPCRs has come from studies investigating spinophilin's regulation of several classes of adrenergic receptors (ARs) and mAchRs (Fujii et al 2008, Kurogi et al 2009, Wang et al 2004, Wang et al 2007, Wang et al 2005). Overexpression of spinophilin in *Xenopus laevis* oocytes suppressed αAR-mediated mobilization of intracellular Ca^{2+} levels. This spinophilin-dependent decrease in αAR signaling was associated with an RGS2-dependent increase in GTP hydrolysis of the active $G_{\alpha q}$ subunit associated with αAR (Wang et al 2005). Similarly, spinophilin expression also decreased M1- and M3-mAChR signaling, which is also coupled to $G_{\alpha q}$ signaling, by promoting RGS8-dependent termination of signaling (Fujii et al 2008, Kurogi et al 2009). Collectively, these studies suggest spinophilin functions to decrease signaling of several $G_{\alpha q}$-coupled GPCRs, but through phosphorylation-independent mechanisms.

Spinophilin also decreases activity of the $G_{\alpha i/o}$-coupled α_{2A}-AR (α_{2A}AR) receptor, but through a different mechanism (Wang et al 2004). Specifically, spinophilin is suggested to compete with β-arrestin to dephosphorylate α_{2A}AR, presumably by targeting PP1. Spinophilin knockout ($Spino^{-/-}$)-derived mouse embryonic fibroblasts (MEFs)

displayed increased MAPK signaling upon agonism of the receptor; however, this increase in activity was short-lived as a result of α_{2A}AR quickly internalizing. Furthermore, Wang et al. also found the same trend after stimulating Spino$^{-/-}$ MEFs for 5-minutes then restimulating after a 30-minute wash, suggesting loss of spinophilin increases α_2AR phosphorylation and the amplitude of MAPK signaling, which quickly results in increased receptor endocytosis (Wang et al 2004).

In addition to spinophilin interacting with ARs, decreasing their signaling, and increasing their membrane expression, spinophilin also interacts with and regulates mGluR5 signaling in a similar manner (Di Sebastiano et al 2016). Specifically, Di Sebastiano et al. found that spinophilin directly interacts with the third intracellular loop of mGluR5. Furthermore, it was determined that loss of spinophilin from Spino$^{-/-}$-derived primary cortical neurons increased mGluR5-dependent increases in MAPK signaling while concomitantly decreasing mGluR5 expression on the membrane surface (Di Sebastiano et al 2016). Although this study did not determine if spinophilin's regulation of mGluR5 signaling and surface expression was due to changes in mGluR5 phosphorylation, the directionality of these findings are consistent with reports of how spinophilin regulates α2AR and M1/3-mAChRs. Collectively, these studies suggest spinophilin expression functions to stabilize GPCR signaling and membrane expression, including mGluR5, which may be required for mGluR5 function to promote excessive grooming behavior.

In addition to spinophilin regulating mGluR5 signaling and membrane expression, we previously found that spinophilin interacts with SAPAP3 in rodent striatum (Morris et al 2018). First, we identified this protein interaction through a proteomics screen, which suggested depletion of dopaminergic projections from the SNc decreased the spinophilin-

SAPAP3 interaction (Hiday et al 2017). In addition to dopamine signaling regulating this protein interaction, we recently found that co-expression of mGluR5 in human embryonic kidney 293 (HEK293) cells increased the spinophilin-SAPAP3 interaction. Interestingly, these data implicate spinophilin, SAPAP3, and mGluR5 in a functional protein network associated with rodent excessive grooming. Although we previously found that loss of spinophilin decreased the learning and performance of a novel motor repertoire (using an accelerating rotarod task) and prevents psychostimulant-induced locomotor sensitization (Areal et al 2019, Edler et al 2018, Morris et al 2018)—a behavioral task that requires mGluR5 signaling (Schwendt et al 2012)—the extent to which spinophilin mediates mGluR5-dependent excessive grooming is unknown.

1.8 Formulation of Central Hypothesis

The information detailed in the subsections above was utilized to formulate a central hypothesis that will be tested throughout the remaining chapters of this dissertation. Specifically, given that 1) corticostriatal dysfunction is a hallmark of OCSDs, 2) MSN subtype-specific adaptations in the DLS underlie repetitive behaviors, 3) increased mGluR5 function underlies excessive grooming in SAPAP3 KO mice, 4) spinophilin regulates mGluR5-depenent signaling and motor function, and 5) co-expression of mGluR5 increases spinophilin's protein interaction with SAPAP3, we hypothesize *that spinophilin expression in striatal medium spiny neurons mediates mGluR5-dependent excessive grooming*.

Chapter Two: Materials and Methods

2.1 Animals

The following genotypes were obtained from Jackson Laboratories or the mutant mouse regional resource center (MMRRC): Whole-body spinophilin KO mice (B6N(Cg)-*Ppp1r9b*$^{tm1.1(KOMP)Vlcg}$/J; bred in house after obtaining from Jackson laboratories); SAPAP3 KO mice (B6.129-Dlgap3^{tm1Gfng}/J); CagCreER (Tg(CAG-cre/Esr1*)5Amc; Drd1-Cre (036916-UCD B6.FVB(Cg)-Tg(Drd1a-cre)FK150Gsat/Mmucd); Adora2a-Cre (MMRRC strain 036158-UCD, B6.FVB(Cg)-Tg(Adora2a-cre)KG139Gsat/Mmucd). Conditional spinophilin KO mice were created by the University of Michigan Transgenic Animal Model Core from ES cells generated by the EUCOMMTOOLS group and obtained from the EuMMCR containing a targeted insert with a beta-gal reporter and neomycin selection cassette surrounded by FRT sites as well as loxP sites flanking exon 3 of the spinophilin gene. Upon crossing these animals with mice expressing Flp recombinase, only the loxp sites surrounding exon 3 of the spinophilin gene, Ppp1r9b, remained. Initial insert was confirmed by the EuMMCR using long-range PCR. Following Flp recombination the following DNA insert remained:

TGCCAGAGGTCCATAGGTCAGGAAGGCGCATAACGATACCACGATATCAACA
AGTTTGTACAAAAAAGCAGGCTGGCGCCGGAACCGAAGTTCCTATTCCGAAG
TTCCTATTCCGAAGTTCCTATTCTCTAGAAAGTATAGGAACTTCGTCGAGATA
ACTTCGTATAGCATACATTATACGAAGTTATGTCGAGATATCTAGACCCAGCT
TTCTTGTACAAAGTGGTTGATATCTCTATAGTCGCAGTAGGCGGCAGGGCAG
GTGTAGCTAGGCAGTGGGTATCCACGTTTGGTCAGTGACGCTCTGGGCTCAG
AAGAGAATAATAGGAGATCAAAGGCTCAGGGCTAAGACCTGGCTCAGTCCCC

ATCCCAGCCACACACCCTTATCTGTATGCACAATAGCCTACCACACCCCAGCC ACCCCTCACACACCCTGCTGCCTGTCAGCTCGTTGGATAGGGCAAAGGGCAG GAAGTAACCCGTATGAGTTAGCCTGGCAAAAGGGAGGTGGGAGGAACCATA ATTCTTTCCCATCATGGGGTGACTCGTAAGCTTGGGTAGAAGATCCCTGCCAG TCATGGCTTACCCCCCTTCTGCCTCACAGACTCTGAGGGCTTGGGCATC. Genotyping primers complementary to the endogenous Ppp1r9b sequence surrounding the insert were made (forward and reverse primers, respectively: TGCCAGAGGTCCATAGGTCAGG and GATGCCCAAGCCCTCAGAGT) to amplify the wild-type band lacking insert (392 base pairs) and mutant band containing insert (624 base pairs) (**Figure 1B**). All genotypes described above were backcrossed at least 6 generations and/or maintained on C57BL/6 background. SAPAP3$^{+/-}$ and/or Spinophilin$^{Fl/Fl,\ Fl/+,\ or\ +/+}$ mice were bred with Drd1- and Adora2a-Cre lines to obtain all genotypes utilized herein. Animals were maintained on a 12-hour light dark cycle (7AM:7PM) and all animal procedures were performed on 7-16 week-old male and female mice between 8AM and 5PM in accordance with the School of Science and School of Medicine Institutional Animal Care and Use Committees at IUPUI (Protocol #s SC270R, SC310R, 21090). All animal experiments include data from male and female mice. Sex was not included as a biological variable in our statistical analyses; however, behavior and electrophysiology experiments were visualized by sex.

2.2 Animal Behavior

All locomotion and repetitive self-grooming experiments were performed in the open field (OF) of Noldus Phenotyper Cages using a validated AI approach. Male and female mice were used for all behavior experiments.

2.2.1 Grooming Classification by Noldus Behavior Recognition Module

Noldus Behavior Recognition Module is a machine learning algorithm that utilizes nose, center, and tail identifiers to measure region-specific changes in animal orientation, which is input into a probabilistic model to predict rodent behavior. We optimized the placement of the nose, center, and tail identifiers (contour-based detection settings) using age-matched C57BL/6 mice. Once optimized, we measured the accuracy of the algorithm in predicting grooming behavior, which we defined as the initiation of any phase of grooming along the cephalo-caudal axis targeting the nose, face, ears, or body (Kalueff et al 2007, Kalueff et al 2016). Grooming duration was manually scored for 163, 30-minute videos and was compared to the results obtained from Noldus' Behavior Recognition Algorithm (default probability settings) (**Figure 5C**). Pearson Correlation analysis determined the Noldus Behavior Recognition Module has a high accuracy when predicting grooming behavior ($N=163$, $r=0.97$, $p \leq 0.0001$), therefore, to increase consistency in grooming classification and prevent bias in manual scoring, we utilized this algorithm to measure changes in grooming behavior for the experiments below.

2.2.2 SAPAP3 Wild-type and Knockout Effects on Open Field Grooming and Locomotion

Singly-housed male and female, 8-week old control (SAPAP3 WT/Spino$^{Fl/Fl\ or\ Fl/+}$ or SAPAP3 KO/Spino$^{Fl/Fl\ or\ Fl/+}$ or SAPAP3 WT/Spino$^{+/+}$/D1-Cre or SAPAP3 WT/Spino$^{+/+}$/A2A-Cre), Spino$^{\Delta dMSN}$ (SAPAP3 WT/Spino$^{Fl/Fl}$/D1-Cre or SAPAP3 KO/Spino$^{Fl/Fl}$/D1-Cre), and Spino$^{\Delta iMSN}$ (SAPAP3 WT/Spino$^{Fl/Fl}$/A2A-Cre or SAPAP3

KO/Spino$^{Fl/Fl}$/A2A-Cre) mice were placed in Noldus Phenotyper Cages (30 cm x 30 cm x 30 cm) where locomotion (distance traveled) and grooming (grooming duration, grooming frequency, mean grooming bout duration) behavior was measured for 1-hour.

2.2.3 mGluR5 PAM Effects on Open Field Grooming and Locomotion

Male and female 7-9 week old control (Spino$^{Fl/Fl\ or\ Fl/+}$ or Spino$^{+/+}$/D1- or A2A-Cre), Spino$^{\Delta dMSN}$ (Spino$^{Fl/Fl}$/D1-Cre), and Spino$^{\Delta iMSN}$ (Spino$^{Fl/Fl}$/A2A-Cre) mice were placed in Noldus Phenotyper Cages (30 cm x 30 cm x 30 cm) where locomotion (distance traveled) and grooming (grooming duration, grooming frequency, mean grooming bout duration) behavior was measured for 30-minutes (pre-injection period). Following the pre-injection period, animals were given an i.p. injection of VU0360172 (1, 3, 10, 20, 30, or 56 mg/kg) or an equivalent volume of vehicle (10% tween-80 in H_2O) and placed back into the same arena and behavior was measured for an additional 30 minutes (post-injection period).

2.3 Electrophysiology

Male and female 7-10 week old control (Spino$^{Fl/Fl}$), Spino$^{\Delta dMSN}$ (Spino$^{Fl/Fl}$/D1-Cre), and Spino$^{\Delta iMSN}$ (Spino$^{Fl/Fl}$/A2A-Cre) mice were isoflurane-anesthetized and the brain was rapidly dissected out. 350 µm thick coronal brain slices containing the dorsal striatum were made using a Leica VT1200S vibratome. The cutting solution was a sucrose-based ice-cold solution that contained 194 mM sucrose, 30 mM NaCl, 4.5 mM KCl, 1 mM MgCl2, 26 mM NaHCO3, 1.2 mM NaH2PO4, 10 mM glucose and was saturated with 95% O2/5% CO2. Slices were then transferred to a 95% O2/5% CO2-saturated artificial cerebral spinal fluid (aCSF) solution that contained 124 mM NaCl,

4.5 mM KCl, 1 mM MgCl2, 26 mM NaHCO3, 1.2 mM NaH2PO4, 10 mM glucose, and 2 mM CaCl2. Slices were stored at 30°C for 1-h then transferred to room temperature until recordings were performed.

Recordings were performed in 95% O2/5% CO2-saturated aCSF at 30° to 32°C with continuous perfusion at a rate of 1 to 2 ml/min. Field excitatory postsynaptic currents (fEPSPs) were recorded with micropipettes filled with 1 M NaCl using a Multiclamp 700B amplifier and Clampex software (Molecular Devices). Tungsten stereotrodes (~1 MW) were used to stimulate the dorsolateral striatum and population spike amplitudes (in mV) were measured. Stimulation parameters were adjusted using a constant current isolated stimulator (Digitimer). Using the stimulation strength that produced 50% of the maximum response, a stable baseline was recorded for 10 min stimulating at 0.05 Hz. LTD was induced similar to previous work (Yin et al 2009). This was done by applying two 1-s trains of 100 pulses (10 μs per pulse) delivered at 100 Hz, with 10 s between trains. Changes in population spike amplitudes were recorded for 30 min after induction monitoring at a rate of 0.05 Hz. This process, applying the LTD protocol and recording the response for 30 min, was repeated two more times. Data were expressed as a percentage of change with respect to the average baseline.

2.4 Tissue Homogenization

Striatal tissue (whole striatum or 2mm striatal punches from 0.5mm coronal sections) was homogenized in low-ionic lysis buffer as previously described (Hiday et al 2017, Morris et al 2018, Salek et al 2019, Watkins et al 2018). Briefly, low-ionic lysis buffer (0.01 M dithiothreitol (DTT), 0.005 M ethylenediaminetetraacetic acid (EDTA), 0.002 M Tris-HCl pH 7.5, 1% Triton X-100) containing protease inhibitors (Bimake) and

phosphatase inhibitors (20 mM sodium fluoride, 20 mM sodium orthovanadate, 20 mM β-glycerophosphate, and 10 mM sodium pyrophosphate; Sigma-Aldrich, St. Louis, MO or ThermoFisher) was used to homogenize tissue. Homogenates were sonicated for 15 s at 25% amplitude, rotated for 4ºC for 5 minutes, and centrifuged at 15,000 X g for 10 minutes at 4ºC. Resulting supernatants were transferred to a clean microfuge tube where prepared lysates were used for protein concentration assay (Thermo BCA Assay, 23227 or 23252), immunoprecipitation (see below), and/or preparation of input sample by diluting lysate 1:4 in 4X Laemmli sample buffer for immunoblot analysis.

2.5 Spinophilin Immunoprecipitations from SAPAP3 Wild-type and Knockout Striatum

Grooming behavior was measured in Noldus Phenotyper Cages (see below) for 2.5 hours in 4-6 month old SAPAP3 WT or KO mice. After behavior recording, whole striata were dissected, flash frozen, and stored at -80ºC. Lysates were prepared by weighing tissue and homogenizing (as described above) in low-ionic lysis buffer (45 µL/mg of tissue) and 500 µL of striatal lysate (1.5 – 2.0 mg total protein) was added to microfuge tube and 2 µg of sheep-spinophilin primary antibody (Thermo; PA5-48102) was spiked into the lysate and tubes incubated overnight at 4ºC with rotation. The following morning, 15 µL of Protein G magnetic beads was spiked into the sample and incubated two-hours at 4ºC with rotation. Beads were washed as described above and resuspended in 40 µL of 2X Laemmli sample buffer.

2.6 mGluR5 Immunoprecipitations from Spinophilin Wild-type and Knockout Striatum

Dissected whole striatum was immediately homogenized (as described above) in 1 mL of low-ionic lysis buffer and 750 µL of striatal lysate was added to a microfuge tube and 1 µg of rabbit-mGluR5 primary antibody (Millipore; AB5675) was spiked into the lysate and tubes incubated for 2.5 hours at 4ºC with rotation, then 15 µL of Protein G magnetic beads was added, and samples were incubated for an additional 2.5 hours at 4ºC with rotation. Samples were placed on magnetic tube rack and the lysate was transferred into a new microfuge tube where an aliquot of lysate was taken to measure immunodepletion and an additional 1 µg of rabbit-mGluR5 primary antibody was spiked into the lysate and samples were incubated overnight at 4ºC with rotation. The next day, another aliquot of lysates was taken to measure immunodepletion. For each round of IP, Protein G magnetic beads were washed three times with immunoprecipitation wash buffer (150 mM NaCl, 50 mM Tris-HCl pH 7.5, 0.5% (v/v) Triton X-100) and washed beads were resuspended in 30 µL of 1X phosphate buffered saline (PBS). Beads from the first and second IP were combined after confirming the sequential IPs sufficiently depleted mGluR5 from lysate via immunoblot (see below) analysis (**Figure 15**).

2.7 Immunoblotting

Immunoblotting was performed as previously described (Hiday et al 2017, Morris et al 2018, Salek et al 2019, Watkins et al 2018). Briefly, inputs (12.5 µg total protein for 2mm tissue punches, 30 µg total protein for whole striatum) or immunoprecipitates were separated by SDS-PAGE and blotted using the following antibodies: sheep-spinophilin (Thermo; PA5-48102), rabbit-SAPAP3 (Millipore; ABN325), mouse-mGluR5

(Millipore; MABN540), goat-PP1g1 (SantaCruz; sc-6108), mouse-PP1a (SantaCruz; sc-7482) and mouse-D_2R (SantaCruz; sc-5303). Appropriate infrared secondary antibodies were used (Donkey anti goat, donkey anti rabbit, or donkey anti mouse conjugated to Alexa Fluor 690 or 780; ThermoFisher or Jackson ImmunoResearch) and imaged using Odyssey CLX or Odyssey M where fluorescence intensity measurements were made using Image Studio or Empiria, respectively (LI-COR Biosciences, Lincoln, NE). We previously confirmed linearity of signal intensity for spinophilin, SAPAP3, and mGluR5 (Morris et al 2018). At least two independent cohorts of animals were utilized for all immunoblot experiments, and each gel was run with at least an N of 2 per condition for each cohort. Samples were normalized to the average control value within each gel to allow for comparisons across gels.

2.8 Proteomics

mGluR5 IPs from Spino$^{+/+}$ and Spino$^{-/-}$ were submitted to the Indiana University Center for Proteome Analysis at the Indiana University School of Medicine for sample preparation, mass spectrometry analysis, bioinformatics, and data evaluation for the GelC-MS run and both quantitative proteomics runs similar to previously published protocols (Grecco et al 2021, Salek et al 2019).

2.8.1 GelC-MS Sample Preparation and Data Analysis

Samples collected from SDS-PAGE were de-stained with 25 mM ammonium bicarbonate in 50 % acetonitrile (I). For all digestion steps, a volume sufficient to cover the gel pieces were used. Next, 10 mM DTT in 25 mM ammonium bicarbonate was added to reduce disulfides. 25 mM iodoacetamide was then added to alkylate free sulfhydryl groups. After addition of iodoacetamide, the reaction was incubated in the

dark for 45 minutes. Gel pieces were incubated in 25 mM ammonium bicarbonate. The gel pieces were then dehydrated with 25 mM ammonium bicarbonate in 50% ACN. The samples were then placed in a rotary vacuum and centrifuged until dry and subsequently digested with 12.5 ng/µl trypsin in 25 mM ammonium bicarbonate at 37°C overnight. The supernatant was collected from all samples. The remaining gel pieces were washed with 5% formic acid in 50% ACN and were vortexed and sonicated for 5 minutes. The supernatants were collected and pooled with previous supernatants and were submitted to the Indiana University Proteomics Core Facility for analysis, where Peptides were separated on an Ultimate 3000 HPLC with loading on a 5 cm C18 trap column Acclaim™ PepMap™ 100 (3 µm particle size, 75 µm diameter; Thermo Scientific, Cat No: 164946) followed by a 15 cm PepMap RSLC C18 EASY-Spray column (Thermo Scientific, Cat No: ES900) and analyzed using a Q-Exactive Plus mass spectrometer (Thermo Fisher Scientific) operated in positive ion mode. Solvent B was increased from 5%-35% over 75 min, to 90% over 2 min, back to 3% over 2 minutes (Solvent A: 95% water, 5% acetonitrile, 0.1% formic acid; Solvent B: 100% acetonitrile, 0.1% formic acid). A data dependent top 15 method was used with MS scan range of 200-2000 m/z, resolution of 70,000, AGC target 3e6, maximum IT of 100 ms. MS2 resolution of 17,500, fixed first mass 100 m/z, normalized collision energy of 30, isolation window of 4 m/z, target AGC of 1e5, and maximum IT of 50 ms. Dynamic exclusion of 30 sec, charge exclusion of 1, 7, 8, >8 and isotopic exclusion parameters were used.

Data were analyzed using Proteome Discoverer 2.4 (Thermo Fisher Scientific). Sequest HT search used a Uniprot *Mus musculus* database downloaded 01_09_2017, full trypsin cleavage with max of 2 missed cleavage sites, precursor tolerance of 10 ppm,

fragment mass tolerance of 0.02 Da, static modifications of carbamidomethyl on C, dynamic modifications (max 3 per peptide) of oxidation on M, phosphorylation on S, T, or Y, and acetylation, met-loss or met-loss plus acetylation on protein N-termini. Fixed value peptide spectrum match (PSM) validator was used as the FDR node with a maximum delta Cn of 0.05. Spectra of interest were hand annotated using Xcalibur (Thermo Fisher Scientific).

2.8.2 Tandem Mass Tag-Liquid Chromatography/Mass Spectrometry

After immunoprecipitation (IP) and wash steps, beads (3 WT and 3 KO in the first batch and 2 WT and 2 KO in the second) were submitted to the Center for Proteome analysis. 30 µL of 8 M Urea in 100 mM Tris pH 8.5 was added and proteins were reduced with 5 mM tris(2-carboxyethyl)phosphine hydrochloride (TCEP, Sigma-Aldrich Cat No: C4706) for 30 minutes at room temperature. The resulting free cysteine thiols were alkylated with 10 mM chloroacetamide (CAA, Sigma Aldrich Cat No: C0267) for 30 min at room temperature in the dark. Samples were diluted with 50 mM Tris.HCl, pH 8.5 to a final urea concentration of 2 M and treated with 1 µL PNGaseF (New England Biolabs, Cat No P0705L) for 2 hrs at 35 ºC. Samples were then digested overnight at 35 ºC with 0.5 µg Trypsin/Lys-C (Mass Spectrometry grade, Promega Corporation, Cat No: V5072).

Digestions were acidified with trifluoracetic acid (TFA, 0.5% v/v) and desalted on SPE columns (Pierce Cat no 89870) with a wash of 300 µL 0.1% TFA followed by elution in 70% acetonitrile 0.1% formic acid (FA). Peptides were dried by speed vacuum and resuspended in 24 µL of 50 mM triethylammonium bicarbonate pH 8.0 (TEAB) and labeled for two hours at room temperature with 0.2 mg of Tandem Mass Tag (TMT)

reagent which was resuspended in 24 µL acetonitrile (Thermo Fisher Scientific, TMT™ Isobaric Label Reagent Set; Cat No 90111, lot no. WC306775 for 6-plex and WD320959 for 4-plex) (Li et al 2020). Labelling reactions were quenched by adding 0.2% hydroxylamine (final v/v) to the reaction mixtures at room temperature for 15 minutes. Labeled peptides were then combined, mixed, and dried by speed vacuum. After drying, samples were resuspended in 0.1% TFA and desalted using Waters SepPak (Waters™ WAT054955) cartridges with a wash of 1 mL 0.1% TFA followed by elution in 70% IACN 0.1% FA. The specific TMT label corresponding to each WT and KO sample are designated in **Figure 15**.

For the initial 6-plex of IP TMT samples, the entire sample was applied to a High-Select™ TiO2 Phosphopeptide enrichment tip (applied 3 times, washed and eluted as per manufacturer's instructions, Thermo Fisher Scientific, Cat No A32993). However, detected phosphopeptides from enriched and non-enriched fractions were combined in analysis due to limited phosphopeptide detection in the enriched fraction. Due to this, the phosphopeptide enrichment was not performed for the validatory 4-plex of IP TMT samples.

Nano-LC-MS/MS analyses were performed on an EASY-nLC HPLC system (SCR: 014993, Thermo Fisher Scientific) coupled to Orbitrap Eclipse™ mass spectrometer (Thermo Fisher Scientific) with a FAIMS pro interface. Twenty and 25 % of each TMT mix was loaded onto a 25 cm aurora column (IonOpticks, AUR2-25075C18A) at 400 nL/min. 1/3 of the phosphopeptide fraction was injected. Peptides were eluted from 5-30% with mobile phase B (Mobile phases A: 0.1% FA, water; B: 0.1% FA, 80% IACN (Thermo Fisher Scientific Cat No: LS122500) over 160 minutes,

30-80% B over 10 mins; and dropping from 80-10% B over the final 10 min. The mass spectrometer was operated in positive ion mode with 3 FAIMS CVs (-45, -55, -70) and 1.3 sec cycle time per CV. Data-dependent acquisition method with advanced peak determination and Easy-IC (internal calibrant) were used. Precursor scans (m/z 400-1600) were done with an orbitrap resolution of 120000, RF lens% 30, maximum inject time 105 ms, standard AGC target, MS2 intensity threshold of 2.5e4, including charges of 2 to 6 for fragmentation with 60 sec dynamic exclusion. MS2 scans were performed with a quadrupole isolation window of 0.7 m/z, 38% HCD CE, 50000 resolution, 200% normalized AGC target, dynamic maximum IT fixed first mass of 100 m/z. The data were recorded using Thermo Fisher Scientific Xcalibur (4.3) software (Thermo Fisher Scientific Inc.).

Resulting RAW files were analyzed in Proteome Discover™ 2.5 (Thermo Fisher Scientific, RRID: SCR_014477) with a *Mus musculus* UniProt FASTA (both reviewed and unreviewed sequences) plus common contaminants (49922 total sequences). Quantification methods utilized isotopic impurity levels available from Thermo Fisher Scientific. SEQUEST HT searches were conducted with a maximum number of 3 missed cleavages; precursor mass tolerance of 10 ppm; and a fragment mass tolerance of 0.02 Da. Static modifications used for the search were carbamidomethylation on cysteine (C) residues. Dynamic modifications used for the search were oxidation of methionines, TMT label on the N-termini of peptides, TMT label on lysine (K) residues, phosphorylation (S, T, Y) and deamidation of N (max 3 dynamic mods). Dynamic Protein terminus modifications allowed were: acetylation (N-terminus), Met-loss or Met-loss plus acetylation (N-terminus). Percolator False Discovery Rate was set to a strict

setting of 0.01 and a relaxed setting of 0.05. IMP-ptm-RS node was used for all modification site localization scores. In the consensus workflows, data were normalized using a fasta file of all 3 GRM5 isoforms. Co-isolation thresholds of 50% and average reporter ion S/N cutoffs of 10 were used for quantification. Lot specific isotopic impurity levels were corrected for. Resulting normalized abundance values for each sample type, abundance ratio and log2(abundance ratio) values; and respective p-values (t-test) from Proteome Discover™ were exported to Microsoft Excel. All processed and raw data are uploaded to ProteomeXchange (PXD034053 and 10.6019/PXD034053) (Deutsch et al 2020).

2.9 Stereotaxic Adeno-Associated Virus Injections

The following procedures were performed to inject AAV5-CMV-EGFP-Cre (Addgene #105545) or AAV5-CMV-EGFP (Addgene #105530) into the striatum of conditional spinophilin mice.

2.9.1 Surgery Preparation

Surgical tools were autoclaved and Kopf Stereotax Alignment System (Model 1900) was wiped down with ethanol to maintain a sterile surgery environment. Glass bead sterilizer, dissecting lamp, and heating pads were turned on and a clean housing-in-place cage was place on the heating pad to preheat cage for post-operative care. AAV was placed on ice and microsyringe pump (World Precision Instruments, UMP3T-1) was turned on and injection parameters were set (syringe type, withdraw and injection volume, volume per step, and injection rate). Importantly, volume per step is specific to individual syringes and is calculated using the following formula:

Volume per Step = (ID/2) x (ID/2) x 3.1415926 x 1000 x 0.003175 where ID is the syringe internal diameter. Here, a 0.5 µL Hamilton Syringe (86259) was used with volume per step = 0.0269 nL. Lastly, stereotax leveling, and isoflurane vaporizer filling was validated.

2.9.2 AAV Injections

Time of surgery and the mouse's weight were documented in animal surgery log. Mice were anesthetized with 5% isoflurane for 5 minutes (flow rate = 2 L/min). The hair on top of the mouse's skull was trimmed and the mouse nose was secured into nose cone. Once secured, eye lubricant was added to mouse eyes (Dechra, Puralube Vet Ointment) and the isoflurane was lowered to 1.5%. Ear bars were inserted into mouse ear canals to stabilize skull, then skull was sterilized with ethanol and iodine successively at least three times each. Once the skull was secured and leveled, a scalpel was used to make an incision down the base of the skull long enough to expose bregma and lambda markings on skull. The skull was next leveled along the X- and Y- axes using Alignment Indicator (Kopf, Model 1905), then a microscope (Kopf, Model 1915) was used to locate the center of bregma, then all stereotaxic coordinates on a Micro Manipulator with Digital Display (Kopf, Model 1940) were re-zeroed. A stereotax drill (Kopf, Model 1911) was used to create two bilateral holes (4 total) in the skull to infuse anterior and posterior regions of the striatum with AAV. Specifically, drill holes for anterior striatal infusions were placed at: anterior/posterior (A/P) +1.00, medial/lateral (M/L) +/-2.05, dorsal/ventral (D/V) -3.5, and drill holes for posterior striatal infusions were placed at: A/P +0.4, M/L +/-2.65, D/V -3.55. The syringe was attached to the stereotax and sufficient AAV for each injection (one at a time) was withdrawn into syringe, such that 150 nL was injected into anterior

drill holes and 300 nL was infused into posterior drill holes. Once the syringe was loaded with the AAV, the syringe was aligned with appropriate drill hole and was quickly lowered to appropriate Z-coordinate where AAV was infused at a rate of 40 nL/min. After infusion, the AAV diffused undisturbed for 5 minutes, then the syringe needle was slowly removed from skull. Between injections, the syringe needle was wiped with isopropanol pad and rinsed by pipetting ethanol and milli Q onto kimwipes. After all injections were completed, the skin on the skull was super glued back together with VetBond and the mouse received a 5 mg/kg ketoprofen and 0.5 ml of warm saline via a subcutaneous injection. Finally, anti-itch cream (Lanacane) was applied to skull and mouse was removed from ear bars and placed into pre-warmed biohazard cage. Animals were weighed and treated with Lanacane inside a biological safety cabinet once a day for 3 days following surgery, then animals were returned to standard housing.

2.10 Statistics

SAPAP3 WT and KO behavior in OF was analyzed by two-way analysis of variance (ANOVA) tests with post-hoc Šídák's or Tukey's multiple comparisons test and Pearson's correlation analyses. mGluR5 PAM behavior in OF was analyzed by two-way ANOVAs with post-hoc Šídák's multiple comparisons test, Pearson's correlation, unpaired t-tests, and one-way ANOVAs with post-hoc Dunnett's multiple comparisons test. Field electrophysiology recordings were analyzed by two-way ANOVA with repeated measures, one-way ANOVA, or one-way ANOVAs with repeated measures with post-hoc Dunnett's multiple comparisons tests. Immunoblots were quantified as previously described (Morris et al 2018) and analyzed by unpaired t-test or one-way ANOVAs with post-hoc Dunnett's multiple comparisons test. Quantitative proteomics

results were first quantified by $\log_2$ fold-change (KO/WT), then one-tailed unpaired t-tests were performed. String-db was used to generate protein-protein interaction networks and perform gene ontology (GO) analyses, which used false discovery rate (FDR) to filter significant GO terms. In all ANOVA tests described above, post-hoc tests were only performed when column, row, or interaction p-value < 0.05. If $p < 0.05$, multiple comparisons were only performed within columns and/or rows that had a significant ANOVA effect. For t-tests of proteomics phosphorylation and interaction data, $p < 0.1$ was used. All statistical analyses, t-, F-, and r-statistics are listed in tables 2, 3, and 5 at the end of Chapters Three-Five.

Chapter Three: MSN Subtype-Specific Spinophilin Knockout Disrupts Plasticity in the Dorsolateral Striatum

3.1 Introduction

Descending cortical projections innervating the striatum—the major basal ganglia input nucleus—are critical for shaping associative, sensorimotor, and limbic aspects of motor function. As described in the introduction, network-wide changes in DLS function are associated with grouping complex action sequences together into cohesive, habitual actions. While these adaptations underlying habit formation are advantageous to simplify complex actions, perturbations in this process can increase the propensity to form habits, a characteristic of OCSD pathology. Recent studies suggest MSN subtype-specific adaptions in the DLS underlie repetitive and habitual motor outputs (see chapter 1.3). Therefore, identifying MSN subtype-specific manipulations capable of modulating network-wide changes in DLS function may in turn modulate repetitive and habitual behaviors.

Habitual behavior in the SAPAP3 knockout model for understanding OCSDs is associated with decreased corticostriatal synaptic transmission in the DLS (Welch et al 2007). Subsequent mechanistic studies suggest this decrease is caused, at least in part, by increased mGluR5 signaling in MSNs that increases 1) AMPAR endocytosis, and 2) eCB-mediated synaptic depression (Chen et al 2011, Wan et al 2011). Given this, identifying molecules capable of increasing corticostriatal synaptic transmission and/or decreasing eCB-mediated plasticity, such as HFS-LTD, may be one strategy to decrease habitual behavior in SAPAP3 KO mice.

Spinophilin is the most abundant PP1-targeting protein in the striatal PSD and directly interacts with mGluR5. Constitutive whole-body loss of spinophilin (Spino$^{-/-}$) prevents HFS-LTD in ex-vivo striatal slices from 3-4 week old mice, but this deficit could be overcome via pharmacological enhancement of D2R, suggesting decreased striatal D2R function may limit HFS-LTD in Spino$^{-/-}$ mice (Allen et al 2006). In addition, whole-body loss of spinophilin also prevented LTD associated with increased activity of group 1 mGluRs (Di Sebastiano et al 2016), albeit this was in the hippocampus where LTD occurs through endocytosis of postsynaptic AMPARs (Gladding et al 2009, Lüscher & Huber 2010). Together, these studies suggest spinophilin mediates plasticity associated with increased mGluR5 function, including HFS-LTD in the DLS. However, it is unclear if MSN subtype-specific loss of spinophilin results in network-wide increases in glutamatergic transmission and/or decreases in HFS-LTD in the DLS.

Here, we created and validated a conditional spinophilin mouse line to knockout spinophilin MSN subtype-specifically. Next, we utilized field electrophysiology to determine that loss of spinophilin in dMSNs results in network-wide increases in evoked corticostriatal synaptic transmission and decreases in HFS-LTD in the DLS. In contrast, loss of spinophilin in iMSNs did not affect evoked corticostriatal synaptic transmission, but decreased HFS-LTD in the DLS. Collectively, these data suggest loss of spinophilin in dMSNs or iMSNs prevents network-wide changes in corticostriatal plasticity, which in turn may modulate motor functions associated with the DLS, such as repetitive and habitual motor programs.

3.2 Results

3.2.1 Creation and Validation of a Conditional Spinophilin Knockout Line.

Spinophilin is expressed in diverse brain regions and cell types (Allen et al 1997, Muhammad et al 2015, Muly et al 2004, Ouimet et al 2004). To directly probe spinophilin's MSN-specific functions, we created a conditional spinophilin knockout line (**Figure 1A-B**). We biochemically validated our conditional spinophilin line (Spino$^{Fl/Fl}$) by crossing them with a global, tamoxifen-inducible Cre-recombinase mouse line (CagCreER) and injecting these mice with tamoxifen to confirm a significant protein depletion in the striatum (~95%), hippocampus (~96%), cortex (~94%), and cerebellum (~90%) (**Figure 1C-R**). Interestingly, Cre expression also decreased PP1 levels in hippocampus, but not striatum, cortex, or cerebellum.

We next injected an adeno-associated virus (AAV) expressing Cre into the striatum of conditional spinophilin line as a secondary method to validate that Cre expression decreases spinophilin levels. Specifically, we injected a viral vector encoding Cre-EGFP (AAV5-CMV-Cre-EGFP) or EGFP alone (AAV5-CMV-EGFP) into the dorsal striatum of Spino$^{Fl/Fl}$ mice (**Figure 2A**). Semi-quantitative immunoblot analysis of striatal tissue punches collected 3- and 5-weeks following surgery determined that Cre expression decreased spinophilin protein levels compared to the EGFP control AAV (**Figure 2B-C)**. Despite a trend toward decreased PP1 levels, one-way ANOVA analysis did not detect a significant reduction in PP1 levels at 3- or 5-weeks following AAV transduction, however, this is likely due to the experiment being underpowered (**Figure 2D-E**). Collectively, **Figures 1-2** demonstrate that Cre expression decreases spinophilin protein levels in a novel conditional spinophilin mouse line.

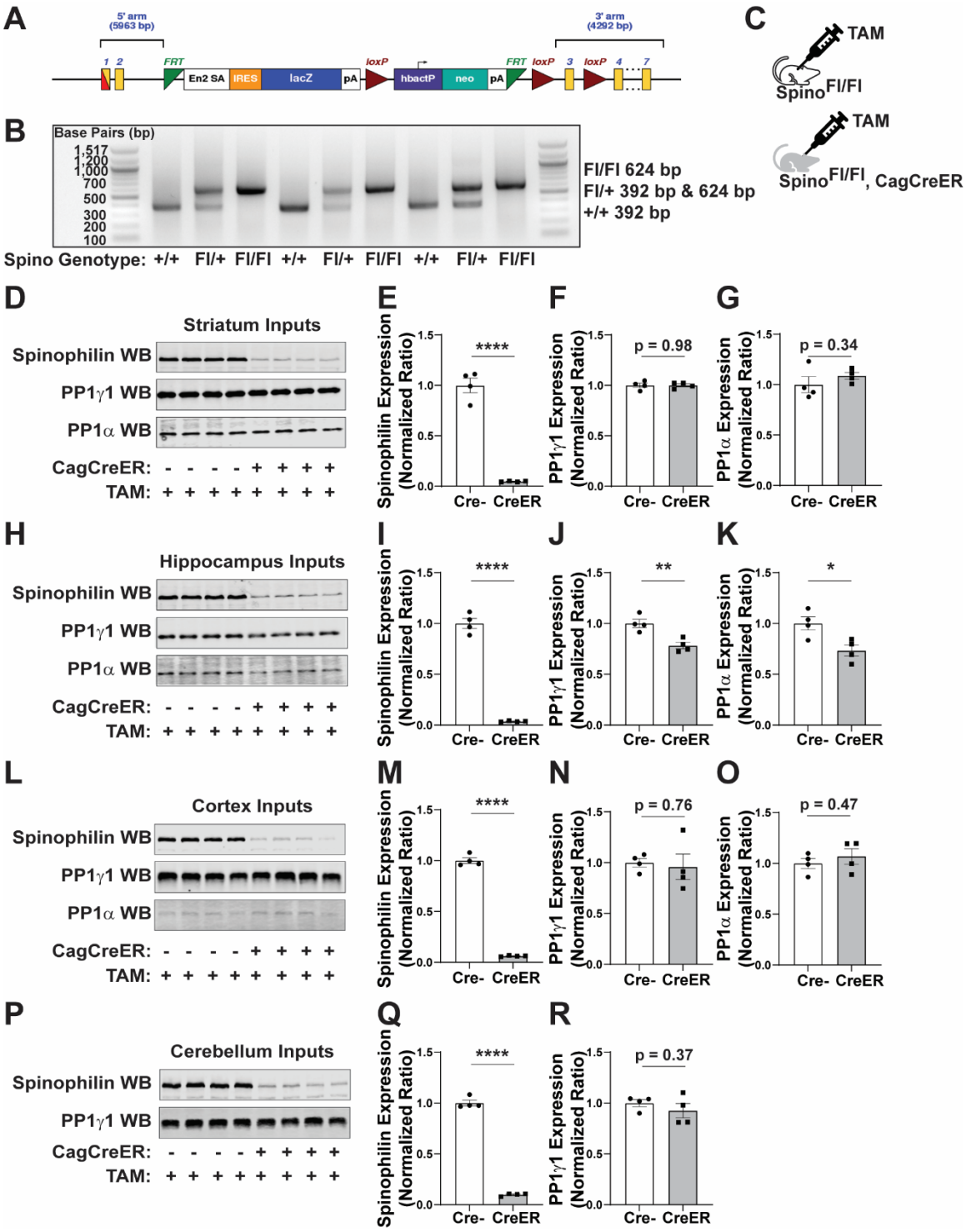
A
5' arm (5963 bp)
3' arm (4292 bp)
1 2 FRT En2 SA IRES lacZ pA loxP hbactP neo pA FRT loxP 3 loxP 4 7
B
Base Pairs (bp)
1,517
1,200
1,000
700
500
300
200
100
Fl/Fl 624 bp
Fl/+ 392 bp & 624 bp
+/+ 392 bp
Spino Genotype: +/+ Fl/+ Fl/Fl +/+ Fl/+ Fl/Fl +/+ Fl/+ Fl/Fl
C
TAM
SpinoFl/Fl
TAM
SpinoFl/Fl, CagCreER
D
Striatum Inputs
Spinophilin WB
PP1γ1 WB
PP1α WB
CagCreER: - - - - + + + +
TAM: + + + + + + + +
E
Spinophilin Expression (Normalized Ratio)
****
Cre- CreER
F
PP1γ1 Expression (Normalized Ratio)
p = 0.98
Cre- CreER
G
PP1α Expression (Normalized Ratio)
p = 0.34
Cre- CreER
H
Hippocampus Inputs
Spinophilin WB
PP1γ1 WB
PP1α WB
CagCreER: - - - - + + + +
TAM: + + + + + + + +
I
Spinophilin Expression (Normalized Ratio)
****
Cre- CreER
J
PP1γ1 Expression (Normalized Ratio)
**
Cre- CreER
K
PP1α Expression (Normalized Ratio)
*
Cre- CreER
L
Cortex Inputs
Spinophilin WB
PP1γ1 WB
PP1α WB
CagCreER: - - - - + + + +
TAM: + + + + + + + +
M
Spinophilin Expression (Normalized Ratio)
****
Cre- CreER
N
PP1γ1 Expression (Normalized Ratio)
p = 0.76
Cre- CreER
O
PP1α Expression (Normalized Ratio)
p = 0.47
Cre- CreER
P
Cerebellum Inputs
Spinophilin WB
PP1γ1 WB
CagCreER: - - - - + + + +
TAM: + + + + + + + +
Q
Spinophilin Expression (Normalized Ratio)
****
Cre- CreER
R
PP1γ1 Expression (Normalized Ratio)
p = 0.37
Cre- CreER

Figure 1: Biochemical Validation of Conditional Spinophilin Knout Mice.

A) Design of targeted DNA insert used to create spinophilin gene conditional line. **B)** Representative example of genotyping +/+, Fl/+, and Fl/Fl spinophilin alleles. **C)** Conditional spinophilin KO mice were crossed with an inducible Cre recombinase (Cre) line expressed under the Cag promotor (CagCreER). Male and female $Spino^{Fl/Fl}$ mice +/- CagCreER were given 5 daily I.P. injections of tamoxifen (TAM, 24 mg/kg) and whole striatum was dissected 28 days later for semi-quantitative immunoblot analysis of **D-G)** striatal, **H-K)** hippocampus, **L-O)** cortex, and **P-R)** cerebellum inputs. Student's t-tests were performed to determine the effect CagCreER has on protein expression. CagCreER significantly decreased **E)** spinophilin ($p<0.0001$) but not **F)** PP1γ1 ($p=0.98$) or **G)** PP1α ($p=0.34$) protein expression in striatum. In hippocampus, CagCreER significantly decreased **I)** spinophilin ($p<0.0001$), **J)** PP1γ1 ($p=0.005$), and **K)** PP1α ($p=0.02$) expression, suggesting there may be compensatory changes in PP1 levels similar to $Spino^{-/-}$ hippocampus (Salek et al 2019). In cortex, CagCreER significant decreased **M)** spinophilin ($p<0.0001$) but not **N)** PP1γ1 ($p=0.76$) or **O)** PP1α ($p=0.47$) expression. In cerebellum, CagCreER significantly decreased **Q)** spinophilin ($p<0.0001$) but not **R)** PP1γ1 ($p=0.37$). Consistent with in-situ hybridization data reported in the Allen Brain Atlas, we detected minimal PP1α expression in cerebellum (data not shown). N=4 TAM-treated $Spino^{Fl/Fl}$ (2 male), 4 TAM-treated $Spino^{Fl/Fl}$/CagCreER (2 male). Data ± SEM. *$p\leq0.05$, **$p\leq0.01$, ****$p<0.0001$.

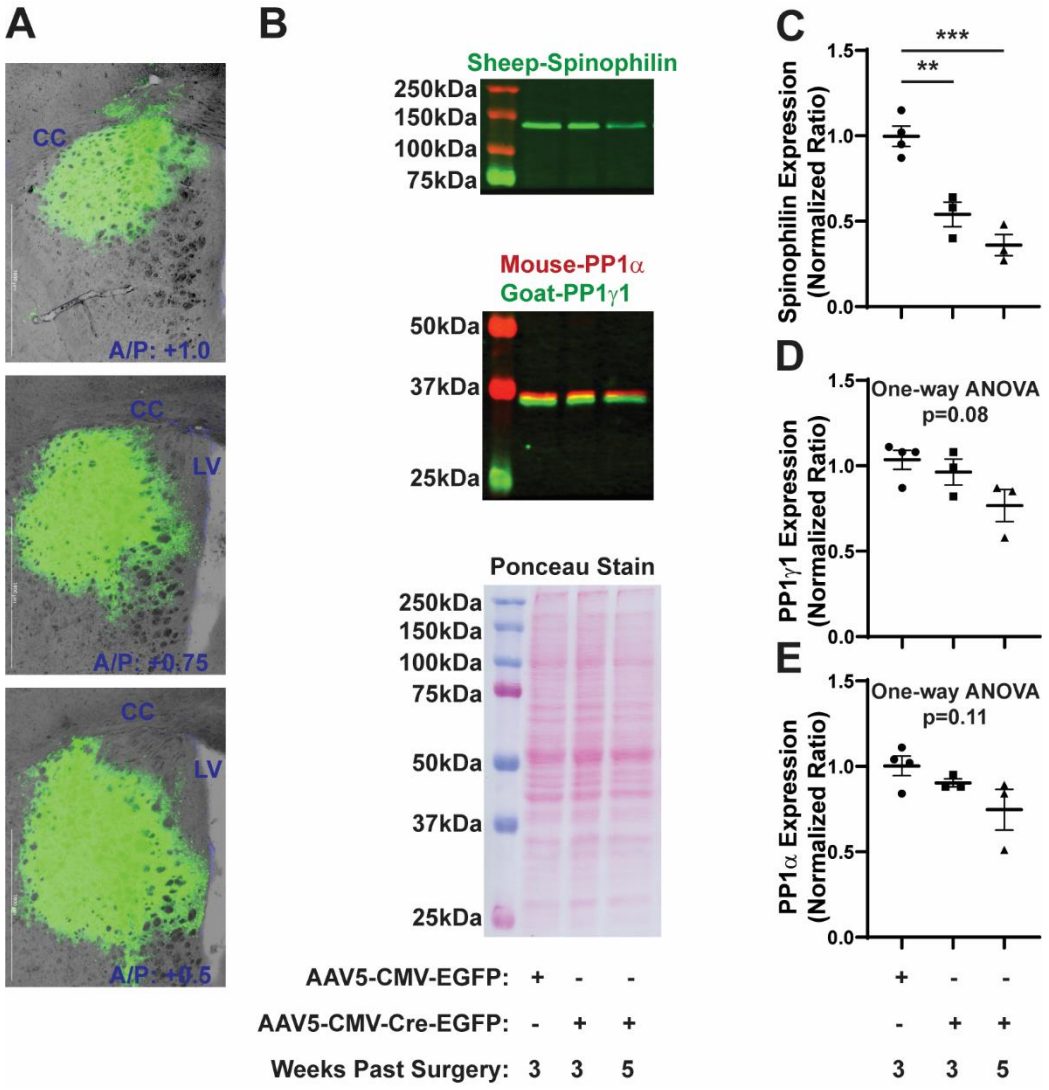
A
CC
A/P: +1.0
CC
LV
A/P: +0.75
CC
LV
A/P: +0.5
B
Sheep-Spinophilin
250kDa
150kDa
100kDa
75kDa
Mouse-PP1α
Goat-PP1γ1
50kDa
37kDa
25kDa
Ponceau Stain
250kDa
150kDa
100kDa
75kDa
50kDa
37kDa
25kDa
AAV5-CMV-EGFP: + - -
AAV5-CMV-Cre-EGFP: - + +
Weeks Past Surgery: 3 3 5
C
Spinophilin Expression (Normalized Ratio)
***
**
1.5
1.0
0.5
0.0
D
PP1γ1 Expression (Normalized Ratio)
One-way ANOVA
p=0.08
1.5
1.0
0.5
0.0
E
PP1α Expression (Normalized Ratio)
One-way ANOVA
p=0.11
1.5
1.0
0.5
0.0
+ - -
- + +
3 3 5

Figure 2: Depletion of Spinophilin Protein Expression Using AAV5-CMre-EGFP.

A) Representative images of AAV5-CMV-EGFP fluorescence in striatum demonstrating placement and spread of AAV in striatum. AAV5-CMV-EGFP or Cre-EGFP was injected into the striatum of $Spino^{Fl/Fl}$ mice. Three- or five-weeks after surgery, 1.0 mm or 1.5 mm tissue punches were collected from coronal sections containing the striatum for **B**) semi-quantitative immunoblot analysis of spinophilin, PP1γ1, and PP1α protein levels. **C**) Significant one-way ANOVA (p=0.0005) with post-hoc Tukey's multiple comparisons test determined that spinophilin protein levels were decreased at 3- (p=0.003) and 5- (p=0.0005) weeks following Cre-AAV injections into the striatum. One-way ANOVAs did not find a significant Cre-AAV effect on PP1γ1 or PP1α, however, this is likely due to being underpowered. N=4 $Spino^{Fl/Fl}$/AAV5-CMV-EGFP 3-week, N=3 $Spino^{Fl/Fl}$/AAV5-CMV-Cre-EGFP 3-week, N=3 $Spino^{Fl/Fl}$/AAV5-CMV-Cre-EGFP 5-week. Data ± SEM. Significant post-hoc tests denoted by **$p \leq 0.01$ and ***$p \leq 0.001$. Abbreviations: CC-corpus callosum, LV-lateral ventricle.

3.2.2 Spinophilin MSN Subtype-Specific Knockout Disrupts Dorsolateral Striatal Plasticity

After confirming Cre expression depletes spinophilin protein levels, we bred $Spino^{Fl/Fl}$ mice with Drd1- or Adora2a-Cre lines to deplete spinophilin from dMSNs ($Spino^{\Delta dMSN}$) or iMSNs ($Spino^{\Delta iMSN}$), respectively. Spinophilin protein expression was significantly reduced (~25%) in $spino^{\Delta dMSN}$ and $spino^{\Delta iMSN}$ mice; however, PP1 levels were unaffected (**Figure 3A-E**).

To measure spinophilin's MSN subtype-specific roles in regulating DLS network excitability and long-term plasticity we recorded field population spike amplitude responses to stimulation and LTD. Specifically, we recorded population spike amplitudes evoked from increasing electrical stimulation intensities (input/output) or high-frequency stimulations that induce LTD (HFS-LTD) in coronal sections from $Spino^{Fl/Fl}$ control, $Spino^{\Delta dMSN}$, and $Spino^{\Delta iMSN}$ mice. We detected a spinophilin genotype X intensity interaction suggesting $Spino^{\Delta dMSN}$ increases DLS network responses; however, we did not detect any post-hoc genotype differences within intensity groups (**Figure 3F**). Both $Spino^{\Delta dMSN}$ and $Spino^{\Delta iMSN}$ had significantly decreased HFS-LTD compared to $Spino^{Fl/Fl}$ control. Unlike control, the population spike amplitude did not decrease in $Spino^{\Delta dMSN}$ or $Spino^{\Delta iMSN}$ following either single or multiple bouts of high-frequency stimulation (**Figure 3G-K**). Although this study was not designed to detect sex differences in input/output curves or HFS-LTD, we visualized these datasets by sex (**Figure 4**).

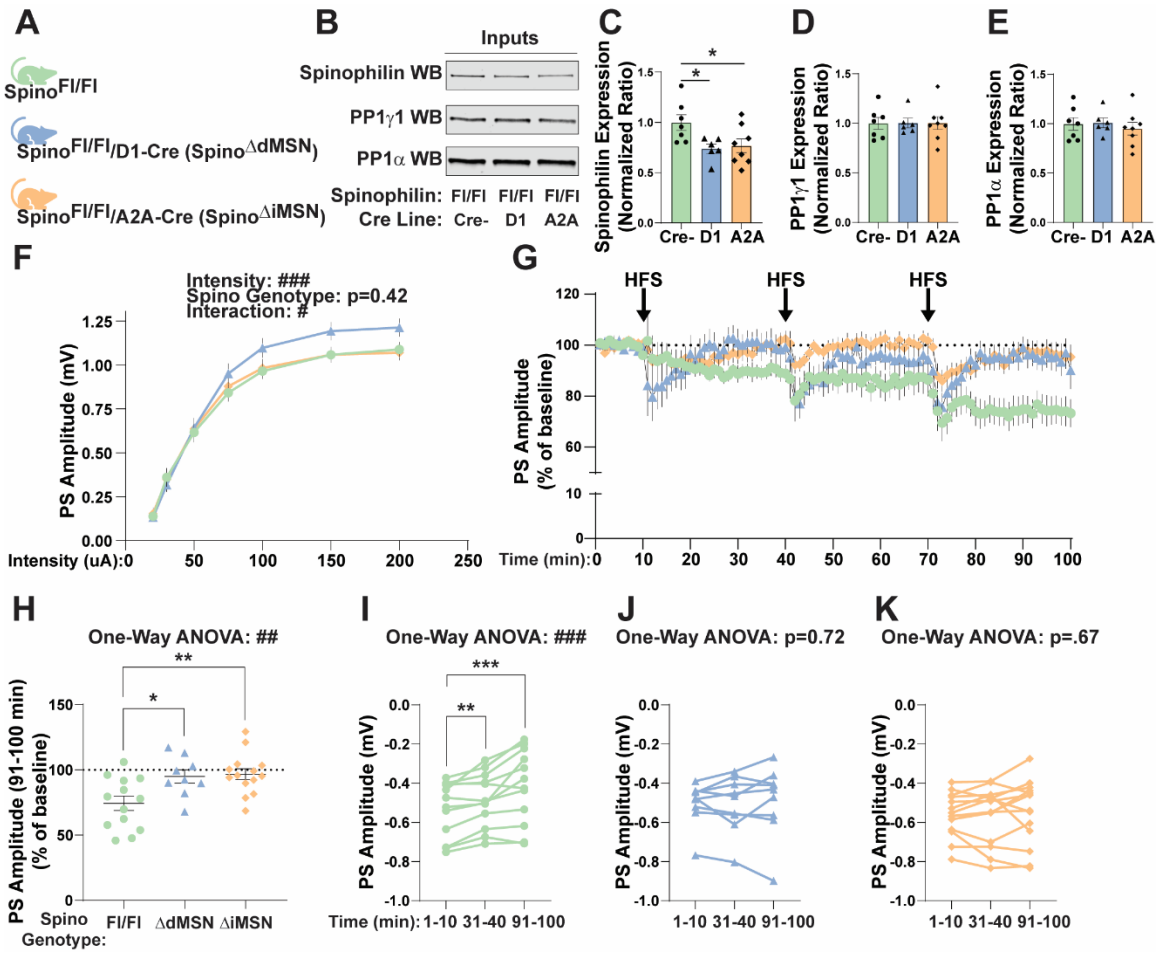
A
SpinoFl/Fl
SpinoFl/Fl/D1-Cre (SpinoΔdMSN)
SpinoFl/Fl/A2A-Cre (SpinoΔiMSN)
B
Inputs
Spinophilin WB
PP1γ1 WB
PP1α WB
Spinophilin: Fl/Fl Fl/Fl Fl/Fl
Cre Line: Cre- D1 A2A
C
Spinophilin Expression (Normalized Ratio)
Cre- D1 A2A
D
PP1γ1 Expression (Normalized Ratio)
Cre- D1 A2A
E
PP1α Expression (Normalized Ratio)
Cre- D1 A2A
F
Intensity: ###
Spino Genotype: p=0.42
Interaction: #
PS Amplitude (mV)
Intensity (uA):0 50 100 150 200 250
G
HFS
HFS
HFS
PS Amplitude (% of baseline)
Time (min):0 10 20 30 40 50 60 70 80 90 100
H
One-Way ANOVA: ##
PS Amplitude (91-100 min) (% of baseline)
Spino Genotype: Fl/Fl ΔdMSN ΔiMSN
I
One-Way ANOVA: ###
PS Amplitude (mV)
Time (min): 1-10 31-40 91-100
J
One-Way ANOVA: p=0.72
PS Amplitude (mV)
1-10 31-40 91-100
K
One-Way ANOVA: p=.67
PS Amplitude (mV)
1-10 31-40 91-100

Figure 3: MSN Subtype-Specific Spinophilin Knockout Disrupts DLS function.

A) Conditional spinophilin mice ($Spino^{Fl/Fl}$) were crossed with Cre constitutively expressed under the Drd1 (D1)- or Adora2a (A2A)- promotor to deplete spinophilin expression in dMSNs ($Spino^{\Delta dMSN}$) or iMSNs ($Spino^{\Delta iMSN}$), respectively. At 2-4 months of age, 2 mm striatal punches were taken from coronal slices isolated from male or female mice for **B)** immunoblot analysis of spinophilin and PP1 protein expression. One-way ANOVA with post hoc Dunnett's multiple comparisons test detected a significant decrease in **C)** spinophilin expression in $Spino^{\Delta dMSN}$ and $Spino^{\Delta iMSN}$ compared to control (p=0.032 and p=0.041, respectively). There was no change in **D)** PP1γ1 (p=0.99) or **E)** PP1α (p=0.75) expression. N=8 $Spino^{Fl/Fl}$ (6 male), 6 $Spino^{\Delta dMSN}$ (2 male), 7 $Spino^{\Delta iMSN}$ (4 male). Field population spike amplitudes from the DLS were measured in response to **F)** stimulation intensity increases or **G)** high-frequency stimulations that result in long-term depression (LTD). Two-way ANOVA with repeated measures detected a spinophilin genotype X stimulation intensity interaction (p=0.02); however, post-hoc Šídák's multiple comparisons test did not detect group differences at any specific intensity **(F)**. N=34 slices from 20 $Spino^{Fl/Fl}$ mice (11 male mice), 27 slices from 17 $Spino^{\Delta dMSN}$ mice (10 male mice), and 28 slices from 17 $Spino^{\Delta iMSN}$ mice (10 male mice). One-way ANOVA with post hoc Dunnett's multiple comparisons test determined that **H)** LTD is decreased in both $Spino^{\Delta dMSN}$ and $Spino^{\Delta iMSN}$ compared to control from 91-100 minutes (p=0.018 and p=0.004, respectively). One-way ANOVAs with repeated measures confirmed LTD in **I)** control at 31-40 and 91-100-minutes relative to the 1-10 minute baseline period (p=0.007 and p=0.0013, respectively), however, neither **J**) $Spino^{\Delta dMSN}$ nor **K**) $Spino^{\Delta iMSN}$ underwent LTD from 31-40 minutes (p=0.97 and p=0.99,

respectively) or 91-100 minutes (p=0.81 and p=0.75, respectively). N=13 slices from 11 $Spino^{Fl/Fl}$ mice (5 male mice), 9 slices from 7 $Spino^{\Delta dMSN}$ mice (3 male mice), and 14 slices from 10 $Spino^{\Delta iMSN}$ mice (5 male mice). Data ± SEM. Significant two- or one-way ANOVA effects denoted by #p≤0.05, ##p≤0.01, ###p≤0.001, ####p<0.0001. Significant post-hoc tests denoted by *p≤0.05, **p≤0.01, ***p≤0.001.

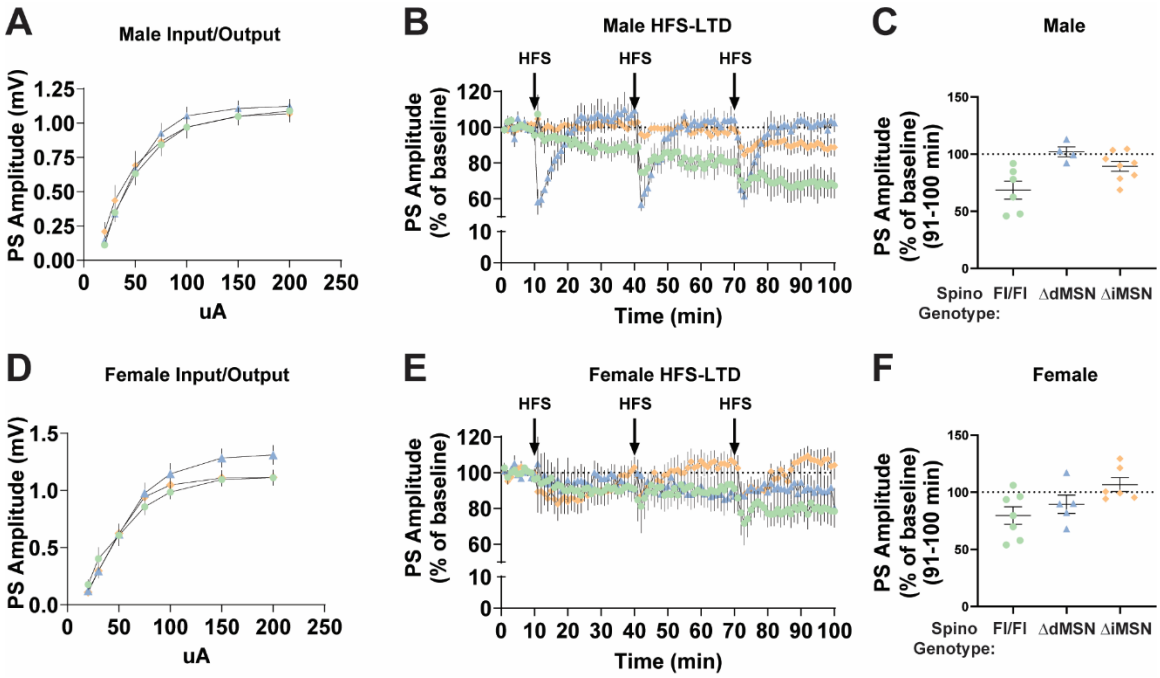
A
Male Input/Output
PS Amplitude (mV)
uA
B
Male HFS-LTD
HFS
HFS
HFS
PS Amplitude (% of baseline)
Time (min)
C
Male
PS Amplitude (% of baseline) (91-100 min)
Spino
Fl/Fl
ΔdMSN
ΔiMSN
Genotype:
D
Female Input/Output
PS Amplitude (mV)
uA
E
Female HFS-LTD
HFS
HFS
HFS
PS Amplitude (% of baseline)
Time (min)
F
Female
PS Amplitude (% of baseline) (91-100 min)
Spino
Fl/Fl
ΔdMSN
ΔiMSN
Genotype:

Figure 4: Field Electrophysiology Input/Output Curves and HFS-LTD Visualized by Sex. Male **A)** input/output curves, **B)** HFS-LTD time-course, and **C)** average population spike amplitude. Female **D)** input/output curves, **E)** HFS-LTD time-course, and **F)** average population spike amplitude from 91-100 minutes.

3.3 Discussion

3.3.1 Biochemical Validation of Conditional Spinophilin Mice

Here, we created a novel conditional spinophilin mouse and biochemically validated this line by demonstrating Cre expression significantly depletes spinophilin protein levels. First, we bred $Spino^{Fl/Fl}$ mice with CagCreER mice to express Cre globally following tamoxifen treatment. Semi-quantitative immunoblot analysis confirmed CagCreER decreased spinophilin protein levels in the striatum (~95%), hippocampus (~96%), cortex (~94%), and cerebellum (~90%), suggesting Cre expression can decrease spinophilin protein to near-knockout levels through the CNS. While the residual spinophilin protein expression (~5-10%) could be a result of not all cells containing conditional spinophilin alleles, we reason it is more likely to be due to a small proportion of cells throughout the body that either do not express CagCreER or do not respond to tamoxifen treatment.

In contrast to CagCreER, we observed a ~60% depletion of spinophilin protein by injecting AAV5-CMV-Cre-EGFP into the striatum of $Spino^{Fl/Fl}$ mice. Although small tissue punches were taken from these animals, we hypothesize this approach resulted in a less robust depletion of spinophilin protein (compared to CagCreER) due to 1) dissecting tissue outside the AAV diffusion range, and 2) less than 100% infection rate of cells within the diffusion range. Despite this, taken together with the CagCreER validation, we hypothesize that spinophilin is completely knocked out of cells that express Cre. Future studies will test this hypothesis by performing spinophilin immunohistochemistry experiments 5-weeks after AAV5-CMV-Cre-EGFP injection into the striatum.

PP1 does not exist on its own; rather it is hypothesized to always be complexed with a targeting protein (Virshup & Shenolikar 2009). Consistent with this hypothesis is the fact PP1 levels are decreased in the striatum and hippocampus following constitutive loss of spinophilin—a major PP1 targeting protein in dendritic spines (Allen et al 1997, Allen et al 2006, Salek et al 2019). Given these reports, we hypothesized that PP1 levels would also decrease after depleting spinophilin with CagCreER or Cre-AAV expression. Interestingly, we detected ~20% decrease in PP1 levels in the hippocampus of $Spino^{Fl/Fl}$/CagCreER mice 4-weeks following tamoxifen treatment, but no change in PP1 levels in striatum, cortex, or cerebellum. Although we detect both PP1γ1 and PP1α in striatum, hippocampus, and cortex, we detected minimal PP1α expression in cerebellum (data not shown)—a finding consistent with in-situ hybridization data reported in the Allen Brain Atlas.

In contrast to our CagCreER validation on conditional spinophilin mice, we detected nearly a 40% reduction in PP1 levels 5-weeks following Cre-AAV injection, however, this effect was not significant likely due to the low number of samples within this study (N=3). One possible explanation for this discrepancy in compensatory changes in striatal PP1 expression (CagCreER vs. Cre-AAV) is the different time-courses of the two experiments. Specifically, striatal tissue was collected 4-weeks after tamoxifen treatment and 5-weeks after Cre-AAV injections, raising the possibility that PP1 decreases in the striatum may take longer than 4-weeks. Alternatively, it is also possible that the lack of compensation in PP1 levels following spinophilin depletion is due to the tamoxifen treatment preventing a decrease in PP1 expression as we observed increases in spinophilin and PP1 expression following tamoxifen treatment of spinophilin replete

animals (Data not shown). These results are not surprising due to estrogen's known role in increasing dendritic spine density (Khan et al 2013). Therefore, given that tamoxifen is a selective estrogen receptor modulator, and that spinophilin, PP1γ1, and PP1α regulate dendritic spine density, it is likely that tamoxifen increases spinophilin and PP1 levels by increasing spine density in the striatum. With this in mind, it is possible that tamoxifen treatment may be occluding decreases in PP1 levels following depletion of spinophilin from striatum, cortex, and cerebellum.

3.3.2 Biochemical Validation of MSN Subtype-Specific Spinophilin Knockout Mice

In addition to depleting spinophilin with CagCreER and Cre-AAV, we also demonstrated that D1- and A2A-Cre expression decrease spinophilin protein levels in the striatum by ~25%, albeit this decrease was not as robust as expected. Specifically, because MSNs account for 90-95% of neurons in the striatum, and dMSNs and iMSNs are roughly equivalent in number (i.e. both subtypes make up ~45% of striatal neurons) (Gerfen & Surmeier 2011), we expected to observe closer to ~40% depletion in both D1- and A2A-Cre mouse lines crossed with $Spino^{Fl/Fl}$ mice. The fact that CagCreER decreased spinophilin protein levels by 95% makes it unlikely that the 25% reduction from D1- and A2A-Cre is due to a large proportion of cells within the striatum lacking conditional spinophilin alleles. Therefore, a more likely explanation for this finding is the fact that spinophilin mRNA and/or protein have been detected in numerous cell types throughout the CNS, including projection neurons, interneurons, presynaptic terminals, even astrocytes (to a lesser extent) (Muhammad et al 2015, Muly et al 2004). Therefore, we hypothesize that spinophilin expression in striatal interneurons, such as cholinergic or fast-spiking interneurons, astrocytes, or axons, may contain other pools of spinophilin

protein, which would not be affected by D1- or A2A-Cre given their cell type-specific expression in dMSNs and iMSNs, respectively, at least within the striatum. Future RNAScope studies will be critical for detailing the unique striatal cell types spinophilin is expressed in. Follow-up biochemical studies will be critical to determine the proportion of spinophilin protein expressed within unique striatal cell types.

Lastly, it is possible that spinophilin protein in striatal interneurons or glial cells does not account for the remaining ~50% of spinophilin in the striatum. If so, this could be due to reduced penetrance of D1- or A2A-Cre in striatal dMSNs or iMSNs, respectively, or that loss of spinophilin in one MSN subtype results in increased spinophilin expression in the other MSN subtype. Although complex, this outcome can be tested by breeding Spino$^{\Delta dMSN}$ and Spino$^{\Delta iMSN}$ mice to generate double transgenic mice, and then measuring spinophilin expression. If expression of D1- and A2A-Cre in the same conditional spinophilin mouse results only in an additive reduction of spinophilin protein levels (~50%) it is unlikely that cell non-autonomous compensation in spinophilin is accounting for the 25% reduction in spinophilin levels from D1- and A2A-Cre alone.

3.3.3 MSN Subtype-Specific Spinophilin Knockout Effects on DLS Excitability and Plasticity

Depletion of spinophilin from dMSNs with D1-Cre increased DLS network excitability, however, we did not detect any post-hoc Spino$^{\Delta dMSN}$ genotype effects overall or within an intensity group. Despite this limitation, published field electrophysiology experiments have determined that excessive grooming in two preclinical models, SAPAP3 KO and SHANK3b KO mice, is associated with decreased DLS excitability—

an effect in the opposite direction compared to Spino$^{\Delta dMSN}$ mice (Peça et al 2011, Welch et al 2007). However, to date, spinophilin's MSN subtype-specific roles in regulating excessive grooming have not been tested.

Loss of spinophilin from dMSNs or iMSNs abrogated network-wide HFS-LTD in the DLS, suggesting MSN subtype-specific loss of spinophilin can disrupt striatal adaptations associated with complex sequential motor programs. Indeed, this form of plasticity (HFS-LTD) in the DLS is suggested to underly increased performance on the accelerating rotarod—a motor skill that requires the concatenation of individual movements into a sequential motor program (Yin et al 2009). Furthermore, increased mGluR5 signaling in MSNs enhances eCB-mediated synaptic depression in the DLS of SAPAP3 KO mice (Chen et al 2011). Therefore, given that plasticity associated with eCB signaling is decreased in MSN subtype-specific spinophilin KO mice, it is possible loss of spinophilin in specific MSN subtypes may disrupt skill performance and/or excessive grooming behavior in SAPAP3 KO mice—another complex sequential motor program associated with DLS function (Kalueff et al 2016). Despite these assumptions based on the directionality of excitability and HFS-LTD in the DLS, it is critical to note that future studies will be critical to determine the mechanisms by which MSN subtype-specific loss of spinophilin disrupts network-wide DLS function.

Striatal HFS-LTD is an eCB-mediated form of plasticity that largely depends on the activity of mGluR5, D2R, and L-type VGCCs (Augustin et al 2018, Kreitzer & Malenka 2005, Wu et al 2015). Collectively, activation of these receptors in the postsynapse promotes unique second messenger systems that converge to increase eCB production, which signal retrogradely to suppress corticostriatal synaptic transmission.

Given this, it is unclear if MSN subtype-specific loss of spinophilin decreases HFS-LTD by decreasing one, multiple, or none of these signaling pathways in the postsynapse. Furthermore, it is critical to note that we cannot conclude from these data alone that MSN subtype-specific spinophilin KO is decreasing HFS-LTD by regulating signaling in the postsynapse. For example, although D1- and A2A-Cre are enriched in striatal dMSNs and iMSNs, respectively, it is possible that extra-striatal D1- and/or A2A-Cre expression depletes spinophilin from cortical neurons that send projections to the striatum. If so, loss of spinophilin in cortical neurons that synapse on MSNs, could directly or indirectly impact neurotransmitter release into the striatum, thus preventing changes in synaptic transmission. Future experiments measuring changes in paired-pulse ratio (PPR) after HFS-LTD will be helpful to determine if loss of spinophilin is decrease presynaptic neurotransmitter release (Ding et al 2008). For example, presynaptic neurotransmitter release probability decreases (PPR increases) following HFS-LTD due to increased retrograde eCB signaling. Therefore, if spinophilin decreases HFS-LTD by decreasing eCB production (via regulating postsynaptic receptors) we would expect no change in PPR following HFS-LTD in MSN subtype-specific spinophilin KO. Alternatively, if PPR is increased in MSN subtype-specific KO mice it is possible loss of spinophilin decreases HFS-LTD via a presynaptic mechanism. In addition to these experiments, coupling pharmacology with HFS-LTD in MSN subtype-specific KOs will also be critical for detailing mechanisms by which spinophilin expression in MSNs mediates plasticity. Inducing LTD in MSN subtype-specific spinophilin KO mice via bath application of a CB1R agonist would demonstrate these genotypes have intact presynaptic machinery required for LTD, further suggesting a postsynaptic mechanism.

Here, we identified spinophilin-dependent changes in field DLS excitability and plasticity following stimulation of the corpus callosum, suggesting spinophilin mediates activity-dependent changes in DLS function. However, future whole-cell electrophysiology experiments measuring MSN properties and changes in basal neurotransmitter release will be needed to confirm spinophilin only mediates changes in striatal function associated with activity (stimulation). Furthermore, although identifying network-wide changes in DLS function following MSN subtype-specific spinophilin knockout is impactful, another limitation of these experiments is the inability to determine if these outcomes are due to cell autonomous or non-autonomous effects. To delineate if cell autonomous loss of spinophilin recapitulates the field electrophysiology results reported herein, future studies will need to measure input/output curves and HFS-LTD using whole-cell electrophysiology recording from dMSNs in Spino$^{\Delta dMSN}$ or iMSNs Spino$^{\Delta iMSN}$ mice.

In summary, we demonstrated that Cre expression decreases spinophilin protein levels in our novel conditional spinophilin mouse line. Furthermore, by breeding our conditional spinophilin line with D1- and A2A-Cre we created MSN subtype-specific spinophilin KO mice. Lastly, we determined that MSN subtype-specific loss of spinophilin disrupts network-wide DLS function. Given that MSN subtype-specific adaptions in the DLS are associated with repetitive motor outputs, future studies will directly probe the extent to which spinophilin expression in striatal dMSNs or iMSNs impacts repetitive motor outputs, such as excessive grooming in SAPAP3 KO mice.

Figure	Panel	Dependent Variable	Statistical Analysis	Statistic (t, F, r), Degrees of freedom (df)	P-Value
1	**E**	Striatum: Spinophilin Expression	Unpaired t-test	t=13.31, df=6	p<0.0001
	F	Striatum: PP1γ1 Expression	Unpaired t-test	t=0.02504, df=6	p=0.98
	G	Striatum: PP1α Expression	Unpaired t-test	t=1.025, df=6	p=0.34
	I	Hippocampus: Spinophilin Expression	Unpaired t-test	t=19.56, df=6	p<0.0001
	J	Hippocampus: PP1γ1 Expression	Unpaired t-test	t=4.254, df=6	p=0.005
	K	Hippocampus: PP1α Expression	Unpaired t-test	t=3.127, df=6	p=0.02
	M	Cortex: Spinophilin Expression	Unpaired t-test	t=33.71, df=6	p<0.0001
	N	Cortex: PP1γ1 Expression	Unpaired t-test	t=0.3117, df=6	p=0.76
	O	Cortex: PP1α Expression	Unpaired t-test	t=0.7642, df=6	p=0.47
	Q	Cerebellum: Spinophilin Expression	Unpaired t-test	t=31.69, df=6	p<0.0001
	R	Cerebellum: PP1α Expression	Unpaired t-test	t=0.9518, df=6	p=0.37
2	**C**	Striatum: Spinophilin Expression	One-way ANOVA	F (2, 7) = 27.75	p=0.0005
	D	Striatum: PP1γ1 Expression	One-way ANOVA	F (2, 7) = 3.589	p=0.08
	E	Striatum: PP1α Expression	One-way ANOVA	F (2, 7) = 3.069	p=0.11
3	**C**	Striatum: Spinophilin Expression	One-way ANOVA	F (2, 18) = 4.372	p=0.02
	D	Striatum: PP1γ1 Expression	One-way ANOVA	F (2, 18) = 0.001	p=0.99
	E	Striatum: PP1α Expression	One-way ANOVA	F (2, 18) = 0.282	p=0.75

3	**F**	Input/Output Curve	Repeated Measures Two-way ANOVA	Intensity: F (2.106, 181.1) = 491.8	p<0.0001
				Genotype: F (2, 86) = 0.8563	p=0.42
				Interaction: F (12, 516) = 1.997	p=0.022
	H	HFS-LTD (91-100 min)	One-way ANOVA	F (2, 33) = 6.604	p=0.0039
	I	Control HFS-LTD	Repeated Measures One-way ANOVA	F (1.433, 15.76) = 15.81	p=0.0004
	J	Spino$^{\Delta dMSN}$ HFS-LTD	Repeated Measures One-way ANOVA	F (1.918, 15.34) = 0.3100	p=0.72
	K	Spino$^{\Delta dMSN}$ HFS-LTD	Repeated Measures One-way ANOVA	F (1.672, 21.74) = 0.3366	p=0.67

Table 2: Chapter 3 Statistics.

Statistical analysis corresponding to Figures 1-3 are reported in the table above.

Chapter Four: MSN Subtype-Specific Spinophilin Knockout Decreases Excessive Grooming in SAPAP3 Knockout Mice

4.1 Introduction

The sensorimotor striatum, a major basal ganglia input nucleus, integrates excitatory and modulatory inputs from diverse cortical and subcortical structures to promote the learning and execution of complex tasks (Graybiel 2008, Jahanshahi et al 2015b). Perturbations within the sensorimotor striatum, or the rodent dorsolateral striatum (DLS), are associated with repetitive motor dysfunction in numerous psychiatric disorders, including OCSDs (Abbott et al 2018, Anticevic et al 2014, Atmaca et al 2007, Beucke et al 2013, Di Martino et al 2011, Grossberg & Kishnan 2018, Harrison et al 2013, O'Sullivan et al 1997, Pujol et al 2004a, Sakai et al 2011). Cell type-specific adaptations in striatal dMSNs and iMSNs within the DLS underlie repetitive and habitual actions (Ade et al 2016, O'Hare et al 2016, Rothwell et al 2014, Rothwell et al 2015, Sheng et al 2019, Wang et al 2017, Wang et al 2016). Functionally, dMSNs, which express D1-type dopamine receptors, promote action execution by increasing thalamic neuronal firing rates, which in turn increase glutamatergic tone in the cortex; whereas, iMSNs, which express D2-type dopamine receptors, inhibit or temper competing motor programs by promoting the inhibition of thalamic output to the cortex, thus decreasing glutamatergic drive (Corbit et al 2003, Cui et al 2013, Gerfen et al 1990, Gerfen & Surmeier 2011, Tecuapetla et al 2014, Trusel et al 2015). Despite bidirectional actions on basal ganglia output, dMSNs and iMSNs work in concert to integrate glutamatergic and dopaminergic signaling to promote complex motor programs, and signaling molecule perturbations within MSNs can increase the propensity to repetitively execute previously

learned motor sequences, a core motor phenotype associated with OCSDs (Barnes et al 2005, Francesconi & Duvoisin 2000, Gillan et al 2014a, Gillan et al 2014b, Graybiel 2008, Greengard 2001, Jin & Costa 2010, Jin et al 2014, Jog et al 1999, Martiros et al 2018, Uematsu et al 2015, Voulalas et al 2005).

Dysfunction in mGluR5 signaling and/or its interaction with postsynaptic density (PSD) scaffolding proteins is associated with repetitive motor dysfunction in numerous preclinical models for understanding psychiatric disorders (D'Antoni et al 2014, Matosin et al 2017, Mehta et al 2011, Pop et al 2014, Ronesi et al 2012, Stewart et al 2013, Wang et al 2016). Of these, mutations in the striatal-enriched mGluR5 scaffold protein, SAPAP3, are associated with repetitive grooming and washing symptoms in OCSDs (Bienvenu et al 2009, Naaz et al 2020, Zuchner et al 2009). Genetic deletion of SAPAP3 in rodents results in striatal circuit abnormalities and increased mGluR5 function that promotes excessive grooming (Ade et al 2016, Chen et al 2011, Corbit et al 2019, Hadjas et al 2019, Hadjas et al 2020, Wan et al 2014, Wan et al 2011, Welch et al 2007), a complex sequential motor program that becomes excessively initiated and sustained despite negative consequences (Kalueff et al 2016).

Reversible phosphorylation of mGluR5's intracellular C-terminal domain is a negative feedback mechanism that promotes receptor desensitization (Alagarsamy et al 2001, Gereau & Heinemann 1998, Ko et al 2012). Protein phosphatases, such as protein phosphatase 1 (PP1), can reverse this endocytic feedback mechanism to stabilize mGluR5 on the membrane surface (Kliewer et al 2017). Promiscuous phosphatases require

targeting proteins to shuttle them into contact with their targets (Cohen 2002). However, the role(s) phosphatase targeting proteins play in promoting increased mGluR5 function to mediate repetitive motor dysfunction are unknown.

Spinophilin is a striatal PSD signaling hub molecule that targets PP1 to diverse substrates (Allen et al 1997, Baucum et al 2010, Colbran et al 1997, Ragusa et al 2010, Sarrouilhe et al 2006, Watkins et al 2018). Spinophilin promotes plasticity and motor behaviors associated with DLS function, stabilizes mGluR5 expression in the neuronal membrane, and prevents G-protein coupled receptor (GPCR) desensitization (Allen et al 2006, Areal et al 2019, Di Sebastiano et al 2016, Edler et al 2018, Fujii et al 2008, Kurogi et al 2009, Morris et al 2018, Wang et al 2004, Wang et al 2007, Wang et al 2005). Recently, we determined that spinophilin interacts with SAPAP3 in mouse striatum, and overexpression of a glutamate binding deficient mGluR5 construct increased the spinophilin-SAPAP3 protein interaction (Morris et al 2018). However, the extent to which spinophilin functions in specific MSN subtypes to mediate SAPAP3-dependent repetitive motor output is unknown. Here, we bred our MSN subtype-specific spinophilin knockout mice (see chapter 3) with SAPAP3 deficient mice to elucidate spinophilin's MSN subtype-specific contributions to excessive grooming in SAPAP3 KO mice. Not only did we determine that MSN subtype-specific spinophilin KO decreases excessive grooming in SAPAP3 KO mice, but we further identify a positive correlation between grooming duration and spinophilin's protein interactions with mGluR5. Collectively, these data suggest spinophilin may mediate excessive grooming in SAPAP3 KO mice by regulating mGluR5 function in MSNs.

4.2 Results

4.2.1 Spinophilin dMSN- and iMSN-Knockout Decrease Excessive Grooming in SAPAP3 Deficient Mice.

Excessive grooming in SAPAP3 KO mice is associated with increased mGluR5 signaling and plasticity in the DLS (Ade et al 2016, Chen et al 2011). Given that spinophilin interacts with SAPAP3 in mouse striatum, mGluR5 expression increases the spinophilin-SAPAP3 protein interaction, and MSN subtype-specific spinophilin knockout decreases DLS plasticity, we generated double knockout mice (SAPAP3 WT and KO/spinophilin MSN subtype-specific KO) to determine if spinophilin in specific MSN subtypes impacts grooming dysfunction. At 8-weeks of age, grooming and locomotion was measured in Noldus Phenotyper cages for 1-hour using a validated artificial intelligence approach (**Figure 5A-C**). Constitutive knockout of SAPAP3 significantly increased grooming duration (percent grooming) in spinophilin replete and Spino$^{\Delta dMSN}$ mice compared to their genotype controls, whereas the increased grooming was abrogated in Spino$^{\Delta iMSN}$ mice compared to their genotype controls. However, percent grooming was significantly decreased in both SAPAP3 KO/Spino$^{\Delta dMSN}$ and SAPAP3 KO/Spino$^{\Delta iMSN}$ mice compared to SAPAP3 KO/spinophilin replete mice (**Figure 5D**). This was a spinophilin-specific effect as D1- or A2A-Cre expression alone does not decrease excessive grooming in SAPAP3 KO mice (**Figure 6**).

Grooming duration can be broken into the number of grooming bouts and the mean duration of each grooming bout. We detected SAPAP3 genotype and spinophilin genotype effects on both grooming frequency and mean grooming bout duration, such that grooming frequency was significantly reduced only in SAPAP3 KO/Spino$^{\Delta iMSN}$ and

mean bout duration was significantly reduced in both SAPAP3 KO/Spino$^{\Delta dMSN}$ and SAPAP3 KO/Spino$^{\Delta iMSN}$ mice (**Figure 5E-F**), suggesting Spino$^{\Delta dMSN}$ and Spino$^{\Delta iMSN}$ mice may decrease SAPAP3 KO grooming via unique mechanisms.

In addition to grooming dysfunction, we also detected SAPAP3 genotype effects causing hypolocomotion in control, Spino$^{\Delta dMSN}$, and Spino$^{\Delta iMSN}$ mice. SAPAP3 KO/Spino$^{\Delta iMSN}$ mice had small, but significantly increased locomotion compared to SAPAP3 KO control mice (**Figure 5G-H**). Given that grooming and locomotion are competing behaviors in the OF, we correlated distance traveled and grooming duration for each genotype, but we only detected a significant negative correlation in SAPAP3 WT and SAPAP3 KO/Spino$^{\Delta iMSN}$ mice (**Figure 5I**). Grooming and locomotion data were also analyzed in 30-minute bins to confirm genotype differences are consistent between the first and second halves of recording (**Figure 7**).

Although this experiment was not designed to detect sex differences in grooming and locomotor behavior, we visualized these datasets by sex (**Figure 8**). Importantly, we detected decreased percent grooming in male and female Spino$^{\Delta dMSN}$ and Spino$^{\Delta iMSN}$ mice. However, we noticed that excessive grooming in male SAPAP3 KO mice was associated with increased grooming frequency, whereas excessive grooming in female SAPAP3 KO mice was associated with increased mean grooming bout duration. Importantly, both Spino$^{\Delta dMSN}$ and Spino$^{\Delta iMSN}$ mice decreased both of these sex-specific increases in SAPAP3 KO excessive grooming.

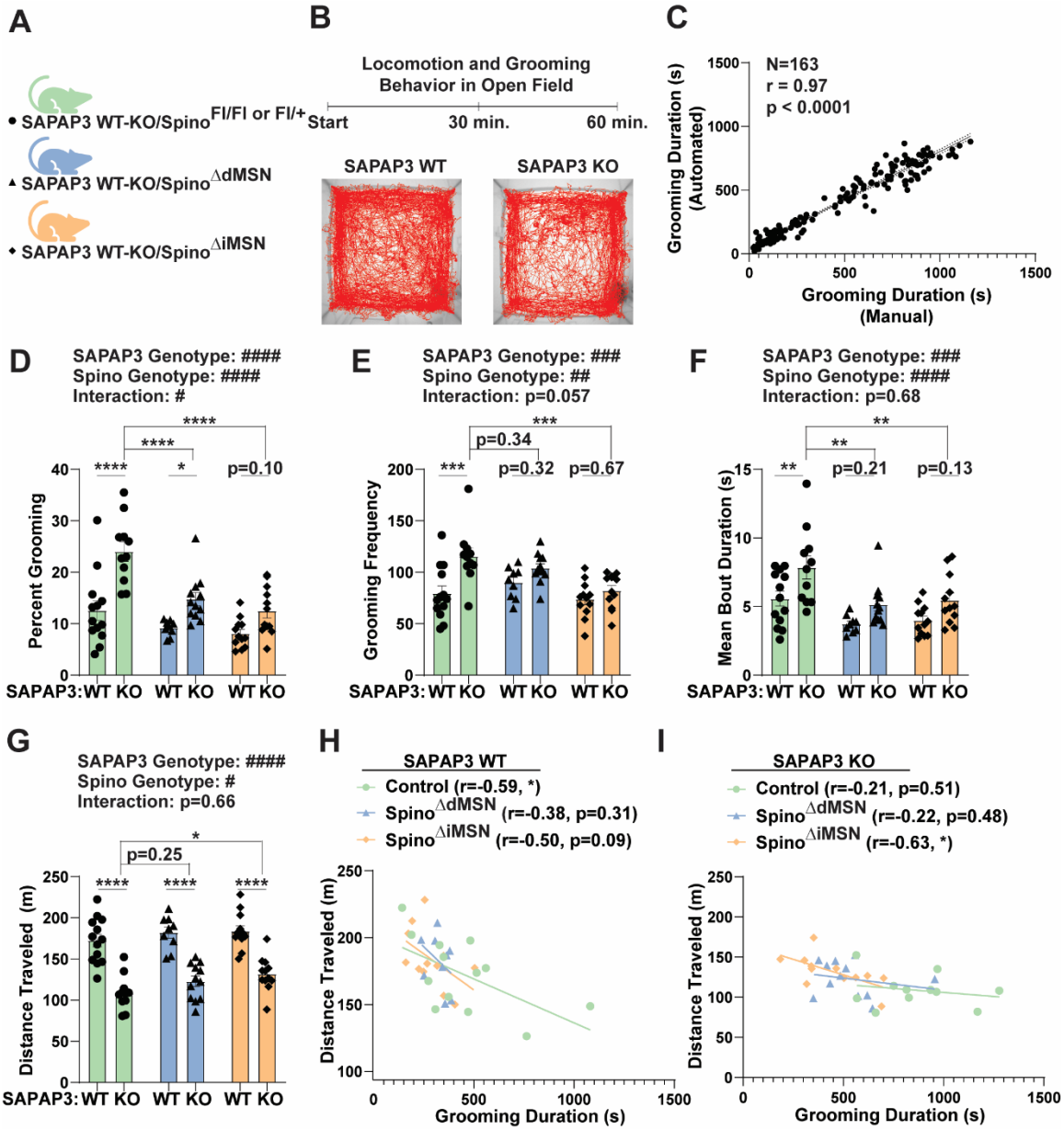
A
SAPAP3 WT-KO/Spino Fl/Fl or Fl/+
SAPAP3 WT-KO/Spino ΔdMSN
SAPAP3 WT-KO/Spino ΔiMSN
B
Locomotion and Grooming Behavior in Open Field
Start
30 min.
60 min.
SAPAP3 WT
SAPAP3 KO
C
N=163
r = 0.97
p < 0.0001
Grooming Duration (s) (Automated)
Grooming Duration (s) (Manual)
D
SAPAP3 Genotype: ####
Spino Genotype: ####
Interaction: #
Percent Grooming
p=0.10
SAPAP3: WT KO WT KO WT KO
E
SAPAP3 Genotype: ###
Spino Genotype: ##
Interaction: p=0.057
Grooming Frequency
p=0.34
p=0.32
p=0.67
SAPAP3: WT KO WT KO WT KO
F
SAPAP3 Genotype: ###
Spino Genotype: ####
Interaction: p=0.68
Mean Bout Duration (s)
p=0.21
p=0.13
SAPAP3: WT KO WT KO WT KO
G
SAPAP3 Genotype: ####
Spino Genotype: #
Interaction: p=0.66
Distance Traveled (m)
p=0.25
SAPAP3: WT KO WT KO WT KO
H
SAPAP3 WT
Control (r=-0.59, *)
Spino ΔdMSN (r=-0.38, p=0.31)
Spino ΔiMSN (r=-0.50, p=0.09)
Distance Traveled (m)
Grooming Duration (s)
I
SAPAP3 KO
Control (r=-0.21, p=0.51)
Spino ΔdMSN (r=-0.22, p=0.48)
Spino ΔiMSN (r=-0.63, *)
Distance Traveled (m)
Grooming Duration (s)

Figure 5: MSN Subtype-Specific Spinophilin Knockout Decreases Excessive Grooming in SAPAP3 Deficient Mice.

A) Eight-week old, double knockout mice (SAPAP3 WT and KO/spinophilin MSN subtype-specific KO) were **B)** placed in open field (OF) Noldus Phenotyper Cages for 60 minutes to measure locomotion and grooming behavior. **C)** Grooming behavior was scored using Noldus' behavior recognition (NBR) algorithm, which was validated by a Pearson's correlation analysis comparing grooming duration scored manually versus the NBR algorithm (N=163 30-minute OF recordings, r=0.97, p<0.0001). Two-way ANOVAs with post-hoc Šídák's multiple comparisons tests determined: **D)** Percent grooming was significantly decreased in SAPAP3 KO/Spino$^{\Delta dMSN}$ (p<0.0001) and SAPAP3 KO/Spino$^{\Delta iMSN}$ mice (p<0.0001) compared to SAPAP3 KO control, and a significant SAPAP3 genotype effect was detected in control (p<0.0001) and Spino$^{\Delta dMSN}$ (0.039) but not Spino$^{\Delta iMSN}$ mice (p=0.10). **E)** Grooming frequency was significantly decreased in SAPAP3 KO/Spino$^{\Delta iMSN}$ mice compared to SAPAP3 KO control mice (p=0.0005). SAPAP3 KO/Spino$^{\Delta dMSN}$ did not affect grooming frequency relative to SAPAP3 KO controls (p=0.34). A significant SAPAP3 genotype effect was detected in control (p=0.0002), but not Spino$^{\Delta dMSN}$ (p=0.32) or Spino$^{\Delta iMSN}$ mice (p=0.67). **F)** Mean grooming bout duration was significantly decreased in SAPAP3 KO/Spino$^{\Delta dMSN}$ (p=0.0014) and SAPAP3 KO/Spino$^{\Delta iMSN}$ mice (p<0.004) compared to SAPAP3 KO control mice. A significant SAPAP3 genotype effect was detected in control (p=0.007), but not Spino$^{\Delta dMSN}$ (p=0.21) or Spino$^{\Delta iMSN}$ mice (p=0.13). **G)** Significant SAPAP3 genotype effects on distance traveled were detected in control (p<0.0001), Spino$^{\Delta dMSN}$ (p<0.0001), and Spino$^{\Delta iMSN}$ mice (p<0.0001). Distance traveled was significantly

increased in SAPAP3 KO/Spino$^{\Delta iMSN}$ compared to SAPAP3 KO control mice (p=0.032), but SAPAP3 KO/Spino$^{\Delta dMSN}$ was not different than SAPAP3 KO control mice (p=0.25). Grooming duration and distance traveled from **H)** SAPAP3 WT and **I)** SAPAP3 KO groups were correlated to determine that grooming behavior negatively correlates with locomotion in SAPAP3 WT control and SAPAP3 KO/Spino$^{\Delta iMSN}$. N=11-13 SAPAP3 WT-KO/Spino$^{Fl/Fl\ or\ Fl/+}$ (7-5 male), N=9-12 SAPAP3 WT-KO/Spino$^{\Delta dMSN}$ (4-6 male), and N=12-12 SAPAP3 WT-KO/Spino$^{\Delta iMSN}$ (4-6 male). Data ± SEM. Significant two-ANOVA effects denoted by #p≤0.05, ##p≤0.01, ###p≤0.001, ####p<0.0001. Significant post-hoc tests denoted by *p≤0.05, **p≤0.01, ***p≤0.001, ****p<0.0001.

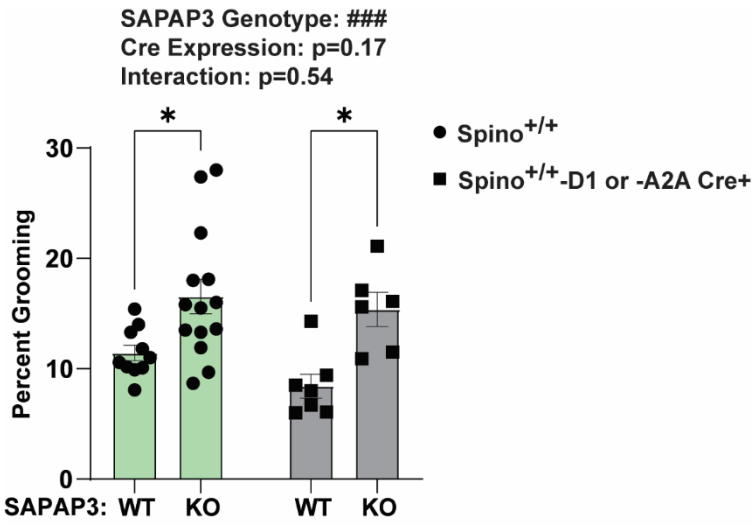
SAPAP3 Genotype: ###
Cre Expression: p=0.17
Interaction: p=0.54
*
*
Spino+/+
Spino+/+-D1 or -A2A Cre+
Percent Grooming
30
20
10
0
SAPAP3: WT KO WT KO

Figure 6: D1- and A2A-Cre Expression Do Not Decrease Excessive Grooming in SAPAP3 Deficient Mice.

Percent grooming behavior of SAPAP3 WT and KO mice expressing wild type spinophilin ($Spino^{+/+}$) and D1- or A2A-Cre and SAPAP3 WT and KO mice Cre- mice was measured for 1-hour at 8-weeks of age. Two-way ANOVA with a post-hoc Šídák's multiple comparisons test detected a significant SAPAP3 genotype effect in Cre- ($p=0.014$) and D1- or A2A Cre+ ($p=0.013$) mice. N=10 SAPAP3 WT (6 male), 14 SAPAP3 KO (5 male), 7 SAPAP3 WT/D1- or A2A-Cre (4 male), 6 SAPAP3 KO/D1- and A2A-Cre (4 male). Data ± SEM. Significant two-ANOVA effects denoted by ###$p\leq0.001$. Significant post-hoc tests denoted by *$p\leq0.05$.

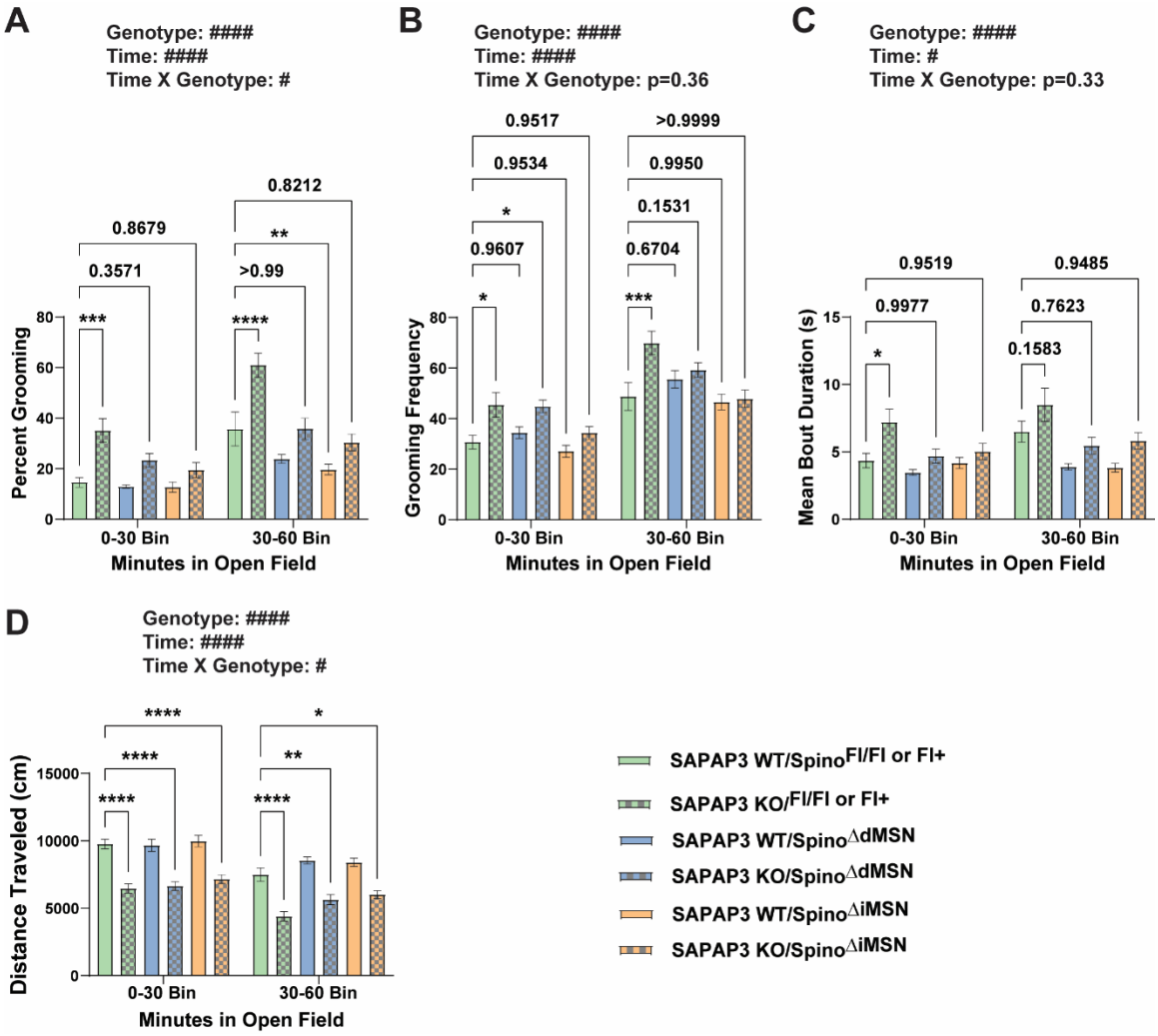
A
Genotype: ####
Time: ####
Time X Genotype: #
Percent Grooming
0.8679
0.3571
0.8212
**
>0.99
***
****
0-30 Bin
30-60 Bin
Minutes in Open Field
B
Genotype: ####
Time: ####
Time X Genotype: p=0.36
Grooming Frequency
0.9517
>0.9999
0.9534
0.9950
*
0.1531
0.9607
0.6704
*
***
0-30 Bin
30-60 Bin
Minutes in Open Field
C
Genotype: ####
Time: #
Time X Genotype: p=0.33
Mean Bout Duration (s)
0.9519
0.9485
0.9977
0.7623
*
0.1583
0-30 Bin
30-60 Bin
Minutes in Open Field
D
Genotype: ####
Time: ####
Time X Genotype: #
Distance Traveled (cm)
****
*
****
**
****
****
0-30 Bin
30-60 Bin
Minutes in Open Field
SAPAP3 WT/Spino^Fl/Fl or Fl+
SAPAP3 KO/^Fl/Fl or Fl+
SAPAP3 WT/Spino^ΔdMSN
SAPAP3 KO/Spino^ΔdMSN
SAPAP3 WT/Spino^ΔiMSN
SAPAP3 KO/Spino^ΔiMSN

Figure 7: MSN Subtype-Specific Spinophilin Knockout Effects on SAPAP3 Knockout Motor Dysfunction Broken into 30-Minute Bins.

The 60-minute open field behavior measurement of SAPAP3 WT and KO/MSN-specific spinophilin knockout was halved into 30-minute bins. Two-way ANOVAs with repeated measures were performed to determine the effect time and genotype have on **A)** percent grooming, **B)** grooming frequency, **C)** mean grooming bout duration, and **D)** distance traveled. N=11-13 SAPAP3 WT-KO/Spino$^{Fl/Fl\ or\ Fl/+}$ (7-5 male), N=9-12 SAPAP3 WT-KO/Spino$^{\Delta dMSN}$ (4-6 male), and N=12-12 SAPAP3 WT-KO/Spino$^{\Delta iMSN}$ (4-6 male). Data ± SEM. Significant two-ANOVA effects denoted by #$p \leq 0.05$ and ####$p < 0.0001$. Significant post-hoc tests denoted by *$p \leq 0.05$, **$p \leq 0.01$, ***$p \leq 0.001$, ****$p < 0.0001$.

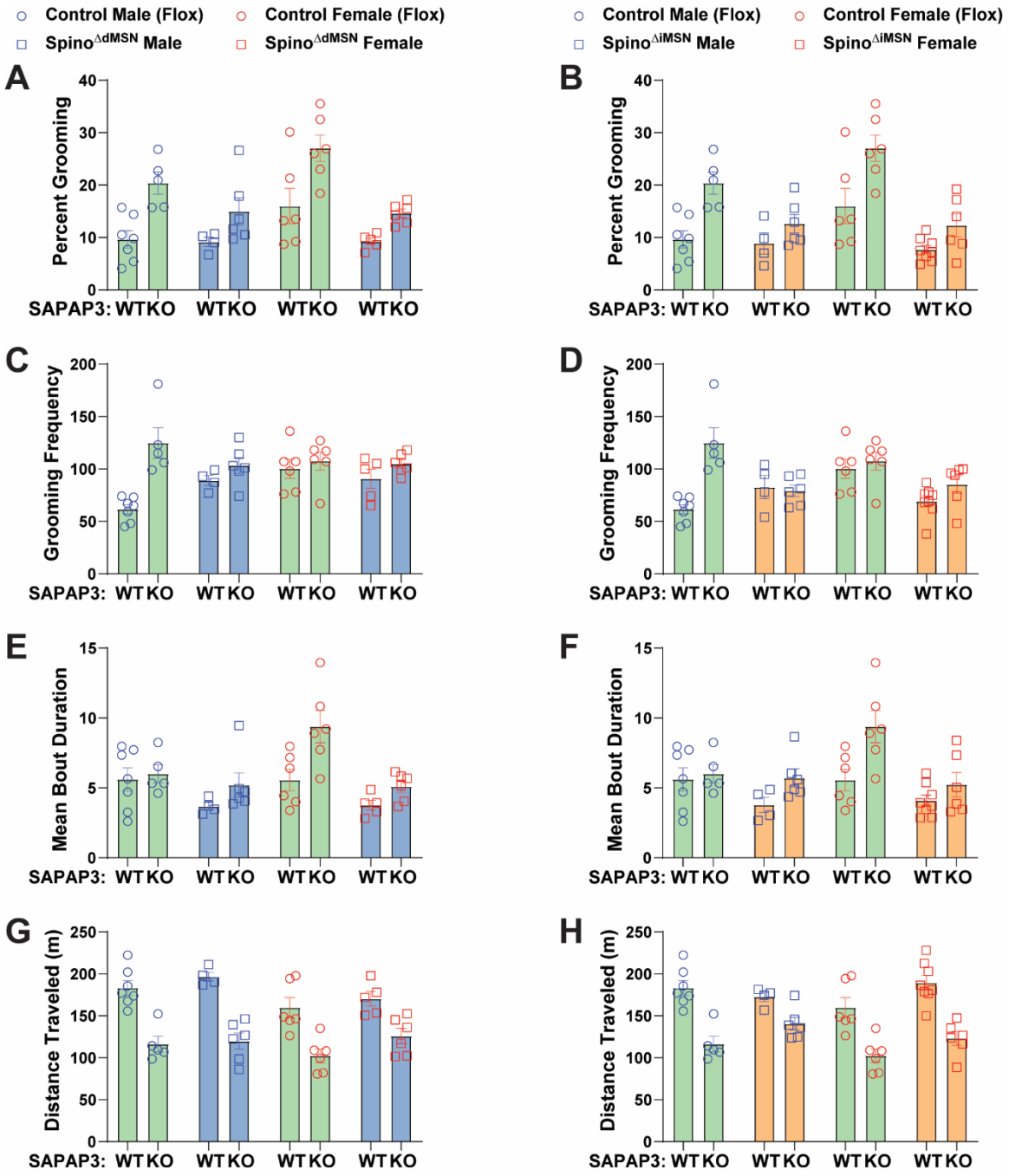
Control Male (Flox)
Control Female (Flox)
Spino$^{\Delta dMSN}$ Male
Spino$^{\Delta dMSN}$ Female
Spino$^{\Delta iMSN}$ Male
Spino$^{\Delta iMSN}$ Female
A
B
C
D
E
F
G
H
Percent Grooming
Grooming Frequency
Mean Bout Duration
Distance Traveled (m)
SAPAP3: WT KO WT KO WT KO WT KO

Figure 8: SAPAP3 Wild-type and Knockout Open Field Behavior Visualized by Sex. Male (blue points) and female (red points) SAPAP3 WT-KO/Spino$^{Fl/Fl\ or\ Fl/+}$ (green bars), SAPAP3 WT-KO/Spino$^{\Delta dMSN}$ (blue bars), and SAPAP3 WT-KO/Spino$^{\Delta iMSN}$ (orange bars) were plotted separately for **A-B.** percent grooming, **C-D.** grooming frequency, **E-F.** mean bout duration, **G-H.** distance traveled. Data ± SEM. N=4-8.

4.2.2 The Interaction of Spinophilin with mGluR5 is Increased in SAPAP3 Knockout Striatum and Correlates with Grooming Duration.

Given that increased striatal mGluR5 signaling is associated with grooming dysfunction in SAPAP3 KO mice we measured spinophilin's interaction with mGluR5 in SAPAP3 KO striatum. In addition, we measured spinophilin's interaction with the D_2R (Smith et al 1999)—another striatal GPCR known to decrease rodent grooming (Berridge & Aldridge 2000a). We harvested striata from 4-6 month-old SAPAP3 WT and KO mice following measurement of grooming behavior and measured the expression and interaction of spinophilin with these GPCRs as well as PP1γ1 (**Figure 9A-B**). Quantitative immunoblot analysis of striatal input samples determined that SAPAP3 KO did not affect spinophilin, mGluR5, or D_2R expression; however, PP1γ1 expression was significantly increased in SAPAP3 KO mice (**Figure 9C-F**). Although we found no change in spinophilin's interaction with PP1γ1, there was significantly more mGluR5 and D_2R in spinophilin IPs from SAPAP3 KO striatum (**Figure 9G-I**). We did not detect any PP1γ1, mGluR5, or D_2R co-IP in spinophilin IPs from Spino$^{-/-}$ striatal tissue (**Figure 9A**, lane 3), indicating co-IPs are specific. Moreover, we detected a significant Pearson's correlation between percent grooming and the $\log_2$ fold-change in the spinophilin-mGluR5 or spinophilin-D_2R interaction (**Figure 9J-K**) as well as a significant correlation between the spinophilin-mGluR5 and spinophilin-D_2R interaction (**Figure 9L**).

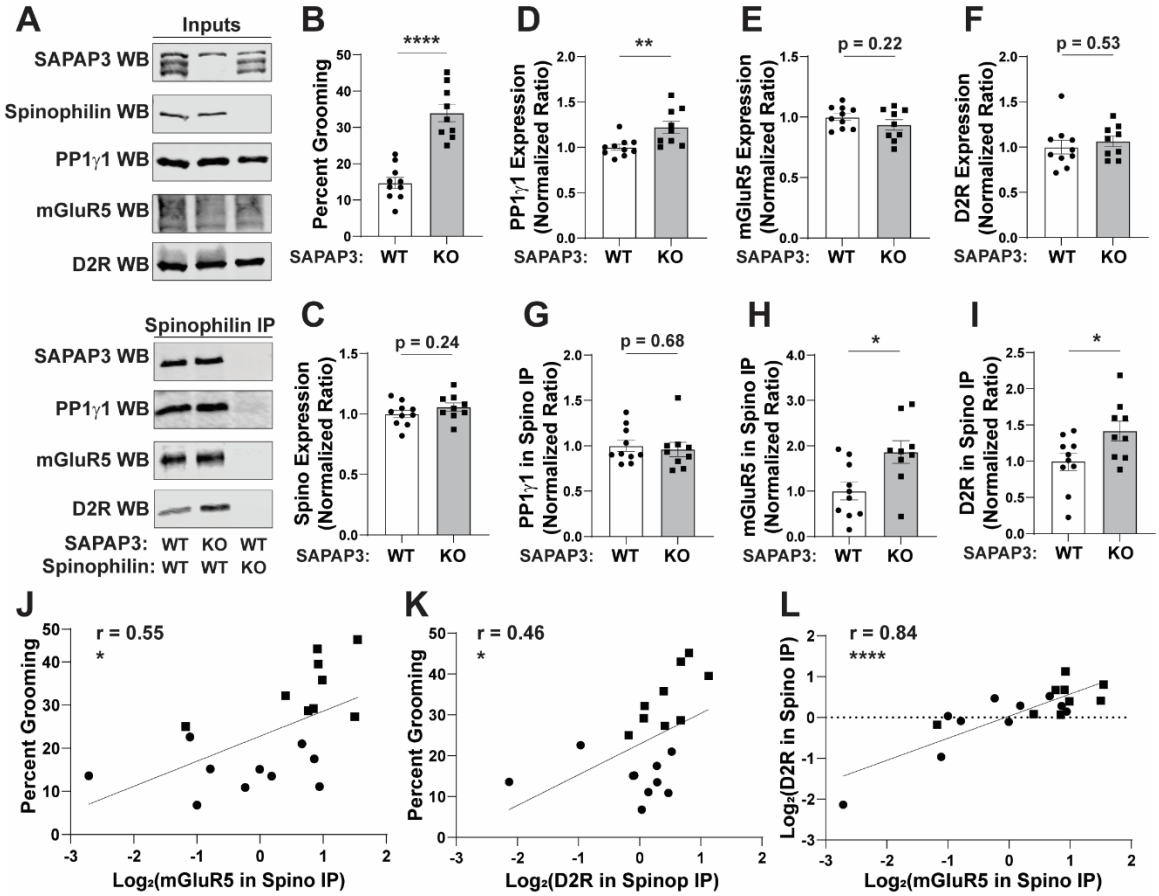
A
Inputs
SAPAP3 WB
Spinophilin WB
PP1γ1 WB
mGluR5 WB
D2R WB
Spinophilin IP
SAPAP3 WB
PP1γ1 WB
mGluR5 WB
D2R WB
SAPAP3: WT KO WT
Spinophilin: WT WT KO
B
****
Percent Grooming
SAPAP3: WT KO
C
p = 0.24
Spino Expression (Normalized Ratio)
SAPAP3: WT KO
D
**
PP1γ1 Expression (Normalized Ratio)
SAPAP3: WT KO
E
p = 0.22
mGluR5 Expression (Normalized Ratio)
SAPAP3: WT KO
F
p = 0.53
D2R Expression (Normalized Ratio)
SAPAP3: WT KO
G
p = 0.68
PP1γ1 in Spino IP (Normalized Ratio)
SAPAP3: WT KO
H
*
mGluR5 in Spino IP (Normalized Ratio)
SAPAP3: WT KO
I
*
D2R in Spino IP (Normalized Ratio)
SAPAP3: WT KO
J
r = 0.55
*
Percent Grooming
Log2(mGluR5 in Spino IP)
K
r = 0.46
*
Percent Grooming
Log2(D2R in Spinop IP)
L
r = 0.84
****
Log2(D2R in Spino IP)
Log2(mGluR5 in Spino IP)

Figure 9: Spinophilin's Interactions with mGluR5 and D2R Correlate with Grooming Behavior.

A-B) Grooming behavior was measured in 4-6 month-old SAPAP3 WT and KO mice for 2.5 hours ($p<0.0001$), then striatal inputs and spinophilin immunoprecipitates (IPs) were prepared for immunoblot analysis of SAPAP3, spinophilin, PP1γ1, mGluR5 and D_2R. Spinophilin KO striatum (lane 3) was used as a qualitative negative control to confirm the specificity of co-immunoprecipitates (co-IPs). Individual unpaired t-tests determined SAPAP3 KO did not change total protein expression of **C)** spinophilin ($p=0.24$), **E)** mGluR5 ($p=0.22$), or **F).** D_2R ($p=0.53$), however, a significant increase in **D)** PP1γ1 ($p=0.007$) was determined. Analysis of IPs determined significantly more **H)** mGluR5 ($p=0.012$) and **I)** D_2R ($p=0.033$) interacting with spinophilin in SAPAP3 KO striatum, however, there is no change in spinophilin's interaction with **G)** PP1γ1 ($p=0.68$). Pearson's correlation analysis determined grooming duration positively correlates with spinophilin's protein interaction with **J)** mGluR5 ($r=0.556$, $p=0.013$) and **K)** D_2R ($r=0.463$, $p=0.045$), and the **L)** spinophilin-mGluR5 interaction positively correlates with the spinophilin-D_2R interaction ($r=0.840$, $p < 0.0001$). N=10 SAPAP3 WT (7 male) and 9 SAPAP3 KO (4 male). Data ± SEM. *$p\leq0.05$, **$p\leq0.01$, ****$p<0.0001$.

4.3 Discussion

Conditional spinophilin knockout from dMSNs or iMSNs decreased excessive grooming caused by constitutive knockout of the striatal-enriched PSD scaffold, SAPAP3. Excessive grooming in SAPAP3 KO mice is associated with MSN subtype-specific adaptations that increase dMSN function relative to neighboring iMSNs in the DLS (Ade et al 2016). Both of these striatal abnormalities—excessive grooming and increased dMSN function—are decreased by treatment with the mGluR5 negative allosteric modulator (NAM), MTEP (Ade et al 2016). Interestingly, we also determined that spinophilin's protein interaction with mGluR5 is increased in SAPAP3 KO striatum and correlates with grooming behavior, suggesting spinophilin may mediate excessive grooming by regulating mGluR5 function. However, to conclude this, future studies will need to analyze spinophilin's contributions to other models of excessive grooming caused by direct activation of mGluR5 function.

Increased grooming duration (percent grooming) is achieved, at least in part, by increased grooming bout initiation (grooming frequency) or by sustained grooming bouts (mean grooming bout duration). Increased dMSN function is essential for initiating and sustaining complex motor programs, including rodent self-grooming (Berridge & Aldridge 2000a, Berridge & Aldridge 2000b, Rothwell et al 2015). Interestingly, SAPAP3 KO/Spino$^{\Delta dMSN}$ mice had decreased mean grooming duration compared to controls, suggesting Spino$^{\Delta dMSN}$ may be important in sustaining complex motor programs.

Decreasing iMSN function with a D_2R agonist decreases grooming initiation, duration, and sequence completion (Berridge & Aldridge 2000a, Berridge & Aldridge 2000b). Interestingly, SAPAP3 KO/Spino$^{\Delta iMSN}$ mice had decreased grooming frequency and mean grooming bout duration compared to SAPAP3 KO control mice. Furthermore, spinophilin's interaction with D2R was also increased in SAPAP3 KO striatum and correlated with grooming behavior. Canonically, D2R is expressed in iMSNs but not dMSNs in the dorsal striatum. Therefore, it is possible that spinophilin mediates grooming frequency and mean grooming bout duration through concerted regulation of mGluR5 and D2R. Although additional experiments would be required to conclude this, we did detect a striking correlation between spinophilin's interaction with mGluR5 and D_2R in the striatum, suggesting spinophilin may regulate these receptors in concert for appropriate integration of glutamatergic and dopaminergic signaling in iMSNs.

Recently, Tecuapetla and colleagues determined that optogenetic inhibition of striatal iMSNs in the dorsomedial striatum (DMS) decreased excessive grooming in SAPAP3 KO mice (Ramírez-Armenta et al 2022). While we elucidated that MSN subtype-specific loss of spinophilin decreases excessive grooming in SAPAP3 KO mice, it is unclear if this is due to spinophilin functioning in specific striatal subregions (i.e. DMS versus DLS). Furthermore, while the D1- and A2A-Cre lines utilized herein are highly expressed within striatal dMSNs or iMSNs, it is possible that spinophilin mediates excessive grooming by functioning in cell types outside the striatum through residual Cre expression in other brain regions, or in a non-cell-autonomous manner. However, in Chapter 3 we determined that both Spino$^{\Delta dMSN}$ and Spino$^{\Delta iMSN}$ mice had abrogated HFS-LTD in the DLS (**Figure 4**)—plasticity that requires mGluR5 and D_2R function (Kreitzer

& Malenka 2005, Wu et al 2015). The role of decreased LTD limiting pathological grooming is consistent with studies showing that SAPAP3 KO mice undergo increased short-term plasticity associated with increased mGluR5 function in the DLS (Chen et al 2011). Furthermore, the increased DLS network responses in Spino$^{\Delta dMSN}$ mice (**Figure 4**) is also an opposite phenotype of preclinical excessive grooming models (Peça et al 2011, Welch et al 2007). Therefore, it is of interest for future studies to directly measure these forms of plasticity in SAPAP3 KO/Spino$^{\Delta dMSN}$ and SAPAP3 KO/Spino$^{\Delta iMSN}$ mice to determine if MSN subtype-specific loss of spinophilin also restores DLS excitability and plasticity. In addition, in-vivo electrophysiology recordings will be necessary to conclude the extent to which increased DLS synaptic transmission and/or decreased LTD correlates with excessive grooming behavior.

Despite these mechanistic limitations, the results reported herein reveal MSN subtype-specific spinophilin knockout mice as novel models capable of identifying cell-autonomous and/or non-autonomous mechanisms required for excessive grooming pathology, a rodent phenotype that has face validity with grooming disorders like trichotillomania. Therefore, future studies will build upon the foundation laid herein to delineate spinophilin's cell-autonomous and non-autonomous functions in specific striatal subregions in mediating plasticity associated with repetitive motor dysfunction.

4	**C**	Automated vs. Manual Scoring	Pearson Correlation	r=0.97	p<0.0001
	D	Percent grooming	Two-way ANOVA	SAPAP3: F (1, 63) = 35.04	p<0.0001
				Spino: F (2, 63) = 17.11	p<0.0001
				Interaction: F (2, 63) = 3.396	p=0.039
	E	Grooming frequency	Two-way ANOVA	SAPAP3: F (1, 63) = 15.61	p=0.0002
				Spino: F (2, 63) = 7.025	p=0.0018
				Interaction: F (2, 63) = 2.992	p=0.057
	F	Mean bout duration	Two-way ANOVA	SAPAP3: F (1, 63) = 15.53	p=0.0002
				Spino: F (2, 63) = 10.86	p<0.0001
				Interaction: F (2, 63) = 0.3881	p=0.68
	G	Distance traveled	Two-way ANOVA	SAPAP3: F (1, 63) = 114.2	p<0.0001
				Spino: F (2, 63) = 3.651	p=0.03
				Interaction: F (2, 63) = 0.4136	p=0.66
	H	SAPAP3 WT: Grooming vs. Locomotion	Pearson Correlation	r=-0.59	p=0.03
				r=-0.38	p=0.31
				R=-0.50	p=0.09
	I	SAPAP3 WT: Grooming vs. Locomotion	Pearson Correlation	r=-0.21	p=0.51
				r=-0.22	p=0.48
				r=-0.63	p=0.02
5	**NA**	Percent grooming	Two-way ANOVA	SAPAP3: F (1, 33) = 16.34	p=0.0003
				Cre: F (1, 33) = 1.964	p=0.17
				Interaction: F (1, 33) = 0.3786	p=0.54
6	**A**	Percent grooming	Repeated Measures Two-way ANOVA	Genotype: F (5, 63) = 14.36	p<0.0001
				Time bin: F (1, 63) = 62.81	p<0.0001
				Interaction: F (5, 63) = 2.549	p=0.036

6	**B**	Grooming frequency	Repeated Measures Two-way ANOVA	Genotype: F (5, 63) = 7.161	p<0.0001
				Time bin: F (1, 63) = 134.3	p<0.0001
				Interaction: F (5, 63) = 1.110	p=0.36
	C	Mean bout duration	Repeated Measures Two-way ANOVA	Genotype: F (5, 63) = 7.200	p<0.0001
				Time bin: F (1, 63) = 6.519	p=0.013
				Interaction: F (5, 63) = 1.160	p=0.33
	D	Distance traveled	Repeated Measures Two-way ANOVA	Genotype: F (5, 63) = 24.11	p<0.0001
				Time bin: F (1, 63) = 128.8	p<0.0001
				Interaction: F (5, 63) = 2.714	p=0.027
8	**B**	Percent grooming	Unpaired t-tests	t=6.924, df=17	p<0.0001
	C	Spinophilin expression	Unpaired t-tests	t=1.210, df=17	p=0.24
	D	PP1g1 expression	Unpaired t-tests	t=3.052, df=17	p=007
	E	mGluR5 expression	Unpaired t-tests	t=1.261, df=17	p=0.22
	F	D2R expression	Unpaired t-tests	t=0.6408, df=17	p=0.53
	G	PP1g1 in Spino IP	Unpaired t-tests	t=0.4102, df=17	p=0.68
	H	mGluR5 in Spino IP	Unpaired t-tests	t=2.784, df=17	p=0.012
	I	D2R in Spino IP	Unpaired t-tests	t=2.316, df=17	p=0.033
	J	Grooming vs. Spino-mGluR5 interaction	Pearson Correlation	r=0.55	p=0.013
	K	Grooming vs. Spino-D2R interaction	Pearson Correlation	r=0.46	p=0.045
	L	Spino-mGluR5 interaction vs. Spino-D2R interaction	Pearson Correlation	r=0.84	p<0.001

Table 3: Chapter 4 Statistics.

Statistical analysis corresponding to Figures 4-7 and 9 are reported in the table above.

Chapter Five: Spinophilin's Role in Regulating Striatal mGluR5 Phosphorylation, Interactions, and Function

5.1 Introduction

Increased mGluR5 function has been postulated as a point of convergence associated with numerous preclinical models for understanding psychiatric disorders, including OCSDs and ASDs (Ade et al 2016, Dölen et al 2007, Kim et al 2017, Matosin & Siegel 2016, Michalon et al 2012, Ronesi et al 2012, Wang et al 2017, Wang et al 2016). Not only is excessive self-grooming in SAPAP3 KO and SHANK3 complete KO mice decreased by mGluR5 NAMs, but mGluR5-specific positive allosteric modulators (PAMs), such as VU0360172 (VU'172) augment self-grooming in wild-type mice (Ade et al 2016, Noetzel et al 2012, Wang et al 2016). Collectively, these studies suggest increased mGluR5 function may be sufficient to cause rodent excessive grooming behavior. Increased mGluR5 function in SAPAP3 KO mice and two models for understanding ASDs is associated with decreased mGluR5 scaffolding into the PSD through homer 1b/c crosslinks, resulting in constitutive mGluR5 function (Ade et al 2016, Ronesi et al 2012, Wang et al 2016). However, the mechanism(s) that uncouple mGluR5 from homer 1b/c, SHANK3, and SAPAP3 to promote mGluR5 dysfunction are unknow.

One mechanism capable of regulating protein-protein interactions is reversible phosphorylation. In the previous chapters, we determined that spinophilin expression in striatal dMSNs or iMSNs mediates striatal plasticity and excessive grooming in SAPAP3 KO mice. Given this, and that spinophilin is the most abundant PP1 targeting protein in the striatal PSD, it is possible that spinophilin mediates excessive grooming by regulating

the abundance of mGluR5 phosphorylation and/or its interactions with PSD protein. Here, we utilize quantitative proteomics approaches to investigate the effects that loss of spinophilin has mGluR5 phosphorylation and interactions with PSD proteins. Moreover, we utilize a recently published pharmacological model of mGluR5-dependent excessive grooming to directly assess spinophilin's MSN subtype-specific roles in mediating overgrooming caused by mGluR5 activity.

5.2 Results

5.2.1 Loss of Spinophilin Modulates mGluR5 Phosphorylation.

To probe consequences of loss of spinophilin on mGluR5, we measured mGluR5 phosphorylation in spinophilin replete (Spino$^{+/+}$) and Spino$^{-/-}$ striatum. First, we performed striatal mGluR5 IPs from one Spino$^{+/+}$ and Spino$^{-/-}$ mouse and excised the mGluR5 band on a Coomassie gel for a targeted GelC-MS run to validate that we can ratiometrically quantify phosphorylation sites on mGluR5 (**Figures 10-13**). Preliminarily, we determined that loss of spinophilin increased mGluR5 phosphorylation at Ser860 and Ser870 (**Table 4**).

A

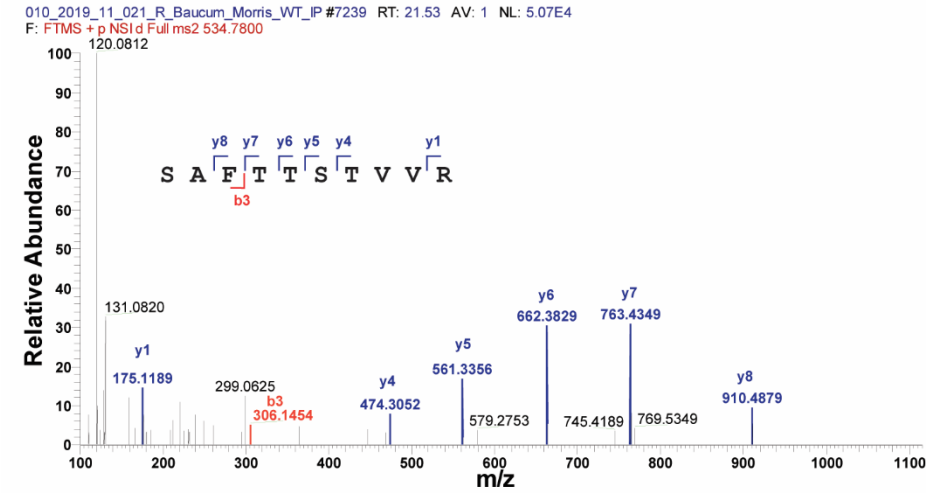
010_2019_11_021_R_Baucum_Morris_WT_IP #7239 RT: 21.53 AV: 1 NL: 5.07E4
F: FTMS + p NSI d Full ms2 534.7800
S A F T T S T V V R
y8 y7 y6 y5 y4 y1
b3
120.0812
131.0820
y1
175.1189
299.0625
b3
306.1454
y4
474.3052
y5
561.3356
579.2753
y6
662.3829
745.4189
y7
763.4349
769.5349
y8
910.4879
Relative Abundance
m/z

B

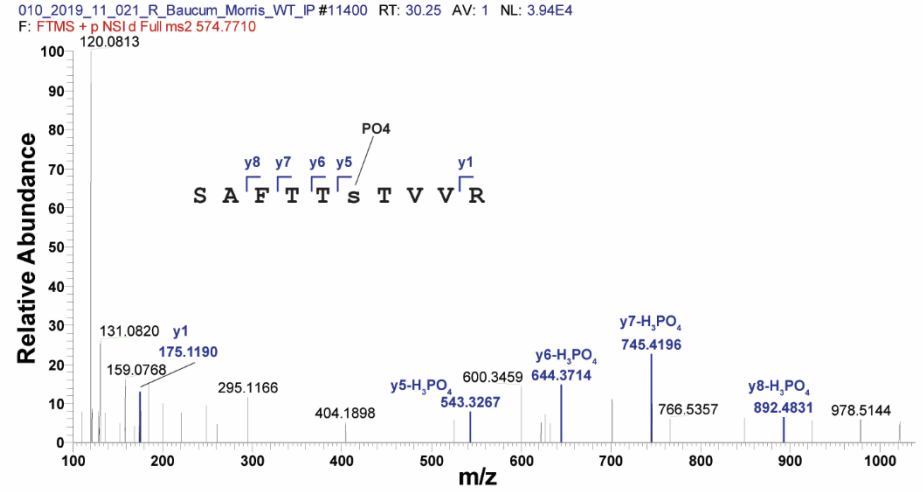
010_2019_11_021_R_Baucum_Morris_WT_IP #11400 RT: 30.25 AV: 1 NL: 3.94E4
F: FTMS + p NSI d Full ms2 574.7710
S A F T T s T V V R
PO4
y8 y7 y6 y5 y1
120.0813
131.0820
y1
175.1190
159.0768
295.1166
404.1898
y5-H3PO4
543.3267
600.3459
y6-H3PO4
644.3714
y7-H3PO4
745.4196
766.5357
y8-H3PO4
892.4831
978.5144
Relative Abundance
m/z

Figure 10: Mass Spectrum of mGluR5 Ser 839 Phosphopeptide.

MS/MS spectrum hand annotated with b- and y-series ions of **A)** total- and **B)** phospho-mGluR5 peptide containing Ser839.

A

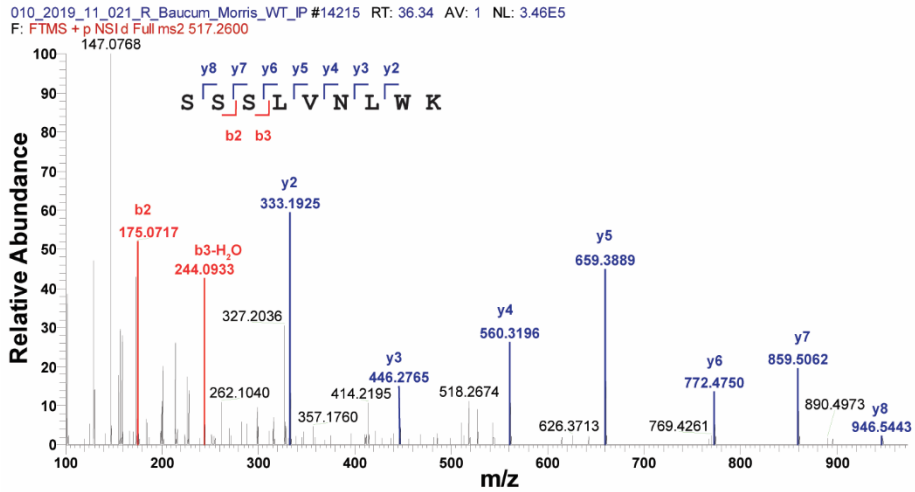
010_2019_11_021_R_Baucum_Morris_WT_IP #14215 RT: 36.34 AV: 1 NL: 3.46E5
F: FTMS + p NSI d Full ms2 517.2600
Relative Abundance
m/z
S S S L V N L W K
y8 y7 y6 y5 y4 y3 y2
b2 b3
147.0768
b2
175.0717
b3-H2O
244.0933
327.2036
y2
333.1925
262.1040
414.2195
y3
446.2765
357.1760
518.2674
y4
560.3196
626.3713
y5
659.3889
769.4261
y6
772.4750
y7
859.5062
890.4973
y8
946.5443

B

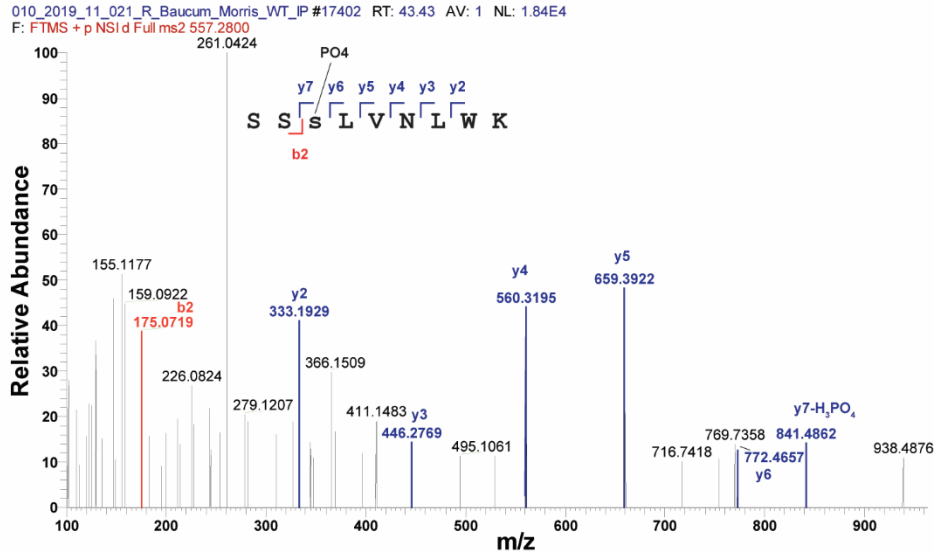
010_2019_11_021_R_Baucum_Morris_WT_IP #17402 RT: 43.43 AV: 1 NL: 1.84E4
F: FTMS + p NSI d Full ms2 557.2800
Relative Abundance
m/z
S S s L V N L W K
PO4
y7 y6 y5 y4 y3 y2
b2
261.0424
155.1177
159.0922
b2
175.0719
226.0824
279.1207
y2
333.1929
366.1509
411.1483
y3
446.2769
495.1061
y4
560.3195
y5
659.3922
716.7418
769.7358
772.4657
y6
y7-H3PO4
841.4862
938.4876

Figure 11: Mass Spectrum of mGluR5 Ser 860 Phosphopeptide.

MS/MS spectrum hand annotated with b- and y-series ions of **A)** total- and **B)** phospho-mGluR5 peptide containing Ser860.

A

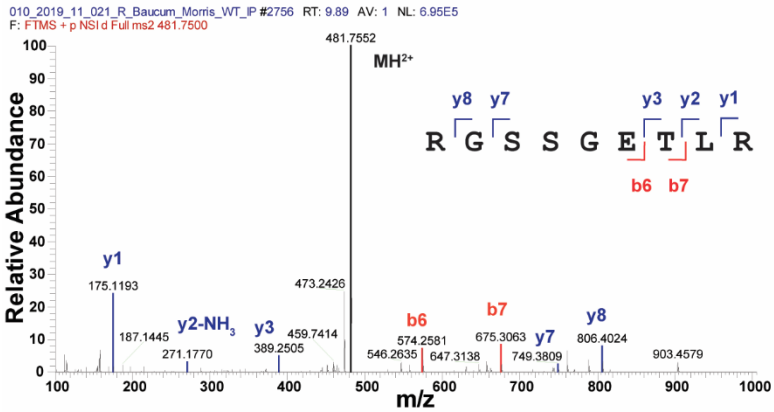
010_2019_11_021_R_Baucum_Morris_WT_IP #2756 RT: 9.89 AV: 1 NL: 6.95E5
F: FTMS + p NSI d Full ms2 481.7500
481.7552
MH2+
y8 y7 y3 y2 y1
R G S S G E T L R
b6 b7
y1
175.1193
473.2426
y2-NH3
y3
459.7414
389.2505
187.1445
271.1770
b6
574.2581
546.2635
647.3138
b7
675.3063
y7
749.3809
y8
806.4024
903.4579
Relative Abundance
m/z

B

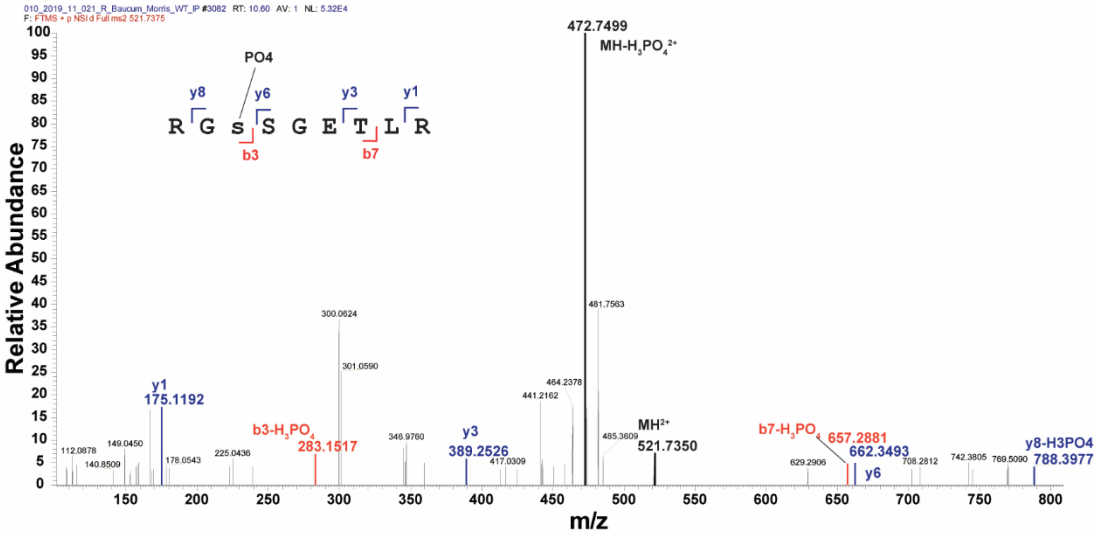
010_2019_11_021_R_Baucum_Morris_WT_IP #3082 RT: 10.60 AV: 1 NL: 5.32E4
F: FTMS + p NSI d Full ms2 521.7375
472.7499
MH-H3PO4 2+
PO4
y8 y6 y3 y1
R G s S G E T L R
b3 b7
481.7563
300.0624
301.0590
464.2378
441.2162
y1
175.1192
b3-H3PO4
283.1517
346.9760
y3
389.2526
417.0309
485.3609
MH2+
521.7350
b7-H3PO4
657.2881
662.3493
y6
y8-H3PO4
788.3977
Relative Abundance
m/z

Figure 12: Mass Spectrum of mGluR5 Ser 870 Phosphopeptide.

MS/MS spectrum hand annotated with b- and y-series ions of **A)** total- and **B)** phospho-mGluR5 peptide containing Ser870.

A

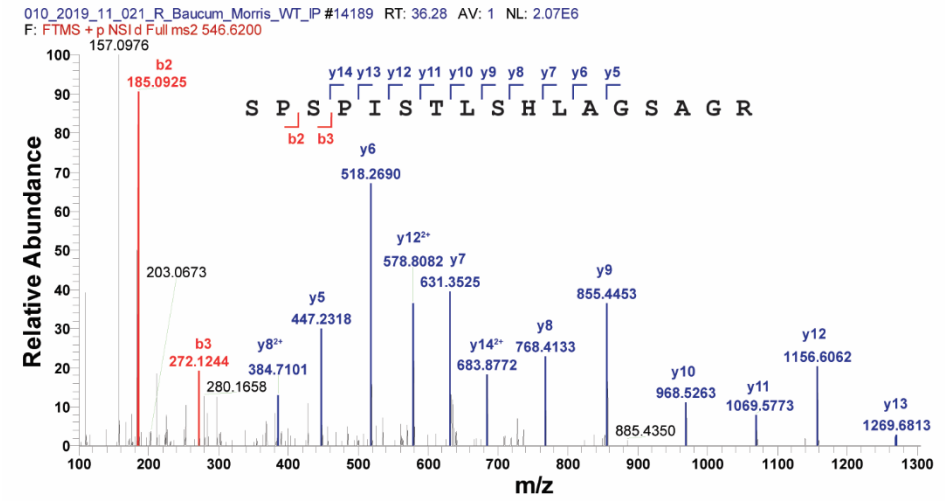
010_2019_11_021_R_Baucum_Morris_WT_IP #14189 RT: 36.28 AV: 1 NL: 2.07E6
F: FTMS + p NSI d Full ms2 546.6200
S P S P I S T L S H L A G S A G R
Relative Abundance
m/z

B

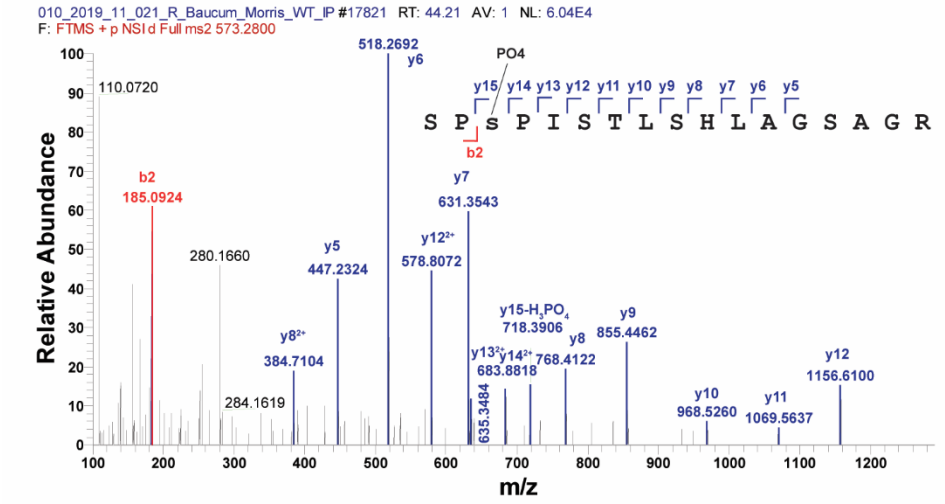
010_2019_11_021_R_Baucum_Morris_WT_IP #17821 RT: 44.21 AV: 1 NL: 6.04E4
F: FTMS + p NSI d Full ms2 573.2800
S P s P I S T L S H L A G S A G R
PO4
Relative Abundance
m/z

Figure 13: Mass Spectrum of mGluR5 Ser 1016 Phosphopeptide.

MS/MS spectrum hand annotated with b- and y-series ions of **A)** total- and **B)** phospho-mGluR5 peptide containing Ser1016.

mGluR5 Peptide	**Amino Acid**	**Abundance Ratio (Log_2)**
SSSLVNLWK	Ser860	0.40
SPSPISTLSHLAGSAGR	Ser1016	0.12
RGSSGETLR	Ser870	0.36
SAFTTsTVVR	Ser839	0.07

Table 4: Loss of Spinophilin Increased mGluR5 Phosphorylation at mGluR5 Ser 860 and Ser 870.

Sequential striatal mGluR5 IPs from one spino$^{+/+}$ and one spino$^{-/-}$ mouse were electrophoresed using an SDS-PAGE gel combined with a total protein Imperial Blue stain. mGluR5 bands at ~150kDa were excised from gel for GelC-MS analysis, which identified mGluR5 phosphorylation at Ser839, Ser860, Ser870, and Ser1016**.** Loss of spinophilin increased the abundance (log_2-fold change > 0.2) of mGluR5 Ser860 and Ser870.

To follow up on these preliminary results, we pooled sequential mGluR5 IPs from spino$^{+/+}$ and spino$^{-/-}$ striatal lysates (N=3 per genotype). These sequential IPs immunodepleted mGluR5 by ~80%, and we found no genotype difference in immunodepletion or mGluR5 expression (**Figure 14A-C**, **Figure 15**). mGluR5 complexes were submitted for protein identification and ratiometric quantification using tandem mass tag-liquid chromatography/mass spectrometry (TMT-LC/MS). Given the inherent variability of IPs coupled with TMT-LC/MS (Stein et al 2019), we utilized a Log_2 Abundance Ratio (KO/WT) < -0.2 or > 0.2 combined with one-tailed t-tests (α<0.10) to identify decreased or increased phosphopeptides, respectively. Interestingly, loss of spinophilin not only increased the abundance of mGluR5 Ser860 and Ser1016 phosphorylation, but we also detected increased phosphorylation of SHANK3 at Ser781 and SAPAP2 at Ser983, proteins with strong genetic associations with autism spectrum disorders (ASDs) and OCSDs (Chien et al 2013, Durand et al 2007, Marshall et al 2008, Pinto et al 2010, Prasad et al 2000, Wilson et al 2003, Wu et al 2013) (**Figure 14D**).

5.2.2 Loss of Spinophilin Shifts mGluR5 Interactions from Lipid Raft Assemblies Toward PSD Scaffolding Proteins Implicated in Psychiatric Disorders

We next analyzed protein abundance of mGluR5 co-IPs in the TMT-LC/MS dataset, which can give insight into consequences of loss of spinophilin on mGluR5 function. We identified 92 downregulated (log_2-fold change < -0.2) and 426 upregulated (log_2-fold change > 0.2) mGluR5 co-IPs isolated from spino$^{-/-}$ striatum that resulted in expansive protein-protein interaction (PPI) networks (**Figures 16-17**). We refined this list of interactors by filtering for significantly decreased/increased proteins (p<0.10 from one-tailed t-tests) that matched at least 6 unique peptides. We identified 27 decreased and

22 increased high-confidence mGluR5 interactors in spino$^{-/-}$ striatum (orange and green points in **Figure 14E**, respectively). We graphed these high-confidence interactors in STRING to generate decreased and increased PPI networks that were used for functional enrichment analysis (**Figure 14F-I**). We determined that spinophilin knockout decreased mGluR5 interactions with glycosylphosphatidylinositol (GPI)-anchored proteins, a class of proteins localized to specialized microdomains in the plasma membrane known as lipid rafts (Um & Ko 2017), and increased mGluR5 interactions with numerous PSD scaffolding proteins, including SAPAP3 and SHANK3. Shifting mGluR5 interactions toward PSD proteins in Spino$^{-/-}$ striatum was associated with multiple Biological Process GO terms, one of which was "regulation of grooming behavior".

We validated these protein interaction findings by submitting a second, small cohort of mGluR5 IPs (N=2 per genotype) for TMT-LC/MS. We replicated that loss of spinophilin decreased ($\log_2$-fold change < 0.2) mGluR5 protein interactions with GPI-anchored proteins and increased ($\log_2$-fold change > 0.2) mGluR5 interactions with PSD proteins implicated in psychiatric disorders, including SAPAP3 and SHANK3.

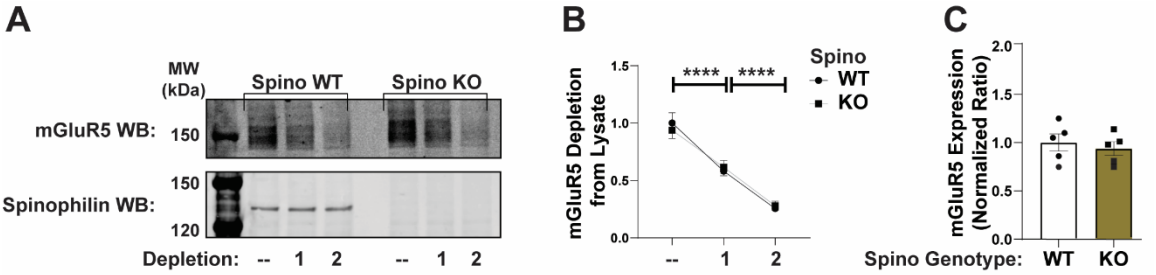

D

Protein	Phospho-Peptide	Amino Acid	Abundance Ratio (log_2)	P-Value
Increased Phospho-Peptides				
mGluR5	[R].SSSLVNLWK.[R]	Ser860	0.40	0.050
mGluR5	[R].SPSPISTLSHLAGSAGR.[T]	Ser1016	0.33	0.073
SHANK3	[R].TKSVGEDEK.[L]	Ser781	1.50	0.052
SAPAP2	[K].IIESPERKEER.[K]	Ser 983	0.88	0.063
UBE3C	[R].LIWLYQNLIK.[H]	Tyr 118	0.56	0.070
Decreased Phospho-Peptides				
MYO9b	[R].TPVVQDLELGALSEEAAG GDEDREK.[E]	Ser 1908	-0.34	0.063

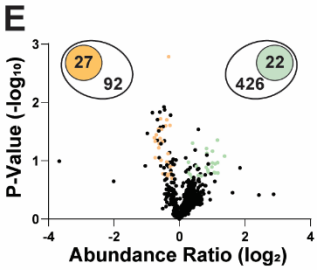

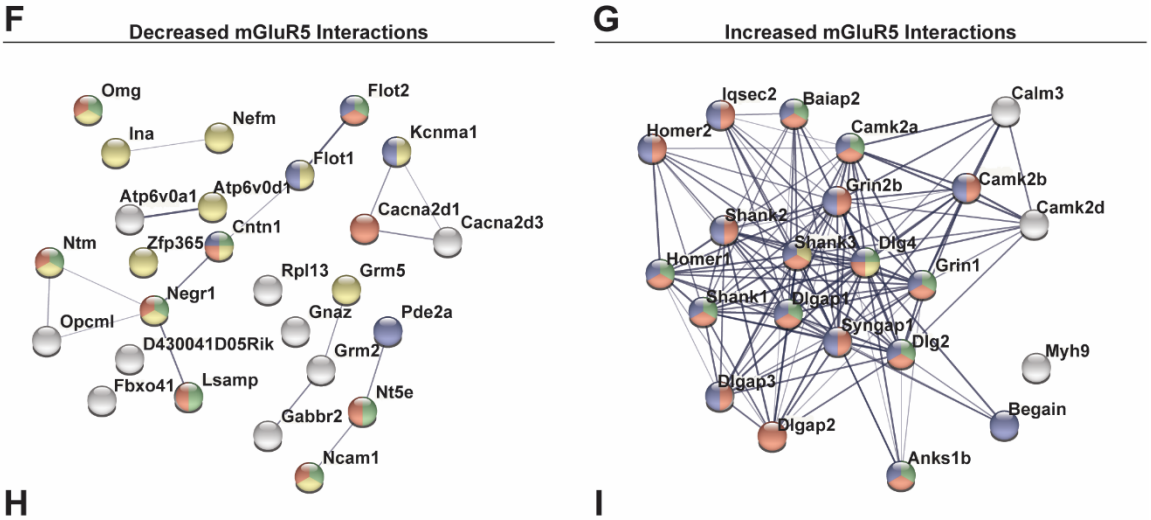

H

GO Term	Description	FDR
Cellular Component Gene Ontology		
GO:0031225	Anchored component of membrane	9.75e-10
GO:0045121	Membrane raft	0.0037
Biological Process Gene Ontology		
GO:0007155	Cell Adhesion	0.02
GO:0007399	Nervous System Development	0.02

I

GO Term	Description	FDR
Cellular Component Gene Ontology		
GO:0014069	Postsynaptic density	1.44e-24
GO:0098978	Glutamatergic synapse	8.22e-24
Biological Process Gene Ontology		
GO:0035418	Protein localization to synapse	2.21e-13
GO:20000821	Regulation of grooming behavior	0.0019

Figure 14: Loss of Spinophilin Shifts mGluR5 Interactions from Lipid Raft Assemblies Toward PSD Proteins Implicated in Psychiatric Disorders.

A) Representative sequential mGluR5 IP from spinophilin WT (Spino$^{+/+}$) and KO (Spino$^{-/-}$) striatal lysates. We detected no difference in **B)** mGluR5 immunodepletion or **C)** mGluR5 protein expression in spino WT and KO inputs. mGluR5 IPs were submitted to the IUSM proteomics core for TMT-MS/MS analysis. **D)** Table showing increased and decreased phospho-peptides that have Abundance Ratio (Log_2) < -0.2 or >0.2 and one-tailed t-test p-value < 0.10. **E)** Volcano plot showing 27 decreased (orange) and 22 increased (green) interactors having Abundance Ratio (Log_2) < -0.2 or >0.2, one-tailed t-test p-value < 0.10, and at least 6 unique peptides matching assigned protein. Protein-protein interaction (PPI) networks corresponding to the **F)** 27 decreased or **G)** 22 increased proteins were graphed in STRING. Graph edges correspond to proteins that participate in a function complex and edge boldness corresponds to the confidence of the interaction. Node colors correspond to gene ontology (GO) terms identified through function enrichment analysis of the **H)** decreased or **I)** increased PPI networks (false discovery rate (FDR) < 0.05). N=3 spino$^{+/+}$ (3 male) and 3 spino$^{-/-}$ (2 male). Data ± SEM. ****p<0.0001.

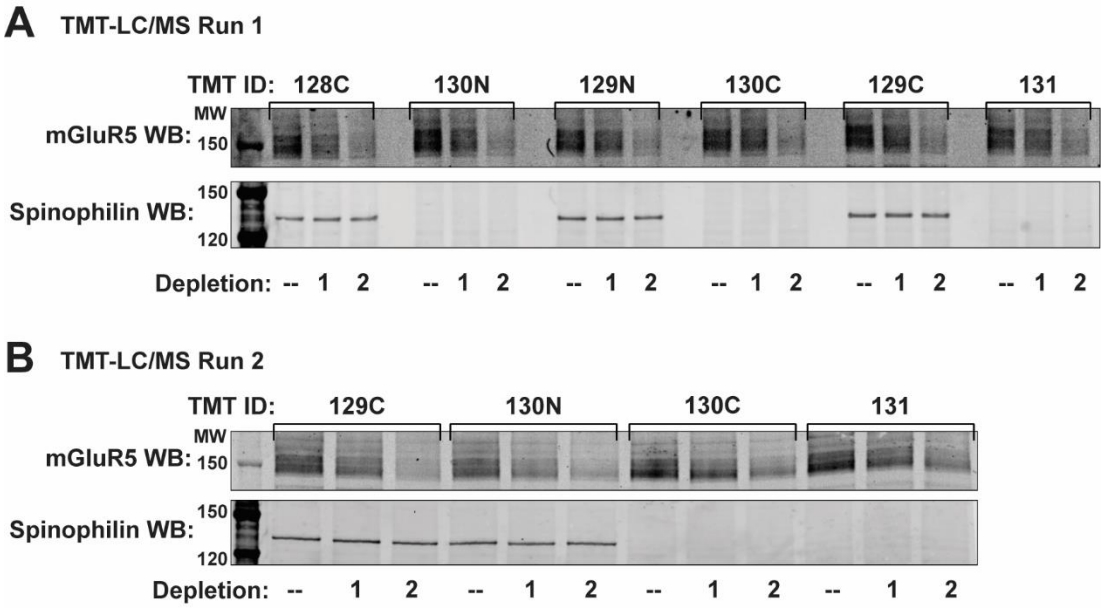
A
TMT-LC/MS Run 1
TMT ID: 128C 130N 129N 130C 129C 131
MW
mGluR5 WB:
150
Spinophilin WB:
150
120
Depletion: -- 1 2 -- 1 2 -- 1 2 -- 1 2 -- 1 2 -- 1 2
B
TMT-LC/MS Run 2
TMT ID: 129C 130N 130C 131
MW
mGluR5 WB:
150
Spinophilin WB:
150
120
Depletion: -- 1 2 -- 1 2 -- 1 2 -- 1 2

Figure 15: Immunoblot Confirmation of Samples Submitted for TMT-LC/MS Runs 1-2. Western blots confirming sequential mGluR5 immunodepletion and spinophilin expression from TMT-LC/MS **A)** run1 and **B)** run 2. TMT IDs above lanes corresponds to isobaric tags listed in Table S2 (run 1) and Table S5 (run 2).

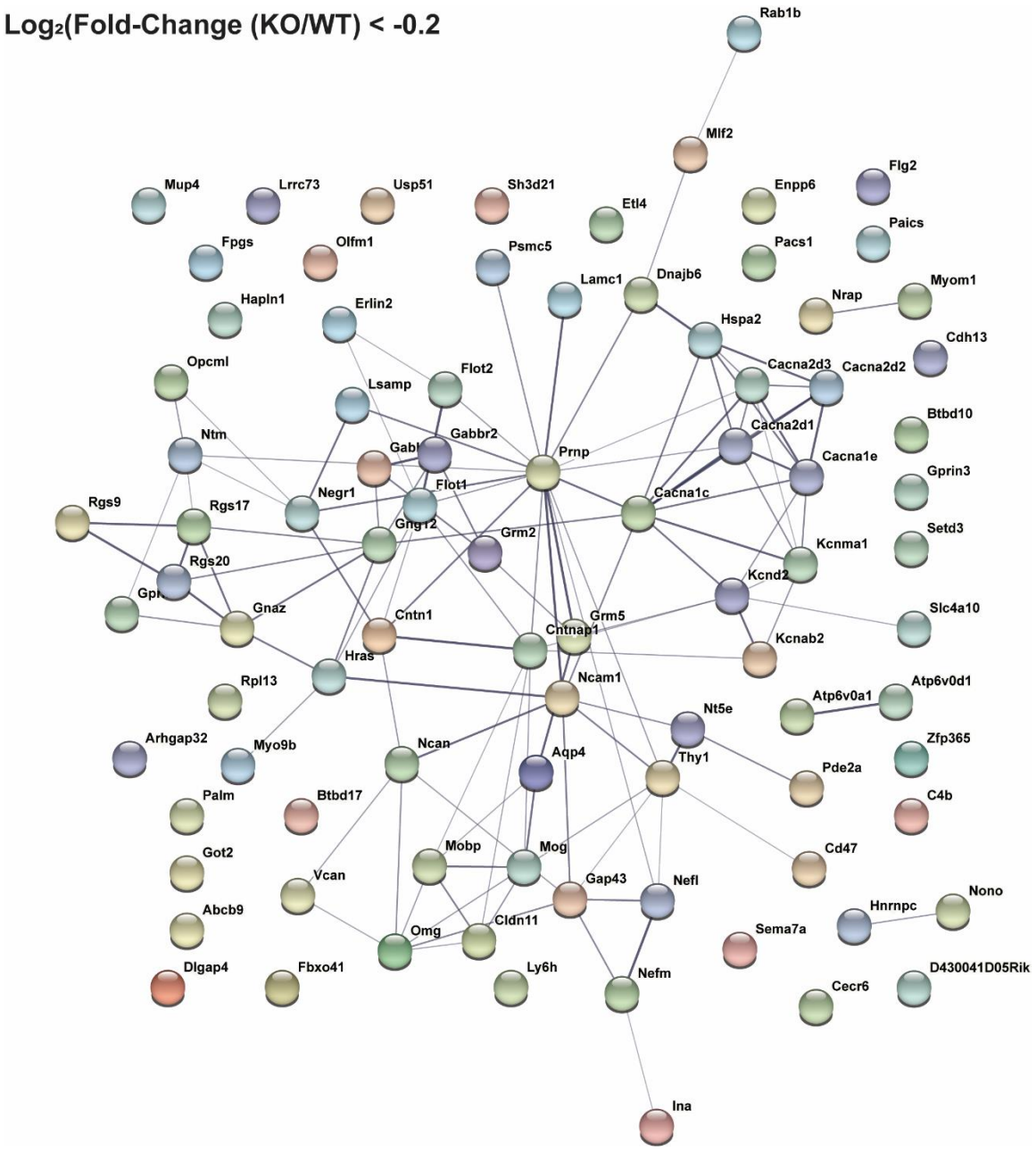
Log2(Fold-Change (KO/WT) < -0.2
Rab1b
Mlf2
Flg2
Mup4
Lrrc73
Usp51
Sh3d21
Etl4
Enpp6
Paics
Fpgs
Olfm1
Psmc5
Pacs1
Lamc1
Dnajb6
Myom1
Hapln1
Erlin2
Nrap
Hspa2
Cdh13
Opcml
Flot2
Cacna2d3
Cacna2d2
Lsamp
Btbd10
Ntm
Gabbr2
Cacna2d1
Gabl
Prnp
Cacna1e
Gprin3
Rgs9
Rgs17
Negr1
Flot1
Cacna1c
Gng12
Grm2
Setd3
Rgs20
Kcnma1
Kcnd2
Gpr
Gnaz
Cntn1
Grm5
Slc4a10
Cntnap1
Kcnab2
Hras
Rpl13
Ncam1
Atp6v0a1
Atp6v0d1
Nt5e
Arhgap32
Myo9b
Ncan
Aqp4
Thy1
Zfp365
Pde2a
Palm
Btbd17
C4b
Mobp
Mog
Cd47
Got2
Vcan
Gap43
Nefl
Nono
Abcb9
Hnrnpc
Omg
Cldn11
Sema7a
Dlgap4
Fbxo41
Ly6h
Nefm
D430041D05Rik
Cecr6
Ina

Figure 16: Complete PPI Network of Decreased mGluR5 Interactions.

All 92 decreased mGluR5 interactors (log_2-fold change < -0.2) were graphed in string-DB to visualize how loss of spinophilin modulates mGluR5's protein-protein interaction (PPIs) network.

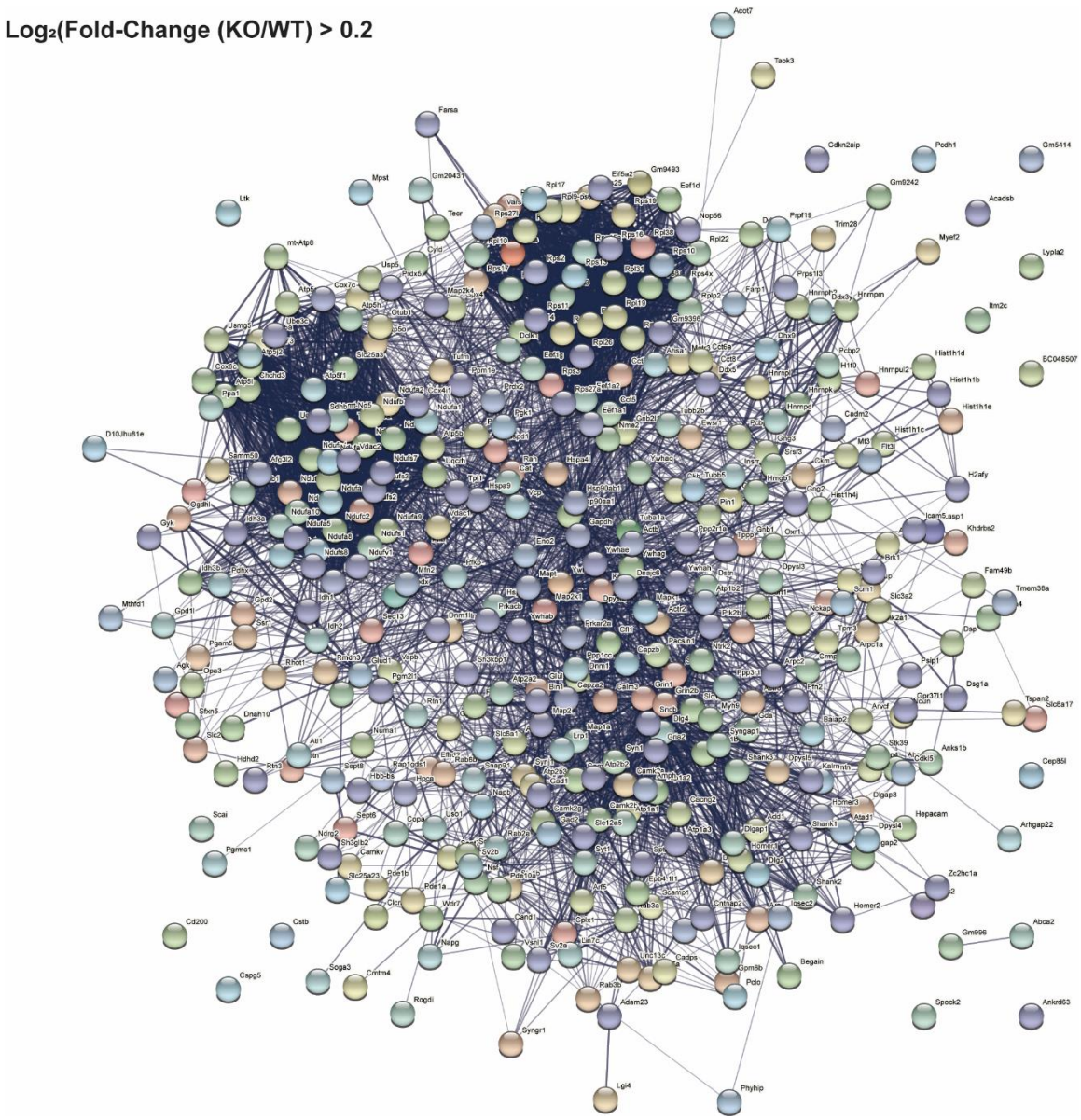
Log₂(Fold-Change (KO/WT) > 0.2

Figure 17: Complete PPI Network of Increased mGluR5 Interactors.

All 426 increased mGluR5 interactors (log_2-fold change > 0.2) were graphed in string-DB to visualize how loss of spinophilin modulates mGluR5's protein-protein interaction (PPIs) network.

5.2.3 Spinophilin MSN Subtype-Specifically Decreases Grooming Caused by the mGluR5 PAM, VU0360172

To directly determine if spinophilin mediates excessive grooming by regulating mGluR5 function we pharmacologically increased grooming behavior by treating mice with the mGluR5 PAM, VU0360172 (VU'172), that selectively increases grooming in wild type, but not mGluR5 KO mice (Ade et al 2016). Specifically, we measured grooming behavior in control, Spino$^{\Delta dMSN}$, and Spino$^{\Delta iMSN}$ mice for 30-minutes before and after an I.P. injection of vehicle or VU'172 (20 mg/kg). We also measured the grooming response to VU'172 in Spino$^{-/-}$ mice to determine any additive or antagonistic effects when spinophilin is knocked out of both MSN subtypes (**Figure 18A**). We found no treatment group effects on percent grooming or distance traveled in the pre-injection period (**Figure 19**); however, percent grooming was decreased, and distance traveled was increased in Spino$^{-/-}$ compared to control mice, a published phenotype of Spino$^{-/-}$ mice (Zhang et al 2020). Vehicle treatment increased grooming (a grooming phenotype that is also decreased in mGluR5 KO mice); however, grooming was further increased by VU'172 treatment in Spino$^{Fl/+ \text{ or } Fl/Fl}$, Spino$^{-/-}$, and Spino$^{+/+}$-D1 or -A2A Cre control mice (**Figure 18B, 20**). Furthermore, we detected significant treatment X spinophilin genotype interaction on percent grooming, such that we did not detect a VU'172 treatment effect on percent grooming in Spino$^{\Delta dMSN}$ and Spino$^{\Delta iMSN}$ mice, and percent grooming in VU'172-treated Spino$^{\Delta dMSN}$ and Spino$^{\Delta iMSN}$ mice was not significantly different from vehicle-treated control mice (**Figure 18B**). Post-injection grooming and locomotion data

were also analyzed in 5-minute bins to confirm genotype effects were consistent across 30-minute recording (**Figure 21**). Collectively, these data suggest MSN subtype-specific spinophilin knockout, but not global knockout, abrogates VU'172-induced grooming.

Although we detected a significant treatment effect on grooming frequency, we found no genotype or genotype X treatment interaction (**Figure 18C**). Also, neither VU'172 (20 mg/kg) nor spinophilin genotype affected mean grooming bout duration (**Figure 18D**). Alternatively, we detected a significant treatment, genotype, and interaction effect on locomotion in OF, but post-hoc tests determined this is due to increased locomotion in vehicle-treated Spino$^{-/-}$ mice (**Figure 18E**). Despite no striking treatment effect across all genotypes, we detected significant negative correlations between grooming duration and distance traveled within 5-minute bins for each vehicle- and VU'172-treated group (**Figure 22**).

To determine how loss of spinophilin in both MSN subtypes modifies VU'172-induced grooming, we bred Spino$^{\Delta dMSN}$ and Spino$^{\Delta iMSN}$ mice to knockout spinophilin from both MSN subtypes (Spino$^{\Delta PanMSN}$). We treated this genotype with VU'172 (20 mg/kg) and compared the grooming response to that of the aforementioned Spino$^{Fl/Fl\ or\ Fl/+}$ and Spino$^{-/-}$ VU'172-treated mice. In contrast to the individual cell type knockouts, there was no significant reduction in percent grooming, grooming frequency, and mean bout duration in the double knockout compared to the control or Spino$^{-/-}$ groups in across the 3 groups (**Figure 23**), suggesting that the lack of effect on VU'172-induced grooming observed in Spino$^{-/-}$ mice was due to loss of spinophilin in both MSN subtypes having an

antagonistic effect on VU'172-induced grooming. Although this experiment was not designed to detect sex differences in grooming and locomotor behavior, we visualized these datasets by sex (**Figure 24**).

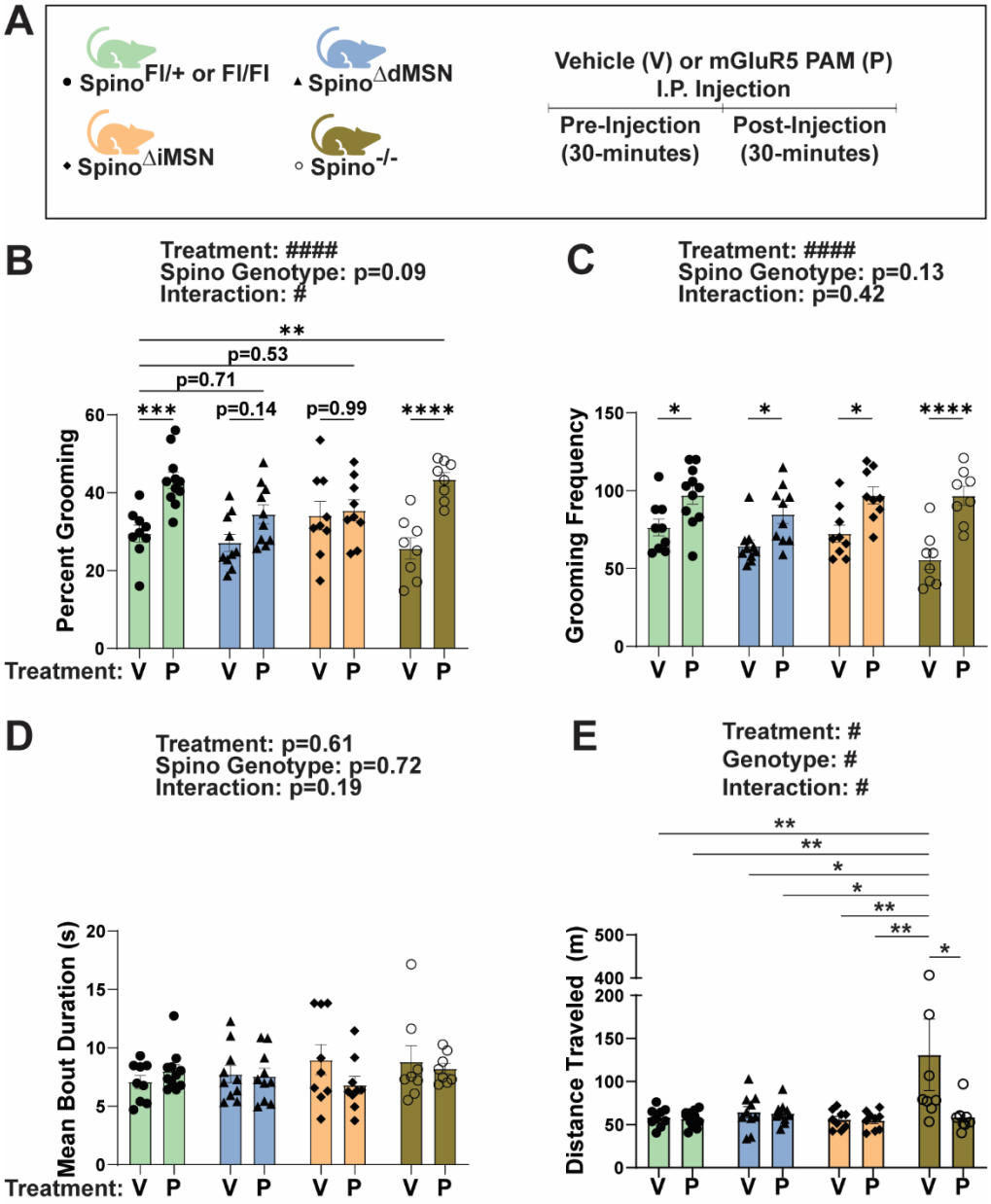
A
Spino Fl/+ or Fl/Fl
Spino ΔdMSN
Spino ΔiMSN
Spino -/-
Vehicle (V) or mGluR5 PAM (P)
I.P. Injection
Pre-Injection (30-minutes)
Post-Injection (30-minutes)
B
Treatment: ####
Spino Genotype: p=0.09
Interaction: #
Percent Grooming
Treatment: V P V P V P V P
C
Treatment: ####
Spino Genotype: p=0.13
Interaction: p=0.42
Grooming Frequency
D
Treatment: p=0.61
Spino Genotype: p=0.72
Interaction: p=0.19
Mean Bout Duration (s)
E
Treatment: #
Genotype: #
Interaction: #
Distance Traveled (m)

Figure 18: MSN Subtype-Specific Spinophilin Knockout Decreases Grooming Caused by the mGluR5 PAM, VU0360172.

A) Control and MSN-specific spinophilin knockout mice were placed in Noldus Phenotyper Cages and basal behavior (pre-injection) was measured for 30-minutes. Following a pre-injection period, mice were removed from the arena and given an I.P. injection of vehicle (V) or the mGluR5 PAM (P), VU0360172 (VU'172) (20 mg/kg). Animals were placed back into the same pre-injection arena immediately following the I.P. injection and behavior was recorded for an additional 30-minutes (post-injection). Two-way ANOVAs with post-hoc Šídák's multiple comparisons tests determined a significant VU'172 treatment effect on **B)** percent grooming in control ($p=0.0007$) and $Spino^{-/-}$ ($p<0.0001$), but not $Spino^{\Delta dMSN}$ ($p=0.139$) or $Spino^{\Delta iMSN}$ ($p=0.99$) mice. Furthermore, percent grooming in the VU'172-treated $Spino^{\Delta dMSN}$ and $Spino^{\Delta iMSN}$ groups was not different from control vehicle ($p=0.71$ and $p=0.53$, respectively), whereas $Spino^{-/-}$ was significantly increased from control vehicle ($p=0.002$). **C)** VU'172 (20 mg/kg) increased grooming frequency in control ($p=0.03$), $Spino^{\Delta dMSN}$ ($p=0.03$), $Spino^{\Delta iMSN}$ ($p=0.01$), and $Spino^{-/-}$ ($p<0.0001$). **D)** VU'172 (20 mg/kg) or spinophilin genotype did not affect mean grooming bout duration. **E)** Two-way ANOVA with post-hoc Dunnett's multiple comparisons test determined distance traveled in vehicle-treated $Spino^{-/-}$ mice was significantly increased compared to all other groups. N=9V/10P $Spino^{Fl/+ \text{ or } Fl/Fl}$ (3/3 male), 10V/10P $spino^{\Delta dMSN}$ (5/6 male), and 9V/9P $spino^{\Delta iMSN}$ (4/4 male), 8V/8P $spino^{-/-}$ (3/4 male).

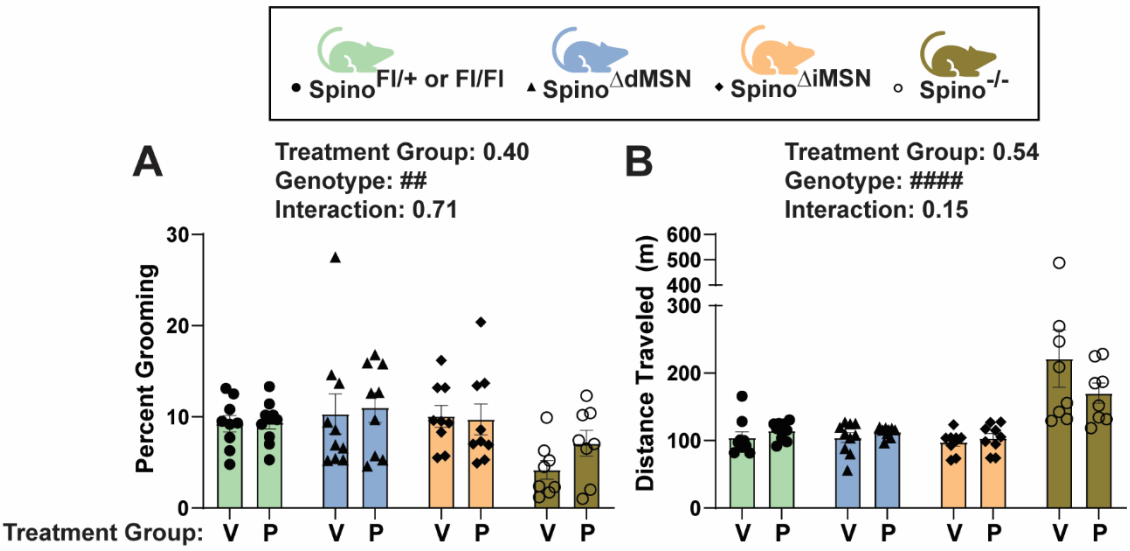
Spino Fl/+ or Fl/Fl
Spino ΔdMSN
Spino ΔiMSN
Spino -/-
A
Treatment Group: 0.40
Genotype: ##
Interaction: 0.71
Percent Grooming
30
20
10
0
Treatment Group: V P V P V P V P
B
Treatment Group: 0.54
Genotype: ####
Interaction: 0.15
Distance Traveled (m)
600
500
400
300
200
100
0
V P V P V P V P

Figure 19: Pre-Injection Open Field Behavior Prior to Treatment with the mGluR5 PAM VU'172 (20 mg/kg).

Two-way ANOVA with post-hoc Dunnett's multiple comparisons test determined there were no pre-existing treatment group effects on **A)** percent grooming or **B)** distance traveled in the 30-minutes pre-injection period, however, percent grooming was significantly decreased ($p=0.04$), and distance traveled was significantly increased ($p<0.0001$) in Spino$^{-/-}$ compared to control. N=9V/10P Spino$^{Fl/+ \text{ or } Fl/Fl}$ (3/3 male), 10V/9P Spino$^{\Delta dMSN}$ (5/5 male), and 9V/9P Spino$^{\Delta iMSN}$ (4/4 male), 8V/8P Spino$^{-/-}$ (3/4 male). Significant two-way ANOVA effects denoted by ##$p\leq0.01$ and ####$p<0.0001$.

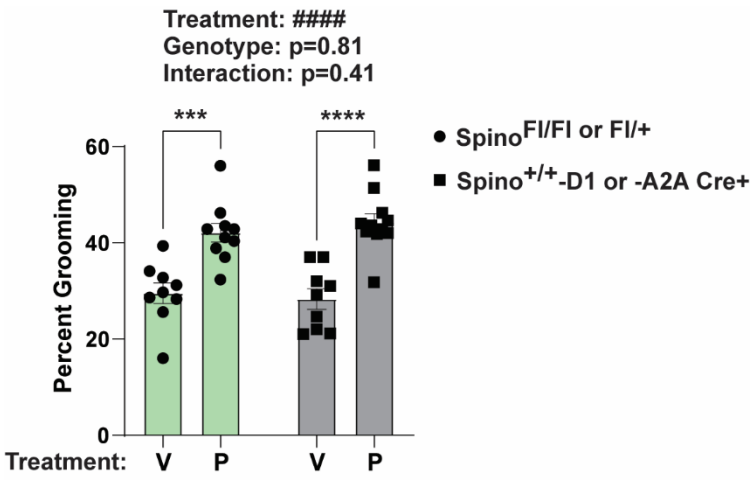
Treatment: ####
Genotype: p=0.81
Interaction: p=0.41
***
****
60
40
20
0
Percent Grooming
Treatment:
V
P
V
P
Spino^Fl/Fl or Fl/+
Spino^+/+-D1 or -A2A Cre+

Figure 20: D1- or A2A-Cre Expression Do Not Affect VU'172 Grooming.

Percent grooming from vehicle- and VU'172-treated Spino$^{Fl/Fl\ or\ Fl/+}$ control groups were compared to vehicle- and VU'172-treated Spino$^{+/+}$-D1 or -A2A Cre control group. Two-way ANOVA with post-hoc Šídák's multiple comparisons test determined a significant VU'172 treatment effect in Spino$^{Fl/Fl\ or\ Fl/+}$ control and Spino$^{+/+}$-D1 or -A2A Cre control groups ($p=0.0002$ and $p<0.0001$, respectively). N=9V/10P Spino$^{Fl/+\ or\ Fl/Fl}$ (3/3 male) and 9V/11P Spino$^{+/+}$-D1 Cre or -A2A Cre (3/4 male). Data ± SEM. Significant two-ANOVA effects denoted by ####$p<0.0001$. Significant post-hoc tests denoted by ***$p\leq0.001$ and ****$p<0.0001$.

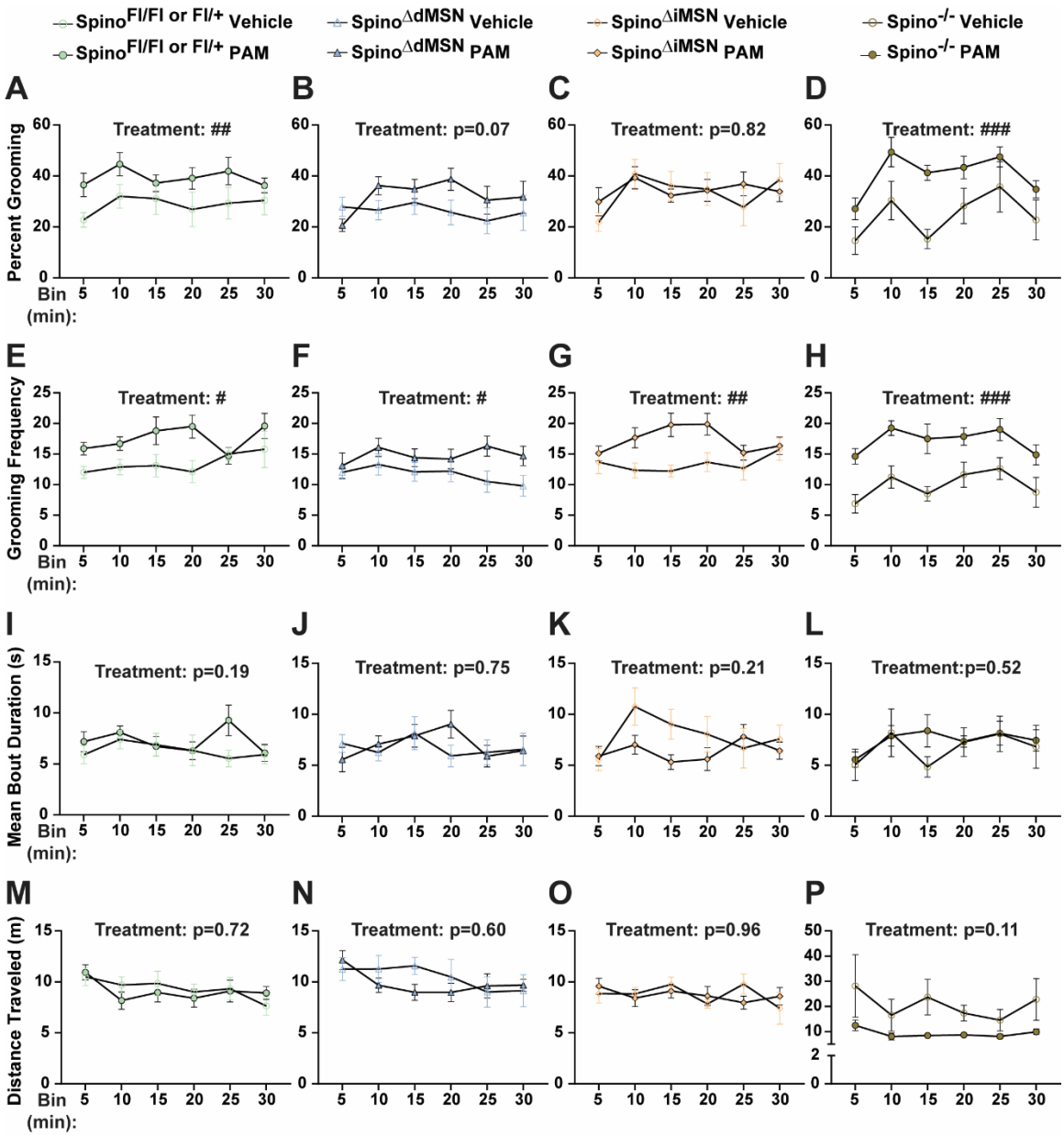
Spino$^{Fl/Fl\ or\ Fl/+}$ Vehicle
Spino$^{Fl/Fl\ or\ Fl/+}$ PAM
Spino$^{\Delta dMSN}$ Vehicle
Spino$^{\Delta dMSN}$ PAM
Spino$^{\Delta iMSN}$ Vehicle
Spino$^{\Delta iMSN}$ PAM
Spino$^{-/-}$ Vehicle
Spino$^{-/-}$ PAM
A
Treatment: ##
B
Treatment: p=0.07
C
Treatment: p=0.82
D
Treatment: ###
Percent Grooming
E
Treatment: #
F
Treatment: #
G
Treatment: ##
H
Treatment: ###
Grooming Frequency
I
Treatment: p=0.19
J
Treatment: p=0.75
K
Treatment: p=0.21
L
Treatment:p=0.52
Mean Bout Duration (s)
M
Treatment: p=0.72
N
Treatment: p=0.60
O
Treatment: p=0.96
P
Treatment: p=0.11
Distance Traveled (m)
Bin (min):
5 10 15 20 25 30

Figure 21: VU'172-Treatment Effects on Grooming and Locomotion Behavior in 5-Minute Bins.

Open field behavior was grouped into 5-minute bins then two-way ANOVAs with repeated measures were performed to determine VU'172 (20 mg/kg)-treatment effects on **A-D)** percent grooming, **E-H)** grooming frequency, **I-L)** mean grooming bout duration, and **M-P)** distance traveled within each genotype. Two-way ANOVAs with repeated measures identified a significant treatment effect on percent grooming in **A)** Spino$^{Fl/Fl\ or\ Fl/+}$ control and **B)** Spino$^{-/-}$, and grooming frequency in all genotypes. However, we did not detect VU'172 treatment effects on mean bout duration or distance traveled. N=9V/10P Spino$^{Fl/+\ or\ Fl/Fl}$ (3/3 male), 10V/10P Spino$^{\Delta dMSN}$ (5/6 male), and 9V/9P Spino$^{\Delta iMSN}$ (4/4 male), 8V/8P Spino$^{-/-}$ (3/4 male). Data ± SEM. Significant two-ANOVA treatment effects denoted by #$p \leq 0.05$, ##$p \leq 0.01$, and ###$p \leq 0.001$.

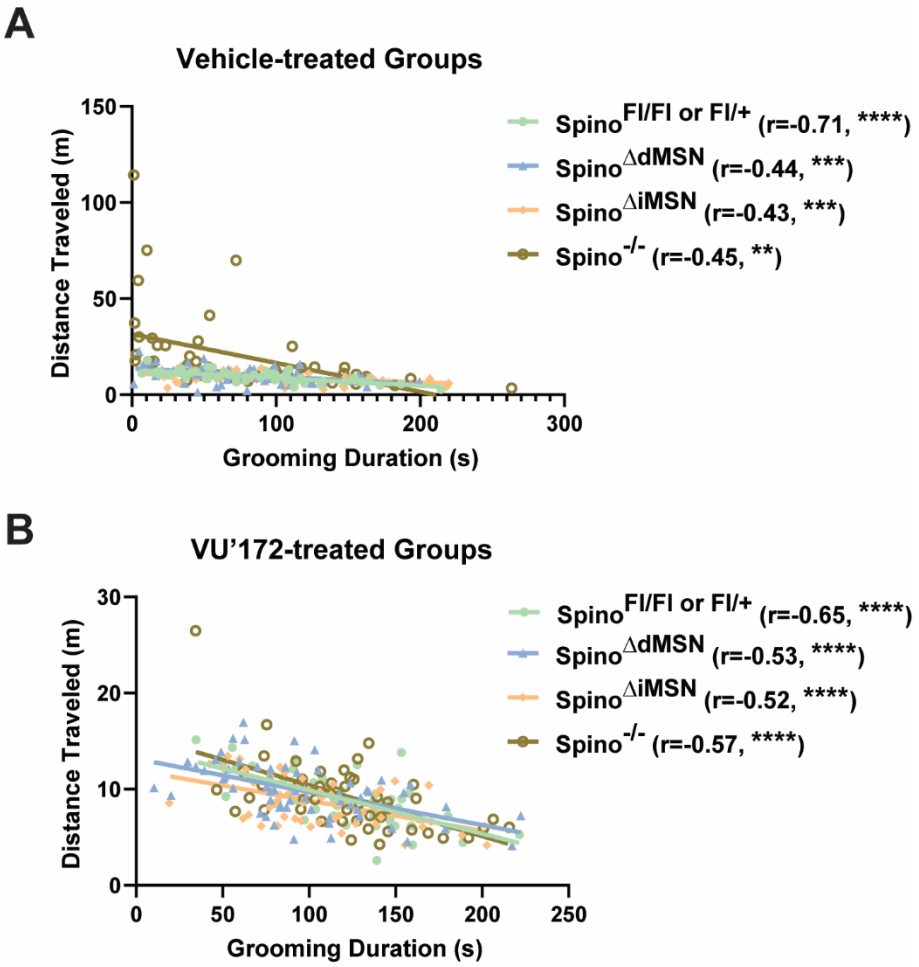
A
Vehicle-treated Groups
Distance Traveled (m)
Grooming Duration (s)
Spino^Fl/Fl or Fl/+ (r=-0.71, ****)
Spino^ΔdMSN (r=-0.44, ***)
Spino^ΔiMSN (r=-0.43, ***)
Spino^-/- (r=-0.45, **)
B
VU'172-treated Groups
Distance Traveled (m)
Grooming Duration (s)
Spino^Fl/Fl or Fl/+ (r=-0.65, ****)
Spino^ΔdMSN (r=-0.53, ****)
Spino^ΔiMSN (r=-0.52, ****)
Spino^-/- (r=-0.57, ****)

Figure 22: Grooming Caused by VU'172 Negatively Correlates with Locomotion in the Open Field.

Person's correlation analysis detected significant negative correlations between grooming duration and distance traveled within 5-minute bins for all **A)** vehicle-treated and **D)** VU'172-treated groups. N=9V/10P Spino$^{Fl/+ \text{ or } Fl/Fl}$ (3/3 male), 10V/10P Spino$^{\Delta dMSN}$ (5/6 male), and 9V/9P Spino$^{\Delta iMSN}$ (4/4 male), 8V/8P Spino$^{-/-}$ (3/4 male). Data ± SEM. Significant two-ANOVA effects denoted by #$p \leq 0.05$. Significant post-hoc tests or correlation coefficients denoted by *$p \leq 0.05$, **$p \leq 0.01$, ***$p \leq 0.001$ ****$p < 0.0001$.

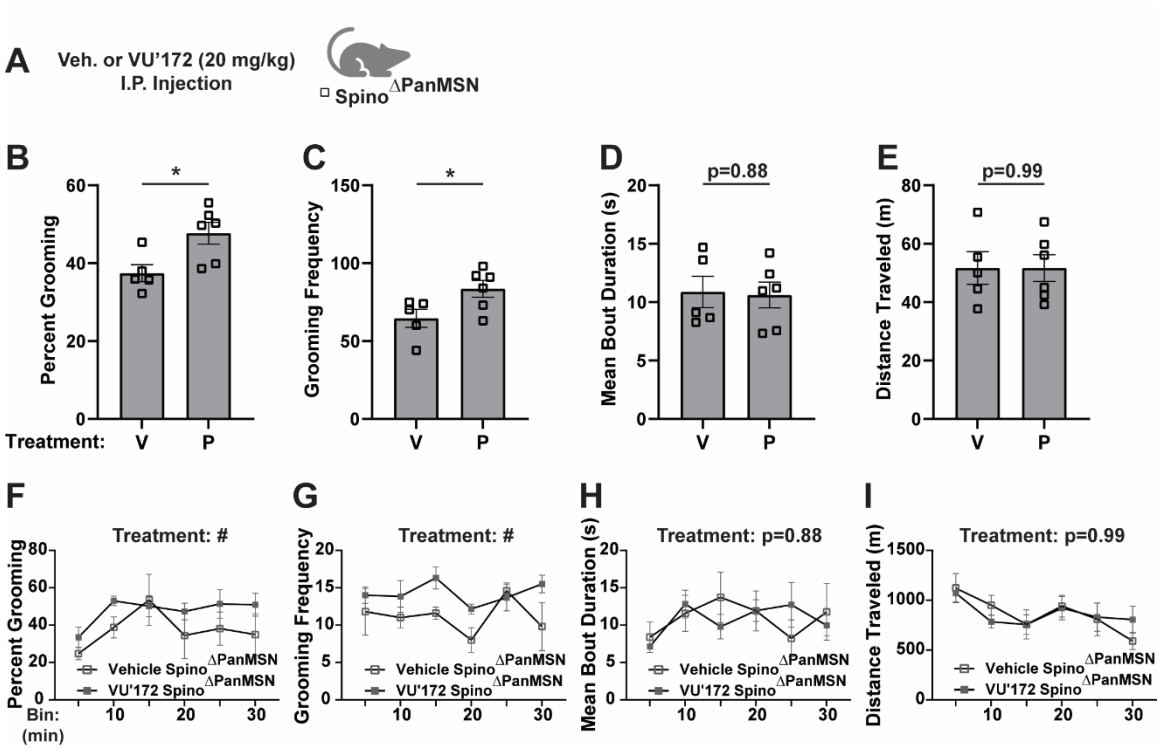
A
Veh. or VU'172 (20 mg/kg)
I.P. Injection
Spino
ΔPanMSN
B
Percent Grooming
Treatment:
V
P
C
Grooming Frequency
D
Mean Bout Duration (s)
p=0.88
E
Distance Traveled (m)
p=0.99
F
Treatment: #
Vehicle Spino ΔPanMSN
VU'172 Spino ΔPanMSN
Bin: (min)
G
H
Treatment: p=0.88
I
Treatment: p=0.99

Figure 23: Depletion of Spinophilin from dMSNs and iMSNs, Together, Does Not Decrease VU'172 Grooming Behavior.

A) Spino$^{\Delta PanMSN}$ were treated with vehicle (Veh.) or VU'172 (20 mg/kg). Student's t-tests determined that VU'172 significantly increased **B)** percent grooming (p=0.02) and **C)** grooming frequency (p=0.04), however, VU'172 did not affect **D)** mean grooming bout duration (p=0.88) and **E)** distance traveled (p=0.99). Two-way ANOVAs with repeated measures were performed to determine treatment effects on grooming and locomotion behavior in 5-minute bins. Consistent with Student's t-tests, two-way ANOVA with repeated measures identified significant VU'172-treatment effects on **F)** percent grooming (p=0.021) and **G)** grooming frequency (p=0.038), however, VU'172 did not affect **H)** mean grooming bout duration (p=0.88) and **I)** distance traveled (p=0.99). N = 5 Veh.- and 6 VU'172-treated Spino$^{\Delta PanMSN}$ (4 male). Data ± SEM. Significant Student's t-test denotes by *p≤0.05. Significant two-ANOVA treatment effects denoted by #p≤0.05.

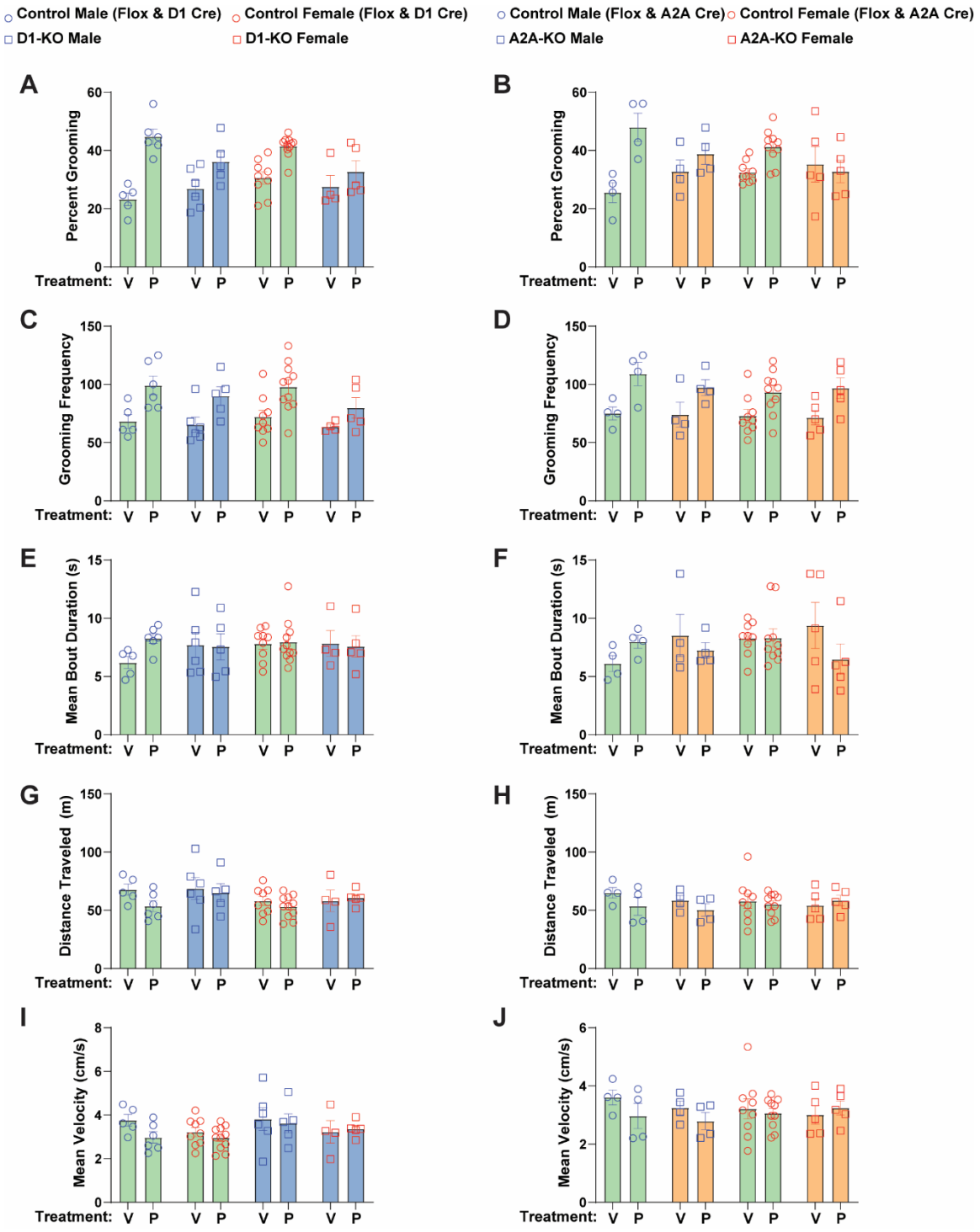
Control Male (Flox & D1 Cre)
Control Female (Flox & D1 Cre)
D1-KO Male
D1-KO Female
Control Male (Flox & A2A Cre)
Control Female (Flox & A2A Cre)
A2A-KO Male
A2A-KO Female
A
B
C
D
E
F
G
H
I
J
Percent Grooming
Grooming Frequency
Mean Bout Duration (s)
Distance Traveled (m)
Mean Velocity (cm/s)
Treatment: V P V P V P V P

Figure 24: mGluR5 PAM Grooming Visualized by Sex.

Male (blue points) and female (red points) control (Spino$^{Fl/Fl}$ and Spino$^{+/+}$-D1 or -A2A Cre) (green bars), Spino$^{\Delta dMSN}$ (blue bars), and Spino$^{\Delta iMSN}$ (orange bars) were plotted separately for **A-B.** percent grooming, **C-D.** grooming frequency, **E-F.** mean bout duration, **G-H.** distance traveled. Data ± SEM. N=4-11.

To further understand why only MSN subtype-specific spinophilin KO decreases VU'172-grooming (not Spino$^{-/-}$ or Spino$^{\Delta PanMSN}$), we performed a VU'172 dose response curve in Spino$^{Fl/Fl}$ control mice using a dose range consistent with published studies administering VU'172 in mice (Noetzel et al 2012, Notartomaso et al 2013, Zuena et al 2018). We not only found significant VU'172 treatment effects on percent grooming but determined percent grooming at low doses is driven by increased mean grooming bout duration, whereas, at high doses, percent grooming is driven by increased grooming frequency (**Figure 25A-D**). Additionally, we also analyzed these data in 5-minute bins to confirm treatment effects are not limited to a specific temporal window (**Figure 25E-H**). Although we did not find a VU'172 treatment effect on distance traveled (**Figure 25D**, **H**), we did find significant negative correlations between grooming duration and distance traveled within 5-minute bins for vehicle, 1 mg/kg, 30 mg/kg and 56 mg/kg doses (**Figure 25I**).

Given this, we treated separate cohorts of Spino$^{\Delta dMSN}$ and Spino$^{\Delta iMSN}$ with a low (1 mg/kg) and high (56 mg/kg) dose of VU'172 and combined these data with our existing 20 mg/kg data (**Figure 18B-E**) to create 4-point dose response curves for grooming duration, grooming frequency, mean grooming bout duration, and distance traveled (**Figure 26A-D**). Furthermore, we grouped these data into 5-minute bins and performed two-way ANOVAs with repeated measures to identify spinophilin genotype effects within each VU'172 dose. We determined that Spino$^{\Delta dMSN}$ decreased percent grooming at 1 and 20 mg/kg compared to control mice (**Figure 27A**). Interestingly, this decrease in percent grooming was associated with a decrease in mean grooming bout duration at 1 mg/kg (**Figure 27C**), and a trend for decreased grooming frequency at 20

mg/kg (p=0.085) (**Figure 27B**), suggesting Spino$^{\Delta dMSN}$ may decrease grooming duration by fractionating the length or initiation of grooming bouts. Although distance traveled was increased in vehicle treated Spino$^{\Delta dMSN}$ mice, we didn't find any genotype effects on distance traveled at other doses (**Figure 27D**). Furthermore, grooming duration negative correlated with distance traveled at all doses for each genotype (**Figure 28**). Interestingly, despite preventing the VU'172 treatment effect at 20 mg/kg (**Figure 18B**), we did not detect any Spino$^{\Delta iMSN}$ genotype effects on VU'172-grooming (**Figure 26**, **27**). Although this experiment was not designed to detect sex differences in grooming and locomotor behavior, we visualized these datasets by sex (**Figure 29**).

While rodent excessive grooming is one form of repetitive/stereotypic behavior, we also measured rearing behavior in our VU'172 dose response animals (**Figure 30A-B**)—another stereotypic behavior in rodents associated with striatal function (Drago et al 1994). Although rearing behavior trended downward as VU'172 dose increased, one-way ANOVA analyses did not detect a significant VU'172 treatment effect on rearing behavior. Furthermore, we also analyzed rearing behavior in 1 and 56 mg/kg-treated Spino$^{\Delta dMSN}$ and Spino$^{\Delta iMSN}$ mice (**Figure 30C-F**); however, we found no spinophilin genotype effects on rearing during the baseline (pre-injection) or post-injection periods. Therefore, these data further suggest VU'172 selectively increases self-directed repetitive behaviors, such as excessive grooming. Furthermore, these data suggest that MSN subtype-specific spinophilin KO mice specifically decrease repetitive grooming behavior without simultaneously increasing other stereotypic behaviors, such as rearing.

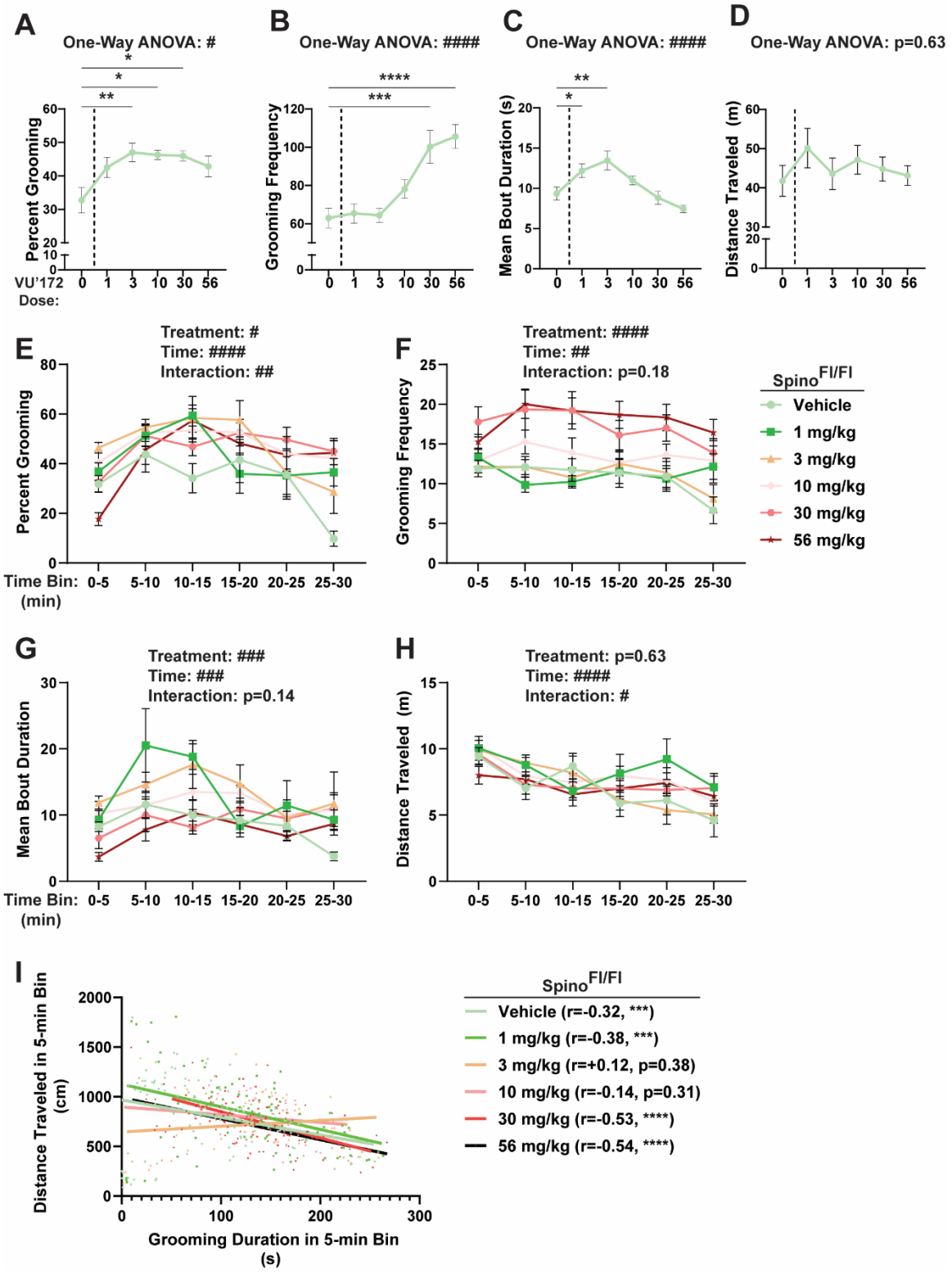
A
One-Way ANOVA: #
Percent Grooming
VU'172 Dose:
0 1 3 10 30 56
B
One-Way ANOVA: ####
Grooming Frequency
C
One-Way ANOVA: ####
Mean Bout Duration (s)
D
One-Way ANOVA: p=0.63
Distance Traveled (m)
E
Treatment: #
Time: ####
Interaction: ##
Percent Grooming
Time Bin: (min)
0-5 5-10 10-15 15-20 20-25 25-30
F
Treatment: ####
Time: ##
Interaction: p=0.18
Grooming Frequency
Spino Fl/Fl
Vehicle
1 mg/kg
3 mg/kg
10 mg/kg
30 mg/kg
56 mg/kg
G
Treatment: ###
Time: ###
Interaction: p=0.14
Mean Bout Duration
H
Treatment: p=0.63
Time: ####
Interaction: #
Distance Traveled (m)
I
Distance Traveled in 5-min Bin (cm)
Grooming Duration in 5-min Bin (s)
Spino Fl/Fl
Vehicle (r=-0.32, ***)
1 mg/kg (r=-0.38, ***)
3 mg/kg (r=+0.12, p=0.38)
10 mg/kg (r=-0.14, p=0.31)
30 mg/kg (r=-0.53, ****)
56 mg/kg (r=-0.54, ****)

Figure 25: VU'172 Dose Response in Conditional Spinophilin Control Mice. Spino$^{Fl/Fl}$ controls were treated with vehicle, 1, 3, 10, 30, or 56 mg/kg VU'172 and grooming behavior was measured as described in **Figure 18A**. One-way ANOVAs with post-hoc Dunnett's multiple comparison's test determined that **A)** percent grooming is significantly increased at 3 mg/kg (p=0.003), 10 mg/kg (p=0.011), and 30 mg/kg (p=0.017), whereas 1 mg/kg (p=0.06) and 56 mg/kg (p=0.056) VU'172 doses were trending toward a significant increase. **B)** Grooming frequency had a classical dose-response curve that significantly increased from vehicle control at 30 mg/kg (p=0.003) and 56 mg/kg (p<0.0001) VU'172. Alternatively, **C)** Mean grooming bout duration, had an inverted U-shaped dose-response curves that is significantly increased at 1 mg/kg (p=0.040) and 3 mg/kg (p=0.005) VU'172, but not 10 mg/kg, 30 mg/kg, or 56 mg/kg (p=0.52, p=0.98, p=0.28, respectively). VU'172 did not affect **D)** distance traveled (p=0.63). Two-way ANOVAs with repeated measures were performed to determine treatment and time-course effects on **E)** percent grooming, **F)** grooming frequency, **G)** mean grooming bout duration, and **H)** distance traveled grouped in 5-minute bins. **I)** Grooming duration and distance traveled within discrete 5-minute bins were correlated for each dose to determine grooming negative correlates with distance traveled in vehicle-, 1 mg/kg-, 30 mg/kg-, and 56 mg/kg-treated Spino$^{Fl/Fl}$ mice, but not at 3 mg/kg or 10 mg/kg. N=8-13 Spino$^{Fl/Fl}$ (6-9 male). Data ± SEM. Significant one- or two-way ANOVA effects denoted by #p≤0.05, ##≤p0.01, ###≤p0.001 and ####p<0.0001. Significant post-hoc tests denoted by *p≤0.05, **p≤0.01,***p≤0.001, ****p<0.0001.

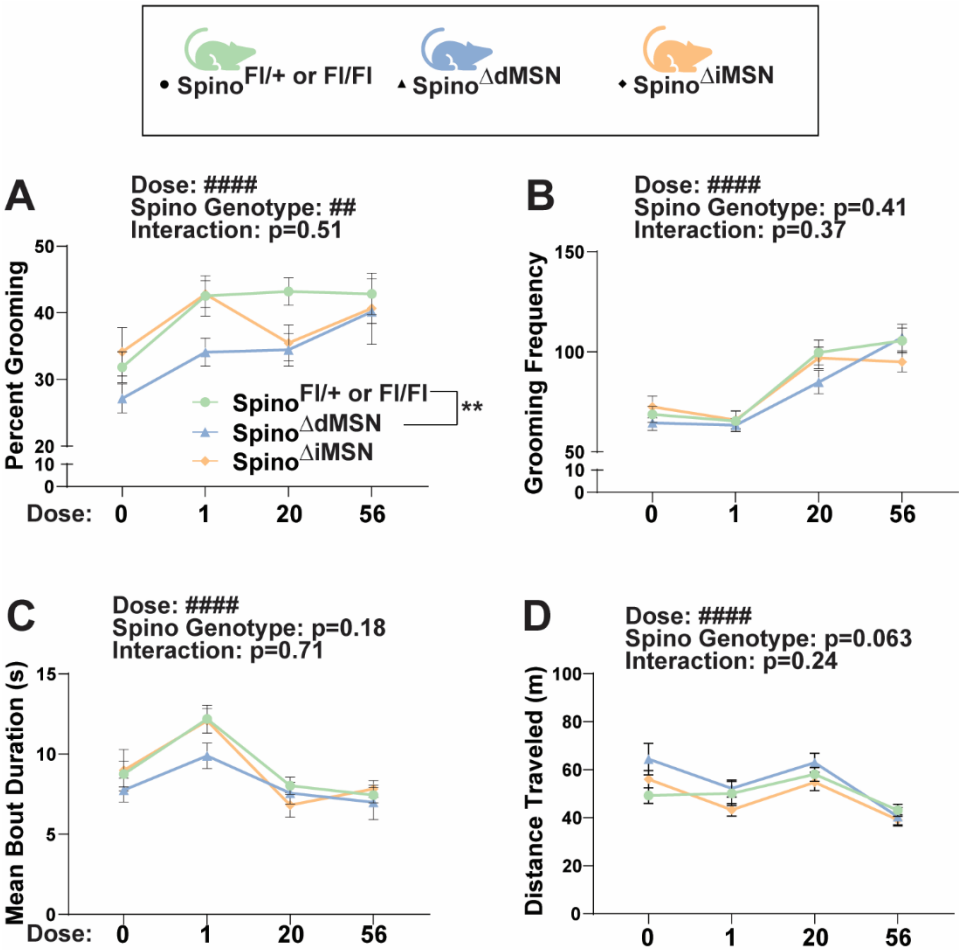
Spino Fl/+ or Fl/Fl
Spino ΔdMSN
Spino ΔiMSN
A
Dose: ####
Spino Genotype: ##
Interaction: p=0.51
Percent Grooming
Spino Fl/+ or Fl/Fl
Spino ΔdMSN
Spino ΔiMSN
**
Dose: 0 1 20 56
B
Dose: ####
Spino Genotype: p=0.41
Interaction: p=0.37
Grooming Frequency
C
Dose: ####
Spino Genotype: p=0.18
Interaction: p=0.71
Mean Bout Duration (s)
D
Dose: ####
Spino Genotype: p=0.063
Interaction: p=0.24
Distance Traveled (m)

Figure 26: Spinophilin MSN Subtype-Specifically Decreases mGluR5-Dependent Grooming.

Separate cohorts of Spino$^{Fl/Fl}$ control, Spino$^{\Delta dMSN}$, and Spino$^{\Delta iMSN}$ mice were treated with vehicle, 1, or 56 mg/kg VU'172 and combined with existing 20 mg/kg data (B-D) to generate 4-point dose response curves. Two-way ANOVAs with post-hoc Dunnett's multiple comparisons tests determined **A)** percent grooming was significantly decreased in Spino$^{\Delta dMSN}$ relative to Spino$^{Fl/Fl}$ control (p=0.004), but Spino$^{\Delta iMSN}$ was not different (0.56). However, spinophilin genotype did not significantly affect **B)** grooming frequency, **C)** mean grooming bout duration, **D)** distance traveled. N=11-22 Spino$^{Fl/Fl\ or\ Fl/+}$ (8-14 male), 8-11 Spino$^{\Delta dMSN}$ (4-6 male), and 9-11 Spino$^{\Delta iMSN}$ (2-5 male). Data ± SEM. Significant two-ANOVA effects denoted by ##p≤0.01 and ####p<0.0001. Significant post-hoc tests denoted by **p≤0.01.

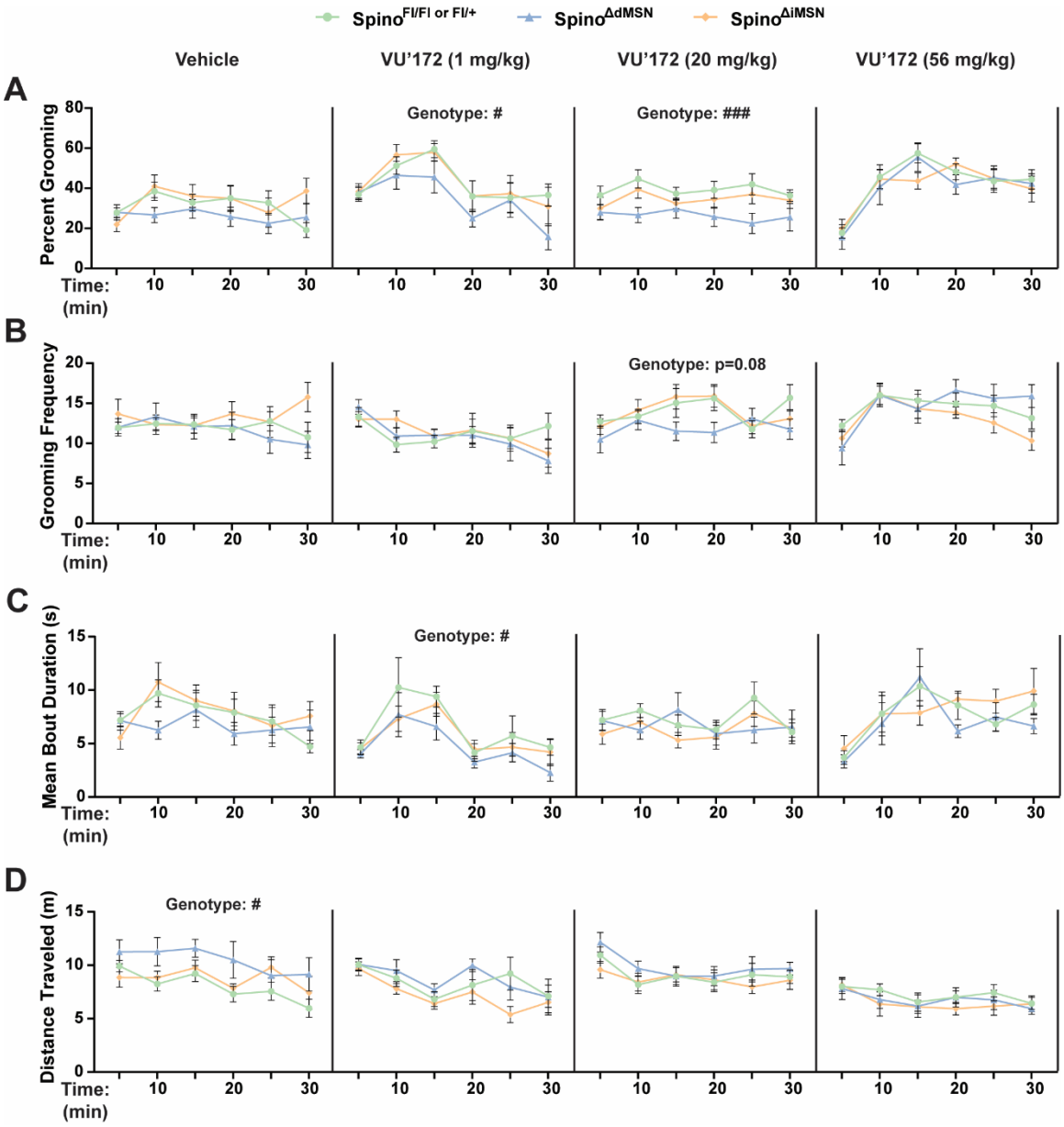
Spino^Fl/Fl or Fl/+
Spino^ΔdMSN
Spino^ΔiMSN
Vehicle
VU'172 (1 mg/kg)
VU'172 (20 mg/kg)
VU'172 (56 mg/kg)
A
Percent Grooming
Genotype: #
Genotype: ###
B
Grooming Frequency
Genotype: p=0.08
C
Mean Bout Duration (s)
Genotype: #
D
Distance Traveled (m)
Genotype: #
Time: (min)

Figure 27: Spinophilin MSN Subtype-Specific Knockout Genotype Effects on Open Field Behavior Following Treatment with Vehicle, 1 mg/kg, 20 mg/kg, and 56 mg/kg VU'172. **A)** Percent grooming, **B)** grooming frequency, **C)** mean grooming bout duration, and **D)** distance traveled from 30-minute post-injection period was analyzed in 5-minute bins for vehicle-, 1 mg/kg-, 20 mg/kg-, and 56 mg/kg-treated $Spino^{Fl/Fl\ or\ Fl/+}$, $Spino^{\Delta dMSN}$, and $Spino^{\Delta iMSN}$ mice. Two-way ANOVAs with repeated measures identified significant spinophilin genotype effects on percent grooming at 1 mg/kg ($p=0.034$) and 20 mg/kg ($p=0.0008$), mean grooming bout duration at 1 mg/kg ($p=0.048$), and distance traveled in vehicle-treated mice ($p=0.045$). Post-hoc Dunnett's multiple comparisons tests determined $Spino^{\Delta dMSN}$ significantly decreased percent grooming at 1 mg/kg ($p=0.042$), percent grooming at 20 mg/kg ($p=0.0004$), mean grooming bout duration at 1 mg/kg ($p=0.027$), and increased distance traveled following vehicle treatment ($p=0.026$). N=11-22 $Spino^{Fl/Fl\ or\ Fl/+}$ (8-14 male), 8-11 $Spino^{\Delta dMSN}$ (4-6 male), and 9-11 $Spino^{\Delta iMSN}$ (2-5 male). Data ± SEM. Significant two-ANOVA effects denoted by #$p \leq 0.05$ and ####$p<0.0001$.

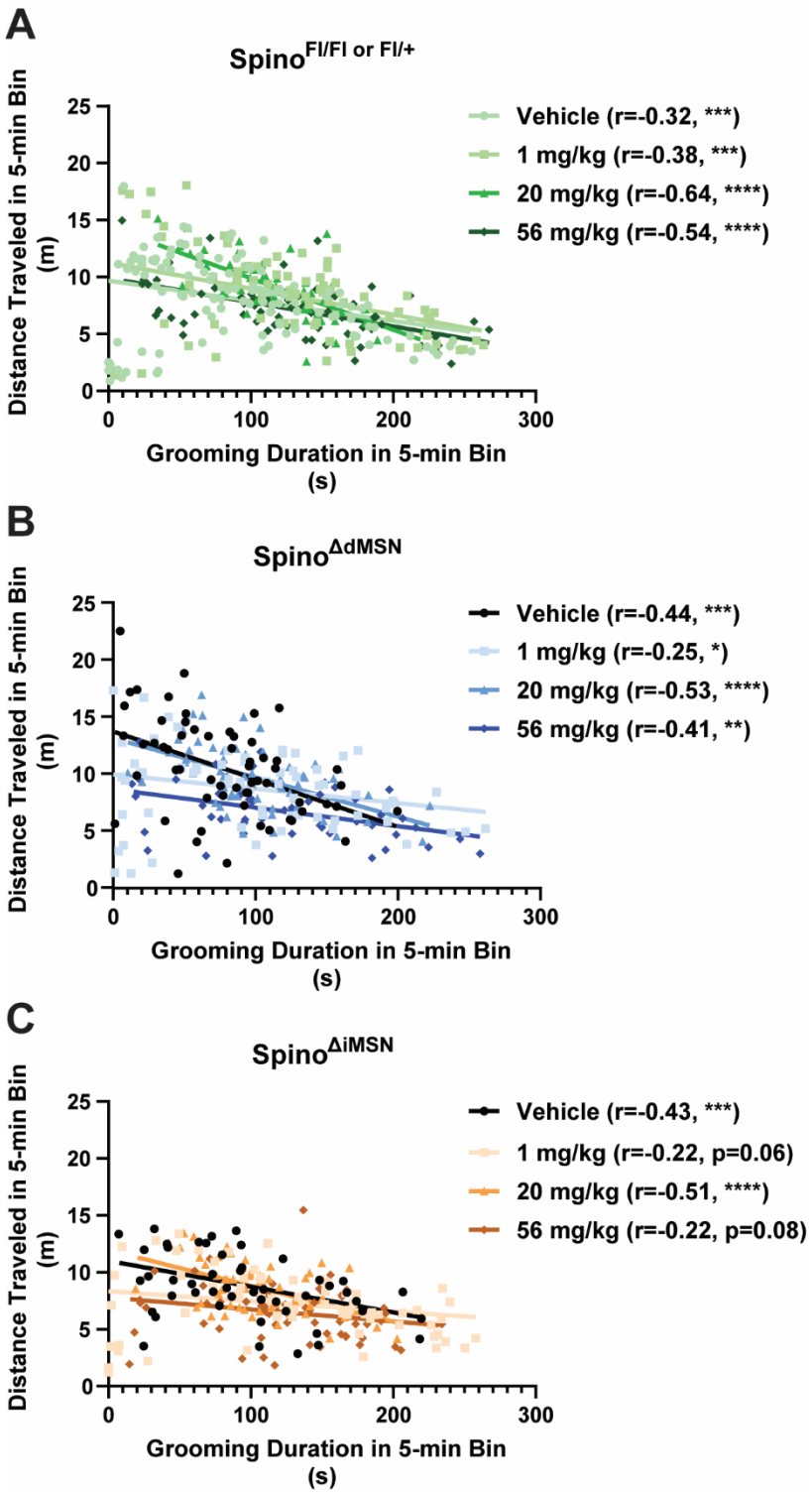
A
Spino^Fl/Fl or Fl/+
Distance Traveled in 5-min Bin (m)
Grooming Duration in 5-min Bin (s)
Vehicle (r=-0.32, ***)
1 mg/kg (r=-0.38, ***)
20 mg/kg (r=-0.64, ****)
56 mg/kg (r=-0.54, ****)
B
Spino^ΔdMSN
Distance Traveled in 5-min Bin (m)
Grooming Duration in 5-min Bin (s)
Vehicle (r=-0.44, ***)
1 mg/kg (r=-0.25, *)
20 mg/kg (r=-0.53, ****)
56 mg/kg (r=-0.41, **)
C
Spino^ΔiMSN
Distance Traveled in 5-min Bin (m)
Grooming Duration in 5-min Bin (s)
Vehicle (r=-0.43, ***)
1 mg/kg (r=-0.22, p=0.06)
20 mg/kg (r=-0.51, ****)
56 mg/kg (r=-0.22, p=0.08)

Figure 28: Grooming Duration Negatively Correlates with Distance Traveled in All Genotypes.

Grooming duration and distance traveled within discrete 5-minute bins were correlated for each dose and genotype. **A)** Pearson's correlation analysis determined grooming duration negatively correlates with distance traveled in vehicle- ($p=0.0003$), 1 mg/kg- ($p=0.0005$), 20 mg/kg- ($p<0.0001$), and 56 mg/kg- ($p<0.0001$) treated 11-22 $Spino^{Fl/Fl\ or\ Fl/+}$ mice. **B)** We also detected significant negative correlations between grooming duration and distance traveled in vehicle- ($p=0.0004$), 1 mg/kg- ($p=0.04$), 20 mg/kg- ($p<0.0001$), and 56 mg/kg- ($p=0.003$) treated $Spino^{\Delta dMSN}$ mice. However, **C)** we only detected significant negative correlations in vehicle- ($p=0.0009$) and 20 mg/kg- ($p<0.0001$) treated $Spino^{\Delta iMSN}$ mice. N=11-22 $Spino^{Fl/Fl\ or\ Fl/+}$ (8-14 male), 8-11 $Spino^{\Delta dMSN}$ (4-6 male), and 9-11 $Spino^{\Delta iMSN}$ (2-5 male). Data ± SEM. Significant Pearson correlation coefficients denoted by *$p\leq0.05$, **$p\leq0.01$, ***$p\leq0.001$, ****$p<0.0001$.

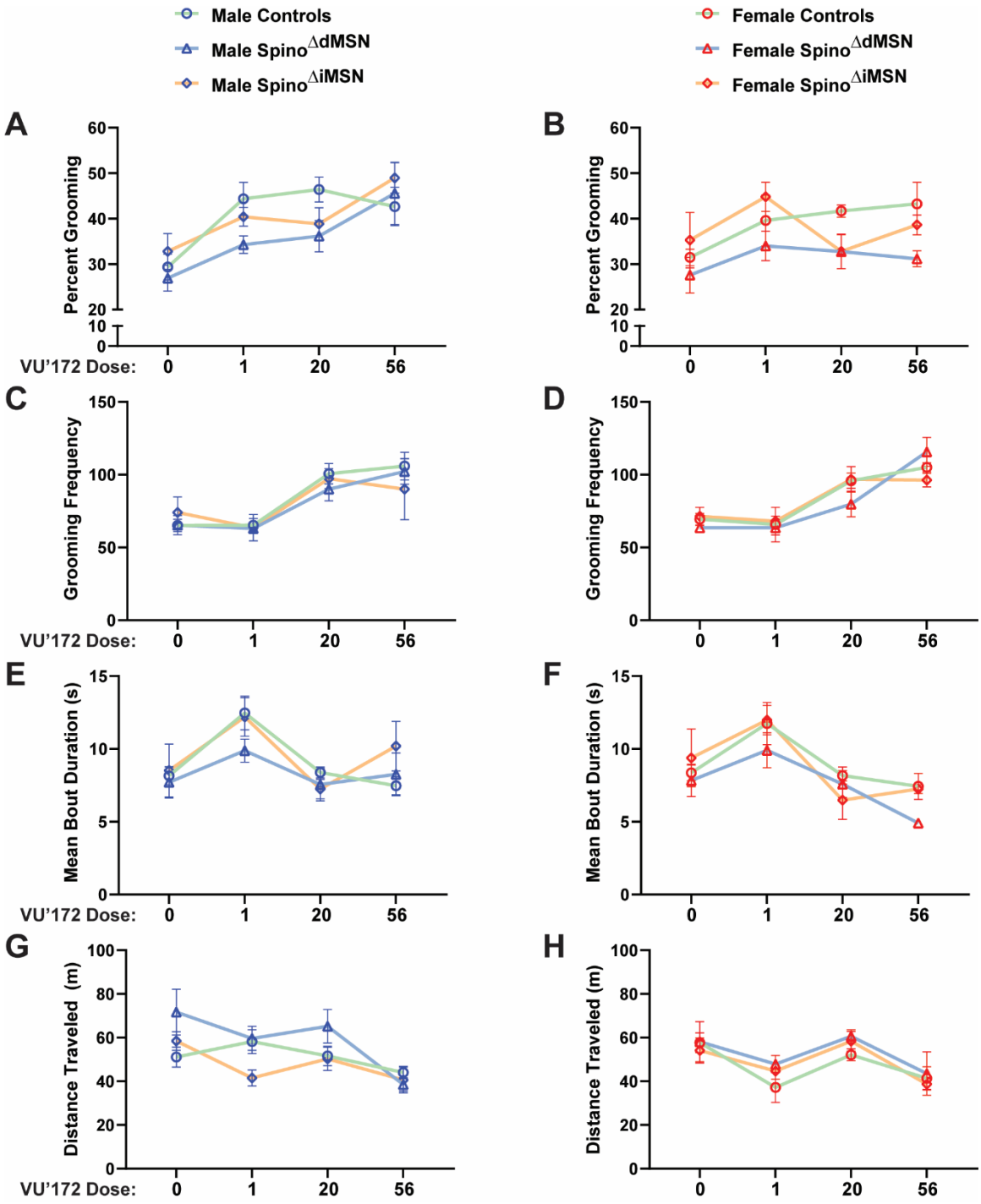
Male Controls
Male Spino$^{\Delta dMSN}$
Male Spino$^{\Delta iMSN}$
Female Controls
Female Spino$^{\Delta dMSN}$
Female Spino$^{\Delta iMSN}$
A
B
C
D
E
F
G
H
Percent Grooming
Grooming Frequency
Mean Bout Duration (s)
Distance Traveled (m)
VU'172 Dose:
0
1
20
56

Figure 29: VU'172 Dose Response Curves Visualized by Sex.

Male (blue points) and female (red points) control (Spino$^{Fl/Fl}$ and Spino$^{+/+}$-D1 or -A2A Cre) (green lines), Spino$^{\Delta dMSN}$ (blue lines), and Spino$^{\Delta iMSN}$ (orange lines) were plotted separately for **A-B.** percent grooming, **C-D.** grooming frequency, **E-F.** mean bout duration, **G-H.** distance traveled. Data ± SEM. N=2-15 male and 3-14 female.

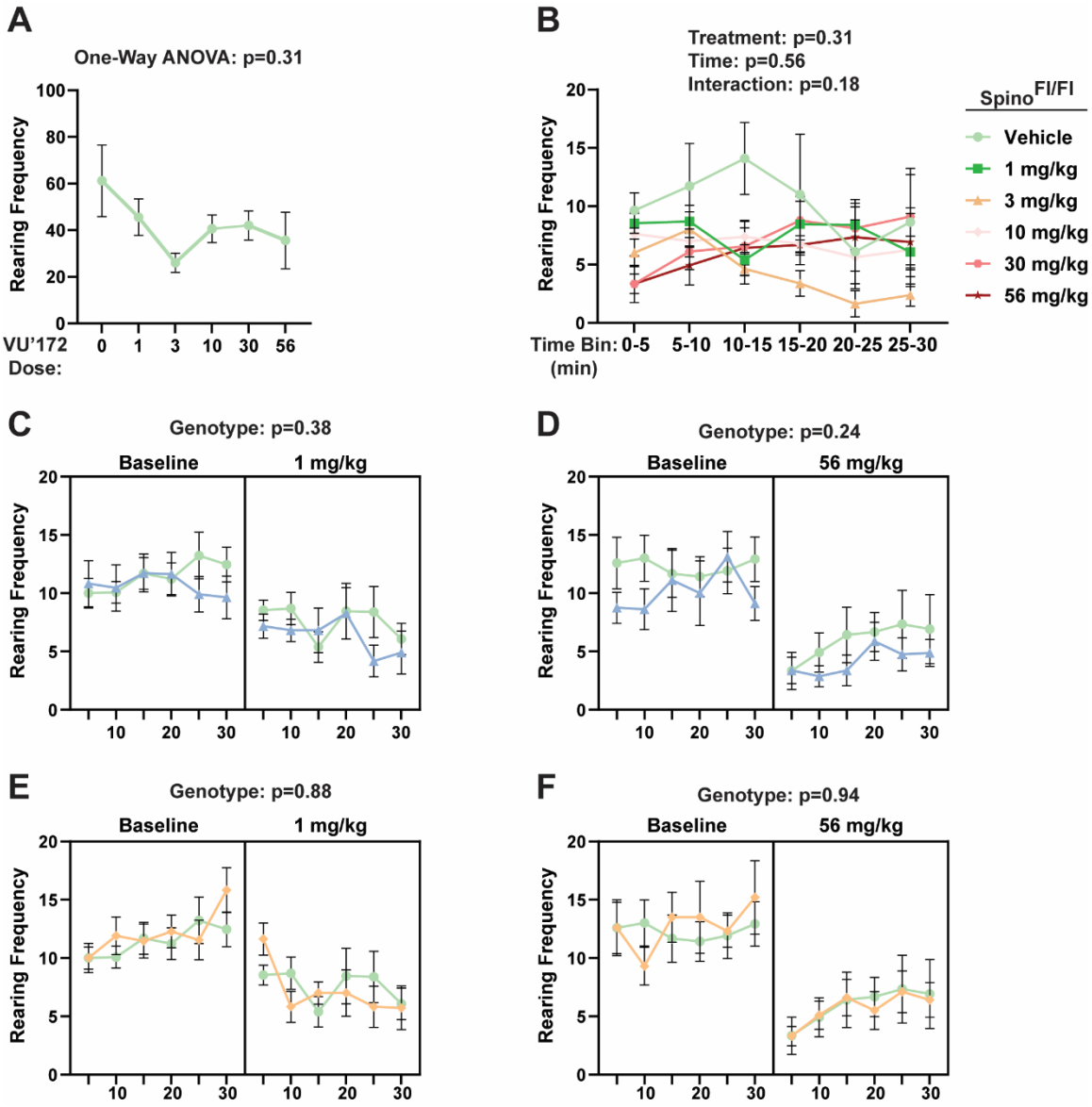
A
One-Way ANOVA: p=0.31
Rearing Frequency
VU'172 Dose:
0 1 3 10 30 56
B
Treatment: p=0.31
Time: p=0.56
Interaction: p=0.18
Rearing Frequency
Time Bin: (min)
0-5 5-10 10-15 15-20 20-25 25-30
Spino Fl/Fl
Vehicle
1 mg/kg
3 mg/kg
10 mg/kg
30 mg/kg
56 mg/kg
C
Genotype: p=0.38
Baseline
1 mg/kg
D
Genotype: p=0.24
Baseline
56 mg/kg
E
Genotype: p=0.88
Baseline
1 mg/kg
F
Genotype: p=0.94
Baseline
56 mg/kg

Figure 30: Spinophilin and VU'172 Do Not Significantly Affect Rearing in Open Field. **A)** One-way ANOVA was performed to determine vehicle, 1 mg/kg, 3 mg/kg, 10 mg/kg, 30 mg/kg and 56 mg/kg VU'172 treatment does not affect rearing frequency in open field (p=0.31). **B)** Rearing behavior from 30-minute post-injection period was grouped into 5-minute bins. Two-way ANOVA with repeated measures did not detect significant treatment (p=0.31), time (p=0.56), or treatment x time interaction (p=0.17) effects. N=8-13 $Spino^{Fl/Fl}$ (6-9 male). Three-way ANOVAs with repeated measures were performed to determine spinophilin genotype effects on rearing frequency in 5-minute bins during the pre-injection (baseline) and post-injection periods. We did not detect genotype affects when comparing $Spino^{Fl/Fl\ or\ Fl/+}$ and $Spino^{\Delta dMSN}$ mice at **C)** 1 mg/kg or **D)** 56 mg/kg VU'172, nor did we detect genotype affects when comparing $Spino^{Fl/Fl\ or\ Fl/+}$ and $Spino^{\Delta iMSN}$ mice at **E)** 1 mg/kg or **F)** 56 mg/kg VU'172. N=11-22 $Spino^{Fl/Fl\ or\ Fl/+}$ (8-14 male), 8-11 $Spino^{\Delta dMSN}$ (4-5 male), and 10-11 $Spino^{\Delta iMSN}$ (2-5 male). Data ± SEM.

5.3 Discussion

Here, we report that loss of spinophilin increases mGluR5 protein interactions with striatal PSD scaffolding proteins implicated in psychiatric disorders, including SAPAP3 and SHANK3. Given that decreased mGluR5 interactions with SAPAP3 or SHANK3 is associated with excessive grooming, we hypothesized a unique role for spinophilin in mediating mGluR5-dependent overgrooming. We further confirmed this hypothesis by demonstrating MSN subtype-specific spinophilin KO mice display decreased grooming (relative to vehicle) when treated with VU'172—a mGluR5-specific PAM that augments grooming behavior in mice. However, we unexpectedly found that only Spino$^{\Delta dMSN}$ mice had decreased VU'172-grooming; whole-body spinophilin KO mice and mice lacking spinophilin in both MSN subtypes had increased grooming similar to controls.

5.3.1 Leveraging Proteomics to Predict Mechanisms by Which Spinophilin Regulates mGluR5

Spinophilin knockout-derived primary cortical neurons have increased mGluR5-dependent MAPK signaling, intracellular calcium (Ca^{2+}) mobilization, and mGluR5 endocytosis (Di Sebastiano et al 2016). Loss of spinophilin significantly upregulated striatal mGluR5 phosphorylation at Ser860 and Ser1016, protein kinase A (PKA) and CaMKII consensus sites, respectively (Raka et al 2015). mGluR5 phosphorylation was also upregulated (Abundance Ratio (Log2) > 0.2) at Ser839 and Ser908, protein kinase C (PKC) sites (Kim et al 2005, Lee et al 2008). Although the function of mGluR5 Ser860 phosphorylation is unknown, phosphorylation of Ser1016, 839, and 908 promote increased MAPK signaling, intracellular Ca^{2+} mobilization, and mGluR5 endocytosis

(Gereau & Heinemann 1998, Kim et al 2005, Ko et al 2012, Lee et al 2008, Raka et al 2015). While these data suggest spinophilin regulates striatal mGluR5 signaling and function in a manner similar to primary cortical neurons (Di Sebastiano et al 2016), future studies will be needed to directly measure spinophilin-dependent changes in mGluR5 signaling and endocytosis in mouse striatum. Furthermore, future studies will determine the extent to which spinophilin-dependent changes in mGluR5 phosphorylation govern its signaling, interactions, and localization within the postsynaptic membrane.

In addition to mGluR5, we also detected increased SHANK3 and SAPAP2 co-IP phosphopeptides in spinophilin knockout striatum—proteins with strong genetic associations with autism spectrum disorders (ASDs) and/or OCSDs (Chien et al 2013, Durand et al 2007, Marshall et al 2008, Pinto et al 2010, Prasad et al 2000, Wilson et al 2003, Wu et al 2013). However, SHANK3 and SAPAP2 co-IP phosphopeptides were only detected in TMT-LC/MS run 1, highlighting documented variability in co-IP quantitative proteins (Stein et al 2019). Given this, future studies will further validate these phosphorylation changes and delineate how changes in mGluR5, SHANK3, or SAPAP phosphorylation modulate mGluR5's protein interactions with striatal PSD proteins.

5.3.2 Spinophilin Organizes the mGluR5 Proteome

Excessive grooming in both SAPAP3 KO and SHANK3 complete KO mice—preclinical models for understanding OCSDs and ASDs, respectively—is decreased by mGluR5 NAMs. Grooming dysfunction in both these preclinical models is associated with decreased mGluR5 scaffolding to PSD proteins (Ade et al 2016, Wang et al 2016).

Strikingly, in addition to MSN subtype-specific spinophilin knockout decreasing mGluR5-depenent excessive grooming, loss of spinophilin in the striatum increased mGluR5 interactions with PSD scaffolding proteins implicated in psychiatric disorders, including SAPAP3 and SHANK3, and decreased mGluR5 interactions with lipid raft-associated membrane proteins. Not only is lipid raft dysfunction associated with psychiatric disorders like the ASD, fragile X syndrome (FXS) (Kalinowska et al 2015, Ronesi et al 2012, Toupin et al 2022, Wang 2014), mGluR5 can differentially signal depending on its interactions with lipid raft signaling complexes or PSD scaffolding proteins (Francesconi et al 2009, Mao et al 2005b, Tu et al 1998). Specifically, mGluR5 interactions with lipid raft complexes attenuates MAPK signaling (Francesconi et al 2009) whereas mGluR5's interaction with Homer1, which couples mGluR5 into the PSD, is associated with agonist-induced increases in MAPK signaling and intracellular Ca^{2+} mobilization (Mao et al 2005b, Tu et al 1998), pathways increased in spinophilin knockout mice (Areal et al 2019, Di Sebastiano et al 2016). While the signaling pathways underlying mGluR5-dependent excessive grooming have not been identified, we hypothesize that our MSN subtype-specific spinophilin knockout mice can elucidate which mGluR5 signaling pathway(s) cause excessive grooming, results that may hold broad therapeutic potential across mGluR5-opathies.

5.3.3 Spinophilin Regulates mGluR5-Dependent Excessive Grooming Cell Type-Specifically

Given that MSN subtype-specific spinophilin knockout prevented excessive grooming in SAPAP3 KO mice (see chapter 4) and VU'172-treated mice (20 mg/kg), it was unexpected that whole-body loss of spinophilin failed to decrease VU'172 grooming.

We further confirmed this by detecting a significant VU'172 grooming response despite depleting spinophilin from both MSN subtypes (Spino$^{\Delta PanMSN}$). Given that repetitive behaviors are associated with an imbalance in dMSN/iMSN activity (see **Table 1**), we reasoned it is possible that Spino$^{\Delta dMSN}$ and Spino$^{\Delta iMSN}$ have bidirectional or antagonistic effects on striatal output, such that loss of spinophilin from both MSNs has no net effect on striatal output. Alternatively, it is also possible that in Spino$^{-/-}$ or Spino$^{\Delta PanMSN}$ mice, a higher-order mechanism outside striatal MSNs overrides decreased VU'172 grooming in Spino$^{\Delta dMSN}$ and Spino$^{\Delta iMSN}$ mice.

To understand why Spino$^{\Delta PanMSN}$ doesn't impact VU'172 grooming, we first analyzed a VU'172 dose-response curve (DRC) in Spino$^{Fl/Fl}$ control mice. We found that percent grooming was significantly increased at 3, 10, and 30 mg/kg doses of VU'172; however, at low (1 mg/kg) and high (56 mg/kg) doses of VU'172, percent grooming was trending upward (1 mg/kg) or downward (56 mg/kg) and not significantly different from vehicle, suggesting a subtle inverted U-shaped DRC (**Figure 25A**). Interestingly, we found that increased grooming duration at low doses (1 and 3 mg/kg) is driven by prolonged grooming bouts (mean bout duration), whereas at high doses (30 and 56 mg/kg), increased grooming duration is driven by increased initiation of grooming bouts (grooming frequency). We further confirmed these unique VU'172 effects on grooming behavior is consistent throughout the 30-minute recording session (**Figure 25E-H**), suggesting unique mechanisms may drive grooming at 3 mg/kg versus 30 mg/kg VU'172.

Given the subtly inverted U-shaped percent grooming DRC, we reasoned it is possible that Spino$^{\Delta dMSN}$ and Spino$^{\Delta iMSN}$ mice bidirectionally regulate VU'172 grooming, such that loss of spinophilin in one MSN subtype decreases, whereas loss in the other MSN subtype increases the VU'172 grooming response. This possibility is consistent with studies suggesting spinophilin prevents GPCR desensitization and VU'172 increases mGluR5 desensitization in cultured striatal neurons (Hellyer et al 2019, Wang et al 2004). Therefore, to understand the directionality by which Spino$^{\Delta dMSN}$ and Spino$^{\Delta iMSN}$ regulate the VU'172 grooming response, we treated these genotypes with a 1 mg/kg or 56 mg/kg VU'172—doses where percent grooming was trending upward (1 mg/kg) or downward (56 mg/kg) but not significantly different from vehicle (**Figure 25A**). Next, we combined these data with data from the existing 20 mg/kg VU'172 experiment (**Figure 18**) to generate 4-point VU'172 DRCs for control, Spino$^{\Delta dMSN}$, and Spino$^{\Delta iMSN}$ mice (**Figure 26**). We also analyzed these behavior data in 5-minute bins to identify spinophilin genotype effects at each dose individually (**Figure 27**). We found that Spino$^{\Delta dMSN}$ mice had significantly decreased percent grooming at 1 mg/kg and 20 mg/kg VU'172. Furthermore, we found that decreased percent grooming in Spino$^{\Delta dMSN}$ mice was associated with decreased mean grooming bout duration at 1 mg/kg VU'172; however, identifying how Spino$^{\Delta dMSN}$ decreased percent grooming at 20 mg/kg is less clear. Specifically, we only found a trend ($p=0.08$) for decreased grooming frequency at 20 mg/kg VU'172, suggesting Spino$^{\Delta dMSN}$ may decrease grooming duration by regulating grooming frequency in combination with other aspects of grooming microstructure, such as an interaction between grooming frequency or mean grooming bout duration. In contrast to Spino$^{\Delta dMSN}$, we did not detect any Spino$^{\Delta iMSN}$ genotype effects on VU'172.

Although grooming behavior wasn't decreased overall, it is worth noting that the VU'172 treatment effect was completely abrogated in Spino$^{\Delta iMSN}$ mice at 20 mg/kg (**Figure 18**). Moreover, we did not detect a treatment effect at 1 mg/kg or 56 mg/kg VU'172 compared to vehicle treated Spino$^{\Delta iMSN}$ mice (**Figure 26A**), however, we did not find a significant dose X genotype interaction effect. Despite these limitations, we hypothesize that Spino$^{\Delta iMSN}$ may cause a ceiling effect on motor output that prevents behavioral adaptations associated with striatal function.

Overall, based off these data, we suggest that spinophilin expression in dMSNs increases grooming duration by sustaining the duration of grooming bouts, whereas spinophilin expression in iMSNs is critical for mediating the VU'172 treatment effect on grooming duration. However, these MSN subtype-specific spinophilin roles are not additive, but rather antagonistic (at least at 20 mg/kg), such that loss of spinophilin from both MSN subtypes does not affect increased grooming caused by VU'172.

5.3.4 Limitations and Future Directions

Some of the major experimental design limitations of this study are 1) grooming caused by injection of vehicle, and 2) administering VU'172 globally to measure striatal function. First, grooming caused by the I.P. injection is likely associated with anxiety or stress-related brain regions, such as the amygdala or hypothalamus via increased hormone signaling (Dunn 1988, Dunn et al 1987, Dunn et al 1979, Hong et al 2014, Roeling et al 1993). Despite this limitation, both knockout and pharmacological inhibition of mGluR5 decrease grooming caused by the vehicle I.P. injection (Ade et al 2016). While these studies further suggest mGluR5 function is associated with increased grooming behavior, to date, the specific regions and/or cell types by which mGluR5

functions in to promote increased grooming is unknown. This limitation is amplified by the fact that we administered VU'172 globally to cause repetitive grooming; it is unclear where this drug is acting in the CNS to drive the grooming response. One strategy to overcome both of these limitations is by microinjecting VU'172 into the rodent striatum. This experiment would eliminate the grooming response from the I.P injection while also directly testing the sufficiency of mGluR5 in the striatum to promote increased grooming. Alternatively, microinjecting an mGluR5 antagonist into the striatum prior to administering vehicle or VU'172 via I.P. injection would further test the necessity of mGluR5 function in the striatum for mediating grooming caused by the injection and/or VU'172. Despite these limitations, here, we utilized D1- and A2A-Cre to specifically deplete spinophilin expression from striatal dMSNs and iMSNs, respectively, thus suggesting spinophilin-dependent effects on VU'172 grooming are associated with changes in striatal function. However, as described in chapter 4, we cannot rule out the possibility that spinophilin mediates repetitive grooming by functioning in cell types outside the striatum that express D1- or A2A-Cre. Furthermore, we cannot conclude that decreased grooming in Spino$^{\Delta dMSN}$ mice, or the abrogated treatment response in Spino$^{\Delta iMSN}$ mice, is due to spinophilin functioning cell-autonomously in dMSNs or iMSNs, respectively.

In addition to microinjection experiments, viral repletion of spinophilin expression in striatal dMSNs or iMSNs is another future direction capable of determining if spinophilin mediates VU'172 grooming by function cell autonomously. Furthermore, in-vivo cell type-specific measurement of mGluR5 signaling will be imperative to detail signaling pathways underlying repetitive grooming behavior. Overall, based off the data

presented herein, we hypothesize that MSN subtype-specific spinophilin knockout disrupts complex sequential motor programs without impacting overall locomotor output, such as basal or hypolocomotion. Due to this, we postulate that our novel MSN subtype-specific spinophilin knockout models are a critical tool to elucidate unique cell autonomous and/or non-autonomous signaling pathways underlying the initiation and/or sustainment of sequential motor programs.

14	**B**	mGluR5 Immunodepletion	Repeated Measures Two-way ANOVA	Genotype: F (1, 8) = 0.0009	p=0.97
				Depletion: F (2, 16) = 142.8	p<0.0001
				Interaction: F (2, 16) = 0.8418	p=0.44
	C	mGluR5 expression	Unpaired t-test	t=0.5651, df=8	p=0.58
18	**B**	VU'172 (20 mg/kg): Percent grooming	Two-way ANOVA	Treatment: F (1, 66) = 31.23	p<0.0001
				Genotype: F (3, 66) = 1.882	p=0.14
				Interaction: F (3, 66) = 3.858	p=0.013
	C	VU'172 (20 mg/kg): Grooming frequency	Two-way ANOVA	Treatment: F (1, 66) = 46.25	p<0.0001
				Genotype: F (3, 66) = 2.453	p=0.071
				Interaction: F (3, 66) = 1.439	p=0.239
	D	VU'172 (20 mg/kg): Mean bout duration	Two-way ANOVA	Treatment: F (1, 66) = 0.7413	p=0.39
				Genotype: F (3, 66) = 0.5025	p=0.68
				Interaction: F (3, 66) = 1.225	p=0.30
	E	VU'172 (20 mg/kg): Distance traveled	Two-way ANOVA	Treatment: F (1, 66) = 4.120	p=0.046
				Genotype: F (3, 66) = 3.412	p=0.022
				Interaction: F (3, 66) = 3.222	p=0.028
19	**A**	Pre-injection: Percent grooming	Two-way ANOVA	Treatment group: F (1, 64) = 0.6927	p=0.69
				Genotype: F (3, 64) = 4.406	p=0.007
				Interaction: F (3, 64) = 0.4551	p=0.71
	B	Pre-injection: Distance traveled	Two-way ANOVA	Treatment group: F (1, 64) = 0.3794	p=0.54
				Genotype: F (3, 64) = 16.30	p<0.0001
				Interaction: F (3, 64) = 1.801	p=0.156

20	**NA**	Cre Controls: Percent grooming	Two-way ANOVA	Treatment: F (1, 35) = 50.11	p<0.0001
				Cre: F (1, 35) = 0.05491	p=0.81
				Interaction: F (1, 35) = 0.6792	p=0.41
21	**A**	Control: Percent grooming	Repeated Measures Two-way ANOVA	Treatment: F (1, 17) = 15.32	p=0.0011
				Time bin: F (3.534, 60.08) = 0.6898	p=0.58
				Interaction: F (5, 85) = 0.2616	p=0.93
	B	Spino$^{\Delta dMSN}$: Percent grooming	Repeated Measures Two-way ANOVA	Treatment: F (1, 18) = 3.772	p=0.06
				Time bin: F (3.453, 62.15) = 1.043	p=0.38
				Interaction: F (5, 90) = 1.143	p=0.34
	C	Spino$^{\Delta iMSN}$: Percent grooming	Repeated Measures Two-way ANOVA	Treatment: F (1, 16) = 0.05484	p=0.81
				Time bin: F (2.665, 42.64) = 2.278	p=0.099
				Interaction: F (5, 80) = 0.9148	p=0.47
	D	Spino$^{-/-}$: Percent grooming	Repeated Measures Two-way ANOVA	Treatment: F (1, 14) = 22.56	p=0.0003
				Time bin: F (5, 70) = 3.650	p=0.0054
				Interaction: F (5, 70) = 0.4508	p=0.81
	E	Control: Grooming frequency	Repeated Measures Two-way ANOVA	Treatment: F (1, 17) = 8.124	p=0.011
				Time bin: F (3.408, 57.94) = 1.417	p=0.24
				Interaction: F (5, 85) = 1.384	p=0.238

21	**F**	Spino$^{\Delta dMSN}$: Grooming frequency	Repeated Measures Two-way ANOVA	Treatment: F (1, 18) = 7.417	p=0.013
				Time bin: F (3.677, 66.19) = 0.6095	p=0.64
				Interaction: F (5, 90) = 0.6939	p=0.62
	G	Spino$^{\Delta iMSN}$: Grooming frequency	Repeated Measures Two-way ANOVA	Treatment: F (1, 16) = 13.88	p=0.0018
				Time bin: F (3.725, 59.59) = 1.044	p=0.389
				Interaction: F (5, 80) = 1.738	p=0.135
	H	Spino$^{-/-}$: Grooming frequency	Repeated Measures Two-way ANOVA	Treatment: F (1, 14) = 23.83	p=0.0002
				Time bin: F (5, 70) = 3.451	p=0.007
				Interaction: F (5, 70) = 0.2891	p=0.91
	I	Control: Mean bout duration	Repeated Measures Two-way ANOVA	Treatment: F (1, 17) = 1.842	p=0.19
				Time bin: F (3.982, 67.70) = 0.9067	p=0.46
				Interaction: F (5, 85) = 1.108	p=0.36
	J	Spino$^{\Delta dMSN}$: Mean bout duration	Repeated Measures Two-way ANOVA	Treatment: F (1, 18) = 0.1006	p=0.75
				Time bin: F (4.170, 75.05) = 0.8267	p=0.51
				Interaction: F (5, 90) = 0.9509	p=0.45
	K	Spino$^{\Delta iMSN}$: Mean bout duration	Repeated Measures Two-way ANOVA	Treatment: F (1, 16) = 1.664	p=0.21
				Time bin: F (2.864, 45.83) = 1.749	p=0.17
				Interaction: F (5, 80) = 1.788	p=0.12

21	**L**	Spino$^{-/-}$: Mean bout duration	Repeated Measures Two-way ANOVA	Treatment: F (1, 14) = 0.4282	p=0.52
				Time bin: F (5, 70) = 1.262	p=0.29
				Interaction: F (5, 70) = 0.5734	p=0.72
	M	Control: Distance traveled	Repeated Measures Two-way ANOVA	Treatment: F (1, 17) = 0.1306	p=0.72
				Time bin: F (3.452, 58.69) = 2.082	p=0.10
				Interaction: F (5, 85) = 0.7348	p=0.59
	N	Spino$^{\Delta dMSN}$: Distance traveled	Repeated Measures Two-way ANOVA	Treatment: F (1, 18) = 0.2800	p=0.60
				Time bin: F (3.387, 60.96) = 2.047	p=0.10
				Interaction: F (5, 90) = 1.399	p=0.23
	O	Spino$^{\Delta iMSN}$: Distance traveled	Repeated Measures Two-way ANOVA	Treatment: F (1, 16) = 0.001950	p=0.96
				Time bin: F (2.496, 39.94) = 1.145	p=0.33
				Interaction: F (5, 80) = 1.198	p=0.31
	P	Spino$^{-/-}$: Distance traveled	Repeated Measures Two-way ANOVA	Treatment: F (1, 14) = 2.922	p=0.109
				Time bin: F (5, 70) = 2.456	p=0.041
				Interaction: F (5, 70) = 0.8232	p=0.53
22	**A**	Vehicle: Grooming vs. Locomotion	Pearson correlation	Control: r=-0.71	p<0.0001
				Spino$^{\Delta dMSN}$: r=-0.44	p=0.0004
				Spino$^{\Delta iMSN}$: r=-0.43	p=0.0009
				Spino$^{-/-}$: r=-0.45	p=0.0013
	B	Vehicle: Grooming vs. Locomotion	Pearson correlation	Control: r=-0.65	p<0.0001
				Spino$^{\Delta dMSN}$: r=-0.53	p<0.0001
				Spino$^{\Delta iMSN}$: r=-0.52	p<0.0001
				Spino$^{-/-}$: r=-0.57	p<0.0001

23	**B**	Percent grooming	Unpaired t-test	t=2.790, df=9	p=0.021
	C	Grooming frequency	Unpaired t-test	t=2.386, df=9	p=0.04
	D	Mean bout duration	Unpaired t-test	t=0.1524, df=9	p=0.88
	E	Distance traveled	Unpaired t-test	t=0.004491, df=9	p=0.99
	F	Percent grooming	Repeated Measures Two-way ANOVA	Treatment: F (1, 9) = 7.791	p=0.021
				Time bin: F (1.980, 17.82) = 1.841	p=0.18
				Interaction: F (5, 45) = 0.4045	p=0.84
	G	Grooming frequency	Repeated Measures Two-way ANOVA	Treatment: F (1, 9) = 5.846	p=0.038
				Time bin: F (2.825, 25.42) = 1.560	p=0.22
				Interaction: F (5, 45) = 1.017	p=0.41
	H	Mean bout duration	Repeated Measures Two-way ANOVA	Treatment: F (1, 9) = 0.02078	p=0.88
				Time bin: F (1.981, 17.83) = 1.029	p=0.37
				Interaction: F (5, 45) = 0.7997	p=0.55
	I	Distance traveled	Repeated Measures Two-way ANOVA	Treatment: F (1, 9) = 2.026e-005	p=0.99
				Time bin: F (3.160, 28.44) = 4.628	p=0.008
				Interaction: F (5, 45) = 0.8993	p=0.48
25	**A**	Percent grooming	One-way ANOVA	F (5, 55) = 3.190	p=0.013
	C	Grooming frequency	One-way ANOVA	F (5, 55) = 10.95	p<0.0001
	B	Mean bout duration	One-way ANOVA	F (5, 55) = 7.794	p<0.0001
	D	Distance traveled	One-way ANOVA	F (5, 55) = 0.6886	p=0.63

25	**E**	Percent grooming	Two-way ANOVA	Dose: F (5, 55) = 3.147	p=0.014
				Time bin: F (5, 275) = 11.43	p<0.0001
				Interaction: F (25, 275) = 2.135	p=0.0017
	F	Grooming frequency	Two-way ANOVA	Dose: F (5, 55) = 10.86	p<0.0001
				Time bin: F (5, 275) = 3.489	p=0.0045
				Interaction: F (25, 275) = 1.271	p=0.179
	G	Mean bout duration	Two-way ANOVA	Dose: F (5, 55) = 5.464	p=0.0004
				Time bin: F (5, 275) = 4.377	p=0.0008
				Interaction: F (25, 275) = 1.325	p=0.14
	H	Distance traveled	Two-way ANOVA	Dose: F (5, 55) = 0.6886	p=0.63
				Time bin: F (5, 275) = 17.08	p<0.0001
				Interaction: F (25, 275) = 1.764	p=0.015
	I	Grooming vs. Locomotion	Pearson Correlation	Vehicle: r=-0.32	p=0.0003
				1 mg/kg: r=-0.38	p=0.0005
				3 mg/kg: r=+0.12	p=0.38
				10 mg/kg: r=-0.14	p=0.31
				30 mg/kg: r=-0.53	p<0.0001
				56 mg/kg: r=-0.54	p<0.0001
26	**A**	Percent grooming	Two-way ANOVA	Dose: F (3, 124) = 7.807	p<0.0001
				Genotype: F (2, 124) = 4.931	p=0.008
				Interaction: F (6, 124) = 0.8824	p=0.51

26	**B**	Grooming frequency	Two-way ANOVA	Dose: F (3, 124) = 36.81	p<0.0001
				Genotype: F (2, 124) = 0.8918	p=0.41
				Interaction: F (6, 124) = 1.086	p=0.37
	C	Mean bout duration	Two-way ANOVA	Dose: F (3, 124) = 14.84	p<0.0001
				Genotype: F (2, 124) = 1.732	p=0.18
				Interaction: F (6, 124) = 0.6153	p=0.71
	D	Distance traveled	Two-way ANOVA	Dose: F (3, 121) = 11.96	p<0.0001
				Genotype: F (2, 121) = 2.824	p=0.063
				Interaction: F (6, 121) = 1.331	p=0.24
27	**A**	Vehicle: Percent grooming	Repeated Measures Two-way ANOVA	Genotype: F (2, 36) = 1.376	p=0.26
				Time bin: F (5, 180) = 1.449	p=0.20
				Interaction: F (10, 180) = 1.200	p=0.29
		VU'172 1 mg/kg: Percent grooming	Repeated Measures Two-way ANOVA	Genotype: F (2, 32) = 3.740	p=0.034
				Time bin: F (5, 160) = 8.255	p<0.0001
				Interaction: F (10, 160) = 0.4679	p=0.90
		VU'172 20 mg/kg: Percent grooming	Repeated Measures Two-way ANOVA	Genotype: F (2, 26) = 9.519	p=0.0008
				Time bin: F (5, 130) = 0.5771	p=0.71
				Interaction: F (10, 130) = 0.4594	p=0.91

27	**A**	VU'172 56 mg/kg: Percent grooming	Repeated Measures Two-way ANOVA	Genotype: F (2, 27) = 0.1830	p=0.18
				Time bin: F (5, 135) = 22.10	p<0.0001
				Interaction: F (10, 135) = 0.8938	p=0.54
	B	Vehicle: Grooming frequency	Repeated Measures Two-way ANOVA	Genotype: F (2, 36) = 1.135	p=0.33
				Time bin: F (5, 180) = 0.1166	p=0.98
				Interaction: F (10, 180) = 0.8091	p=0.62
		VU'172 1 mg/kg: Grooming frequency	Repeated Measures Two-way ANOVA	Genotype: F (2, 32) = 0.1122	p=0.89
				Time bin: F (5, 160) = 3.822	p=0.0027
				Interaction: F (10, 160) = 1.194	p=0.29
		VU'172 20 mg/kg: Grooming frequency	Repeated Measures Two-way ANOVA	Genotype: F (2, 26) = 2.708	p=0.085
				Time bin: F (5, 130) = 2.167	p=0.061
				Interaction: F (10, 130) = 1.303	p=0.23
		VU'172 56 mg/kg: Grooming frequency	Repeated Measures Two-way ANOVA	Genotype: F (2, 27) = 1.184	p=0.32
				Time bin: F (5, 135) = 7.438	p<0.0001
				Interaction: F (10, 135) = 1.266	p=0.25
	C	Vehicle: Mean bout duration	Repeated Measures Two-way ANOVA	Genotype: F (2, 36) = 0.5898	p=0.55
				Time bin: F (5, 180) = 2.199	p=0.056
				Interaction: F (10, 180) = 0.9637	p=0.47

27	**C**	VU'172 1 mg/kg: Mean bout duration	Repeated Measures Two-way ANOVA	Genotype: F (2, 32) = 3.341	p=0.048
				Time bin: F (5, 160) = 7.967	p<0.0001
				Interaction: F (10, 160) = 0.2918	p=0.98
		VU'172 20 mg/kg: Mean bout duration	Repeated Measures Two-way ANOVA	Genotype: F (2, 26) = 0.6501	p=0.53
				Time bin: F (5, 130) = 1.192	p=0.31
				Interaction: F (10, 130) = 0.9135	p=0.52
		VU'172 56 mg/kg: Mean bout duration	Repeated Measures Two-way ANOVA	Genotype: F (2, 27) = 0.5114	p=0.60
				Time bin: F (5, 135) = 6.474	p<0.0001
				Interaction: F (10, 135) = 0.8673	p=0.56
	D	Vehicle: Distance traveled	Repeated Measures Two-way ANOVA	Genotype: F (2, 36) = 3.360	p=0.045
				Time bin: F (5, 180) = 4.620	p=0.0005
				Interaction: F (10, 180) = 0.8643	p=0.56
		VU'172 1 mg/kg: Distance traveled	Repeated Measures Two-way ANOVA	Genotype: F (2, 32) = 1.274	p=0.29
				Time bin: F (5, 160) = 6.636	p<0.0001
				Interaction: F (10, 160) = 1.017	p=0.43
		VU'172 20 mg/kg: Distance traveled	Repeated Measures Two-way ANOVA	Genotype: F (2, 26) = 1.179	p=0.32
				Time bin: F (5, 130) = 4.023	p=0.002
				Interaction: F (10, 130) = 0.5368	p=0.86

27	**D**	VU'172 56 mg/kg: Distance traveled	Repeated Measures Two-way ANOVA	Genotype: F (2, 27) = 0.6097	p=0.55
				Time bin: F (5, 135) = 2.618	p=0.02
				Interaction: F (10, 135) = 0.3148	p=0.97
28	**A**	Control: Grooming vs. Locomotion	Pearson Correlation	Vehicle: r=-0.32	p=0.0003
				1 mg/kg: r=-0.38	p=0.0005
				20 mg/kg: r=-0.64	p<0.0001
				56 mg/kg: r=-0.54	p<0.0001
	B	Spino$^{\Delta dMSN}$: Grooming vs. Locomotion	Pearson Correlation	Vehicle: r=-0.44	p=0.0004
				1 mg/kg: r=-0.25	p=0.040
				20 mg/kg: r=-0.53	p<0.0001
				56 mg/kg: r=-0.41	p=0.0031
	C	Spino$^{\Delta iMSN}$: Grooming vs. Locomotion	Pearson Correlation	Vehicle: r=-0.43	p=0.0009
				1 mg/kg: r=-0.22	p=0.064
				20 mg/kg: r=-0.51	p<0.0001
				56 mg/kg: r=-0.22	P=0.086
30	**A**	Rearing: VU'172 DRC	One-way ANOVA	F (5, 55) = 1.221	p=0.31
	B	Rearing: Binned VU'172 DRC	Repeated Measures Two-way ANOVA	Dose: F (5, 55) = 1.221	p=0.31
				Time bin: F (5, 275) = 0.7806	p=0.56
				Interaction: F (25, 275) = 1.271	p=0.17

30	**C**	Baseline and VU'172 1 mg/kg Rearing: Control vs. Spino$^{\Delta dMSN}$	Three-way ANOVA	IP Injection: F (1, 44) = 12.97	p=0.0008
				Genotype: F (1, 44) = 0.7560	p=0.38
				Time: F (5, 220) = 0.6628	p=0.65
				Time X IP Injection: F (5, 220) = 1.427	p=0.21
				Time X Genotype: F (5, 220) = 1.626	p=0.15
				IP Injection X Genotype: F (1, 44) = 0.04348	p=0.83
				IP Injection X Genotype X Time: F (5, 220) = 0.4316	p=0.82
	D	Baseline and VU'172 56 mg/kg Rearing: Control vs. Spino$^{\Delta dMSN}$	Three-way ANOVA	IP Injection: F (1, 36) = 12.74	p=0.001
				Genotype: F (1, 36) = 1.269	p=0.26
				Time: F (5, 180) = 1.527	p=0.18
				Time X IP Injection: F (5, 180) = 0.6868	p=0.63
				Time X Genotype: F (5, 180) = 0.5420	p=0.74
				IP Injection X Genotype: F (1, 36) = 0.01237	p=0.91
				IP Injection X Genotype X Time: F (5, 180) = 1.219	p=0.30

30	**E**	Baseline and VU'172 1 mg/kg Rearing: Control vs. Spino$^{\Delta iMSN}$	Three-way ANOVA	IP Injection: F (1, 44) = 18.75	p<0.0001
				Genotype: F (1, 44) = 0.02077	p=0.88
				Time: F (5, 220) = 0.5442	p=0.74
				Time X IP Injection: F (5, 220) = 4.379	p=0.0008
				Time X Genotype: F (5, 220) = 1.158	p=0.33
				IP Injection X Genotype: F (1, 44) = 0.3110	p=0.579
				IP Injection X Genotype X Time: F (5, 220) = 1.417	p=0.21
	F	Baseline and VU'172 56 mg/kg Rearing: Control vs. Spino$^{\Delta iMSN}$	Three-way ANOVA	IP Injection: F (1, 40) = 16.96	p=0.0002
				Genotype: F (1, 40) = 0.004558	p=0.94
				Time: F (5, 200) = 1.745	p=0.12
				Time X IP Injection: F (5, 200) = 1.093	p=0.36
				Time X Genotype: F (5, 200) = 0.4911	p=0.78
				IP Injection X Genotype: F (1, 40) = 0.05284	p=0.81
				IP Injection X Genotype X Time: F (5, 200) = 0.8109	p=0.54

Table 5: Chapter 5 Statistics.

Statistical analysis corresponding to Figures 14, 18-23, 25-28, and 30.

Chapter Six: Discussion

6.1 Integrated Discussion

This dissertation applied behavioral, electrophysiological, biochemical, and proteomics approaches to test the hypothesis *that spinophilin expression in striatal medium spiny neurons mediates mGluR5-dependent excessive grooming*. Specifically, we manipulated spinophilin expression in dMSNs or iMSNs using a novel conditional spinophilin knockout mouse to determine that both $Spino^{\Delta dMSN}$ and $Spino^{\Delta iMSN}$ mice decrease excessive grooming and plasticity associated with increased mGluR5 function. Furthermore, we detail that spinophilin's protein interaction with mGluR5 and D_2R correlate with grooming duration. Lastly, using a quantitative proteomics approach, we found that loss of spinophilin increases mGluR5 interactions with PSD scaffolding proteins implicated in psychiatric disorders, including OCSDs and ASDs. Despite the reported phenotypes in MSN subtype-specific KO mice, it is critical to note these genotypes did not display any basal alterations in locomotion or grooming behavior. Therefore, we proposed that $Spino^{\Delta dMSN}$ and $Spino^{\Delta iMSN}$ mice are poised to elucidate cell type-specific adaptations required for a basal motor program, such as grooming, to become excessively initiated and/or sustained.

6.1.1 Spinophilin dMSN-Knockout Effects on Repetitive Grooming and DLS Physiology

We bred our conditional spinophilin line with D1-Cre to deplete spinophilin from striatal dMSNs ($Spino^{\Delta dMSN}$). We confirmed this depletion biochemically by observing a ~25% reduction in spinophilin protein levels in striatum. We found that $Spino^{\Delta dMSN}$ mice decreased excessive grooming caused by constitutive knockout of SAPAP3 and treatment

with 1 mg/kg and 20 mg/kg VU'172. Interestingly, spinophilin decreased grooming duration caused by SAPAP3 KO and 1 mg/kg VU'172 by decreasing the mean duration of grooming bouts, suggesting spinophilin expression in dMSNs may be critical to sustained motor output. Robert Malenka and colleagues previously determined the dMSN function in the rodent DLS is required for the completion, but not the initiation, of sequential motor programs, further implicating dMSN function in sustaining the duration of complex motor programs (Rothwell et al 2015). Rodent grooming is a complex sequential behavior that progresses along the cephalocaudal axis; however, we did not directly measure changes in grooming microstructure in Spino$^{\Delta dMSN}$ mice. Therefore, it will be of interest for future studies to determine if Spino$^{\Delta dMSN}$ initiate grooming bouts similar to control mice but fail to sustain grooming bouts along the cephalocaudal axis.

Excessive grooming in SAPAP3 KO mice is associated with decreased corticostriatal synaptic transmission and increased eCB-mediated plasticity in the DLS (Chen et al 2011, Wan et al 2011, Welch et al 2007). In addition to Spino$^{\Delta dMSN}$ mice decreasing excessive grooming, we also found that Spino$^{\Delta dMSN}$ mice displayed network-wide increases in DLS excitability and decreases in DLS HFS-LTD, suggesting loss of spinophilin may increase corticostriatal synaptic transmission under conditions of activity. Specifically, both input/output curves and HFS-LTD require stimulation of the corpus callosum to induce neurotransmitter release at corticostriatal synapses. Therefore, the Spino$^{\Delta dMSN}$-dependent effects on input/output curves and HFS-LTD further suggest spinophilin mediates activity-dependent changes in striatal function. As described in Chapter 3, future studies measuring basal changes in synaptic transmission and dMSN

properties in Spino$^{\Delta dMSN}$ mice will be critical to determine if spinophilin selectively mediates activity-dependent changes in striatal function, or also impacts basal striatal function.

6.1.2 Spinophilin iMSN-Knockout Effects on Repetitive Grooming and DLS Physiology

We bred our conditional spinophilin line with A2A-Cre to deplete spinophilin protein expression from striatal iMSNs (Spino$^{\Delta iMSN}$). We found that Spino$^{\Delta iMSN}$ mice abrogated the SAPAP3 KO genotype effect on percent grooming, such that SAPAP3 KO/Spino$^{\Delta iMSN}$ mice were not significantly different from SAPAP3 WT/Spino$^{\Delta iMSN}$ mice. Unlike Spino$^{\Delta dMSN}$ mice, which decreased the duration of grooming bouts, we found that decreased grooming in SAPAP3 KO/Spino$^{\Delta iMSN}$ mice was associated with both decreased grooming bout frequency and the duration of grooming bouts, suggesting grooming behavior was decreased overall. In addition to the strong Spino$^{\Delta iMSN}$-dependent effect on SAPAP3 KO grooming, we found that Spino$^{\Delta iMSN}$ mice abrogated the 20 mg/kg VU'172 treatment-dependent increase in grooming duration. However, despite the abrogated treatment effect, we did not detect any Spino$^{\Delta iMSN}$ genotype effects on percent grooming, grooming frequency, or mean grooming bout duration at any VU'172 dose. These complex results suggest Spino$^{\Delta iMSN}$ mice may prevent the treatment effect without decreasing overall grooming (i.e. an interaction effect rather than a genotype effect). Two-way ANOVA did detect a significant interaction effect at the 20 mg/kg VU'172 dose, however, we did not detect a significant interaction when analyzing the VU'172 DRC data. My colleague Darryl Watkins determined that Spino$^{\Delta iMSN}$ mice, but not Spino$^{\Delta dMSN}$, have an attenuated ability to perform a novel motor program using an accelerating rotarod task,

further suggesting Spino$^{\Delta iMSN}$ mice have a limited ability to increase motor output to mediate adaptations associated with striatal function (Morris et al 2022).

The unique results from SAPAP3 KO/Spino$^{\Delta iMSN}$ mice and Spino$^{\Delta iMSN}$ mice treated with VU'172 suggest unique mechanisms may underlie increased grooming in these two models. Interestingly, we found that spinophilin's protein interaction with D_2R, a striatal GPCR expressed in iMSNs but not dMSNs, is increased in SAPAP3 KO mice and correlates with grooming behavior, possibly providing a unique mechanism by which Spino$^{\Delta iMSN}$ mice could regulate excessive grooming in SAPAP3 KO mice compared to VU'172-treated mice, which we assume to be an mGluR5-specific form of repetitive grooming. Recently, Fatuel Tecuapetla and colleagues determined that optogenetic inhibition of striatal iMSNs, but not dMSNs, in the DMS decreased excessive grooming in SAPAP3 KO mice (Ramírez-Armenta et al 2022). Together, these results not only suggest unique iMSN-specific mechanisms could underlie excessive grooming in SAPAP3 KO, but further suggest spinophilin expression in iMSNs may regulate excessive grooming through unique mechanisms (as opposed to spinophilin expression in dMSNs).

Like the similarities and differences between Spino$^{\Delta dMSN}$ and Spino$^{\Delta iMSN}$ effects on repetitive grooming, we also found overlapping and unique effects in our field electrophysiology studies between the two genotypes. Specifically, like Spino$^{\Delta dMSN}$ mice, we found that HFS-LTD was abrogated in Spino$^{\Delta iMSN}$ mice, further suggesting spinophilin expression in striatal MSNs is critical for activity-dependent changes in striatal function. However, unlike Spino$^{\Delta dMSN}$ mice, loss of spinophilin from iMSNs did not impact DLS excitability. Given that excessive grooming is associated with decreased

DLS excitability, it is possible that this small difference in DLS excitability in Spino$^{\Delta dMSN}$ and Spino$^{\Delta iMSN}$ mice could be one explanation why Spino$^{\Delta dMSN}$ mice decrease repetitive grooming in SAPAP3 KO mice and VU'172-treated mice. However, in-vivo electrophysiology experiments would be required to directly probe the relationship between increased DLS function and grooming behavior in Spino$^{\Delta dMSN}$ and Spino$^{\Delta iMSN}$ mice.

6.1.3 Spinophilin Mediates mGluR5-Dependent Excessive Grooming MSN Subtype-Specifically

We hypothesized that spinophilin functions in striatal MSNs to mediate mGluR5-dependent excessive grooming. While the Spino$^{\Delta dMSN}$ and Spino$^{\Delta iMSN}$ grooming data discussed above support this hypothesis, it was unexpected that loss of spinophilin in the whole-body, or in both MSN subtypes, had no effect on 20 mg/kg VU'172. These data suggest that Spino$^{\Delta dMSN}$ and Spino$^{\Delta iMSN}$ mice mediate mGluR5-dependent repetitive grooming in an antagonistic, MSN subtype-specific manner. Although it is unknown why this is the case, numerous studies suggest a balance in dMSN and iMSN function underlies motor output, and increased dMSN function relative to iMSNs underlies repetitive motor behaviors. Therefore, it is possible that MSN subtype-specific spinophilin knockout disrupts the balance in the MSN subtypes, thus preventing repetitive grooming behavior. However, future studies testing this hypothesis would be essential.

Nicole Calakos and colleagues developed a two-photon laser scanning microscopy calcium imaging approach to measure dMSN and iMSN intracellular calcium levels following stimulation of corpus callosum in ex-vivo striatal slices (Ade et al 2016,

O'Hare et al 2016). This approach is capable of measuring calcium oscillations in red fluorescently labeled dMSNs and non-fluorescent iMSNs simultaneously in the DLS, which could be adapted in Spino$^{\Delta dMSN}$ and Spino$^{\Delta iMSN}$ mice to determine if MSN subtype-specific loss of spinophilin disrupts the balance in dMSN/iMSN activity, thus providing a unique hypothetical mechanism to decrease repetitive grooming.

Although Spino$^{-/-}$ mice increased grooming following a 20 mg/kg VU'172 treatment, it is interesting to note that basal grooming levels are decreasing in Spino$^{-/-}$ mice. Moreover, we found that more mGluR5 associates with PSD scaffolding proteins in naive Spino$^{-/-}$ mice—an effect suggested to be protective against preclinical models that display excessive grooming (Ade et al 2016, Wang et al 2016). Therefore, even though Spino$^{-/-}$ mice increase grooming following VU'172 treatment, our data still suggest loss of spinophilin impacts the mGluR5 interactome in the opposite direction of preclinical models that display excessive grooming. While interesting, critical question arise from these data which should be explored as future directions. First, determining how spinophilin regulates mGluR5 phosphorylation and interactions under conditions of increased mGluR5 activity, such as in SAPAP3 KO mice and/or mice treated with VU'172, will be important to understand how mGluR5 activity is affected in Spino$^{-/-}$ mice. Second, it is unclear if increased mGluR5 interactions with PSD scaffolding proteins are specific to dMSNs, iMSNs, or occurs in both MSN subtypes. Unfortunately, classical biochemical approaches do not have cell type-specific resolution; however, recent advances in proximity labeling enable the coupling of a biotin ligase to a seed protein which can be expressed in specific cell types through a double floxed inverted

open reading frame (DIO) AAV. Recently, we created a DIO-PSD95 AAV that has the biotin ligase, miniTurbo (Branon et al 2018), attached to the C-terminus of PSD95 and have biochemically confirmed this AAV expresses only in Cre+ neurons (**Figure 31**).

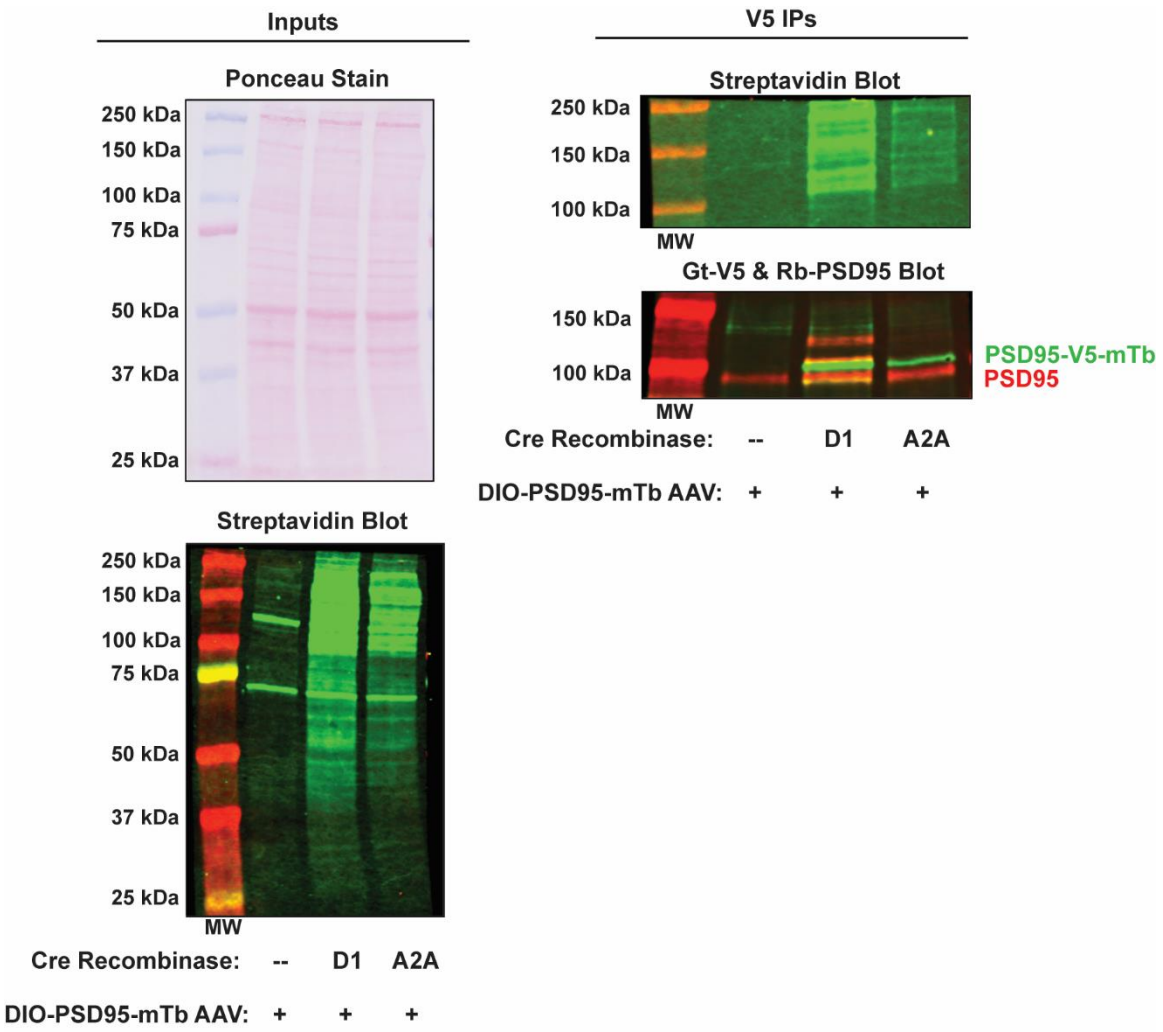
Inputs
Ponceau Stain
250 kDa
150 kDa
100 kDa
75 kDa
50 kDa
37 kDa
25 kDa
Streptavidin Blot
250 kDa
150 kDa
100 kDa
75 kDa
50 kDa
37 kDa
25 kDa
MW
Cre Recombinase: -- D1 A2A
DIO-PSD95-mTb AAV: + + +
V5 IPs
Streptavidin Blot
250 kDa
150 kDa
100 kDa
MW
Gt-V5 & Rb-PSD95 Blot
150 kDa
100 kDa
MW
PSD95-V5-mTb
PSD95
Cre Recombinase: -- D1 A2A
DIO-PSD95-mTb AAV: + + +

Figure 31: Biochemical Validation of AAV9-DIO-CBh-PSD95-V5-mTb Expression and Function.

AAV9-CBh-DIO-PSD95-V5-mTb was injected into the dorsal striatum of Cre negative, D1-Cre, or A2A-Cre mice (N=1 per genotype). Three weeks following viral transduction, mice received three daily subcutaneous injections of D-biotin (24 mg/kg), then whole striatum was dissected for immunoblot analysis of PSD95-mTb expression and biotinylation function. Inputs (left) were immunoblotted with streptavidin conjugated to an Alexa790 fluorophore (green) to qualitatively show an increased abundance of biotinylated proteins in D1- and A2A-Cre mice (lanes 2 and 3) compared to Cre negative mice (lane 1). V5-IPs were immunoblotted for 1) streptavidin-Alexa790 (top right, green) to quantitatively show biotinylated proteins co-IP with PSD95-V5-mTb, and 2) V5 (bottom right, green) to show PSD95-V5-mTb expression only in D1- and A2A-Cre cells. Collectively, these results suggest AAV9-DIO-PSD95-V5-mTb expresses in Cre+ cells and can biotinylate interacting proteins. Future immunohistochemistry studies will be needed to confirm PSD95-V5-mTb localizes to dendritic spines.

Future studies can leverage this DIO-PSD95-mTb AAV to identify MSN subtype-specific protein interactions in the PSD of Spino$^{\Delta dMSN}$ and Spino$^{\Delta iMSN}$ mice to determine if increased mGluR5 is detected in a specific MSN subtype or both. We hypothesize the loss of spinophilin increases mGluR5 interactions with PSD scaffolding protein in both MSN subtypes. While some may suggest this effect likely occurs exclusively in dMSNs due to the protective effect Spino$^{\Delta dMSN}$ has on repetitive grooming behavior, we reason it is also possible that Spino$^{\Delta dMSN}$ and Spino$^{\Delta iMSN}$ mice differentially contribute to excessive grooming due to cytochemical and anatomical differences within the basal ganglia.

6.1.4 Spinophilin and OCSDs

Given the protective effect that Spino$^{\Delta dMSN}$ and Spino$^{\Delta iMSN}$ mice have on repetitive grooming behavior, a critical question arises: to what extent do these preclinical experiments inform future OCSD therapeutic strategies? Although this question is difficult to address due 1) the unassessed generalizability of Spino$^{\Delta dMSN}$ and Spino$^{\Delta iMSN}$ effects on other repetitive/habitual behaviors that may be more informative for OCSD pathology (such as punishment-resistant reward seeking paradigms (Seiler et al 2022)), and 2) the limited mechanistic conclusions we can provide from the experiments presented herein. Despite these limitations, it is critical to note that because both Spino$^{\Delta dMSN}$ and Spino$^{\Delta iMSN}$ mice decreased excessive grooming, future studies can leverage these effects to identify MSN subtype-specific signaling pathways that are required for increased grooming behavior. These studies, in combination with the extent to which these mechanisms generalize to other measures of habitual and compulsive behavior in rodents, can begin to elucidate novel therapeutic strategies capable of decreasing repetitive behaviors in OCSDs.

Recent preclinical studies suggest increased mGluR5 function is associated with OCD-like behavior, and current OCSD treatments target the serotonergic and D2-dopamine receptor system. The fact that spinophilin's protein interaction with mGluR5 and D_2R are increased in SAPAP3 KO mice and correlate with grooming behavior raise hope that understanding mechanisms by which spinophilin mediates repetitive behaviors will both confirm existing mechanisms associated with the pathology (i.e. efficacy of atypical anti-psychotics in reducing grooming) while adding novel signaling pathways associated with mGluR5 function that also contribute to OCSDs, thus holding potential to reshape physicians' strategies to treat OCSDs.

The experiments reported herein were not designed to include sex as a biological variable. However, we visualized grooming in SAPAP3 KO mice and the VU'172 DRCs by sex (**Figure 8** and **29**). Interestingly, we saw unique trends for male and female MSN subtype-specific spinophilin KO mice, such that percent grooming appeared to be decreased to a greater extent in female MSN subtype-specific spinophilin KO mice. Specifically, although MSN subtype-specific spinophilin KO decreases excessive grooming in both male and female SAPAP3 KO mice, we visually noticed a larger effect size in female SAPAP3 KO mice (**Figure 8**). By visualizing our VU'172 DRC data by sex we saw that percent grooming was decreased in female $Spino^{\Delta dMSN}$ mice at all doses, and female $Spino^{\Delta iMSN}$ mice displayed decreased grooming at 20 mg/kg and 56 mg/kg VU'172 doses (**Figure 29**). Interestingly, the prevalence of OCD is suggested to be higher in females than males (NIMH 2017). Therefore, it is possible that female-specific sex difference in MSN subtype-specific spinophilin KO mice may hold translational value for understanding sex-specific mechanisms associated with repetitive behaviors in

OCSDs. Although these trends are interesting, it will be critical for future studies to include sex as a biological variable to fully determine if female MSN subtype-specific spinophilin KO decreases repetitive behaviors to a greater extent than male mice.

6.2 Alternative Interpretations

6.2.1 "Results are Due to Compensation, Not a Direct Action of Spinophilin"

Here, we report that cell type-specific loss of spinophilin decreases mGluR5-dependent excessive grooming, abrogates striatal plasticity, and shifts mGluR5's interactome to favor interactions with PSD scaffolding proteins. While it is easy to assume these phenotypes are a due to spinophilin's direct actions, it is also possible that compensatory changes due to development without spinophilin could underlie the results reported here. To test this alternative interpretation, these experiments could be performed following knockout of spinophilin in adulthood using inducible Cre lines and/or Cre-AAV as shown feasible in Chapter 3. Additionally, viral repletion of spinophilin expression using a recently created and validated DIO-HA-Spinophilin AAV (**Figure 32**) will also be helpful to determine if spinophilin's direct actions mediate repetitive grooming.

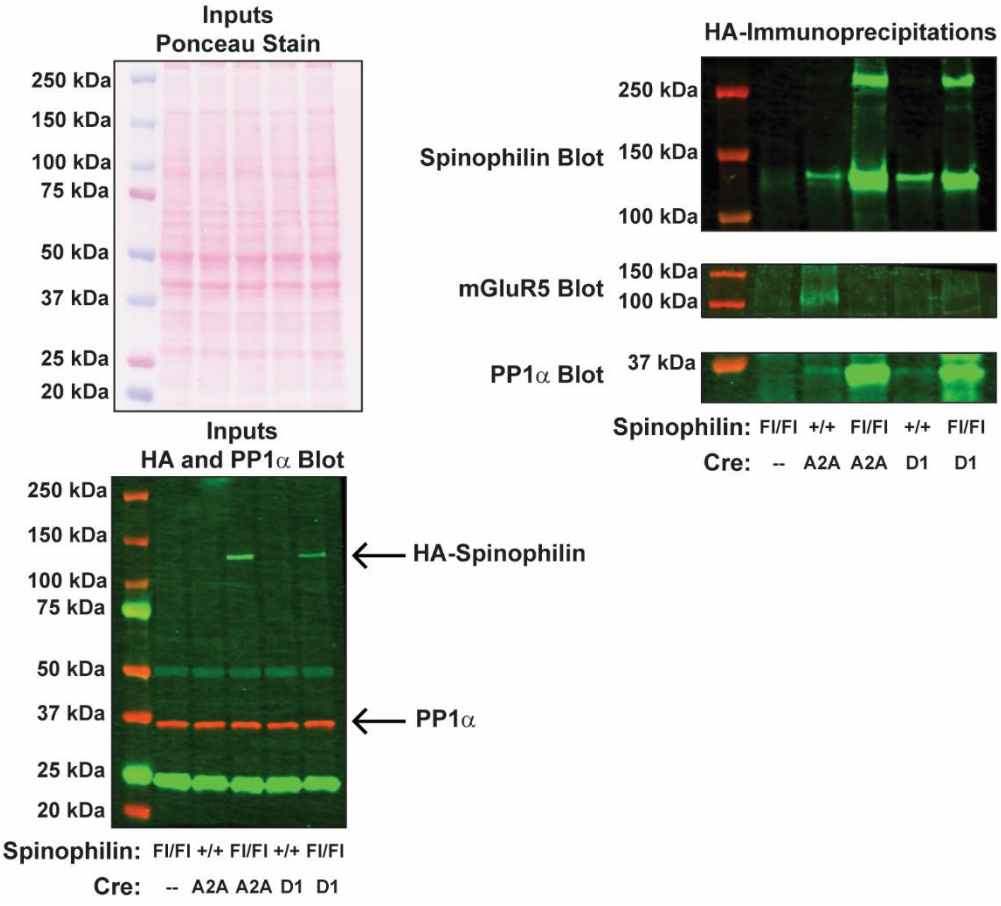
Inputs
Ponceau Stain
250 kDa
150 kDa
100 kDa
75 kDa
50 kDa
37 kDa
25 kDa
20 kDa
HA-Immunoprecipitations
Spinophilin Blot
mGluR5 Blot
PP1α Blot
250 kDa
150 kDa
100 kDa
150 kDa
100 kDa
37 kDa
Spinophilin: Fl/Fl +/+ Fl/Fl +/+ Fl/Fl
Cre: -- A2A A2A D1 D1
Inputs
HA and PP1α Blot
250 kDa
150 kDa
100 kDa
75 kDa
50 kDa
37 kDa
25 kDa
20 kDa
HA-Spinophilin
PP1α
Spinophilin: Fl/Fl +/+ Fl/Fl +/+ Fl/Fl
Cre: -- A2A A2A D1 D1

Figure 32: Biochemical Validation of AAV9-DIO-CBh-HA-Spinophilin Expression and Interactions.

AAV9-DIO-CBh-HA-spinophilin was expressed in the dorsal striatum of Spino$^{Fl/Fl}$/Cre-, Spino$^{+/+}$/D1-Cre, Spino$^{+/+}$/A2A-Cre, Spino$^{Fl/Fl}$/D1-Cre, Spino$^{Fl/Fl}$/A2A-Cre mice. Four-weeks following surgery, striatum was dissected for immunoblot analysis of inputs (left) and HA-IPs (right). Immunoblotting inputs with an antibody specific to the HA-epitope tag revealed robust HA-spinophilin expression in Spino$^{\Delta dMSN}$ and Spino$^{\Delta iMSN}$ mice, but no expression in Spino$^{Fl/Fl}$/Cre-, Spino$^{+/+}$/D1-Cre, and Spino$^{+/+}$/A2A-Cre mice. Immunoblotting HA-IPs with for the HA-tagged spinophilin revealed no expression in Spino$^{Fl/Fl}$/Cre- mice, limited AAV expression in Spino$^{+/+}$/D1-Cre and Spino$^{+/+}$/A2A-Cre mice, and robust expression in Spino$^{\Delta dMSN}$ and Spino$^{\Delta iMSN}$ mice. Additionally, we detected PP1γ1 co-IP with HA-spinophilin in mice expressing DIO-HA-spinophilin, but no PP1γ1 co-IP was detected in the Spino$^{Fl/Fl}$ negative control. These results suggest that 1) AAV9-DIO-CBh-HA-spinophilin expresses in Cre+ cells (but its expression may be limited when endogenous spinophilin is present), and 2) that HA-spinophilin expressed from this virus can interact with PP1. Future immunohistochemical studies will be needed to confirm HA-spinophilin localizes to dendritic spines.

Changes in PP1 expression is one possible compensatory mechanism. Whole-body loss of spinophilin results in decreased PP1 levels in the striatum (Allen et al 2006). While depletion of spinophilin by injecting Cre-AAV in the striatum also decreased PP1 levels 5-weeks following surgery, inducible knockout of spinophilin with CagCreER did not affect PP1 levels. Therefore, although these two methods to deplete spinophilin expression introduce additional confounding variables (i.e. tamoxifen treatment, syringe being plunged into brain), these approaches could be used to determine the extent to which 1) loss of spinophilin in adulthood decreases mGluR5-dependent grooming, and 2) PP1 compensation correlates with repetitive grooming. Despite future studies being needed to test if our results are due to the direct actions of spinophilin, we still propose that our MSN subtype-specific KO mice are useful for detailing required spinophilin-dependent or -independent mechanisms underlying repetitive motor dysfunction.

6.2.2 "Decreased Grooming in Spinophilin MSN Subtype-Specific Knockout Mice is a Result of Decreased Anxiety"

In addition to excessive grooming, increased anxiety-like behavior in SAPAP3 KO mice is decreased by viral repletion of SAPAP3 in the striatum and global administration of an mGluR5 NAM. Furthermore, wild-type mice treated with the mGluR5 PAM, VU'172, display increased anxiety-like behavior, suggesting increased mGluR5 function, possibly within the striatum, also underlies increased anxiety phenotypes in SAPAP3 KO mice. However, little is known regarding the extent to which conditional loss of mGluR5 using D1- or A2A-Cre impact anxiety-like behavior in models for understanding OCSDs. A recent study found that conditional knockout of mGluR5 with D1-Cre increases active avoidance of stress (measured using a two-way

active avoidance test) but decreases passive avoidance of stress (measured using a forced swim test) (Zangrandi et al 2021). Given that increased active avoidance behavior is hypothesized to underlie increased habit formation in individuals with OCD (Gillan et al 2014b), and depletion of mGluR5 with D1-Cre increases avoidance, it is possible that mGluR5 function in D1-Cre expressing neurons may decrease active avoidance, which could in-turn decrease compulsive-like behavior in mice.

Although it is unclear which brain region(s) mGluR5 functions in to decrease active avoidance behavior, we hypothesize these affects are unlikely to explain why depletion of spinophilin expression with D1-Cre decreases mGluR5-dependent repetitive grooming. Specifically, if mice increased grooming as an avoidance response to stressful or anxiogenic stimuli, it would be expected that depletion of mGluR5 with D1- Cre (which increases active avoidance stress) would increasing grooming behavior (i.e. increased grooming to avoid anxiogenic stimuli). In contrast, we report that depletion of spinophilin with D1-Cre decreases repetitive grooming in SAPAP3 KO and VU'172-treated mice. Although these speculations do not rule out the possibility that spinophilin decreases grooming by decreasing anxiety, it is critical to note that previous studies did not find any basal changes in anxiety-like behavior in Spino$^{-/-}$ between 3-5 months of age (Wu et al 2017). However, these studies in Spino$^{-/-}$ mice do not prevent the possibility of unique spinophilin KO/SAPAP3 KO or spinophilin KO/VU'172 interaction effects on anxiety-like behavior. Therefore, although these studies lead us to hypothesize spinophilin mediates repetitive grooming by regulating motor function, future studies measuring anxiety-like behavior will be required to conclude changes in grooming are not due to changes in anxiety.

6.2.3 "You are Measuring Excessive Itching, Not Repetitive Grooming"

A common alternative interpretation of rodent repetitive grooming behavior is simply that the animals are itching themselves, suggesting hyperactivity of skin sensory receptors and/or perturbations within the peripheral nervous system (PNS) cause the repetitive behavior. Welch et al. ruled out this alternative interpretation in SAPAP3 KO mice through histological analyses comparing facial skin from SAPAP3 WT mice and SAPAP3 KO mice that displayed increased grooming but had not yet formed lesions. Specifically, they found no lymphocytic or granulocytic infiltration of the skin tissue, nor did they find any histological differences in skin sensory innervation, suggesting increased grooming is not likely due to inflammation or PNS dysfunction.

Although this alternative interpretation has been explored in SAPAP3 KO mice, the extent to which VU'172 increases grooming by inducing an acute immune response in the periphery, or by augmenting mGluR5 function in the spinal cord to promote nociception is unknown. Although mGluR5 is expressed in microglia, numerous reports suggest mGluR5 activation decreases neuroinflammation (Byrnes et al 2009, Wang et al 2013, Zhang et al 2021). Similarly, mGluR5 activity is also hypothesized to decrease astrocytic release of pro-inflammatory cytokines (Shah et al 2012), making it unlikely that the mGluR5 PAM, VU'172, increases grooming by inducing an acute immune response. Given these data, we hypothesize that increased grooming caused by VU'172 treatment is due to mGluR5-specific actions within neurons in the CNS.

Despite mGluR5 negatively regulating neuroinflammation, mGluR5 activity in the spinal cord dorsal horn (SCDH) promotes nociception (Shah et al 2012). Specifically, intracellular mGluR5 activity in the SCDH promotes nociception (Dogrul et al 2000, Hu

et al 2007, Vincent et al 2016). Interestingly, intrathecal expression of spinophilin has analgesic effects, whereas viral knockdown of spinophilin in the SCDH increased nociception (Hu et al 2015, Wang et al 2021). Given that both mGluR5 activity and reductions in spinophilin expression in the SCDH increase nociception, it seems unlikely that loss of spinophilin would decrease grooming by negatively regulating mGluR5-dependent nociception. Furthermore, we reason it is unlikely that nociception would present as increased grooming behavior, and that conditional knockout of spinophilin with D1- or A2A-Cre would affect spinophilin protein expression in the spinal cord. Therefore, based on these data, we suggest it is unlikely that decreased repetitive grooming in Spino$^{\Delta dMSN}$ and Spino$^{\Delta iMSN}$ mice is due to altered nociception.

6.3 Conclusions and Future Directions

The major finding of this thesis is that spinophilin expression in striatal dMSNs or iMSNs is required for repetitive grooming behavior associated with increased mGluR5 function. Although the experiments detailed above implicate spinophilin in mGluR5-dependent repetitive grooming, they do not provide a deep mechanistic understanding of how spinophilin functions cell autonomously in each MSN subtype to regulate repetitive grooming. Therefore, future studies determining cell type-specific mechanisms by which spinophilin mediates mGluR5-dependent repetitive grooming will be the essential next step to build upon the foundation laid herein.

My working hypothesis is that spinophilin mediates repetitive grooming by regulating specific mGluR5 signaling pathways in MSNs. We found that loss of spinophilin shifts mGluR5 interactions from lipid raft complexes toward PSD scaffolding proteins. Given that mGluR5 can signal through unique signaling pathways depending on

its interaction with PSD scaffolding proteins, it is possible that spinophilin decreases repetitive grooming by selectively decreasing mGluR5 signaling at lipid raft complexes. mGluR5 interactions with PSD scaffolding proteins (indirectly through Homer 1b/c) promotes increased intracellular Ca^{2+} levels and MAPK signaling. Alternatively, decreasing mGluR5 interactions with PSD scaffolding proteins is associated with constitutive, agonist-independent activity, but the signaling pathways associated with this form of mGluR5 activity are inconsistent. A recent study induced constitutive mGluR5 activity in the prefrontal cortex by disrupting mGluR5's interaction with PSD scaffolds to reveal that increased mTOR signaling can promote local protein synthesis of AMPARs. However, other preclinical models suggest constitutive mGluR5 activity can also increase ERK signaling (Michalon et al 2012), even in the SHANK3 complete knockout model that displays excessive grooming (Wang et al 2016). Although these studies are complex, and often seem to be inconsistent, overall they demonstrate the possibility that specific mGluR5 signaling pathways underlie pathological conditions.

Loss of spinophilin increases ERK signaling basally within the striatum, but occludes amphetamine-dependent increases in ERK activity (Areal et al 2019, Di Sebastiano et al 2016). Therefore, if increased ERK activity underlies repetitive grooming associated with mGluR5 function, it is possible that spinophilin decreases repetitive grooming by occluding mGluR5-dependent increases in ERK activity. Given these data, future studies measuring ERK activity in dMSNs and iMSNs in real time would be critical to determine if ERK signaling underlies repetitive grooming. One strategy to achieve this is by utilizing a fluorescence resonance energy transfer (FRET)-based ERK and AKT biosensors (He et al 2019) that can be packed into a DIO-AAV. In

turn, these ERK and AKT biosensor could be used to measure spikes in ERK and/or AKT signaling during grooming bouts, and further determine if MSN subtype-specific loss of spinophilin selectively decreases ERK or AKT activity that may underlie grooming dysfunction.

Lastly, it is also possible that spinophilin expression in dMSNs or iMSNs mediates mGluR5-dependent excessive grooming without directly regulating mGluR5 activity within MSNs. For example, it is also possible that behavioral phenotypes presented herein are due to circuit-specific changes in presynaptic glutamate release from the cortical and/or thalamic inputs into the striatum, thus modulating dMSN or iMSN function independent postsynaptic mGluR5. Additionally, it is possible that increased mGluR5 activity in the cortex and/or VTA/SNc increases glutamate and dopamine release into the striatum. In this scenario, it is possible that spinophilin's regulation of ionotropic glutamate receptors and/or dopaminergic signaling in MSNs may be responsible for decreased mGluR5-depedent repetitive grooming. Therefore, utilizing other in-vivo approaches to measure presynaptic activity and/or dopamine signaling withing each MSN subtype may also be necessary to elucidate how MSN subtype-specific loss of spinophilin decreases excessive grooming. Although these next steps will be challenging, identifying the cell type-specific mechanisms by which spinophilin mediates repetitive grooming can elucidate specific signaling pathways that mediate unique aspects of repetitive behaviors, such as their frequency and how long repetitive behaviors are sustained.

Bibliography

Abbott AE, Linke AC, Nair A, Jahedi A, Alba LA, et al. 2018. Repetitive behaviors in autism are linked to imbalance of corticostriatal connectivity: a functional connectivity MRI study. *Soc Cogn Affect Neurosci* 13: 32-42

Ade KK, Wan Y, Hamann HC, O'Hare JK, Guo W, et al. 2016. Increased Metabotropic Glutamate Receptor 5 Signaling Underlies Obsessive-Compulsive Disorder-like Behavioral and Striatal Circuit Abnormalities in Mice. *Biol Psychiatry* 80: 522-33

Alagarsamy S, Sorensen SD, Conn PJ. 2001. Coordinate regulation of metabotropic glutamate receptors. *Curr Opin Neurobiol* 11: 357-62

Albin RL, Young AB, Penney JB. 1989. The functional anatomy of basal ganglia disorders. *Trends Neurosci* 12: 366-75

Alexander GE, Crutcher MD. 1990. Functional architecture of basal ganglia circuits: neural substrates of parallel processing. *Trends Neurosci* 13: 266-71

Alexander GE, DeLong MR, Strick PL. 1986. Parallel organization of functionally segregated circuits linking basal ganglia and cortex. *Annu Rev Neurosci* 9: 357-81

Allen JA, Halverson-Tamboli RA, Rasenick MM. 2007. Lipid raft microdomains and neurotransmitter signalling. *Nature Reviews Neuroscience* 8: 128-40

Allen PB, Ouimet CC, Greengard P. 1997. Spinophilin, a novel protein phosphatase 1 binding protein localized to dendritic spines. *Proceedings of the National Academy of Sciences of the United States of America* 94: 9956-61

Allen PB, Zachariou V, Svenningsson P, Lepore AC, Centonze D, et al. 2006. Distinct roles for spinophilin and neurabin in dopamine-mediated plasticity. *Neuroscience* 140: 897-911

Ango F, Prézeau L, Muller T, Tu JC, Xiao B, et al. 2001. Agonist-independent activation of metabotropic glutamate receptors by the intracellular protein Homer. *Nature* 411: 962-5

Anticevic A, Hu S, Zhang S, Savic A, Billingslea E, et al. 2014. Global resting-state functional magnetic resonance imaging analysis identifies frontal cortex, striatal, and cerebellar dysconnectivity in obsessive-compulsive disorder. *Biol Psychiatry* 75: 595-605

Areal LB, Hamilton A, Martins-Silva C, Pires RGW, Ferguson SSG. 2019. Neuronal scaffolding protein spinophilin is integral for cocaine-induced behavioral sensitization and ERK1/2 activation. *Mol Brain* 12: 15

Atmaca M, Yildirim H, Ozdemir H, Tezcan E, Poyraz AK. 2007. Volumetric MRI study of key brain regions implicated in obsessive-compulsive disorder. *Prog Neuropsychopharmacol Biol Psychiatry* 31: 46-52

Augustin SM, Chancey JH, Lovinger DM. 2018. Dual Dopaminergic Regulation of Corticostriatal Plasticity by Cholinergic Interneurons and Indirect Pathway Medium Spiny Neurons. *Cell Reports* 24: 2883-93

Balleine BW, O'Doherty JP. 2010. Human and Rodent Homologies in Action Control: Corticostriatal Determinants of Goal-Directed and Habitual Action. *Neuropsychopharmacology : official publication of the American College of Neuropsychopharmacology* 35: 48-69

Banca P, Voon V, Vestergaard MD, Philipiak G, Almeida I, et al. 2015. Imbalance in habitual versus goal directed neural systems during symptom provocation in obsessive-compulsive disorder. *Brain* 138: 798-811

Barbera G, Liang B, Zhang L, Gerfen Charles R, Culurciello E, et al. 2016. Spatially Compact Neural Clusters in the Dorsal Striatum Encode Locomotion Relevant Information. *Neuron* 92: 202-13

Barnes TD, Kubota Y, Hu D, Jin DZ, Graybiel AM. 2005. Activity of striatal neurons reflects dynamic encoding and recoding of procedural memories. *Nature* 437: 1158-61

Baucum AJ, 2nd, Jalan-Sakrikar N, Jiao Y, Gustin RM, Carmody LC, et al. 2010. Identification and validation of novel spinophilin-associated proteins in rodent striatum using an enhanced ex vivo shotgun proteomics approach. *Molecular & cellular proteomics : MCP* 9: 1243-59

Baxter LR, Jr., Phelps ME, Mazziotta JC, Guze BH, Schwartz JM, Selin CE. 1987. Local cerebral glucose metabolic rates in obsessive-compulsive disorder. A comparison with rates in unipolar depression and in normal controls. *Arch Gen Psychiatry* 44: 211-8

Bernard V, Normand E, Bloch B. 1992. Phenotypical characterization of the rat striatal neurons expressing muscarinic receptor genes. *J Neurosci* 12: 3591-600

Berntson GG, Jang JF, Ronca AE. 1988. Brainstem systems and grooming behaviors. *Ann N Y Acad Sci* 525: 350-62

Berridge KC. 1989. Progressive degradation of serial grooming chains by descending decerebration. *Behav Brain Res* 33: 241-53

Berridge KC, Aldridge JW. 2000a. Super-stereotypy I: enhancement of a complex movement sequence by systemic dopamine D1 agonists. *Synapse* 37: 194-204

Berridge KC, Aldridge JW. 2000b. Super-stereotypy II: enhancement of a complex movement sequence by intraventricular dopamine D1 agonists. *Synapse* 37: 205-15

Berridge KC, Aldridge JW, Houchard KR, Zhuang X. 2005. Sequential super-stereotypy of an instinctive fixed action pattern in hyper-dopaminergic mutant mice: a model of obsessive compulsive disorder and Tourette's. *BMC Biol* 3: 4

Berridge KC, Fentress JC, Parr H. 1987. Natural syntax rules control action sequence of rats. *Behav Brain Res* 23: 59-68

Berridge KC, Whishaw IQ. 1992. Cortex, striatum and cerebellum: control of serial order in a grooming sequence. *Experimental brain research* 90: 275-90

Berridge MJ, Irvine RF. 1984. Inositol trisphosphate, a novel second messenger in cellular signal transduction. *Nature* 312: 315-21

Beucke JC, Sepulcre J, Talukdar T, Linnman C, Zschenderlein K, et al. 2013. Abnormally high degree connectivity of the orbitofrontal cortex in obsessive-compulsive disorder. *JAMA Psychiatry* 70: 619-29

Bienvenu OJ, Wang Y, Shugart YY, Welch JM, Grados MA, et al. 2009. Sapap3 and pathological grooming in humans: Results from the OCD collaborative genetics study. *Am J Med Genet B Neuropsychiatr Genet* 150b: 710-20

Bockaert J, Perroy J, Ango F. 2021. The Complex Formed by Group I Metabotropic Glutamate Receptor (mGluR) and Homer1a Plays a Central Role in Metaplasticity and Homeostatic Synaptic Scaling. *The Journal of Neuroscience* 41: 5567-78

Bosch-Bouju C, Hyland BI, Parr-Brownlie LC. 2013. Motor thalamus integration of cortical, cerebellar and basal ganglia information: implications for normal and parkinsonian conditions. *Front Comput Neurosci* 7: 163

Branon TC, Bosch JA, Sanchez AD, Udeshi ND, Svinkina T, et al. 2018. Efficient proximity labeling in living cells and organisms with TurboID. *Nature Biotechnology* 36: 880

Brautigan DL, Shenolikar S. 2018. Protein serine/threonine phosphatases: keys to unlocking regulators and substrates. *Annual review of biochemistry* 87: 921-64

Burguiere E, Monteiro P, Feng G, Graybiel AM. 2013. Optogenetic stimulation of lateral orbitofronto-striatal pathway suppresses compulsive behaviors. *Science* 340: 1243-6

Byrnes KR, Stoica B, Loane DJ, Riccio A, Davis MI, Faden AI. 2009. Metabotropic glutamate receptor 5 activation inhibits microglial associated inflammation and neurotoxicity. *Glia* 57: 550-60

Calabresi P, Maj R, Pisani A, Mercuri NB, Bernardi G. 1992. Long-term synaptic depression in the striatum: physiological and pharmacological characterization. *J Neurosci* 12: 4224-33

Calabresi P, Pisani A, Mercuri NB, Bernardi G. 1996. The corticostriatal projection: from synaptic plasticity to dysfunctions of the basal ganglia. *Trends Neurosci* 19: 19-24

Calabresi P, Saiardi A, Pisani A, Baik JH, Centonze D, et al. 1997. Abnormal synaptic plasticity in the striatum of mice lacking dopamine D2 receptors. *J Neurosci* 17: 4536-44

Calipari ES, Huggins KN, Mathews TA, Jones SR. 2012. Conserved dorsal-ventral gradient of dopamine release and uptake rate in mice, rats and rhesus macaques. *Neurochem Int* 61: 986-91

Callender JA, Newton AC. 2017. Conventional protein kinase C in the brain: 40 years later. *Neuronal Signal* 1: Ns20160005

Caporale N, Dan Y. 2008. Spike timing-dependent plasticity: a Hebbian learning rule. *Annu Rev Neurosci* 31: 25-46

Chamberlain SR, Menzies LA, Fineberg NA, Del Campo N, Suckling J, et al. 2008. Grey matter abnormalities in trichotillomania: morphometric magnetic resonance imaging study. *Br J Psychiatry* 193: 216-21

Chen M, Wan Y, Ade K, Ting J, Feng G, Calakos N. 2011. Sapap3 deletion anomalously activates short-term endocannabinoid-mediated synaptic plasticity. *J Neurosci* 31: 9563-73

Chen Q, Veenman CL, Reiner A. 1996. Cellular expression of ionotropic glutamate receptor subunits on specific striatal neuron types and its implication for striatal vulnerability in glutamate receptor-mediated excitotoxicity. *Neuroscience* 73: 715-31

Chevalier G, Vacher S, Deniau JM, Desban M. 1985. Disinhibition as a basic process in the expression of striatal functions. I. The striato-nigral influence on tecto-spinal/tecto-diencephalic neurons. *Brain Res* 334: 215-26

Chien W-H, Gau S-F, Liao H-M, Chiu Y-N, Wu Y-Y, et al. 2013. Deep exon resequencing of DLGAP2 as a candidate gene of autism spectrum disorders. *Molecular Autism* 4: 26

Choi S, Lovinger DM. 1997. Decreased probability of neurotransmitter release underlies striatal long-term depression and postnatal development of corticostriatal synapses. *Proceedings of the National Academy of Sciences of the United States of America* 94: 2665-70

Claire M. Gillan, B.A. ,, Martina Papmeyer, M.A. ,, Sharon Morein-Zamir, Ph.D. ,, Barbara J. Sahakian, Ph.D. ,, Naomi A. Fineberg, M.A., M.R.C.Psych. ,, et al. 2011. Disruption in the Balance Between Goal-Directed Behavior and Habit Learning in Obsessive-Compulsive Disorder. *American Journal of Psychiatry* 168: 718-26

Cohen PT. 2002. Protein phosphatase 1--targeted in many directions. *J Cell Sci* 115: 241-56

Colbran RJ, Bass MA, McNeill RB, Bollen M, Zhao S, et al. 1997. Association of brain protein phosphatase 1 with cytoskeletal targeting/regulatory subunits. *J Neurochem* 69: 920-9

Conquet F, Bashir ZI, Davies CH, Daniel H, Ferraguti F, et al. 1994. Motor deficit and impairment of synaptic plasticity in mice lacking mGluR1. *Nature* 372: 237-43

Corbit LH, Janak PH. 2010. Posterior dorsomedial striatum is critical for both selective instrumental and Pavlovian reward learning. *The European journal of neuroscience* 31: 1312-21

Corbit LH, Muir JL, Balleine BW. 2003. Lesions of mediodorsal thalamus and anterior thalamic nuclei produce dissociable effects on instrumental conditioning in rats. *The European journal of neuroscience* 18: 1286-94

Corbit VL, Manning EE, Gittis AH, Ahmari SE. 2019. Strengthened Inputs from Secondary Motor Cortex to Striatum in a Mouse Model of Compulsive Behavior. *J Neurosci* 39: 2965-75

Croci C, Sticht H, Brandstatter JH, Enz R. 2003. Group I metabotropic glutamate receptors bind to protein phosphatase 1C. Mapping and modeling of interacting sequences. *J Biol Chem* 278: 50682-90

Cromwell HC, Berridge KC. 1996. Implementation of action sequences by a neostriatal site: a lesion mapping study of grooming syntax. *J Neurosci* 16: 3444-58

Cui G, Jun SB, Jin X, Pham MD, Vogel SS, et al. 2013. Concurrent activation of striatal direct and indirect pathways during action initiation. *Nature* 494: 238-42

Cunha RA. 2001. Adenosine as a neuromodulator and as a homeostatic regulator in the nervous system: different roles, different sources and different receptors. *Neurochem Int* 38: 107-25

Cunha RA, Ribeiro JA. 2000. ATP as a presynaptic modulator. *Life Sci* 68: 119-37

D'Antoni S, Spatuzza M, Bonaccorso CM, Musumeci SA, Ciranna L, et al. 2014. Dysregulation of group-I metabotropic glutamate (mGlu) receptor mediated signalling in disorders associated with Intellectual Disability and Autism. *Neuroscience and biobehavioral reviews* 46 Pt 2: 228-41

DeLong MR. 1990. Primate models of movement disorders of basal ganglia origin. *Trends Neurosci* 13: 281-5

Deniau JM, Chevalier G. 1985. Disinhibition as a basic process in the expression of striatal functions. II. The striato-nigral influence on thalamocortical cells of the ventromedial thalamic nucleus. *Brain Res* 334: 227-33

Deutsch EW, Bandeira N, Sharma V, Perez-Riverol Y, Carver JJ, et al. 2020. The ProteomeXchange consortium in 2020: enabling 'big data' approaches in proteomics. *Nucleic Acids Res* 48: D1145-d52

Di Martino A, Kelly C, Grzadzinski R, Zuo X-N, Mennes M, et al. 2011. Aberrant striatal functional connectivity in children with autism. *Biological psychiatry* 69: 847-56

Di Sebastiano AR, Fahim S, Dunn HA, Walther C, Ribeiro FM, et al. 2016. Role of Spinophilin in Group I Metabotropic Glutamate Receptor Endocytosis, Signaling, and Synaptic Plasticity. *J Biol Chem* 291: 17602-15

Ding J, Peterson JD, Surmeier DJ. 2008. Corticostriatal and thalamostriatal synapses have distinctive properties. *J Neurosci* 28: 6483-92

Dogrul A, Ossipov MH, Lai J, Malan TP, Jr., Porreca F. 2000. Peripheral and spinal antihyperalgesic activity of SIB-1757, a metabotropic glutamate receptor (mGLUR(5)) antagonist, in experimental neuropathic pain in rats. *Neurosci Lett* 292: 115-8

Dölen G, Osterweil E, Rao BSS, Smith GB, Auerbach BD, et al. 2007. Correction of Fragile X Syndrome in Mice. *Neuron* 56: 955-62

Drago J, Gerfen CR, Lachowicz JE, Steiner H, Hollon TR, et al. 1994. Altered striatal function in a mutant mouse lacking D1A dopamine receptors. *Proceedings of the national academy of sciences* 91: 12564-68

Dudman JT, Krakauer JW. 2016. The basal ganglia: from motor commands to the control of vigor. *Curr Opin Neurobiol* 37: 158-66

Dunn AJ. 1988. Studies on the neurochemical mechanisms and significance of ACTH-induced grooming. *Ann N Y Acad Sci* 525: 150-68

Dunn AJ, Berridge CW, Lai YI, Yachabach TL. 1987. CRF-induced excessive grooming behavior in rats and mice. *Peptides* 8: 841-4

Dunn AJ, Green EJ, Isaacson RL. 1979. Intracerebral adrenocorticotropic hormone mediates novelty-induced grooming in the rat. *Science* 203: 281-3

Durand CM, Betancur C, Boeckers TM, Bockmann J, Chaste P, et al. 2007. Mutations in the gene encoding the synaptic scaffolding protein SHANK3 are associated with autism spectrum disorders. *Nature Genetics* 39: 25-27

Edler MC, Salek AB, Watkins DS, Kaur H, Morris CW, et al. 2018. Mechanisms Regulating the Association of Protein Phosphatase 1 with Spinophilin and Neurabin. *ACS chemical neuroscience* 9: 2701-12

Elste AM, Benson DL. 2006. Structural basis for developmentally regulated changes in cadherin function at synapses. *Journal of Comparative Neurology* 495: 324-35

Evans JC, Robinson CM, Shi M, Webb DJ. 2015. The guanine nucleotide exchange factor (GEF) Asef2 promotes dendritic spine formation via Rac activation and spinophilin-dependent targeting. *J Biol Chem* 290: 10295-308

Everitt BJ, Robbins TW. 2016. Drug Addiction: Updating Actions to Habits to Compulsions Ten Years On. *Annual Review of Psychology* 67: 23-50

Fagni L, Chavis P, Ango F, Bockaert J. 2000. Complex interactions between mGluRs, intracellular Ca2+ stores and ion channels in neurons. *Trends Neurosci* 23: 80-8

Feng J, Yan Z, Ferreira A, Tomizawa K, Liauw JA, et al. 2000. Spinophilin regulates the formation and function of dendritic spines. *Proceedings of the National Academy of Sciences of the United States of America* 97: 9287-92

Ferré S, Fredholm BB, Morelli M, Popoli P, Fuxe K. 1997. Adenosine-dopamine receptor-receptor interactions as an integrative mechanism in the basal ganglia. *Trends Neurosci* 20: 482-7

Ferré S, Karcz-Kubicha M, Hope BT, Popoli P, Burgueño J, et al. 2002. Synergistic interaction between adenosine A2A and glutamate mGlu5 receptors: implications for striatal neuronal function. *Proceedings of the National Academy of Sciences of the United States of America* 99: 11940-45

Francesconi A, Duvoisin RM. 2000. Opposing effects of protein kinase C and protein kinase A on metabotropic glutamate receptor signaling: selective desensitization of the inositol trisphosphate/Ca2+ pathway by phosphorylation of the receptor-G protein-coupling domain. *Proceedings of the National Academy of Sciences of the United States of America* 97: 6185-90

Francesconi A, Kumari R, Zukin RS. 2009. Regulation of group I metabotropic glutamate receptor trafficking and signaling by the caveolar/lipid raft pathway. *J Neurosci* 29: 3590-602

Frederick AL, Yano H, Trifilieff P, Vishwasrao HD, Biezonski D, et al. 2015. Evidence against dopamine D1/D2 receptor heteromers. *Mol Psychiatry* 20: 1373-85

Fujii S, Yamazoe G, Itoh M, Kubo Y, Saitoh O. 2008. Spinophilin inhibits the binding of RGS8 to M1-mAChR but enhances the regulatory function of RGS8. *Biochemical and biophysical research communications* 377: 200-4

Gandhi NJ, Katnani HA. 2011. Motor functions of the superior colliculus. *Annu Rev Neurosci* 34: 205-31

Gereau RWt, Heinemann SF. 1998. Role of protein kinase C phosphorylation in rapid desensitization of metabotropic glutamate receptor 5. *Neuron* 20: 143-51

Gerfen CR, Engber TM, Mahan LC, Susel Z, Chase TN, et al. 1990. D1 and D2 dopamine receptor-regulated gene expression of striatonigral and striatopallidal neurons. *Science* 250: 1429-32

Gerfen CR, Surmeier DJ. 2011. Modulation of striatal projection systems by dopamine. *Annual review of neuroscience* 34: 441-66

Gillan CM, Morein-Zamir S, Kaser M, Fineberg NA, Sule A, et al. 2014a. Counterfactual processing of economic action-outcome alternatives in obsessive-compulsive disorder: further evidence of impaired goal-directed behavior. *Biol Psychiatry* 75: 639-46

Gillan CM, Morein-Zamir S, Urcelay GP, Sule A, Voon V, et al. 2014b. Enhanced avoidance habits in obsessive-compulsive disorder. *Biol Psychiatry* 75: 631-8

Gillan CM, Papmeyer M, Morein-Zamir S, Sahakian BJ, Fineberg NA, et al. 2011. Disruption in the balance between goal-directed behavior and habit learning in obsessive-compulsive disorder. *Am J Psychiatry* 168: 718-26

Gladding CM, Fitzjohn SM, Molnár E. 2009. Metabotropic glutamate receptor-mediated long-term depression: molecular mechanisms. *Pharmacological reviews* 61: 395-412

Golani I, Fentress JC. 1985. Early ontogeny of face grooming in mice. *Dev Psychobiol* 18: 529-44

Graybiel AM. 1998. The basal ganglia and chunking of action repertoires. *Neurobiol Learn Mem* 70: 119-36

Graybiel AM. 2008. Habits, rituals, and the evaluative brain. *Annu Rev Neurosci* 31: 359-87

Graybiel AM, Rauch SL. 2000. Toward a Neurobiology of Obsessive-Compulsive Disorder. *Neuron* 28: 343-47

Grecco GG, Haggerty DL, Doud EH, Fritz BM, Yin F, et al. 2021. A multi-omic analysis of the dorsal striatum in an animal model of divergent genetic risk for alcohol use disorder. *J Neurochem* 157: 1013-31

Greengard P. 2001. The neurobiology of slow synaptic transmission. *Science* 294: 1024-30

Grossberg S, Kishnan D. 2018. Neural Dynamics of Autistic Repetitive Behaviors and Fragile X Syndrome: Basal Ganglia Movement Gating and mGluR-Modulated Adaptively Timed Learning. *Frontiers in psychology* 9: 269

Grossman SD, Futter M, Snyder GL, Allen PB, Nairn AC, et al. 2004. Spinophilin is phosphorylated by Ca2+/calmodulin-dependent protein kinase II resulting in regulation of its binding to F-actin. *J Neurochem* 90: 317-24

Gubellini P, Saulle E, Centonze D, Bonsi P, Pisani A, et al. 2001. Selective involvement of mGlu1 receptors in corticostriatal LTD. *Neuropharmacology* 40: 839-46

Hadjas LC, Lüscher C, Simmler LD. 2019. Aberrant habit formation in the Sapap3-knockout mouse model of obsessive-compulsive disorder. *Sci Rep* 9: 12061

Hadjas LC, Schartner MM, Cand J, Creed MC, Pascoli V, et al. 2020. Projection-specific deficits in synaptic transmission in adult Sapap3-knockout mice. *Neuropsychopharmacology : official publication of the American College of Neuropsychopharmacology*

Harrison BJ, Pujol J, Cardoner N, Deus J, Alonso P, et al. 2013. Brain corticostriatal systems and the major clinical symptom dimensions of obsessive-compulsive disorder. *Biol Psychiatry* 73: 321-8

Hayashi MK, Ames HM, Hayashi Y. 2006. Tetrameric hub structure of postsynaptic scaffolding protein homer. *Journal of Neuroscience* 26: 8492-501

He J, Wink S, de Bont H, Le Dévédec S, Zhang Y, van de Water B. 2019. FRET biosensor-based kinase inhibitor screen for ERK and AKT activity reveals differential kinase dependencies for proliferation in TNBC cells. *Biochem Pharmacol* 169: 113640

Hellyer SD, Albold S, Sengmany K, Singh J, Leach K, Gregory KJ. 2019. Metabotropic glutamate receptor 5 (mGlu5)-positive allosteric modulators differentially induce or potentiate desensitization of mGlu5 signaling in recombinant cells and neurons. *J Neurochem* 151: 301-15

Hiday AC, Edler MC, Salek AB, Morris CW, Thang M, et al. 2017. Mechanisms and Consequences of Dopamine Depletion-Induced Attenuation of the Spinophilin/Neurofilament Medium Interaction. *Neural plasticity* 2017: 4153076

Hikosaka O, Takikawa Y, Kawagoe R. 2000. Role of the basal ganglia in the control of purposive saccadic eye movements. *Physiol Rev* 80: 953-78

Holz A, Mülsch F, Schwarz MK, Hollmann M, Döbrössy MD, et al. 2019. Enhanced mGlu5 Signaling in Excitatory Neurons Promotes Rapid Antidepressant Effects via AMPA Receptor Activation. *Neuron* 104: 338-52.e7

Hong W, Kim DW, Anderson DJ. 2014. Antagonistic control of social versus repetitive self-grooming behaviors by separable amygdala neuronal subsets. *Cell* 158: 1348-61

Hou JM, Zhao M, Zhang W, Song LH, Wu WJ, et al. 2014. Resting-state functional connectivity abnormalities in patients with obsessive-compulsive disorder and their healthy first-degree relatives. *J Psychiatry Neurosci* 39: 304-11

Hsieh-Wilson LC, Allen PB, Watanabe T, Nairn AC, Greengard P. 1999. Characterization of the neuronal targeting protein spinophilin and its interactions with protein phosphatase-1. *Biochemistry* 38: 4365-73

Hu HJ, Alter BJ, Carrasquillo Y, Qiu CS, Gereau RWt. 2007. Metabotropic glutamate receptor 5 modulates nociceptive plasticity via extracellular signal-regulated kinase-Kv4.2 signaling in spinal cord dorsal horn neurons. *J Neurosci* 27: 13181-91

Hu XD, Liu YN, Zhang ZY, Ma ZA, Suo ZW, Yang X. 2015. Spinophilin-Targeted Protein Phosphatase-1 Alleviated Inflammatory Pain by Negative Control of MEK/ERK Signaling in Spinal Cord Dorsal Horn of Rats. *J Neurosci* 35: 13989-4001

Hunnicutt BJ, Jongbloets BC, Birdsong WT, Gertz KJ, Zhong H, Mao T. 2016. A comprehensive excitatory input map of the striatum reveals novel functional organization. *Elife* 5

Hunnicutt BJ, Long BR, Kusefoglu D, Gertz KJ, Zhong H, Mao T. 2014. A comprehensive thalamocortical projection map at the mesoscopic level. *Nat Neurosci* 17: 1276-85

Isobe M, Redden SA, Keuthen NJ, Stein DJ, Lochner C, et al. 2018. Striatal abnormalities in trichotillomania: A multi-site MRI analysis. *NeuroImage: Clinical* 17: 893-98

Jahanshahi M, Obeso I, Rothwell JC, Obeso JA. 2015a. A fronto-striato-subthalamic-pallidal network for goal-directed and habitual inhibition. *Nature reviews. Neuroscience* 16: 719-32

Jahanshahi M, Obeso I, Rothwell JC, Obeso JA. 2015b. A fronto–striato–subthalamic–pallidal network for goal-directed and habitual inhibition. *Nature Reviews Neuroscience* 16: 719

Jin X, Costa RM. 2010. Start/stop signals emerge in nigrostriatal circuits during sequence learning. *Nature* 466: 457-62

Jin X, Tecuapetla F, Costa RM. 2014. Basal ganglia subcircuits distinctively encode the parsing and concatenation of action sequences. *Nat Neurosci* 17: 423-30

Jog MS, Kubota Y, Connolly CI, Hillegaart V, Graybiel AM. 1999. Building neural representations of habits. *Science* 286: 1745-9

Kalinowska M, Castillo C, Francesconi A. 2015. Quantitative Profiling of Brain Lipid Raft Proteome in a Mouse Model of Fragile X Syndrome. *PLOS ONE* 10: e0121464

Kalueff AV, Aldridge JW, LaPorte JL, Murphy DL, Tuohimaa P. 2007. Analyzing grooming microstructure in neurobehavioral experiments. *Nat Protoc* 2: 2538-44

Kalueff AV, Stewart AM, Song C, Berridge KC, Graybiel AM, Fentress JC. 2016. Neurobiology of rodent self-grooming and its value for translational neuroscience. *Nature reviews. Neuroscience* 17: 45-59

Kammermeier PJ, Xiao B, Tu JC, Worley PF, Ikeda SR. 2000. Homer proteins regulate coupling of group I metabotropic glutamate receptors to N-type calcium and M-type potassium channels. *The Journal of neuroscience : the official journal of the Society for Neuroscience* 20: 7238-45

Kang J, Kim H, Hwang SH, Han M, Lee S-H, Kim HF. 2021. Primate ventral striatum maintains neural representations of the value of previously rewarded objects for habitual seeking. *Nature communications* 12: 2100

Karno M, Golding JM, Sorenson SB, Burnam MA. 1988. The epidemiology of obsessive-compulsive disorder in five US communities. *Arch Gen Psychiatry* 45: 1094-9

Khakh BS. 2019. Astrocyte-Neuron Interactions in the Striatum: Insights on Identity, Form, and Function. *Trends in neurosciences* 42: 617-30

Khan MM, Dhandapani KM, Zhang QG, Brann DW. 2013. Estrogen regulation of spine density and excitatory synapses in rat prefrontal and somatosensory cerebral cortex. *Steroids* 78: 614-23

Kim CH, Braud S, Isaac JT, Roche KW. 2005. Protein kinase C phosphorylation of the metabotropic glutamate receptor mGluR5 on Serine 839 regulates Ca2+ oscillations. *J Biol Chem* 280: 25409-15

Kim H, Lee Y, Park JY, Kim JE, Kim TK, et al. 2017. Loss of Adenylyl Cyclase Type-5 in the Dorsal Striatum Produces Autistic-Like Behaviors. *Mol Neurobiol* 54: 7994-8008

Kimchi EY, Laubach M. 2009. Dynamic encoding of action selection by the medial striatum. *J Neurosci* 29: 3148-59

Kliewer A, Reinscheid RK, Schulz S. 2017. Emerging Paradigms of G Protein-Coupled Receptor Dephosphorylation. *Trends Pharmacol Sci* 38: 621-36

Ko SJ, Isozaki K, Kim I, Lee JH, Cho HJ, et al. 2012. PKC phosphorylation regulates mGluR5 trafficking by enhancing binding of Siah-1A. *J Neurosci* 32: 16391-401

Kolb B, Milner B. 1981. Performance of complex arm and facial movements after focal brain lesions. *Neuropsychologia* 19: 491-503

Koralek AC, Jin X, Long JD, 2nd, Costa RM, Carmena JM. 2012. Corticostriatal plasticity is necessary for learning intentional neuroprosthetic skills. *Nature* 483: 331-5

Kravitz AV, Freeze BS, Parker PR, Kay K, Thwin MT, et al. 2010. Regulation of parkinsonian motor behaviours by optogenetic control of basal ganglia circuitry. *Nature* 466: 622-6

Kravitz AV, Kreitzer AC. 2012. Striatal mechanisms underlying movement, reinforcement, and punishment. *Physiology (Bethesda)* 27: 167-77

Kreitzer AC. 2009. Physiology and pharmacology of striatal neurons. *Annu Rev Neurosci* 32: 127-47

Kreitzer AC, Malenka RC. 2005. Dopamine modulation of state-dependent endocannabinoid release and long-term depression in the striatum. *Journal of Neuroscience* 25: 10537-45

Kreitzer AC, Malenka RC. 2007. Endocannabinoid-mediated rescue of striatal LTD and motor deficits in Parkinson's disease models. *Nature* 445: 643-47

Kruk MR, Westphal KG, Van Erp AM, van Asperen J, Cave BJ, et al. 1998. The hypothalamus: cross-roads of endocrine and behavioural regulation in grooming and aggression. *Neuroscience and biobehavioral reviews* 23: 163-77

Kupferschmidt DA, Juczewski K, Cui G, Johnson KA, Lovinger DM. 2017. Parallel, but Dissociable, Processing in Discrete Corticostriatal Inputs Encodes Skill Learning. *Neuron* 96: 476-89.e5

Kurogi M, Nagatomo K, Kubo Y, Saitoh O. 2009. Effects of spinophilin on the function of RGS8 regulating signals from M2 and M3-mAChRs. *Neuroreport* 20: 1134-9

Lacey CJ, Boyes J, Gerlach O, Chen L, Magill PJ, Bolam JP. 2005. GABA(B) receptors at glutamatergic synapses in the rat striatum. *Neuroscience* 136: 1083-95

Lang DM, Lommel S, Jung M, Ankerhold R, Petrausch B, et al. 1998. Identification of reggie-1 and reggie-2 as plasmamembrane-associated proteins which cocluster with activated GPI-anchored cell adhesion molecules in non-caveolar micropatches in neurons. *J Neurobiol* 37: 502-23

Lee JH, Lee J, Choi KY, Hepp R, Lee JY, et al. 2008. Calmodulin dynamically regulates the trafficking of the metabotropic glutamate receptor mGluR5. *Proceedings of the National Academy of Sciences of the United States of America* 105: 12575-80

Li J, Van Vranken JG, Pontano Vaites L, Schweppe DK, Huttlin EL, et al. 2020. TMTpro reagents: a set of isobaric labeling mass tags enables simultaneous proteome-wide measurements across 16 samples. *Nat Methods* 17: 399-404

Lim SAO, Kang UJ, McGehee DS. 2014. Striatal cholinergic interneuron regulation and circuit effects. *Frontiers in Synaptic Neuroscience* 6

Lovinger DM, Tyler E. 1996. Synaptic transmission and modulation in the neostriatum. *International review of neurobiology* 39: 77-111

Lüscher C, Huber KM. 2010. Group 1 mGluR-dependent synaptic long-term depression: mechanisms and implications for circuitry and disease. *Neuron* 65: 445-59

Ma T, Cheng Y, Roltsch Hellard E, Wang X, Lu J, et al. 2018. Bidirectional and long-lasting control of alcohol-seeking behavior by corticostriatal LTP and LTD. *Nat Neurosci* 21: 373-83

Mahon S, Deniau J-M, Charpier S. 2004. Corticostriatal plasticity: life after the depression. *Trends in Neurosciences* 27: 460-67

Mailly P, Aliane V, Groenewegen HJ, Haber SN, Deniau JM. 2013. The rat prefrontostriatal system analyzed in 3D: evidence for multiple interacting functional units. *J Neurosci* 33: 5718-27

Mao L, Yang L, Arora A, Choe ES, Zhang G, et al. 2005a. Role of protein phosphatase 2A in mGluR5-regulated MEK/ERK phosphorylation in neurons. *J Biol Chem* 280: 12602-10

Mao L, Yang L, Tang Q, Samdani S, Zhang G, Wang JQ. 2005b. The scaffold protein Homer1b/c links metabotropic glutamate receptor 5 to extracellular signal-regulated protein kinase cascades in neurons. *J Neurosci* 25: 2741-52

Mao LM, Wang JQ. 2016. Dopamine D2 receptors are involved in the regulation of Fyn and metabotropic glutamate receptor 5 phosphorylation in the rat striatum in vivo. *J Neurosci Res* 94: 329-38

Marshall CR, Noor A, Vincent JB, Lionel AC, Feuk L, et al. 2008. Structural Variation of Chromosomes in Autism Spectrum Disorder. *The American Journal of Human Genetics* 82: 477-88

Martiros N, Burgess AA, Graybiel AM. 2018. Inversely Active Striatal Projection Neurons and Interneurons Selectively Delimit Useful Behavioral Sequences. *Curr Biol* 28: 560-73.e5

Mathur BN, Lovinger DM. 2012. Endocannabinoid-dopamine interactions in striatal synaptic plasticity. *Frontiers in pharmacology* 3: 66

Matosin N, Fernandez-Enright F, Lum JS, Newell KA. 2017. Shifting towards a model of mGluR5 dysregulation in schizophrenia: consequences for future schizophrenia treatment. *Neuropharmacology* 115: 73-91

Matosin N, Siegel SJ. 2016. Metabotropic Glutamate Receptor 5 as a Point of Convergence for Models of Obsessive-Compulsive Disorder and Autism Spectrum Disorder. *Biological Psychiatry* 80: 504-06

Mattheisen M, Samuels JF, Wang Y, Greenberg BD, Fyer AJ, et al. 2015. Genome-wide association study in obsessive-compulsive disorder: results from the OCGAS. *Mol Psychiatry* 20: 337-44

McGeorge AJ, Faull RLM. 1989. The organization of the projection from the cerebral cortex to the striatum in the rat. *Neuroscience* 29: 503-37

Mehta MV, Gandal MJ, Siegel SJ. 2011. mGluR5-antagonist mediated reversal of elevated stereotyped, repetitive behaviors in the VPA model of autism. *PLoS One* 6: e26077

Michalon A, Sidorov M, Ballard Theresa M, Ozmen L, Spooren W, et al. 2012. Chronic Pharmacological mGlu5 Inhibition Corrects Fragile X in Adult Mice. *Neuron* 74: 49-56

Monakow KH, Akert K, Künzle H. 1978. Projections of the precentral motor cortex and other cortical areas of the frontal lobe to the subthalamic nucleus in the monkey. *Experimental brain research* 33: 395-403

Morató X, Luján R, Gonçalves N, Watanabe M, Altafaj X, et al. 2018. Metabotropic glutamate type 5 receptor requires contactin-associated protein 1 to control memory formation. *Human Molecular Genetics* 27: 3528-41

Morris CW, Watkins DS, Pennington T, Doud EH, Qi G, et al. 2022. Spinophilin limits metabotropic glutamate receptor 5 scaffolding to the postsynaptic density and cell type-specifically mediates excessive grooming. *bioRxiv*: 2022.05.24.493240

Morris CW, Watkins DS, Salek AB, Edler MC, Baucum AJ, 2nd. 2018. The association of spinophilin with disks large-associated protein 3 (SAPAP3) is regulated by metabotropic glutamate receptor (mGluR) 5. *Molecular and cellular neurosciences* 90: 60-69

Muhammad K, Reddy-Alla S, Driller JH, Schreiner D, Rey U, et al. 2015. Presynaptic spinophilin tunes neurexin signalling to control active zone architecture and function. *Nature communications* 6: 8362

Muly EC, Allen P, Mazloom M, Aranbayeva Z, Greenfield AT, Greengard P. 2004. Subcellular distribution of neurabin immunolabeling in primate prefrontal cortex: comparison with spinophilin. *Cerebral cortex (New York, N.Y. : 1991)* 14: 1398-407

Naaz S, Balachander S, Srinivasa Murthy N, Ms B, Sud R, et al. 2020. Association of SAPAP3 allelic variants with symptom dimensions and pharmacological treatment response in obsessive-compulsive disorder. *Exp Clin Psychopharmacol*

Nakano K. 2000. Neural circuits and topographic organization of the basal ganglia and related regions. *Brain Dev* 22 Suppl 1: S5-16

Nambu A, Tokuno H, Hamada I, Kita H, Imanishi M, et al. 2000. Excitatory cortical inputs to pallidal neurons via the subthalamic nucleus in the monkey. *J Neurophysiol* 84: 289-300

Nambu A, Tokuno H, Takada M. 2002. Functional significance of the cortico-subthalamo-pallidal 'hyperdirect' pathway. *Neurosci Res* 43: 111-7

Nazeer A, Latif F, Mondal A, Azeem MW, Greydanus DE. 2020. Obsessive-compulsive disorder in children and adolescents: epidemiology, diagnosis and management. *Transl Pediatr* 9: S76-s93

Nazzaro C, Greco B, Cerovic M, Baxter P, Rubino T, et al. 2012. SK channel modulation rescues striatal plasticity and control over habit in cannabinoid tolerance. *Nat Neurosci* 15: 284-93

NIMH. 2017. Prevalence of Obsessive-Compulsive Disorder Among Adults. Harvard Medical School: National Comorbidity Survey

Niswender CM, Conn PJ. 2010. Metabotropic glutamate receptors: physiology, pharmacology, and disease. *Annu Rev Pharmacol Toxicol* 50: 295-322

Noetzel MJ, Rook JM, Vinson PN, Cho HP, Days E, et al. 2012. Functional impact of allosteric agonist activity of selective positive allosteric modulators of metabotropic glutamate receptor subtype 5 in regulating central nervous system function. *Mol Pharmacol* 81: 120-33

Notartomaso S, Zappulla C, Biagioni F, Cannella M, Bucci D, et al. 2013. Pharmacological enhancement of mGlu1 metabotropic glutamate receptors causes a prolonged symptomatic benefit in a mouse model of spinocerebellar ataxia type 1. *Molecular Brain* 6: 48

Nuñez A, Malmierca E. 2007. Corticofugal modulation of sensory information. *Adv Anat Embryol Cell Biol* 187: 1 p following table of contents, 1-74

Nusser Z, Mulvihill E, Streit P, Somogyi P. 1994. Subsynaptic segregation of metabotropic and ionotropic glutamate receptors as revealed by immunogold localization. *Neuroscience* 61: 421-27

O'Hare JK, Ade KK, Sukharnikova T, Van Hooser SD, Palmeri ML, et al. 2016. Pathway-Specific Striatal Substrates for Habitual Behavior. *Neuron* 89: 472-9

O'Sullivan RL, Rauch SL, Breiter HC, Grachev ID, Baer L, et al. 1997. Reduced basal ganglia volumes in trichotillomania measured via morphometric magnetic resonance imaging. *Biological Psychiatry* 42: 39-45

Orlando LR, Dunah AW, Standaert DG, Young AB. 2002. Tyrosine phosphorylation of the metabotropic glutamate receptor mGluR5 in striatal neurons. *Neuropharmacology* 43: 161-73

Ouimet CC, Katona I, Allen P, Freund TF, Greengard P. 2004. Cellular and subcellular distribution of spinophilin, a PP1 regulatory protein that bundles F-actin in dendritic spines. *J Comp Neurol* 479: 374-88

Page G, Khidir FA, Pain S, Barrier L, Fauconneau B, et al. 2006. Group I metabotropic glutamate receptors activate the p70S6 kinase via both mammalian target of rapamycin (mTOR) and extracellular signal-regulated kinase (ERK 1/2) signaling pathways in rat striatal and hippocampal synaptoneurosomes. *Neurochem Int* 49: 413-21

Park J, Coddington LT, Dudman JT. 2020. Basal Ganglia Circuits for Action Specification. *Annu Rev Neurosci* 43: 485-507
Peça J, Feliciano C, Ting JT, Wang W, Wells MF, et al. 2011. Shank3 mutant mice display autistic-like behaviours and striatal dysfunction. *Nature* 472: 437-42
Pelkey KA, Askalan R, Paul S, Kalia LV, Nguyen TH, et al. 2002. Tyrosine phosphatase STEP is a tonic brake on induction of long-term potentiation. *Neuron* 34: 127-38
Perrin E, Venance L. 2019. Bridging the gap between striatal plasticity and learning. *Curr Opin Neurobiol* 54: 104-12
Pinto D, Pagnamenta AT, Klei L, Anney R, Merico D, et al. 2010. Functional impact of global rare copy number variation in autism spectrum disorders. *Nature* 466: 368-72
Pop AS, Gomez-Mancilla B, Neri G, Willemsen R, Gasparini F. 2014. Fragile X syndrome: a preclinical review on metabotropic glutamate receptor 5 (mGluR5) antagonists and drug development. *Psychopharmacology (Berl)* 231: 1217-26
Prasad C, Prasad AN, Chodirker BN, Lee C, Dawson AK, et al. 2000. Genetic evaluation of pervasive developmental disorders: the terminal 22q13 deletion syndrome may represent a recognizable phenotype. *Clinical Genetics* 57: 103-09
Pujol J, Soriano-Mas C, Alonso P, Cardoner N, Menchon JM, et al. 2004a. Mapping structural brain alterations in obsessive-compulsive disorder. *Arch Gen Psychiatry* 61: 720-30
Pujol J, Soriano-Mas C, Alonso P, Cardoner N, Menchón JM, et al. 2004b. Mapping structural brain alterations in obsessive-compulsive disorder. *Arch Gen Psychiatry* 61: 720-30
Ragusa MJ, Dancheck B, Critton DA, Nairn AC, Page R, Peti W. 2010. Spinophilin directs protein phosphatase 1 specificity by blocking substrate binding sites. *Nature structural & molecular biology* 17: 459-64
Raka F, Di Sebastiano AR, Kulhawy SC, Ribeiro FM, Godin CM, et al. 2015. Ca2+/Calmodulin-dependent protein Kinase II interacts with group I Metabotropic Glutamate and facilitates Receptor Endocytosis and ERK1/2 signaling: role of β-Amyloid. *Molecular Brain* 8: 21
Ramírez-Armenta KI, Alatriste-León H, Verma-Rodríguez AK, Llanos-Moreno A, Ramírez-Jarquín JO, Tecuapetla F. 2022. Optogenetic inhibition of indirect pathway neurons in the dorsomedial striatum reduces excessive grooming in Sapap3-knockout mice. *Neuropsychopharmacology : official publication of the American College of Neuropsychopharmacology* 47: 477-87
Rasmussen AH, Rasmussen HB, Silahtaroglu A. 2017. The DLGAP family: neuronal expression, function and role in brain disorders. *Mol Brain* 10: 43
Rauch SL, Jenike MA, Alpert NM, Baer L, Breiter HC, et al. 1994. Regional cerebral blood flow measured during symptom provocation in obsessive-compulsive disorder using oxygen 15-labeled carbon dioxide and positron emission tomography. *Arch Gen Psychiatry* 51: 62-70
Reynolds JN, Wickens JR. 2002. Dopamine-dependent plasticity of corticostriatal synapses. *Neural networks* 15: 507-21
Robbins TW, Vaghi MM, Banca P. 2019. Obsessive-Compulsive Disorder: Puzzles and Prospects. *Neuron* 102: 27-47

Roeling TA, Veening JG, Peters JP, Vermelis ME, Nieuwenhuys R. 1993. Efferent connections of the hypothalamic "grooming area" in the rat. *Neuroscience* 56: 199-225

Ronesi JA, Collins KA, Hays SA, Tsai NP, Guo W, et al. 2012. Disrupted Homer scaffolds mediate abnormal mGluR5 function in a mouse model of fragile X syndrome. *Nat Neurosci* 15: 431-40, s1

Rothwell PE, Fuccillo MV, Maxeiner S, Hayton SJ, Gokce O, et al. 2014. Autism-associated neuroligin-3 mutations commonly impair striatal circuits to boost repetitive behaviors. *Cell* 158: 198-212

Rothwell PE, Hayton SJ, Sun GL, Fuccillo MV, Lim BK, Malenka RC. 2015. Input-and output-specific regulation of serial order performance by corticostriatal circuits. *Neuron* 88: 345-56

Sakai Y, Narumoto J, Nishida S, Nakamae T, Yamada K, et al. 2011. Corticostriatal functional connectivity in non-medicated patients with obsessive-compulsive disorder. *Eur Psychiatry* 26: 463-9

Salek AB, Edler MC, McBride JP, Baucum AJ, 2nd. 2019. Spinophilin regulates phosphorylation and interactions of the GluN2B subunit of the N-methyl-d-aspartate receptor. *J Neurochem* 151: 185-203

Sarrouilhe D, di Tommaso A, Metaye T, Ladeveze V. 2006. Spinophilin: from partners to functions. *Biochimie* 88: 1099-113

Saugstad JA, Marino MJ, Folk JA, Hepler JR, Conn PJ. 1998. RGS4 Inhibits Signaling by Group I Metabotropic Glutamate Receptors. *The Journal of Neuroscience* 18: 905-13

Schiffmann SN, Fisone G, Moresco R, Cunha RA, Ferré S. 2007. Adenosine A2A receptors and basal ganglia physiology. *Prog Neurobiol* 83: 277-92

Schuler H, Peti W. 2008. Structure-function analysis of the filamentous actin binding domain of the neuronal scaffolding protein spinophilin. *The FEBS journal* 275: 59-68

Schwendt M, McGinty JF. 2007. Regulator of G-protein signaling 4 interacts with metabotropic glutamate receptor subtype 5 in rat striatum: relevance to amphetamine behavioral sensitization. *J Pharmacol Exp Ther* 323: 650-7

Schwendt M, Sigmon SA, McGinty JF. 2012. RGS4 overexpression in the rat dorsal striatum modulates mGluR5- and amphetamine-mediated behavior and signaling. *Psychopharmacology* 221: 621-35

Seiler JL, Cosme CV, Sherathiya VN, Schaid MD, Bianco JM, et al. 2022. Dopamine signaling in the dorsomedial striatum promotes compulsive behavior. *Curr Biol* 32: 1175-88.e5

Seo M, Lee E, Averbeck BB. 2012. Action selection and action value in frontal-striatal circuits. *Neuron* 74: 947-60

Shah A, Silverstein PS, Singh DP, Kumar A. 2012. Involvement of metabotropic glutamate receptor 5, AKT/PI3K signaling and NF-κB pathway in methamphetamine-mediated increase in IL-6 and IL-8 expression in astrocytes. *J Neuroinflammation* 9: 52

Shan Q, Christie MJ, Balleine BW. 2015. Plasticity in striatopallidal projection neurons mediates the acquisition of habitual actions. *The European journal of neuroscience* 42: 2097-104

Shen W, Flajolet M, Greengard P, Surmeier DJ. 2008. Dichotomous dopaminergic control of striatal synaptic plasticity. *Science* 321: 848-51

Sheng M, Hoogenraad CC. 2007. The Postsynaptic Architecture of Excitatory Synapses: A More Quantitative View. *Annual Review of Biochemistry* 76: 823-47

Sheng M, Kim E. 2000. The Shank family of scaffold proteins. *J Cell Sci* 113 (Pt 11): 1851-6

Sheng MJ, Lu D, Shen ZM, Poo MM. 2019. Emergence of stable striatal D1R and D2R neuronal ensembles with distinct firing sequence during motor learning. *Proceedings of the National Academy of Sciences of the United States of America*

Shigemoto R, Nomura S, Ohishi H, Sugihara H, Nakanishi S, Mizuno N. 1993. Immunohistochemical localization of a metabotropic glutamate receptor, mGluR5, in the rat brain. *Neuroscience letters* 163: 53-57

Smith FD, Oxford GS, Milgram SL. 1999. Association of the D2 dopamine receptor third cytoplasmic loop with spinophilin, a protein phosphatase-1-interacting protein. *J Biol Chem* 274: 19894-900

Smith Y, Raju DV, Pare J-F, Sidibe M. 2004. The thalamostriatal system: a highly specific network of the basal ganglia circuitry. *Trends in neurosciences* 27: 520-27

Stein BD, Herzig S, Martínez-Bartolomé S, Lavallée-Adam M, Shaw RJ, Yates JR. 2019. Comparison of CRISPR Genomic Tagging for Affinity Purification and Endogenous Immunoprecipitation Coupled with Quantitative Mass Spectrometry To Identify the Dynamic AMPKα2 Interactome. *Journal of Proteome Research* 18: 3703-14

Stein DJ, van Heerden B, Hugo C, van Kradenburg J, Warwick J, et al. 2002. Functional brain imaging and pharmacotherapy in trichotillomania: single photon emission computed tomography before and after treatment with the selective serotonin reuptake inhibitor citalopram. *Progress in Neuro-Psychopharmacology and Biological Psychiatry* 26: 885-90

Stewart SE, Yu D, Scharf JM, Neale BM, Fagerness JA, et al. 2013. Genome-wide association study of obsessive-compulsive disorder. *Molecular Psychiatry* 18: 788-98

Sugiyama H, Ito I, Hirono C. 1987. A new type of glutamate receptor linked to inositol phospholipid metabolism. *Nature* 325: 531-33

Surmeier DJ, Song W-J, Yan Z. 1996. Coordinated expression of dopamine receptors in neostriatal medium spiny neurons. *Journal of neuroscience* 16: 6579-91

Swedo SE, Rapoport JL, Leonard H, Lenane M, Cheslow D. 1989. Obsessive-compulsive disorder in children and adolescents. Clinical phenomenology of 70 consecutive cases. *Arch Gen Psychiatry* 46: 335-41

Tallaksen-Greene SJ, Kaatz KW, Romano C, Albin RL. 1998. Localization of mGluR1a-like immunoreactivity and mGluR5-like immunoreactivity in identified populations of striatal neurons. *Brain research* 780: 210-17

Taylor JL, Rajbhandari AK, Berridge KC, Aldridge JW. 2010. Dopamine receptor modulation of repetitive grooming actions in the rat: potential relevance for Tourette syndrome. *Brain Res* 1322: 92-101

Tecuapetla F, Matias S, Dugue GP, Mainen ZF, Costa RM. 2014. Balanced activity in basal ganglia projection pathways is critical for contraversive movements. *Nature communications* 5: 4315

Tepper JM, Bolam JP. 2004. Functional diversity and specificity of neostriatal interneurons. *Curr Opin Neurobiol* 14: 685-92

Tepper JM, Wilson CJ, Koós T. 2008. Feedforward and feedback inhibition in neostriatal GABAergic spiny neurons. *Brain Res Rev* 58: 272-81

Terry-Lorenzo RT, Roadcap DW, Otsuka T, Blanpied TA, Zamorano PL, et al. 2005. Neurabin/protein phosphatase-1 complex regulates dendritic spine morphogenesis and maturation. *Molecular biology of the cell* 16: 2349-62

Testa CM, Standaert DG, Landwehrmeyer GB, Penney JB, Jr., Young AB. 1995. Differential expression of mGluR5 metabotropic glutamate receptor mRNA by rat striatal neurons. *J Comp Neurol* 354: 241-52

Thamby A, Jaisoorya TS. 2019. Antipsychotic augmentation in the treatment of obsessive-compulsive disorder. *Indian J Psychiatry* 61: S51-s57

Thorn CA, Atallah H, Howe M, Graybiel AM. 2010. Differential dynamics of activity changes in dorsolateral and dorsomedial striatal loops during learning. *Neuron* 66: 781-95

Ting JT, Peca J, Feng G. 2012. Functional consequences of mutations in postsynaptic scaffolding proteins and relevance to psychiatric disorders. *Annual review of neuroscience* 35: 49-71

Toupin A, Benachenhou S, Abolghasemi A, Laroui A, Galarneau L, et al. 2022. Association of lipid rafts cholesterol with clinical profile in fragile X syndrome. *Scientific Reports* 12: 2936

Tricomi E, Balleine BW, O'Doherty JP. 2009. A specific role for posterior dorsolateral striatum in human habit learning. *European Journal of Neuroscience* 29: 2225-32

Trusel M, Cavaccini A, Gritti M, Greco B, Saintot PP, et al. 2015. Coordinated Regulation of Synaptic Plasticity at Striatopallidal and Striatonigral Neurons Orchestrates Motor Control. *Cell Rep* 13: 1353-65

Tu JC, Xiao B, Naisbitt S, Yuan JP, Petralia RS, et al. 1999. Coupling of mGluR/Homer and PSD-95 Complexes by the Shank Family of Postsynaptic Density Proteins. *Neuron* 23: 583-92

Tu JC, Xiao B, Yuan JP, Lanahan AA, Leoffert K, et al. 1998. Homer binds a novel proline-rich motif and links group 1 metabotropic glutamate receptors with IP3 receptors. *Neuron* 21: 717-26

Tunstall MJ, Oorschot DE, Kean A, Wickens JR. 2002. Inhibitory interactions between spiny projection neurons in the rat striatum. *J Neurophysiol* 88: 1263-9

Turner KM, Svegborn A, Langguth M, McKenzie C, Robbins TW. 2022. Opposing Roles of the Dorsolateral and Dorsomedial Striatum in the Acquisition of Skilled Action Sequencing in Rats. *The Journal of Neuroscience* 42: 2039-51

Uematsu K, Heiman M, Zelenina M, Padovan J, Chait BT, et al. 2015. Protein kinase A directly phosphorylates metabotropic glutamate receptor 5 to modulate its function. *J Neurochem* 132: 677-86

Um Ji W, Kaufman Adam C, Kostylev M, Heiss Jacqueline K, Stagi M, et al. 2013. Metabotropic Glutamate Receptor 5 Is a Coreceptor for Alzheimer Aβ Oligomer Bound to Cellular Prion Protein. *Neuron* 79: 887-902

Um JW, Ko J. 2017. Neural Glycosylphosphatidylinositol-Anchored Proteins in Synaptic Specification. *Trends Cell Biol* 27: 931-45

Vaghi MM, Cardinal RN, Apergis-Schoute AM, Fineberg NA, Sule A, Robbins TW. 2019. Action-Outcome Knowledge Dissociates From Behavior in Obsessive-Compulsive Disorder Following Contingency Degradation. *Biological Psychiatry: Cognitive Neuroscience and Neuroimaging* 4: 200-09

Valentin VV, Dickinson A, O'Doherty JP. 2007. Determining the neural substrates of goal-directed learning in the human brain. *Journal of Neuroscience* 27: 4019-26

Vincent K, Cornea VM, Jong Y-JI, Laferrière A, Kumar N, et al. 2016. Intracellular mGluR5 plays a critical role in neuropathic pain. *Nature communications* 7: 10604

Virshup DM, Shenolikar S. 2009. From promiscuity to precision: protein phosphatases get a makeover. *Molecular cell* 33: 537-45

Voulalas PJ, Holtzclaw L, Wolstenholme J, Russell JT, Hyman SE. 2005. Metabotropic glutamate receptors and dopamine receptors cooperate to enhance extracellular signal-regulated kinase phosphorylation in striatal neurons. *J Neurosci* 25: 3763-73

Walitza S, Melfsen S, Jans T, Zellmann H, Wewetzer C, Warnke A. 2011. Obsessive-compulsive disorder in children and adolescents. *Dtsch Arztebl Int* 108: 173-9

Wan Y, Ade KK, Caffall Z, Ilcim Ozlu M, Eroglu C, et al. 2014. Circuit-selective striatal synaptic dysfunction in the Sapap3 knockout mouse model of obsessive-compulsive disorder. *Biol Psychiatry* 75: 623-30

Wan Y, Feng G, Calakos N. 2011. Sapap3 deletion causes mGluR5-dependent silencing of AMPAR synapses. *J Neurosci* 31: 16685-91

Wang H. 2014. Lipid rafts: a signaling platform linking cholesterol metabolism to synaptic deficits in autism spectrum disorders. *Frontiers in behavioral neuroscience* 8: 104

Wang JL, Wang Y, Sun W, Yu Y, Wei N, et al. 2021. Spinophilin modulates pain through suppressing dendritic spine morphogenesis via negative control of Rac1-ERK signaling in rat spinal dorsal horn. *Neurobiology of disease* 152: 105302

Wang JW, Wang HD, Cong ZX, Zhang XS, Zhou XM, Zhang DD. 2013. Activation of metabotropic glutamate receptor 5 reduces the secondary brain injury after traumatic brain injury in rats. *Biochemical and biophysical research communications* 430: 1016-21

Wang Q, Zhao J, Brady AE, Feng J, Allen PB, et al. 2004. Spinophilin blocks arrestin actions in vitro and in vivo at G protein-coupled receptors. *Science* 304: 1940-4

Wang W, Li C, Chen Q, van der Goes MS, Hawrot J, et al. 2017. Striatopallidal dysfunction underlies repetitive behavior in Shank3-deficient model of autism. *J Clin Invest* 127: 1978-90

Wang X, Bey AL, Katz BM, Badea A, Kim N, et al. 2016. Altered mGluR5-Homer scaffolds and corticostriatal connectivity in a Shank3 complete knockout model of autism. *Nature communications* 7: 11459

Wang X, Zeng W, Kim MS, Allen PB, Greengard P, Muallem S. 2007. Spinophilin/neurabin reciprocally regulate signaling intensity by G protein-coupled receptors. *Embo j* 26: 2768-76

Wang X, Zeng W, Soyombo AA, Tang W, Ross EM, et al. 2005. Spinophilin regulates Ca2+ signalling by binding the N-terminal domain of RGS2 and the third intracellular loop of G-protein-coupled receptors. *Nature cell biology* 7: 405-11

Wang Z, Kai L, Day M, Ronesi J, Yin HH, et al. 2006. Dopaminergic control of corticostriatal long-term synaptic depression in medium spiny neurons is mediated by cholinergic interneurons. *Neuron* 50: 443-52

Watkins DS, True JD, Mosley AL, Baucum AJ, 2nd. 2018. Proteomic Analysis of the Spinophilin Interactome in Rodent Striatum Following Psychostimulant Sensitization. *Proteomes* 6

Welch JM, Lu J, Rodriguiz RM, Trotta NC, Peca J, et al. 2007. Cortico-striatal synaptic defects and OCD-like behaviours in Sapap3-mutant mice. *Nature* 448: 894-900

Welch JM, Wang D, Feng G. 2004. Differential mRNA expression and protein localization of the SAP90/PSD-95-associated proteins (SAPAPs) in the nervous system of the mouse. *J Comp Neurol* 472: 24-39

Wilson HL, Wong ACC, Shaw SR, Tse W-Y, Stapleton GA, et al. 2003. Molecular characterisation of the 22q13 deletion syndrome supports the role of haploinsufficiency of SHANK3/PROSAP2 in the major neurological symptoms. *Journal of Medical Genetics* 40: 575-84

Wu H, Cottingham C, Chen L, Wang H, Che P, et al. 2017. Age-dependent differential regulation of anxiety- and depression-related behaviors by neurabin and spinophilin. *PLoS One* 12: e0180638

Wu K, Hanna GL, Easter P, Kennedy JL, Rosenberg DR, Arnold PD. 2013. Glutamate system genes and brain volume alterations in pediatric obsessive-compulsive disorder: a preliminary study. *Psychiatry Res* 211: 214-20

Wu Y-W, Kim J-I, Tawfik Vivianne L, Lalchandani Rupa R, Scherrer G, Ding Jun B. 2015. Input- and Cell-Type-Specific Endocannabinoid-Dependent LTD in the Striatum. *Cell Reports* 10: 75-87

Xiao B, Tu JC, Worley PF. 2000. Homer: a link between neural activity and glutamate receptor function. *Curr Opin Neurobiol* 10: 370-4

Xie K, Martemyanov KA. 2011. Control of striatal signaling by g protein regulators. *Front Neuroanat* 5: 49

Yamagata M, Sanes JR, Weiner JA. 2003. Synaptic adhesion molecules. *Current Opinion in Cell Biology* 15: 621-32

Yan Z, Flores-Hernandez J, Surmeier DJ. 2001. Coordinated expression of muscarinic receptor messenger RNAs in striatal medium spiny neurons. *Neuroscience* 103: 1017-24

Yan Z, Hsieh-Wilson L, Feng J, Tomizawa K, Allen PB, et al. 1999. Protein phosphatase 1 modulation of neostriatal AMPA channels: regulation by DARPP-32 and spinophilin. *Nat Neurosci* 2: 13-7

Yin HH, Knowlton BJ, Balleine BW. 2004. Lesions of dorsolateral striatum preserve outcome expectancy but disrupt habit formation in instrumental learning. *European Journal of Neuroscience* 19: 181-89

Yin HH, Mulcare SP, Hilário MR, Clouse E, Holloway T, et al. 2009. Dynamic reorganization of striatal circuits during the acquisition and consolidation of a skill. *Nat Neurosci* 12: 333-41

Yin HH, Ostlund SB, Knowlton BJ, Balleine BW. 2005. The role of the dorsomedial striatum in instrumental conditioning. *The European journal of neuroscience* 22: 513-23

Yttri EA, Dudman JT. 2018. A Proposed Circuit Computation in Basal Ganglia: History-Dependent Gain. *Mov Disord* 33: 704-16

Zangrandi L, Schmuckermair C, Ghareh H, Castaldi F, Heilbronn R, et al. 2021. Loss of mGluR5 in D1 Receptor-Expressing Neurons Improves Stress Coping. *Int J Mol Sci* 22

Zhang JM, Wang HK, Ye CQ, Ge W, Chen Y, et al. 2003. ATP released by astrocytes mediates glutamatergic activity-dependent heterosynaptic suppression. *Neuron* 40: 971-82

Zhang Y-N, Fan J-K, Gu L, Yang H-M, Zhan S-Q, Zhang H. 2021. Metabotropic glutamate receptor 5 inhibits α-synuclein-induced microglia inflammation to protect from neurotoxicity in Parkinson's disease. *Journal of Neuroinflammation* 18: 23

Zhang Y, Song L, Dong H, Kim DS, Sun Z, et al. 2020. Spinophilin-deficient mice are protected from diet-induced obesity and insulin resistance. *Am J Physiol Endocrinol Metab* 319: E354-e62

Zhang Y, Venkitaramani DV, Gladding CM, Zhang Y, Kurup P, et al. 2008. The Tyrosine Phosphatase STEP Mediates AMPA Receptor Endocytosis after Metabotropic Glutamate Receptor Stimulation. *The Journal of Neuroscience* 28: 10561-66

Zimmermann H. 2000. Extracellular metabolism of ATP and other nucleotides. *Naunyn Schmiedebergs Arch Pharmacol* 362: 299-309

Zuchner S, Wendland JR, Ashley-Koch AE, Collins AL, Tran-Viet KN, et al. 2009. Multiple rare SAPAP3 missense variants in trichotillomania and OCD. *Mol Psychiatry* 14: 6-9

Zuena AR, Iacovelli L, Orlando R, Di Menna L, Casolini P, et al. 2018. In Vivo Non-radioactive Assessment of mGlu5 Receptor-Activated Polyphosphoinositide Hydrolysis in Response to Systemic Administration of a Positive Allosteric Modulator. *Frontiers in pharmacology* 9

Curriculum Vitae

Cameron W. Morris

Education

Indiana University
Doctor of Philosophy in Medical Neuroscience earned at Indiana University-Purdue University Indianapolis (IUPUI)
September 2022

Purdue University
Bachelor of Science earned in Chemistry and Neuroscience earned at IUPUI
December 2016

Manuscripts

In Preparation

Prita R. Asih*, **Cameron W. Morris***, Hong Wang, Steve Pedrini, Kathryn Goozee, Preeti Dave, Simon M. Laws, Kevin Taddei, Hamid Sohrabi, Pratishtha Chatterjee, and Ralph N Martins (2022). Association of plasma soluble TREM2 with neocortical amyloid-β load, neuroinflammation, and neurodegeneration in cognitively normal older adults at risk of Alzheimer's disease.

In Review

Cameron W. Morris, Darryl S. Watkins, Taylor Pennington, Emma H. Doud, Guihong Qi, Amber L. Mosley, Brady K. Atwood, Anthony J. Baucum II (2022). Spinophilin limits metabotropic glutamate receptor 5 scaffolding to the postsynaptic density and cell type-specifically mediates excessive grooming. In review at Biological Psychiatry. Preprint posted on BioRXiv. 10.1101/2022.05.24.493240

Published

Grecco, G.G., Mork, B., Huang, J.-Y., Metzger, C.E., Haggerty, D.L., Reeves, K.C., Gao, Y., Hoffman, H., Katner, S.N., Masters, A.R., **Morris, C.W**., Newell, E.A., Engleman, E.A., Baucum, II A.J., Kim, J., Yamamoto, B.K., Allen, M.R., Wu, Y.-C., Lu, H.-C., Sheets, P.L., Atwood, B.K. (2020). Prenatal methadone exposure disrupts behavioral development and alters motor neuron intrinsic properties and local circuitry. eLife. PMID: 33724184

Cameron W. Morris*, Darryl S. Watkins*, Asma B. Salek*, Michael C. Edler Jr., Anthony J Baucum II. The association of spinophilin with disks large-associated protein 3 (SAPAP3) is regulated by metabotropic glutamate receptor (mGluR) 5. Molecular and Cellular Neuroscience. PMID: 29908232

Michael C. Edler, Asma B. Salek, Darryl S. Watkins, Harjot Kaur, **Cameron W. Morris**, Bryan K. Yamamoto, Anthony J. Baucum II. Mechanisms Regulating the Association of Protein Phosphatase 1 with Spinophilin and Neurabin. ACS Chem Neurosci. PMID: 29786422

Andrew C. Hiday, Michael C. Edler, Asma B. Salek, **Cameron W. Morris**, Morrent Thang, Tyler J. Rentz, Kristie L. Rose, Lisa M Jones, Anthony J. Baucum II. Mechanisms and consequences of dopamine depletion-induced attenuation of the spinophilin/neurofilament medium interaction. Neural Plasticity. PMID: 28634551

* Indicates co-first authorship

Abstracts

Invited Talks

C. W. Morris. (2022) Spinophilin mediates mGluR5-dependent excessive grooming cell type-specifically. Stark Neuroscience Research Institute (SNRI) Seminar. April 2022, SNRI, Indianapolis, IN 46202

C. W. Morris. (2021) Conditional spinophilin knockout mice as a novel model for detailing striatal MSN-specific mechanism underlying rodent repetitive behavior. SNRI Summer Symposium. September 2021, SNRI, Indianapolis, IN 46202

C. W. Morris. (2020) Post-synaptic Signaling Mechanisms Underlying Striatal Dysfunction. SNRI Summer Symposium, October 2020, SNRI, Indianapolis, IN 46202

C. W. Morris. (2016) Molecular Cascades and Potential Implications of the Spinophilin and SAPAP3 Interaction on Basal Ganglia Disorders. Indiana University Undergraduate Research Conference (IUUCR), December 2016, IUPUI Center for Research and Learning, Indianapolis, IN 46202

C. W. Morris. (2016) Mechanisms Underlying the SAPAP3 and Spinophilin Interaction: Implications in OCD and Parkinson's Disease. Midwest Undergraduate Cognitive Science Conference (MUCSC), April 2016, Indiana University Cognitive Science Program, Bloomington, IN 47406

Poster Presentations

C. W. Morris, Darryl S. Watkins, Anthony J. Baucum II. (2021) Conditional spinophilin knockout mice as a novel model for detailing striatal MSN-specific mechanism underlying rodent repetitive behavior. Society for Neuroscience Poster Symposium, November 2021, Society for Neuroscience National Meeting, Chicago, IL 60610

C W. Morris, Darryl S. Watkins, Anthony J. Baucum II. (2019) The spinophilin, SAPAP3, and mGlu5 complex as a potential regulatory node of obsessive-compulsive disorder-like behavior. Society for Neuroscience Poster Symposium, October 2019, Society for Neuroscience National Meeting, Chicago, IL 60610

C W. Morris, Darryl S. Watkins, Anthony J. Baucum II. (2019) The spinophilin, SAPAP3, and mGlu5 complex as a potential regulatory node of obsessive-compulsive disorder-like behavior. Society for Neuroscience Poster Symposium, October 2019, Society for Neuroscience National Meeting, Chicago, IL 60610

C. W. Morris, M. C. Edler, A. J. Baucum. (2016) Function and Physiological Implications of the SAPAP3 and Spinophilin Interaction. Society for Neuroscience Poster Symposium, November 2016, Society for Neuroscience Nation Meeting, San Diego, CA 92101

C. W. Morris, M. C. Edler, A. J. Baucum. (2016) Mechanisms Underlying Synaptic Complex Formation in Parkinson's Disease and Obsessive-Compulsive Disorder. Indiana University-Purdue University Indianapolis Research Day, April 2016, Center for Research and Learning, Indianapolis, IN 46202

C. W. Morris, M. C. Edler, A. J. Baucum. (2016) Mechanisms Underlying Synaptic Complex Formation in Parkinson's Disease and Obsessive-Compulsive Disorder. Society for Neuroscience Poster Symposium, March 2016, Society for Neuroscience Regional Meeting, Indianapolis, IN 46202

C. W. Morris, M. C. Edler, A. J. Baucum. (2015) Spinophilin Association with SAPAP3 is regulated by Dopamine Depletion, mGluR5, and PKC. IUPUI International Scientific Exchange Symposium and Poster Session, October 2015, Indianapolis, IN 46202

C. W. Morris, M. C. Edler, A. J. Baucum. (2015) Spinophilin Association with SAPAP3 is Regulated by Dopamine Depletion, mGluR5, and PKC. Society for Neuroscience Poster Symposium, October 2015, Society for Neuroscience National Meeting, Chicago, IL 60610, 382.15

C. W. Morris, M. C. Edler, A. J. Baucum. (2015) PKC Regulates the SAPAP3 and Spinophilin Association. Summer Research Program Poster Session, July 2015, Center for Research and Learning, Indianapolis, IN 46202

C. W. Morris, M. C. Edler, A. J. Baucum. (2015) mGluR5 Dependent Regulation of the SAPAP3 and Spinophilin Interaction. Honors Capstone Research Poster Session, May 2015, Department of Psychology, Indianapolis, IN 46202

C. W. Morris, M. C. Edler, A. J. Baucum. (2015) mGluR5 Dependent Regulation of the SAPAP3 and Spinophilin Interaction. Indiana University-Purdue University Research Day Poster Symposium, April 2015, Center for Research and Learning, Indianapolis, IN 46202

C. W. Morris, M. C. Edler, A. J. Baucum. (2015) Research in the Baucum Laboratory. Hoosier Association of Science Teachers Inc. Poster Session, February 2015, IUPUI Undergraduate Recruitment, Indianapolis, IN 46202

J. Yang, A. Long, **C. W. Morris**. (2014) Quantitative and Qualitative Analysis of Nitrite Teratogenicity. Biology K102 Honors Research Poster Session, December 2014, IUPUI Department of Biology, Indianapolis, IN 46202

Honors and Awards
IUPUI University Fellowship ($27,000 for one year)
2018-2019

Neuroscience Outstanding Research Award; IUPUI
February 2017

IUPUI Honors Scholar
December 2017

Honorary Mention in Research; IUURC
December 2016

Stark Neurosciences Research Institute Grant
Summer 2016

Honorary Mention in Research; MUCSC
April 2016

UROP Grant
Summer 2015

Professional Experience
Research
Dissertation Research: Striatal Signaling Molecules in Repetitive Behaviors
May 2019-August 2022

Eli Lilly & Company Co-Op Internship
May 2017 – August 2018

Research Technician
February 2017 – May 2017

Undergraduate Researcher
August 2015 – December 2016

Stark Neurosciences Research Institute Summer Internship
June – July 2016

Undergraduate Research Opportunities Summer Fellowship
June - July 2015

Development
Stark Neurosciences Research Institute Internship Seminar
June – July 2016

Physician Shadowing Program Externship
Spring 2016

Methods in Teaching Chemistry Seminar
Fall 2015; Spring 2016

UROP Workshops
June - July 2015

Capstone Honors Research Seminar
August 2015 – May 2016

Teaching
IUPUI Department of Chemistry Laboratory Instruct
Fall 2016

General Chemistry I Recitation Peer Led Team Learning Leader
Fall 2015

Introduction to Chemistry Recitation Leader
Fall 2014 – Spring 2015

Mentoring
Best Practices Tutor
May 2016 – October 2016

Bepko Learning Center Genetics Tutor
Fall 2016

IUPUI National Mentoring Symposium Presenter
Fall 2015

Chemistry Resource Center
Spring 2013

Commitment to Service
Licensed Indiana Foster Parent
August 2020 – August 2022

Center for Research and Learning Ambassador
December 2015 – December 2016

Lay Children's Ministry Director
2015 – 2019